Universitat de Girona

NEW INSIGHTS IN THE STUDY OF THE PHYSIOLOGY OF THE ADIPOSE TISSUE

Núria Oliveras Cañellas

Universitat de Girona

DOCTORAL THESIS

New insights in the study of the physiology of the adipose tissue

Núria Oliveras Cañellas

2024

Universitat de Girona

DOCTORAL THESIS

New insights in the study of the physiology of the adipose tissue

Núria Oliveras Cañellas

2024

Doctoral Programme in Molecular Biology, Biomedicine and Health

Co-directed by:

Prof. José Manuel Fernández-Real Lemos

Prof. Rémy Burcelin

Tutor:

Prof. José Manuel Fernández-Real Lemos

Presented to obtain the degree of PhD at the University of Girona

Prof. **José Manuel Fernández-Real Lemos**, group leader of the *Biomedical Research Institute of Girona (IDIBGI), Endocrinology, Diabetes and Nutrition Research Unit (UDEN)*, lead investigator of the CIBER *de la Fisiopatología de la Obesidad y la Nutrición (CIBEROBN, ISCIII)*, and professor of medicine at the *University of Girona (UdG)*.

Prof. **Rémy Burcelin**, Research Director Inserm. I^{2}MC, Institute for Research on Cardiometabolic Diseases, Inserm U 1027. Team Dynamix. *Centre Hospitalier Universitaire Rangueil,* Toulouse, France.

WE DECLARE:

That the thesis entitled "New insights in the study of the physiology of the adipose tissue" presented by Núria Oliveras Cañellas to obtain the doctoral degree in *Molecular Biology, Biomedicine and Health* by the *Universitat de Girona*, has been completed under our supervision and fulfils all the requirements to qualify for an International Doctorate.

For all intents and purposes, we hereby sign this document.

José Manuel Fernández-Real Lemos   Rémy Burcelin

Girona, 2024

"La vida no és fàcil, per ningú de nosaltres.
Però… No importa!
S'ha de perseverar, i sobre tot,
tenir confiança en un mateix.
S'ha de sentir-se dotat per realitzar
alguna cosa i que aquesta cosa
s'ha d'aconseguir, costi el que costi"

Marie Curie

A la meva família

ACKNOWLEDGEMENT

Recordo perfectament el dia que vaig arribar a l'IdIBGi, sense saber ben bé què m'esperava i mai m'hauria imaginat que després més de cinc anys estaria escrivint aquestes línies de la meva tesi doctoral. Tota aquesta feina ha estat possible gràcies a la contribució i ajuda de moltes persones que d'una manera o altre m'han acompanyat al llarg d'aquest camí.

Primer de tot, voldria donar les gràcies als directors d'aquesta tesi, al Dr. José Manuel Fernández-Real per donar-me l'oportunitat de participar en aquest projecte, confiar en mi i ajudar-me a créixer com a investigadora; and to Prof. Rémy Burcelin for giving me the opportunity to work in his laboratory for three months, I really appreciate all the scientific help and facilities.

José, gràcies per la teva disposició a ajudar-me en tot moment i per haver-me transmès la teva passió per la recerca. Paco, gràcies pels teus consells i per fer-me veure la realitat de la ciència, que tot i no ser idíl·lic és molt gratificant. Jordi, gràcies pels teus coneixements i sobretot en la part estadística d'aquesta tesi.

Aina, gràcies pel recolzament i entendre'm en tot moment, qui millor que tu per fer-ho, juntes vam començar aquesta aventura i mà a mà l'hem acabat. No saps la tranquil·litat que m'ha donat saber que estaves darrere meu, esquena amb esquena. Gràcies per les estones juntes. Només desitjo el millor per tu en el que vindrà, perquè no dubto que ho serà. T'ho mereixes!

Gràcies a les noies de la Fly Room per ser-hi en tot moment. Anna, vam arribar gairebé de la mà, gràcies per tots els consells durant tots aquests anys, per escoltar-me quan ho he necessitat i donar-me una perspectiva diferent, gràcies per ensenyar-me tant i fer que les coses difícils semblin una mica més fàcils. Liss, gràcies per les nostres converses arreglant el món que feien que m'oblidés de la tesis per una estona, per l'ajuda desinteressada, simplement gràcies per ser-hi en tot moment. Irene, gràcies per estar disposada a escoltar-me i entendre'm en tot moment, gràcies pels consells i sobretot per ensenyar-me el camí en aquesta nova etapa. Cristina, gràcies per preguntar i ser-hi en tot moment de la manera més desinteressada possible.

Especial menció a dos UDENs que actualment ja no hi són, Jess i Ferran, gràcies per fer de la meva arribada una adaptació fàcil. Jess, gràcies per ser allà, per preguntar en tot moment, per ensenyar-me tot el que sé, pels consells i l'ajuda quan ho he necessitat. Ferran, gràcies

per ser-hi des de la distància i per interessar-te com va tot. Perquè no se m'acut una millor manera de ser-hi, sense ser aquí.

A la resta d'UDENs que m'han acompanyat durant tots aquests anys, Yenny, Isma, Kenia, María, Irene, Anna, Elena, Andrea, Sara... gràcies. També voldria agrair a tots els col·laboradors que han format part d'aquest projecte d'una manera o altra proporcionant les eines necessàries per a l'elaboració d'aquesta tesi.

A tota la família de l'IdIBGi, gràcies a tots per compartir amb mi tot aquest camí. Ariadna i Berta, gràcies per les estones de desconnexió durant el dinar, per les xerrades posar-nos al dia, per estar disposades a preguntar i donar-nos suport en tota l'aventura. Marina, gràcies per ser l'alegria de l'IdIBGi, perquè una estona amb tu et treu un somriure per tot el dia, gràcies per ser sempre tant positiva. També vull agrair a la resta de l'IdIBGi l'agradable convivència, Lucía, Alba, Adri, Laia, Mar, Albert, Joana, Ester, Àngela, ... Moltes gràcies a tots!

Moving to Toulouse, I sincerely thank to Dr. Christophe Heymes for giving me the opportunity to participate in one of his projects and to Dra. Anne Bouloumie for welcoming me to the laboratory. Finally, I would like to say thanks to Alex, Kévin and Jiuwen, for their kindness and for helping me whenever I needed it.

Gràcies a la meva família, papes, Josep, iaia i tieta. Gràcies per recolzar-me i animar-me, respectar les meves decisions i donar-me suport. Gràcies per la vostra paciència i escoltar-me en tot moment. Per intentar entendre'm sense entendre gairebé res. Gràcies per ensenyar-me a lluitar pel que m'agrada i ensenyar-me que la constància dóna els seus fruits.

Per últim, voldria agrair d'una manera molt especial a en Joel, gràcies pel teu suport incondicional durant tots aquests anys, per recolzar-me en tot moment en les meves decisions, per confiar en mi més del que jo ho faig, per tota l'ajuda dins i fora d'aquesta tesi i per la infinita paciència que tens. Molts ànims pel que et queda, perquè encara que l'última etapa és la més dura, quan s'acaba és la més gratificant. Gràcies per ser-hi en tot moment i caminar amb mi de la mà.

LIST OF ORIGINAL MANUSCRIPTS

This thesis is presented as a compendium of manuscripts:

Manuscript I

Oliveras-Cañellas N*, Castells-Nobau A*, de la Vega-Correa L*, Latorre-Luque J, Motger-Albertí A, Arnoriaga-Rodriguez M, Garre-Olmo J, Zapata-Tona C, Coll-Martínez C, Ramió-Torrentà L, Moreno-Navarrete JM, Puig J, Villarroya F, Ramos R, Casadó-Anguera V, Martín-García E, Maldonado R, Mayneris-Perxachs J, Fernández-Real JM. **Adipose tissue coregulates cognitive function.** Sci Adv. 2023 Aug 11; 9(32):eadg4017. doi: 10.1126/sciadv.adg4017

Impact factor (JCR 2022): 13.6 (D1, 7/73 Multidisciplinary Sciences)

Manuscript II

Oliveras-Cañellas N, Moreno-Navarrete JM, Lorenzo PM, Garrido-Sánchez L, Becerril S, Rangel O, Latorre J, de la Calle Vargas E, Pardo M, Valentí V, Romero-Cabrera JL, Oliva-Olivera W, Silva C, Diéguez C, Villarroya F, López M, Crujeiras AB, Seoane LM, López-Miranda J, Frühbeck G, Tinahones FJ, Fernández-Real JM. **Downregulated adipose tissue expression of browning genes with increased environmental temperatures.** J Clin Endocrinol Metab. 2023 Dec 21; 109(1):e145-e154. doi: 10.1210/clinem/dgad469

Impact factor (JCR 2022): 5.8 (Q1, 31/145 Endocrinology & Metabolism)

Additional publications generated by this thesis topic during the PhD are shown in **Appendix 2**.

LIST OF ABREVIATIONS

Abbreviation	Description
1tub23cf	γ – Tubulin 23
¹H NMR	Proton Nuclear Magnetic Resonance
AAV	Adeno-Associated Virus
ABCC1	ATP Binding Cassette Subfamily C Member 1 (ABCC1 Blood Group)
ACC	Acetyl-CoA Carboxylase Enzyme
Acetyl – CoA	Acetyl Coenzyme A
ACLY	ATP – Citrate Lyase
ACS	Acetyl – CoA Synthetase
ACTB	β – Actin
AD	Alzheimer's Disease
ADIPOQ	Adiponectin
ADRB2	Adrenoceptor β2
AEMET	National Meteorological Agency of Spain
Akt	Protein Kinase B
Aβ42	Amiloid β (aa 1 – 42)
Amn	Amnesiac
AMPH	Amphiphysin
ANOVA	Analysis of variance
ApoB	Apolipoprotein B
ARHGAP23	Rho GTPase Activating Protein 23
AT	Adipose Tissue
ATGL	Adipocyte Triglyceride Lipase
ATP	Adenosine Triphosphate
ATP1B1	ATPase Na+/K+ Transporting Subunit β1
BAT	Brown Adipose Tissue
BBB	Blood – Brain Barrer
BCHE	Butyrylcholinesterase
BDSC	Bloomington *Drosophila* Stock Centre
BMI	Body Mass Index
BMP	Bone Morphogenetic Protein
BSA	Bovine Serum Albumin
C4A	Complement C4A (Chido/Rodgers Blood Group)
C4B	Complement C4B (Chido/Rodgers Blood Group)
C/EBP	CCAAT / Enhancer – Binding Protein
CAMKII	Calcium/Calmodulin Dependent Protein Kinase II
cAMP	Cyclic Adenosine 5' – Monophosphate
CEIC	Committee for Clinical Investigation
CEEA – PRB	Comitè Ètic d'Experimentació Animal – Parc de Recerca Biomèdica de Barcelona
CI	Courtship Index
CIBEROBN	Centro de Investigación Biomédica en Red Fisiopatología de la Obesidad y Nutrición
CIDEA1	Cell Death Inducing DNA Fragmentation Factor α Subunit Like Effector A
cDNA	Complementary DNA
CD36	Cluster of Differentiation 36
CNS	Central Nervous System

CPM	Count per Million
CPMG	Carr – Purcell – Meiboom – Gill
CRP	C – Reactive Protein
Ct	Cycle Threshold
cVA	Cis – Vaccenyl Acetate
CVLT – II	California Verbal Learning Test
CXCR-1	C-X-C Motif Chemokine Receptor 1
Cyp4	Cytochrome P450
DAG	Diacylglycerol
DALYs	Disability – Adjusted Life Years
DBP	Diastolic Blood Pressure
Dcr – 2	Dicer Enzyme
DEG	Differential Expression Gene
DIAPH3	Diaphanous Related Formin 3
DLG	Discs Large MAGUK Scaffold Protein
DLGAP1	DLG Associated Protein 1
DNA	Deoxyribonucleic Acid
DNase	Deoxyribonuclease
Dnc	Dunce
DSM-5	Diagnostic and Statistical Manual of Mental Disorders 5th edition
DST	Digit Span Test
dNTP	Deoxynucleotides Triphosphate
EDTA	Ethylenediaminetetraacetic Acid
ELISA	Enzyme – Linked Immunosorbent Assay
ESI	Electrospray Ionization
ER	Endoplasmic Reticulum
EZR	Ezrin
FAS	Fatty Acid Synthetase
FASN	Fatty Acid Synthase
FDR	False Discovery Rate
FFA	Free Fatty Acids
G3P	Glyceraldehyde 3 – Phosphate
GAPDH	Gyceraldehyde-3 – Phosphate Dehydrogenase
GD	Georg Dietz
GFP	Green Fluorescence Protein
GLUT4	Glucose Transporter 4
GO	Gene Ontology
GPAT	Glycerol 3-Phosphate Acyltransferase
GPC4	Glypican 4
GTPase	Rho Guanosine Triphosphatase
Hb	Haemoglobin
HbA1c	Glycosylated Haemoglobin
HCV	Hepatitis C Virus
HDL	High – Density Lipoprotein

HFD	High – Fat Diet
HOMER1	Homer Scaffold Protein 1
HPLC	High – Performance Liquid Chromatography
HRP	Horsedish Peroxidase
HSL	Hormone Sensitive Lipase
IDIBGI	Institut d'Investigació biomèdica de Girona
IL	Interleukin
ILC2	Group 2 Innate Lymphoid Cells
INMT	Indolethylamine N – Methyltransferase
IR	Insulin Resistance
iWAT	Inguinal White Adipose Tissue
KCNN3	Potassium Calcium – Activated Channel Subfamily N Member 3
KK	Krystyna Keleman
KYNU	Kynureninase
LBP	Lipopolysaccharide Binding Protein
LD	Lipid Droplet
LDL	Low – Density Lipoprotein
LI	Learning Index
LPA	Lysophosphatidic Acid
LPC	Lysophosphatidylcholine
LPL	Lipoprotein Lipase
LSD	Least Significant Difference
LTM	Long Term Memory
MAG	Monoacylglycerol
Malonyl – CoA	Malonyl Coenzyme A
MARK study	Improving Intermediate Risk Management Study
MCI	Mild Cognitive Impairment
MESGI50 study	Maturity and satisfactory ageing in Girona Study
MGL	Monoacylglycerol Lipase
microRNA	Micro – Ribonucleic Acid
ML	Machine Learning
MRI	Magnetic Resonance Imaging
mRNA	Messenger RNA
MS/MS	Tandem Mass Spectrometry
MSCs	Mesenchymal Stem Cells
mWAT	Mesenteric White Adipose Tissue
Myf5	Myogenic 5
MZSA	Maximum Normalized Importance Among Shadow Attributes
Na,K-ATPase	Sodium and Potassium Dependent Adenosine Triphosphatase
NAFLD	Non – Alcoholic Fatty Liver Disease
NCAM2	Neural Cell Adhesion Molecule 2
ND	Normal Diet
NEFA	Non – Esterified Fatty Acids
NIG – FLY	Fly Stocks of National Institute of Genetics
NKAL	Na,K – ATPase Oxidant Amplification Loop
NLGN3	Neuroligin 3
NLRP3	Nucleotide Oligomerization Domain (NOD) like Receptor Family, Pyrin Domain – Containing 3
NNMT	Nicotinamide N – Methyltransferase

NOR	Novel Object Recognition
NR4A family	Nuclear Receptor Subfamily 4 Group A (Member 1 / 2 / 3)
NUDT2	Nudix Hydrolase 2
OAT	Ornithine Aminotransferase
PA	Palmitate
PAI – 1	Plasminogen Activator Inhibitor – 1
PBMC	Peripheral Blood Mononuclear Cells
PBS	Phosphate Buffered Saline
PCR	Polymerase Chain Reaction
PGE2	Prostaglandin E2
PIK3C2	Phophatidylinositol – 4 – Phosphate 3 – Kinase Catalytic Subunit Rype 2
PIP	Phosphatidylinositol
PKA	Protein Kinase A
PLA2G6	Phospholipase A2 Group VI
PLEKHA6	Pleckstrin Homology Domain Containing A6
PLIN1	Perilipin 1
PNS	Peripheral Nervous System
PODXL	Podocalyxin like
PPARγ	Peroxisome Proliferator Activated Receptor Gamma
PPIA	Peptidylprolyl Isomerase A
PRDM16	PR/SET Domain 1
PTPRD	Protein Tyrosine Phosphatase Receptor Type D
qPCR	Quantitative Polymerase Chain Reaction
QPRT	Quinolinate Phosphoribosyltransferase
RBP1	Retinol Binding Protein 1
RD	Recycling Delay
RF	Random Forest
RHOBTB1	Rho Related BTB Domain Containing 1
RIMS1	Regulating Synaptic Membrane Exocytosis 1
RISC	RNA – Induced Silencing Complex
RNA	Ribonucleic Acid
RNAi	Interference RNA
RNApol2	RNA Polymerase II
RNase	Ribonuclease
RNA-seq	RNA Sequencing
ROCF	Rey – Osterrieth Complex Figure
ROS	Reactive Oxygen Species
rRNA	Ribosomal RNA
RSEM	RNA – Seq by Expectation Maximization
RT	Reverse Transcription
RTA	Real Time Analysis
Rut	Rutabaga
SAT	Subcutaneous Adipose Tissue
SBP	Systolic Blood Pressure

SCWT	Stroop Colour and Word Test
SEM	Standard Error of Mean
SG02	Shugoshin 2
siRNAs	Small Interference RNA
SHARE	Survey of Health, Ageing and Retirement in Europe Project
shRNA	Short Hairpin RNA
SLC2A4	Solute Carrier Family 2 Member 4
SLC18A2	Solute Carrier Family 18 Member A2
SMAD	Mother Against Decapentaplegic Homolog
SNCA	Synuclein α
SNS	Sympathetic Nervous System
SRF	Serum Response Factor
STAR	Spliced Transcripts Alignment to a Reference
STM	Short Term Memory
STRING	Search Tool for Retrieval of Interacting Proteins/Genes
SVF	Stroma Vascular Fraction
SYN1	Synapsin I
T2D	Type 2 Diabetes
TBS	Tris – Buffered Saline
TC	Total Cholesterol
TCA	Tricarboxylic Acid Cycle
TCN2	Transcobalamin 2
TG	Triglycerides
TIMP1	Tissue Inhibitor of Metallopeptidase 1
TMB	3,3',5,5' – Tetramethylbenzidine
TMT	Trail Making Test
TNF-α	Tumor Necrosis Factor – α
TRiP	Transgenic RNAi Project
TSP	3 – Trimethyl-Silyl – 1 – [2,2,3,3, – ^{2}H4]
UAS – GAL4	Upstream Activating System – Galactosidase 4
UCP1	Uncoupled Protein 1
UNC5B	Unc – 5 Netrin Receptor B
VAT	Visceral Adipose Tissue
VDRC	Vienna *Drosophila* RNAi Centre
VLDL	Very – Low Density Lipoprotein
VMAT	Vesicle Monoamine Transporter Member 2
WAIS-III	Wechsler Adult Intelligence Scale – III
WAT	White Adipose Tissue
WHO	World Health Organization
WHR	Waist – to – Hip Ratio
Z	Normalized Permutation Importance

LIST OF FIGURES

x

LIST OF TABLES

TABLE OF CONTENTS

SUMMARY

The prevalence of obesity has increased dramatically in recent years and has reached epidemic proportions. Obesity is a chronic multifactorial disease associated with an abnormal accumulation of dysfunctional adipose tissue and has been associated with multiple related disorders, including cognitive dysfunction. It is known that cognitive decline is a major health problem and is found to be exacerbated by metabolic comorbidities such as obesity. The aetiology of obesity is multifactorial, including environmental factors. Nowadays, environmental factors are changing due to global warming which is increasing the temperature of the Earth. It is known that the browning process is very important in the physiology of adipose tissue.

The aim of this thesis is to describe the bidirectional interaction between adipose tissue and cognitive performance in human subjects with morbid obesity, as well as in animal models, and to investigate how environmental temperature might affect adipose tissue physiology and metabolic traits in white adipose tissue. For this purpose, several cohorts of subjects, with and without obesity, were recruited and transcriptomic analysis were performed in the adipose tissue of these subjects. Brain function was assessed through neurocognitive tests. Temperature data was obtained from a cohort of more than 1,000 subjects from five different regions of Spain. *Drosophila melanogaster* and mice animal models were used to study the cognitive function by altering the expression of target genes in the fat body or adipose tissue.

Here, we identified 188 genes from RNA sequencing of adipose tissue in three cohorts that were associated with performance in different cognitive domains. These genes were mostly involved in synaptic function, phosphatidylinositol metabolism, the complement cascade, anti-inflammatory signalling, and vitamin metabolism. These findings were translated into the plasma metabolome. The circulating blood expression levels of most of these genes were also associated with several cognitive domains in a cohort of 816 participants. Targeted misexpression of candidate gene ortholog in the *Drosophila* fat body significantly altered memory and learning in flies. Among them, down-regulation of the neurotransmitter release cycle-associated gene *SLC18A2* improved cognitive abilities in *Drosophila* and in mice. Up-regulation of *RIMS1* in *Drosophila* fat body improved cognitive abilities.

The expression of genes associated with browning and *ADIPOQ* in adipose tissue were significantly and negatively associated with environmental temperatures. The latter temperatures were also negatively associated with the expression of genes involved in

adipogenesis. Decreased expression of *UCP1* and *ADIPOQ* messenger RNA and circulating adiponectin were observed with increasing temperatures in all individuals as a whole and in participants with obesity in univariate, multivariate and artificial intelligence analysis. The differences remained statistically significant in individuals without type 2 diabetes and in samples collected during winter.

Taken together, these findings suggest a bidirectional interaction between the adipose tissue transcriptome and brain function in humans, as well as in animal models. Furthermore, given the North-South gradient in obesity prevalence in the study regions, the present observations may have implications for the relationship between the obesity pandemic and global warming.

RESUM

La prevalença de l'obesitat ha augmentat dràsticament en els últims anys arribant a assolir proporcions epidèmiques. L'obesitat és una malaltia crònica multifactorial associada a una acumulació anormal de teixit adipós no funcional i, s'ha associat a múltiples desordres relacionats, incloent la disfunció cognitiva. Es sap que el declivi cognitiu és un greu problema per la salut i s'ha trobat que és més pronunciat en malalties metabòliques com és l'obesitat. L'etiologia de l'obesitat és multifactorial, entre el que s'inclouen factors ambientals. Actualment, els factors ambientals estan en constant canvi degut al canvi climàtic que està augmentant la temperatura de la terra. Es sap que el procés de *browning* és molt important en la fisiologia del teixit adipós.

L'objectiu d'aquesta tesis és descriure la interacció bidireccional entre el teixit adipós i la funció cognitiva en subjectes humans amb obesitat mòrbida, així com també en models animals, i investigar com la temperatura ambiental pot afectar la fisiologia del teixit adipós i els trets metabòlics del teixit adipós blanc. Per a aquest propòsit, diferents cohorts de participants, amb i sense obesitat, s'han reclutat i s'han dut a terme anàlisis transcriptòmics en el teixit adipós d'aquests subjectes. La funció cerebral s'ha avaluat a través de testos neurocognitius. Les dades de temperatura s'han obtingut d'una cohort de més de 1000 participants de cinc regions diferents d'Espanya. *Drosophila melanogaster* i ratolins s'han utilitzat com a models animal per estudiar la funció cognitiva, on s'ha alterat l'expressió de gens diana en el *fat body* o al teixit adipós.

Aquí, hem identificat 188 gens a través de seqüenciació de RNA del teixit adipós de tres cohorts que s'han associat amb rendiment en diferent dominis cognitius. Aquests gens estan involucrats en funció sinàptica, metabolisme de fosfatidil-inositol, cascada de complements, senyalització anti-inflamatòria, i metabolisme de vitamines. Aquestes troballes van ser traslladades al metaboloma plasmàtic. Els nivells d'expressió circulant en sang de la majoria d'aquests gens també estan associats amb diferent dominis cognitius en una cohort de més de 816 participants. L'expressió dirigida d'un gen ortòleg candidat al *fat body* de *Drosophila* altera de manera significativa la memòria i l'aprenentatge de les mosques. De tots ells, la disminució de l'expressió del gen *SLC18A2*, associat al cicle d'alliberament de neurotransmissors, millora les capacitats cognitives, tant a *Drosophila* com en ratolí. La sobre-expressió de *RIMS1* al *fat body* de *Drosophila* millora les capacitats cognitives.

L'expressió de gens associats a *browning* i *ADIPOQ* en el teixit adipós està associat negativament de manera significativa amb la temperatura ambiental. Aquestes mateixes temperatures estan negativament associades amb l'expressió de gens involucrats en adipogènesis. Una disminució de l'expressió de *UCP1* i *ADIPOQ* en RNA missatger i, adiponectina circulant, s'ha observat amb l'augment de temperatures en tots els participants com un conjunt i entre els participants obesos tant en anàlisis univariants, multivariants com també en intel·ligència artificial. Les diferències es mantenen significants en participants sense diabetis tipus 2 i en les mostres recollides durant l'hivern.

En conjunt, aquestes troballes suggereixen una interacció bidireccional entre el transcriptoma del teixit adipós i la funció cerebral en humans, així com també en models animals. A més, atès al gradient nord-sud de la prevalença de l'obesitat en les regions d'estudi, les observacions actuals poden tenir implicacions en la relació entre la pandèmia de l'obesitat i el canvi climàtic.

RESUMEN

La incidencia de la obesidad ha aumentado drásticamente en los últimos años llegando a alcanzar proporciones epidémicas. La obesidad es una enfermedad crónica multifactorial asociada a una acumulación anormal de tejido adiposo no funcional y se ha asociado a múltiples desórdenes relacionados, incluyendo la disfunción cognitiva. Se conoce que el declive cognitivo es un grave problema para la salud y se ha encontrado que es más pronunciado en enfermedades metabólicas, como es la obesidad. La etiología de la obesidad es multifactorial, incluyendo factores ambientales. Actualmente, los factores ambientales están en constante cambio debido al cambio climático que está aumentando la temperatura de la tierra. Se conoce que el proceso de *browning* es muy importante en la fisiología el tejido adiposo.

El objetivo de esta tesis es describir la interacción bidireccional entre el tejido adiposo y la función cognitiva en sujetos humanos con obesidad mórbida, así como también en modelos animales, e investigar como la temperatura ambiental puede afectar la fisiología del tejido adiposo y los rasgos metabólicos del tejido adiposo blanco. Por este propósito, distintas cohortes de participantes, con y sin obesidad, se han reclutado y se han llevado a cabo análisis transcriptómicos en el tejido adiposo de éstos. La función cerebral se ha evaluado a través de pruebas neurocognitivas. Los datos de temperatura se han obtenido de una cohorte de más de 1000 participantes de cinco regiones diferentes de España. *Drosophila melanogaster* y ratones se han utilizado como modelos animal para estudiar la función cognitiva, donde se ha alterado la expresión de genes diana en el *fat body* o en el tejido adiposo.

Aquí, hemos identificado 188 genes a través de secuenciación de RNA del tejido adiposo de tres cohortes que se han asociado con el rendimiento en diferentes dominios cognitivos. Estos genes están involucrados en función sináptica, metabolismo del fosfatidil-inositol, cascada de complementos, señalización anti-inflamatoria, y metabolismo de vitaminas. Estos hallazgos fueron trasladados al metaboloma plasmático. Los niveles de expresión circulante en sangre de la mayoría de estos genes también están asociados con distintos dominios cognitivos en una cohorte de más de 816 participantes. La expresión dirigida de un gen ortólogo candidato en el *fat body* de *Drosophila* altera de manera significativa la memoria y el aprendizaje en moscas. Entre todos ellos, la disminución de la expresión del gen *SLC18A2*, asociado al ciclo de liberación de neurotransmisores, mejora las capacidades cognitivas en

Drosophila y en ratón. La sobre-expresión de *RIMS1* en el *fat body* de *Drosophila* mejora las capacidades cognitivas.

La expresión de genes asociados a *browning* y *ADIPOQ* en el tejido adiposo está asociado negativamente de manera significativa a la temperatura ambiental. Estas mismas temperaturas están negativamente asociadas a la expresión de genes involucrados en adipogénesis. Una disminución de la expresión de *UCP1* y *ADIPOQ* en RNA mensajero y, adiponectina circulante, se ha observado con el aumento de temperaturas en todos los participantes como un conjunto y en los participantes con obesidad tanto en análisis univariantes, multivariantes como también en inteligencia artificial. Las diferencias se mantienen significativas en participantes sin diabetes tipo 2 y en las muestras recogidas durante invierno.

En conjuntos, estos hallazgos sugieren una interacción bidireccional entre el transcriptoma del tejido adiposo y la función cerebral en humanos, así como también en modelos animales. Además, dado el gradiente norte-sur de la incidencia de la obesidad en las regiones de estudio, las observaciones actuales pueden tener implicaciones en la relación entre la pandemia de la obesidad y el cambio climático.

1. INTRODUCTION

1.1 OBESITY

1.1.1 Definition and classification of obesity

Obesity is a multifactorial chronic disease characterised by an excessive fat accumulation (globally, regionally and/or in organs) that increases the risk of adverse health outcomes [1,2] and reduces life expectancy [3]. Specifically, the World Health Organization (WHO) defines overweight and obesity as abnormal or excessive accumulation of fat that presents a risk to health [4]. This accumulation is usually due to an imbalance between energy intake and energy expenditure, resulting in a chronic positive energy balance [5].

The WHO defines obesity as a percentage of fat mass greater than 25% in men and 33% in women. This definition is currently considered inadequate, as we know that obesity is a chronic, relapsing disease with a more complex etiopathogenesis than expected, causing multiple comorbidities, reducing patient life expectancy and lacking effective treatment.

The body mass index (BMI) is a simple and available weight-for-height index that is widely used to classify overweight and obesity in adults. It is defined as a body weight in kilograms divided by the square of his height in meters (kg/m^2). WHO uses BMI to classify obesity into different groups (**Table 1**).

Table 1 | Classification of overweight and obesity in adults based on BMI. *Table taken and adapted from Purnell J. Q. (2000)* [1]

Status	BMI (kg/m2)
Underweight	< 18.5
Normal	18.5 – 24.9
Overweight	25.0 – 29.9
Obesity	≥ 30
Class I	30.0 – 34.9
Class II	35.0 – 39.9
Severe Obesity (class III)	≥ 40

Overweight is defined as a BMI equal to or greater than 25 kg/m^2; obesity is defined as a BMI equal to or greater than 30 kg/m^2; and severe obesity is defined as a BMI equal to or greater than 40 kg/m^2 [4]. BMI correlates with the percentage of body fat, which is independently influenced by sex, age and race [1].

1.1.2 Pathophysiology of obesity

Although obesity is a multifactorial and multisystem disease, its pathophysiology is well understood. The hallmark for understanding the pathophysiology of obesity is based on the energy homeostasis, a biological process responsible for maintaining a balance between energy intake and energy expenditure over time [6].

Energy homeostasis is achieved by a system whereby circulating signals inform the brain of available energy stores (a process known as 'adipose negative feedback') and the brain makes corrective adjustments to food intake in response [7]. The two main hormones involved in energy homeostasis are leptin, secreted by the adipose tissue (AT), and insulin, secreted by the pancreas. Both circulate at levels in proportional to body fat stores and act in the brain to reduce food intake [6]. Negative feedback from adiposity reduces food intake by increasing brain responsiveness to satiety signals, an effect mediated by neuronal input from leptin and insulin [8].

Obesity is defined as a pathological state based on peripheral accumulation of adiposity [9], which results when caloric intake exceeds current requirements [7]. Humans consume carbohydrates, proteins, fats and non-nutritive bioactive compounds such as dietary fibre, polyphenols or terpenoids as part of the substrate required for life. When more macronutrients are consumed than are used, the excess is stored in the form of glycogen and fats. This storage fat is mainly made up of triglycerides (TG), which accumulate in aggregated adipocytes to form white adipose tissue (WAT). These energy stores provide energy to support the ongoing metabolic needs of the organism [10,11].

As weight increases, insulin secretion must increase in basal state and in response to meals to compensate for insulin resistance (IR) if normal glucose homeostasis is to be maintained. Increased insulin secretion as obesity progresses, increases insulin delivery to the brain, where it helps to limit further weight gain. Leptin has a more important role than insulin in central nervous system (CNS) control of energy homeostasis [6].

The lipid depot function of WAT is to mobilise TG for systemic utilisation when other tissues require energy. Fat accumulation becomes pathogenic when the energy balance between the ingested and burnt energy become too positive, resulting in weight gain [2,12]. This excess energy intake triggers several morphological and metabolic changes, such as hypertrophy and hyperplasia of the adipocytes, in addition to fibrosis and inflammatory processes [13].

Hypertrophy is an adaptive response to excess fat that maintains the nutrient buffering capacity of the AT by increasing the size of the existing adipocytes [14,15]. Hyperplasia is the ability to generate new mature adipocytes by differentiating resident preadipocytes to increase they in number [14,16]. In addition, hyperplasia attempts to balance hypertrophy to maintain AT homeostasis [16]. The higher the degree of hypertrophy, the lower the rate of adipocyte formation occurs [17].

In a chronic state of positive energy balance, the adipocyte initially expands until it reaches a critical cell size and becomes lipid overloaded [12]. Adipocytes experience increased mechanical stress as their contact with neighbouring cells increases and they experience hypoxia [18]. Then, developed a pro-inflammatory role, leading to fibrosis, apoptosis, and finally IR [12,18]. The increased mechanical and hypoxic stress of hypertrophic adipocytes contributes to AT inflammation [18]. In contrast, hyperplasia attempts unsuccessfully to repair the metabolic changes caused by the excess fat [12] (**Figure 1**).
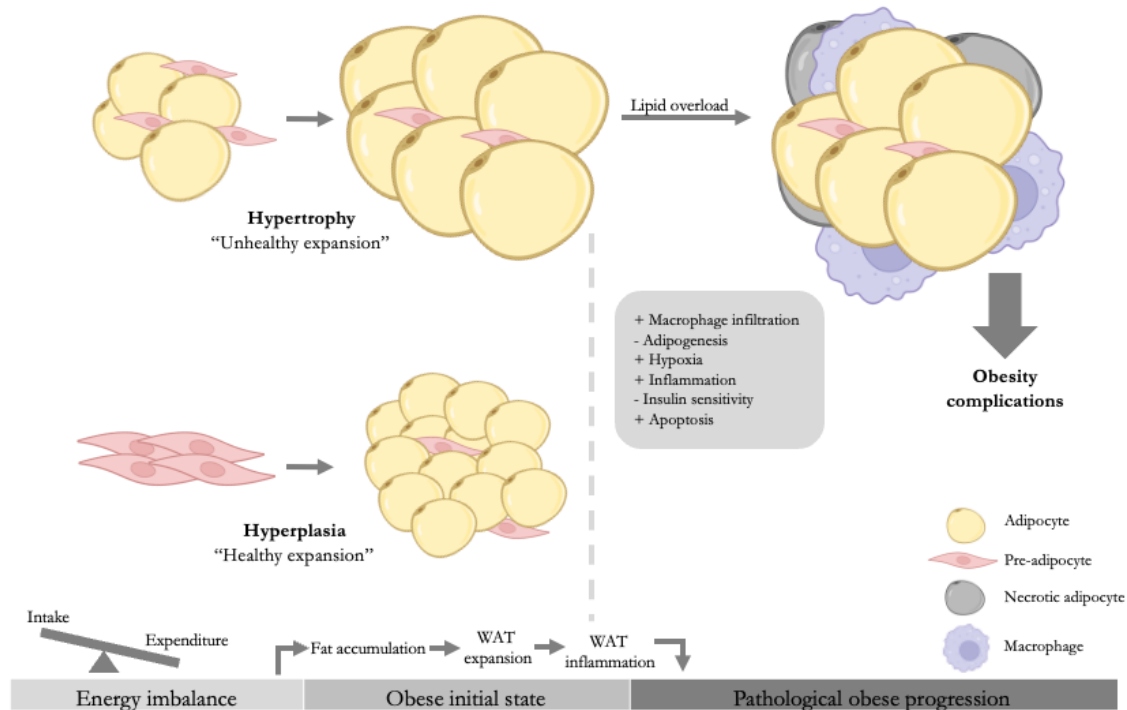
Figure 1 | Comparative scheme between hypertrophy and hyperplasia processes in AT. Once the energy imbalance is presented, fat accumulation begins in the AT. In this sense, the AT tries to manage this excess in two ways: in a healthy mode generating new adipocytes (hyperplasia) or in a pernicious manner with the enlargement of the existing ones (hypertrophy). In the case of hypertrophy, this happens because of an inability to manage such excess of lipids which leads to lipid overload and consequently to a pathological state. Thus, begins the infiltration of macrophages among other immune cells and the consequent inflammatory response of the AT. *Figure taken and adapted from Ghaben A. L. (2019)* [18]

1.1.3   Aetiology of obesity

The exact cause of obesity is complex and unknown. Given the increasing epidemiology of obesity and the fact that several factors have been described as causally influencing the aetiology of obesity, there is a need to understand [19]. There appears to be an interplay between hereditary, environmental, physiological, behavioural, social and economic factors [9,20–23] (**Table 2**).

Hereditary factors and our particular socio-economic and socio-cultural environment, such as a sedentary lifestyle combined with excessive energy intake, have been shown to influence the risk of obesity. These factors create an obesogenic environment. An obesogenic environment is any influence on the environment, opportunities or living conditions that can promote obesity. Not all of us who live in obesogenic environments experience the same

increase in our waistlines. While body weight regulation is and should be viewed as a complex interaction between environmental, socio-economic and genetic factors; personal behaviours in response to these conditions continues to play a dominant role in preventing obesity [2].

Table 2 | Major risk factors that influenced the aetiology of obesity. *Table taken and adapted from Hruby A. (2015)* [2]

Hereditary factors	Environmental factors	Behavioural factors	Socioeconomic factors
Genetics Epigenetics Family history	Environment Gut microbiota Endocrine-disrupting chemicals Chronodisruption	Dietary patterns Sedentary lifestyle / physical exercise Stress Sleep Several disorders and medication	Socio-demographic indicators Globalisation Urbanisation Lack of education Poverty

1.1.3.1   Hereditary factors

Genetic factors: Genetic factors account for 20 – 40% of the causes of obesity [24], more than 140 genetic regions have been related to different adiposity measures [22]. Obesity is a polygenic disease, generally not caused by a mutation in a single gene, but rather by the accumulation of multiple genes that predispose an individual to obesity [25,26]. However, several loss-of-function mutations have been identified that cause monogenic obesity and act in the appetite-regulating leptin-melanocortin pathway [22] including leptin [27], leptin receptor [28,29], pro-opiomelanocortin and melanocortin 4 receptor [30]. Of these, the melanocortin 4 receptor mutation is the most common cause of monogenic obesity in humans [8].

Epigenetics: Epigenetics is defined as heritable changes in gene function that occur without a change in deoxyribonucleic acid (DNA) sequence, suggesting that is a heritable trait [31]. It includes DNA methylation, histone modifications and micro–ribonucleic acid (microRNA)-mediated processes [26]. Epigenetic modifications of gene expression during early life are increasingly recognised as contributing to obesity [25]. Genetic predisposition and ageing are factors that contribute to epigenetic variability, and, several environmental factors, including exercise and diet, further interact with the human epigenome [31].

Family history: The likelihood of becoming obese can be influenced by family history. A child with an obese parent has a three-fold risk of becoming obese as an adult, while a child with both parents obese has a ten-fold risk of future obesity [26].

1.1.3.2 Environmental factors

Environment: It is well known that environmental factors are important precursors of health and disease [19], which play a role in the development of obesity [32]. This refers to the built environment (fast food restaurants, parks, transport or the healthiness of the neighbourhood) and to the environmental pathogens such as viruses, microbiomes and social networks [2]. The presence of neighbourhood recreational spaces for physical activity has been associated with increased levels of physical activity [2].

Over the last 20 years, environmental changes have increased obesity rates [26]. With the rise in the obesity pandemic and the increase in the overall temperature of the Earth's atmosphere, there is a growing trend that environmental temperatures may be influencing the obesity pandemic [33].

Gut microbiota: The body's microbiome has the potential to influence our physiology in several ways and contribute to metabolic function acting through an integrated host to regulate energy storage [34]. Normally, the gut microbiota plays a beneficial role in the host, but dysbiosis between microbial populations [26] can increase dietary energy harvest, resulting in an obese microbiome [20] and developing some diseases, such as neurological disorders, inflammatory bowel disease, malnutrition, cancer or diabetes [26]. Furthermore, specific bacterial profiles have been identified in obese individuals that promote the storage of dietary energy [35].

Endocrine-disrupting chemicals: Endocrine-disrupting chemicals are exogenous chemicals that can mimic or block the action of hormones by binding to or interfering with their receptors. This interference disrupts signalling processes throughout the body, leading to diseases of the endocrine system, or indirectly by disrupting hormone levels of altering hormone transport. In particular, obesogens, a subclass of endocrine-disrupting chemicals, can disrupt sensitive metabolic processes if exposure occurs during early development, predisposing individuals to weight gain, increasing the number and size of adipocytes. Endocrine-

disrupting chemicals can cause changes in hypothalamus, which have a role in eating behaviour [6,36].

Chronodisruption: It is defined as a disruption of the internal temporal ordering of biochemical, physiological and behavioural circadian rhythms that results in an alteration of the normal pattern. It can be caused by various environmental factors or external common situations such as jet lag, shift work, night light pollution or night-time leisure activities. Other factors are internal, caused by changes in the core machinery of the molecular circadian clock. Mutations in clock genes are associated with obesity and may interact with obesogenic behaviours for obesity or weight-control parameters [37].

1.1.3.3 Behavioural factors

It has been suggested that behavioural and lifestyle changes in wide sectors of the population are responsible for the persistent imbalance between the total energy intake and the energy expenditure [38].

Dietary patterns: The shift away from low-calorie, high-fibre diets towards energy-dense, palatable diets is thought to be contributing to the increased prevalence of obesity. In addition, many of the low-cost foods available are salty, fatty and/or sweet, relatively palatable, with large amounts of sweetened beverages. Exposure to these food cues constitutes a challenge to homeostasis [25,26].

Sedentary lifestyle / Physical exercise: Sedentary lifestyle has been positively associated with obesity [38]. Physical activity, sedentary time and screen time were associated with weight change and maintenance in adulthood [2].

Stress: The modern environment and the hectic lifestyles have increased psychological stress [25]. Stress is known to induce overeating and, per se, obesity [39].

Sleep: The link between short sleep duration and obesity is well established [40].

Several disorders and medication: There are some syndromes, disorders and/or drugs that can increase the risk of obesity [20] (**Table 3**).

Table 3 | Syndromes, disorders and drugs that can promote obesity. *Table taken and adapted from Apovian C. M (2014)* [20]

Syndromes, disorders and drugs that can promote obesity	
Syndromes	Prader-Willi Bardet-Biedl Cohen Alstrom Frohlich
Neurologic disorders	Brain injury Brain tumour Consequences of cranial irradiation Hypothalamic obesity
Endocrine disorders	Hypothyroidism Cushing Growth hormone deficiency Pseudohypoparathyroidism
Psychological disorders	Depression Eating disorders
Drug-induced	Tricyclic antidepressants Oral contraceptives Antipsychotics Antiepileptic Corticosteroids Sulfonylureas Thiazolidinediones Insulin Beta-blockers

1.1.3.4   *Social and economic factors*

Socio-economic factors play a significant role in food choices, leading to unhealthy weight gain and increased risk of obesity. Increasing age, low income and low education are associated with high BMI [26]. Gender differences may be due to lower paid jobs, which tend to be more physically demanding for men [2].

1.1.4 Related disorders associated to obesity

Obesity comprises a significant public health threat and have negative effects of the quality of life [11] declining life expectancy [23,41]. Obesity predisposes patients to a large number of comorbidities and increased mortality rates. Overall, health risks and mortality increase as the degree of overweight increases [41]. For every increase in 5 units of BMI higher than 25 kg/m^2, the total mortality increases 30% [42].

1.1.4.1 Metabolic syndrome

Metabolic syndrome is a condition defined by a cluster of risk factors that directly promote the development of cardiovascular diseases and type 2 diabetes (T2D) [43]. Increased abdominal obesity, or waist circumference, has been recognised as an independent component of the metabolic syndrome. Elevated TG concentrations, low high-density lipoprotein (HDL) cholesterol levels, elevated blood pressure, and high fasting glucose concentrations are also recognised as components of metabolic syndrome. Subjects with three or more factors are classified as having metabolic syndrome [41] (**Table 4**).

Table 4 | Factors that defines the metabolic syndrome. *N Oliveras-Cañellas (2024)*

Risk factor	Defining level
Waist circumference	
Men	> 102 cm
Women	> 88 cm
TG	≥ 150 mg/dL
HDL – Cholesterol	
Men	< 40 mg/dL
Women	< 50 mg/dL
Blood pressure	≥ 130 / ≥ 85 mmHg
Fasting glucose	≥ 100 mg/dL

Specifically, hypertriglyceridemia and low HDL-cholesterol, together with an increase in the total cholesterol and/or low-density lipoprotein (LDL) cholesterol, is known as dyslipidaemia [44].

1.1.4.2   Type 2 Diabetes

T2D is strongly associated with obesity and with the central distribution of body fat [41]. Overweight raises risk of developing T2D by a factor of 3, and obesity by a factor of 7 [2]. The risk of having T2D is 40 times higher in people with BMI higher than 35 kg/m^2 than BMI lower than 23 kg/m^2 [43].

T2D is characterised by an alteration on the metabolism of carbohydrates, fatties and proteins, which depends on changes in insulin secretion and/or insulin sensitivity producing a continuous hyperglycaemic status [45]. Obesity can modify these factors. T2D is diagnosed when fasting glucose is higher than 126 mg/dL and/or glycosylated haemoglobin (HbA1c) higher than 6.5%.

Insulin is the responsible of reducing blood glucose levels through the induction of glucose uptake for insulin-sensible tissues like muscle, heart or AT; and inhibited the glucose production in liver, kidney and small intestine. IR is a dysregulation of blood glucose uptake due to a loss of tissue insulin sensitivity as a result of inhibition of the insulin signalling pathway [46].

1.1.4.3   Cardiovascular disease

Hypertension, dyslipidaemia and hyperglycaemia, components of metabolic syndrome, are obesity-related risk factors for the developing of cardiovascular diseases. In addition, overweight and obesity, with and without metabolic syndrome, are a risk factor for heart disease, such as myocardial infarction, ischemic heart disease [47], and ischemic stroke [2,48]. Cardiovascular diseases, specifically ischemic heart disease and stroke, are the leading cause of BMI-related deaths globally [2].

The dysfunctional AT, present in an obese subject, produces pro-inflammatory factors that induce a chronic stress and release lipids into bloodstream. As a consequence, increase blood

pressure, which is proportional to the percentage of fat body. This increase led to also increase fat ectopic deposition and coagulation factors, which increase the formation and breaking of atherosclerotic plates, characteristic from cardiovascular disease [49].

1.1.4.4 *Gastrointestinal and hepatic diseases*

There are many gastrointestinal and hepatic diseases for which obesity is the direct cause or a significant risk factor. When obesity is a risk factor, it may interact with other pathogenic mechanisms and result in earlier presentation of disease or complications [50].

Gastrointestinal tract plays a role in obesity through contributions to satiation, production of gut hormones that influence appetite and the absorption of nutrients that determine the positive energy balance that results in obesity [50]. It is well known that obese subjects had micronutrient deficiencies of vitamins D [51], A, C and E, as well as, iron, copper, calcium and magnesium [52]. Increase body fat increases the turnover of cholesterol, this extra load of cholesterol may be the tipping point for the development of stone formation and gall bladder disease [50] being a strong association with gallstone diseases [50].

Obesity is the main factor associated to fatty depot at hepatic level. Around 75% of obese patients have some fatty depots in hepatic tissue [53]. Exist a positive correlation between BMI and non-alcoholic fatty liver disease (NAFLD), which shared pathogenic mechanisms [50]. NAFLD is the more prevalent abnormality in patients with obesity, which progress to steatohepatitis and cirrhosis [54].

1.1.4.5 *Neurological manifestations and psychiatric conditions*

Obesity is associated with anatomic and functional changes in human brain [2], but the link that led to neurological disorders is complex and multifactorial, from both CNS and peripheral (PNS) nervous system impairments. CNS and PNS are quite distinct in form and function, but both are susceptible to obesity-driven dysfunction, suggesting that common mechanisms contributing to disease progression may be perpetuated by visceral adiposity [55].

In older population, BMI is inversely correlated with brain volume, and obese older adults show atrophy in the frontal lobe, anterior cingulate gyrus, hippocampus and thalamus. In

addition, overweight in midlife increases risk of Alzheimer's disease (AD) or degenerative disorders such as dementia, and higher risk is observed for obesity [2]. Some studies show a relation between T2D and dementia [56], in which T2D acts as an accelerated of cognitive dysfunction [57]. Subjects with obesity and metabolic syndrome, but without hyperglycaemia, are more properly to have a global cognitive dysfunction [58].

Related to psychosocial disorders, obesity is associated with increased risk of them, which include major depression, anxiety, manic episode, alcohol abuse [59,60] and eating disorders [61]. Persons with higher BMI showed a slightly increased risk of developing depression [20].

1.1.4.6   *Other disorders developed as a consequence of obesity*

Other important disorders developed as a consequence of obesity are found in **Table 5**:

Table 5 |Disorders developed as a consequence of obesity. *N Oliveras-Cañellas (2024)*

Other disorders developed as a consequence of obesity	
Obstructive sleep apnoea	Obese individuals, like a consequence of anatomic characteristics collapse the superior airway and have an elevated risk of obstructive sleep apnoea [62,63]. Around 60% of the people who are obese have obstructive sleep apnoea.
Cancer	Obesity contributes to around 6% of cancers diagnosed in 2007 [2] and up to 14% of all deaths from cancer [64–66]. The most common cancers developed by the contribution of obesity are breast, endometrial, ovarian, colorectal, oesophageal, kidney, pancreatic and prostate cancer [67].
Hypothyroidism	Undiagnosed hypothyroidism may go to weight gain, but obesity also affect thyroid function [68]. Thyroid hormones are linked to body composition because they are integral in basal metabolism and thermogenesis, and also affect in the metabolism of glucose and lipid, fat oxidation and food intake. In obesity, an increase in the thyroid-stimulating hormone levels has seen, suggesting that obesity has an impact on the hypothalamic-pituitary-thyroid axis, leading to changes in thyroid function [20].

Polycystic ovary syndrome and infertility	Obesity exacerbates the incidence, prevalence and severity of polycystic ovary syndrome [69,70]. Around 80% of women with polycystic ovary syndrome are obese [20]. Women with polycystic ovary syndrome have greater metabolic pregnancy complications and the offspring have increased risk of congenital abnormalities [70]. Weigh loss improve reproductive, metabolic and psychological features in polycystic ovary syndrome [69].
Osteoarthritis	The global prevalence of osteoarthritis continues to escalate, as a result of an ageing population and as a result of the current obesity epidemic [45]. Body weight influences the severity of osteoarthritis, every 5kg of weight gain conferring a 36% increase in the risk of knee osteoarthritis. Obesity and osteoarthritis reduce mobility and activity, further weight gain and decreased muscle strength [71]. Weight loss coupled with exercise, is recognised as an important approach in the management of obese patients with osteoarthritis [71].
Dermatological entities	Obesity causes alteration in skin physiology that predisposes obese individuals to the development of various skin manifestations and diseases, such as psoriasis [72] .
Trauma and infection	Hospital mortality increased in 30% and the risk of major complications after a surgery double in obese patients [2].

1.1.5   Diagnosis and treatment of obesity

The most commonly used method for estimating body fat is based on BMI. It is a very simple, easy and inexpensive way to identify obesity [73]. BMI can be used as a screening tool to estimate adiposity, but it is an anthropometric measure that clearly underperforms as a predictor of health and as a sole guide for clinical decision-making [74]. It has been recognised that is an imperfect index, unable to correctly quantify adiposity [9].

The diagnostic accuracy of BMI for obesity is not optimal, especially in individuals with higher body fat percentage but normal and intermediate BMI values [75]. Another limitation is that BMI does not take into account important variables such as gender, age [3] or ethnicity [76].

Loss of muscle mass makes BMI a less accurate predictor [77]. Although, BMI correlates with fat accumulation and metabolic health in large populations, it is insensitive to body fat distribution [73]. BMI is not used as the sole measure of obesity, but as a complement to others measures.

Waist circumference or waist-to-hip Ratio (WHR) can predict obesity-related diseases [78]. Both are anthropometric markers used in clinical practice to measure abdominal or central obesity, which is a better indicator of the risk of developing obesity-related diseases [2,76]. Abdominal adiposity is thought to be primarily visceral, metabolically active fat surrounding organs, and is associated with metabolic dysregulation that predisposes individuals to cardiovascular disease and related conditions [2]. In Caucasians, central obesity is diagnosed when the waist circumference is at least 88 cm for women and 102 cm for men [79], and when the WHR is >0.5 and abdominal adiposity is high [76]. In conjunction with BMI, which indicates general adiposity, waist circumference and WHR are used as proxies for central adiposity and intra-abdominal visceral fat [3].

A better way to define obesity is by percentage of total body fat, although this is rarely used in clinical practice because of inconvenience and cost. Obesity can be defined as 25% or more in men and 35% or more in women [79]. Fat mass can be measured directly using imaging techniques that can provide accurate and repeatable body composition [9]. These include Dual-Energy X-ray Absorptiometry, Computed Tomography and magnetic resonance imaging (MRI). In addition, fat mass can be measured indirectly using Hydrostatic Weighing (densitometry), Air Displacement or Bioelectrical Impedance Analysis [1].

In obese people it is recommended that lose at least 10% of their body weight [80]. Treatment of obesity has goals beyond weight loss, such as reducing obesity-related risks and improving overall patient health. Early intervention and effective treatment of obesity are needed to manage obesity-related co-morbidities and improve the quality of life and well-being of obese patients. Weight management goals should emphasise realistic weight loss to reduce health risks and include promotion of weight loss, maintenance of weight loss and prevention of weight regain [81]. The best recommended treatments are lifestyle changes, pharmacotherapy and bariatric surgery.

Weight loss interventions may be recommended for people with a BMI ≥ 30 or BMI ≥ 25 and weight-related complications. A multifactorial lifestyle program, including dietary modifications with reduced calorie intake, increased physical activity and behavioural

changes, is recommended as basic therapy [80,82–84]. Loss of 5 – 10% of initial weight to reduce the impact of obesity-related complications. Weight loss is greater when diet is combined with physical activity.

Pharmacological weight loss with medications is used in combination with lifestyle interventions [84] in adult obese individuals with a BMI $\geq$ 30 kg/m^2 or with a BMI $\geq$ 27 kg/m^2 and obesity-related comorbidities [80,82,83] or in those patients who have not lost >5% of their baseline weight after 3 – 6 months of participation in a lifestyle program [32].

Bariatric surgery is recommended for adult obese individuals with a BMI $\geq$ 40 kg/m^2 or a BMI $\geq$ 35 kg/m^2 with obesity-related comorbidities such as diabetes, dyslipidaemia or hypertension, or when all non-surgical weight loss interventions have failed [32,83,84].

Weight loss is associated with improvements in intermediate risk factors for disease and could reduce mortality [85]. In addition, bariatric surgery reduces chronic inflammation associated with obesity and alters biomarkers, gut microbiota, and long-term remission of diabetes [80]. After weight loss, long-term measures are needed to maintain the lost weight. This should include a low-calorie and balanced diet, increased physical activity and behavioural support [83].

1.1.6   Epidemiology of obesity

The prevalence of overweight and obesity has increased worldwide in recent decades, reaching epidemic proportions [2,86]. Currently, obesity and related disorders constitute a serious threat to the future health of all the world's population [87].

According to the WHO, the global prevalence of obesity has tripled since 1975 and continues to grow exponentially, making it one of the most prevalent diseases in the world (**Figure 2**). In 2016, approximately 1.9 billion of the world's adult population were overweight (38.9%) of which 650 million were obese (13.1%) [4]. The distribution of obesity prevalence is heterogeneous around the world, with obesity tending to be higher in the richer countries of Europe, North America and Oceania, and very low in the Southern Asia and Africa (**Figure 2B)**.
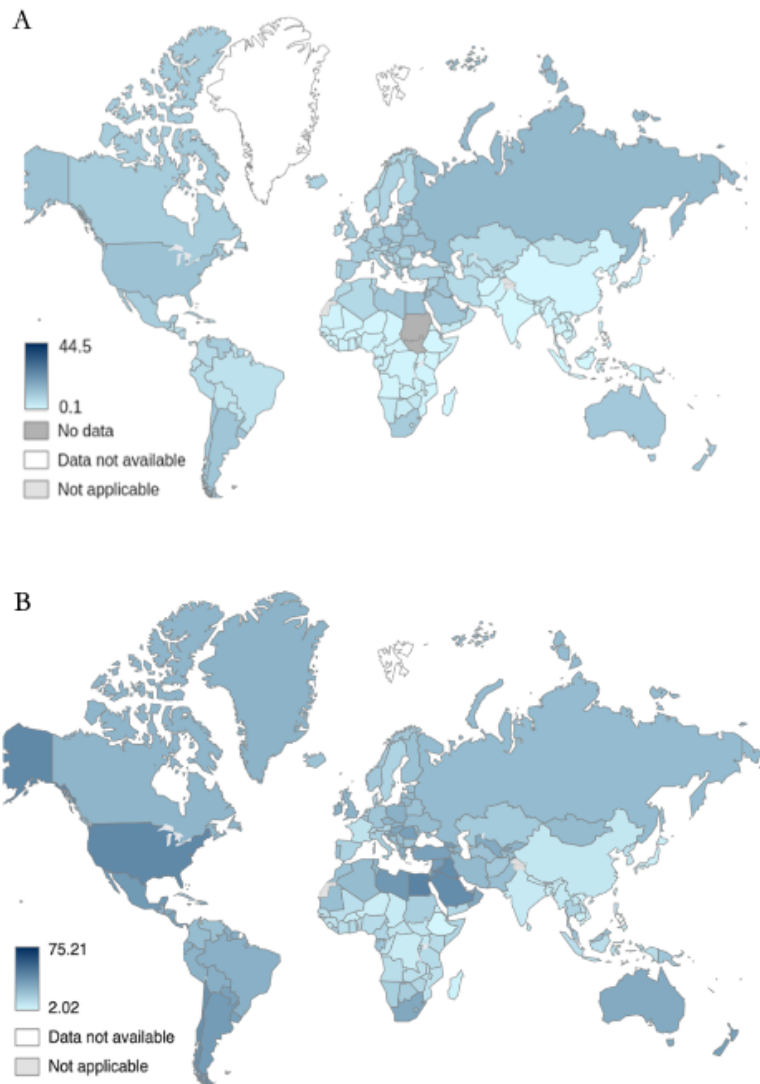
Figure 2 | Epidemiology data from obesity prevalence worldwide. *A.* Percentage of BMI ≥ 30 kg/m2 in 1976. **B.** Percentage of BMI ≥ 30 kg/m2 in 2022. *Figure taken and adapted from WHO* [4]

Overweight and obesity affect adults of all ages, ethnicities and socioeconomic levels. However, it is generally more prevalent among older people and women (15.1%, compared to 11.1% among men) [11].

Focusing on Europe, the incidence of obesity was 23.3%, specifically 23.3% for men and 24.5% for women. A similar trend was observed in Spain, where the prevalence of obesity was 23.8%, 24.6% for men and 22.8% for women [4].

Changes in the food environment and food systems are likely to be important drivers. Increased availability and accessibility of energy-dense foods may explain weight gain in different populations. In addition, more time spent in sedentary work and less time spent in leisure activities have also contributed to the increasing prevalence of obesity [86].

Global mortality related to high BMI increased by 28.3% in 2015. Excess body weight is a major risk factor for mortality and morbidity, contributing to 4 million deaths and 120 million disability-adjusted life years (DALYs) among adults worldwide [86]. Most of the health consequences of obesity are due to non-communicable diseases, cardiovascular disease, diabetes and some cancers [23]. For every 5 units increase in BMI above 25 kg/m^2, all-cause mortality increases by 29%, vascular mortality by 41% and diabetes-related mortality by 210% [20].

In addition to excess mortality, obesity is also associated with poorer quality of life for patients, leading to many social and work limitations and, as a consequence, high healthcare costs [88]. Obesity also contributes to a reduction in life expectancy of up to 4.2 years for men and 3.5 years for women. In the case of morbid obesity, the reduction increases to 7.7 and 9.1 years, respectively [89].

Obesity is associated with a 36% increase in annual healthcare costs in developed countries, mainly due to associated comorbidities, and a 77% increase in medication costs compared to average weight [20]. Obesity patients incur 46% more hospital costs, 27% more outpatient visits and 80% more of medication costs. These costs focus on healthcare and ignore the economic impact of lost productivity due to disability and obesity-related diseases [90].

1.2   ADIPOSE TISSUE

1.2.1   Description of the adipose tissue

The AT is a complex endocrine organ that contributes to the systemic [91]. In addition, AT provides a physical barrier for thermal insulation and acts as a mechanical cushion to protect internal organs from mechanical stress. Fat mass can range from 5 to 60% of total body weight [92] and its distribution is influenced by sex [93], race [94] and age [92].

The AT is made up of connective tissue, specifically mesenchymal tissue, composed mainly of fat cells called adipocytes, surrounded by the stromal vascular fraction (SVF). Adipocytes are the predominant cell type in the AT and are considered the functional unit of the tissue.

The SVF is a mixture of a variety of other cell types such as preadipocytes, human adipose stromal cells, vascular endothelial cells, fibroblasts and several immunological cells (macrophages, lymphocytes, eosinophils, T and B cells, mast cells and neutrophils) [95]. The proportions of the cellular populations of the SVF vary according to the type, localisation and metabolic state of the AT to which they belong and can be influenced by local and systemic factors related to inflammation, IR or obesity [96]. These support cells represent approximately 60% of the cells in AT, although 90% of the tissue volume is occupied by fat [97].

The AT is categorised on the basis of its anatomical location and the main cell type it contains. Traditionally, adipocytes have been classified into two types that differ in function, morphology and location. White unilocular adipocytes, which make up the WAT, are a tissue mainly specialised in fat storage. However, brown multilocular adipocytes have many mitochondria that are used to consume the stored energy through heat dissipation in a process called non-shivering thermogenesis, these adipocytes make up brown adipose tissue (BAT). WAT accounts for more than 95% of AT mass; whereas BAT accounts for only 1 – 2% [98]. More recently, a third type of AT, known as beige or *brite*, has been identified [99]. Beige adipocytes, which have morphological and biochemical characteristics of classical brown fat, have a flexible phenotype depending on the physiological circumstances, they can store or release energy [100].

Although they all belong to AT, their developmental origin is different [101]. It was once thought that brown and white adipocytes shared a common precursor, but it is now known that brown fat develops differently from white fat. WAT formation begins in utero from a

mesenchymal origin and its development is stimulated after birth when adipocytes are needed for energy storage. Most white adipocytes are thought to originate from mesenchymal progenitor cells of the mesoderm, but white adipocytes from different depots seem to have different origins [102].

Brown adipocytes express some myogenic genes not seen in white adipocytes. Skeletal muscle and brown fat are derived from the same or very similar precursors that share a common developmental origin [14,103]. Myocytes and brown adipocytes are derived from mesenchymal stem cells (MSCs) that express the myogenic factor 5 (Myf5) [101,102,104]. Myf5 is a myogenic determinant with metabolic similarities between brown fat and skeletal muscle in terms of high oxygen consumption and fuel use, and the metabolic difference between BAT and the less metabolically active and energy storing WAT depots [14].

Although beige adipocytes share characteristics with brown fat, they do not originate from the Myf5 lineage [99]. Beige adipocytes share the white adipocytes program [103].

1.2.2 Types of adipose tissue

1.2.2.1 White Adipose Tissue

WAT is the predominant tissue type in mammals and represent around 95% of AT mass [98,105]. The distribution of AT depends on sex. Normal weight women have a higher proportion of fat mass, around 25 – 30%, compared to men with 10 – 20% [106,107].

White adipocytes appear as polyhedral and round cells with a large diameter, characterised by a single large lipid droplet (LD) occupying most of their cytoplasm (95% of cell volume), forcing the nucleus and all other organelles to the periphery of the cell, with a low content of mitochondria and other organelles in their lateralised cytoplasm [66,92,107–109]. During development, young adipocytes contain multiple small LD that coalesce into a single lipid inclusion as the cell matures and becomes unilocular [105].

WAT accumulates in discrete sites, which are recognised as specific depots [97] and are classified according to their localisation. The different depots are distinguished by their distinct anatomical locations [98,110] and endocrine and metabolic characteristics [111]. The largest WAT depots are found in the subcutaneous region and around the viscera [105]. Subcutaneous adipose tissue (SAT) and visceral adipose tissue (VAT) not only differ in localisation, also in

the progenitor cells that give rise to each tissue, giving them a different functions and characteristics [112].

SAT is located under the skin and outside the peritoneal cavity in several body regions [97], mainly around the abdomen, hips and thighs, and accounts for approximately 80% of total body fat [14,66,111]. VAT represents 5 – 20% of total body fat mass [14,97] and it surrounds many organs intra-abdominally and provides a protective cushion [66]. VAT is found in the mesenteric region connected to the intestine, within the abdominal musculature and in the thoracic region [97], in the omental region around the stomach and spleen, in the perirenal region covering the kidneys [66] and in the epicardial region around the heart [113].

The adipocytes of SAT started to differentiate in the prenatal stages, whereas VAT is made after birth [114]. The SAT depot is heterogeneous and contains mature unilocular adipocytes interspersed with small multilocular adipocytes, whereas the VAT depot is more uniform and appears to consist mainly of large unilocular adipocytes [102].

SAT and VAT depots are likely to make different contributions to metabolism. SAT is considered a healthy metabolic tissue, especially when localised in the femoral and gluteal areas, where it protects against metabolic changes, improves glucose tolerance and negatively correlates with IR [115]. SAT secretes circulating adiponectin, an anti-inflammatory adipokine with beneficial metabolic effects [107,112], an essential hormone in the regulation of glucose levels and fatty acid catabolism during caloric restriction [116]. However, VAT depots are associated with metabolic complications and appear to increase the risk of diabetes, hyperlipidaemia and cardiovascular disease [102]. The size of VAT adipocytes is higher than SAT because when they become hypertrophic, they have more IR and lipolytic capacity, being one of the factors linking abdominal adiposity and cardiovascular risk [112].

Studies in the last decades have shown that AT play a key role in metabolic systemic health, because besides being the main energy stores, they can also secrete cytokines and hormones that act as paracrine or endocrine in other tissues and organs, regulating or modulating their function (lipid and glucose homeostasis, energy balance, inflammation and tissue repair) [109,117].

The main function of WAT is to store energy into LD in the form of TG, according to energy needs [99,102,118]. TG accumulation is achieved by *de novo* fatty acid synthesis, also known as lipogenesis, as well as fatty acid uptake, whereas TG mobilisation is achieved by lipolysis

(**Figure 3**). AT adapt rapidly to different nutritional conditions, remodelling fast and dynamic, producing high number of molecules that cause high metabolic changes at systemic level [117] and promote changes in the number and /or in size of adipocytes [119].
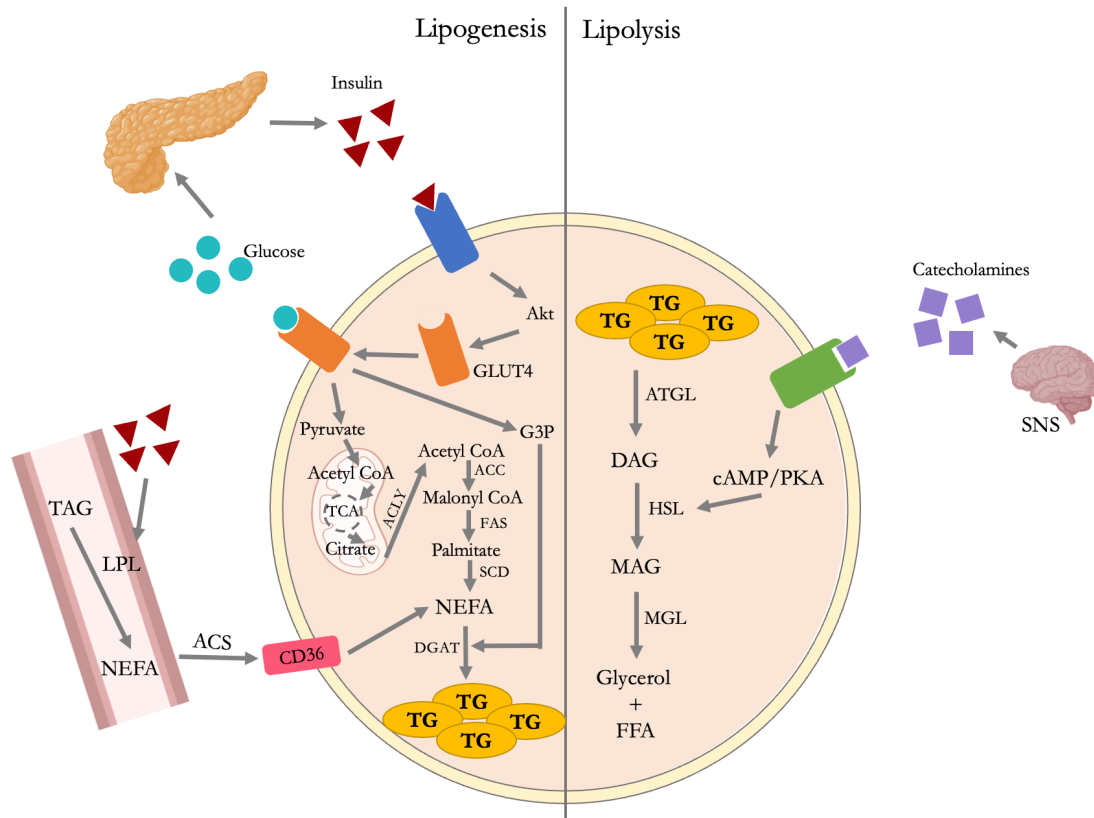
Figure 3 | Lipogenesis and lipolysis in AT. The figure shows the two main metabolic processes of the white adipocyte, separated by a grey line. Lipogenesis is represented in the left side of the image and lipolysis in the right side. Stimulated by energy excess, lipogenesis leads to the formation of TG-containing LD in adipocytes. Lipolysis is induced by energy demand and causes the release of glycerol and FFA from adipocytes. *Figure taken and adapted from Richard A. J. (2000)* [120]

When there is an energy surplus, adipocytes store the excess of energy as TGs in the process of lipogenesis. Glucose, which is the first stimulator of the lipogenic pathway, triggers the synthesis and secretion of insulin from the pancreas. The action of insulin induces two major aspects of this pathway, *de novo* lipogenesis and circulating TG pathway.

Firstly, insulin binds to its receptors on the surface of adipocytes and activates the protein kinase B (Akt) pathway, which leads to the mobilisation of the glucose transporter 4 (GLUT4), allowing glucose to be taken up by the cell. Glucose enters adipocytes via GLUT4 and is metabolised by glycolysis to pyruvate. Under aerobic conditions, pyruvate is converted

by pyruvate dehydrogenase to acetyl coenzyme A (acetyl-CoA), which enters the tricarboxylic acid cycle (TCA) to produce citrate, which is transported to the cytosol and converted by adenosine triphosphate (ATP)-citrate lyase (ACLY) to acetyl-CoA. This acetyl-CoA is converted to malonyl coenzyme A (malonyl-CoA) by the enzyme acetyl-CoA carboxylase (ACC) and, finally, fatty acid synthetase (FAS) converts this malonyl-CoA to palmitate (PA) [121]. Glyceraldehyde 3-phosphate (G3P) is a limiting substrate for lipogenesis, more than that provided by glucose via glycolysis, gluconeogenesis is another source of non-carbohydrate substrates such as pyruvate, amino acids or lactate.

On the other hand, adipocytes take up dietary lipids from the bloodstream as non-esterified fatty acids (NEFA) released from circulating TGs. Circulating TGs are bound to chylomicrons (formed in the small intestine) and very-low density lipoprotein (VLDL) (formed in the liver) [122]. Insulin induces the activity of lipoprotein lipase (LPL), which is secreted by adipocytes and released into blood vessels where it interacts with VLDL and chylomicrons to hydrolysed them. After hydrolysis, the entry of NEFA into cells requires the facilitation of the cluster of differentiation 36 (CD36). Insulin also stimulates the translocation of these fatty acid transporters to cell membranes, making insulin the predominant stimulus on the lipogenesis process. Once free fatty acids (FFA) are inside the adipocyte, NEFA is converted to acetyl-CoA by Acetyl-CoA synthetase (ACS).

At this step, the two pathways converge, the circulating TGs pathway and the *de novo* lipogenesis pathway, which starts with glycolysis and continues with a series of reactions leading to the synthesis of TGs. Next, G3P is acylated by glycerol 3-phosphate acyltransferase (GPAT) to form lysophosphatidic acid (LPA), which is converted to PA and dephosphorylated to form diacylglycerols (DAG). The final step in TGs synthesis depends on the conversion of DAG to TGs by the enzyme diacylglycerol acyltransferase [121,123–126].

Conversely, during periods of energy demand such as fasting, exercise or cold exposure, lipolysis is stimulated. Lipolysis is the catabolic process that leads to the release of FFA and glycerol from TGs stored in the LD of adipocytes [127]. In a state of high energy demand, decreased levels of circulating insulin with increased levels of glucagon suppress lipogenesis and induce the lipolytic pathway. Glucagon and other factors such as catecholamines, natriuretic peptides, growth hormone and thyroid-stimulating hormone are stimulators of lipolysis. Glucagon and catecholamines induce cyclic adenosine 3'-5'-monophosphate (cAMP) -dependent protein kinase A (PKA) activity by increasing cAMP production and

activating PKA. Catecholamines, which include epinephrine and norepinephrine, are released by the sympathetic nervous system (SNS). This action is exerted by binding to membrane-bound β-adrenergic receptors found on adipocytes [127,128].

TGs are broken down into DAGs by the action of the adipocyte triglyceride lipase (ATGL). Activated PKA phosphorylates hormone sensitive lipase (HSL), which hydrolyses DAG to monoacylglycerols (MAG) and allows their translocation to the LD through the phosphorylation of LD-associated proteins such as Perilipin 1 (PLIN1). The final step is the hydrolyses of MAG into fully liberated glycerol and FFA by the enzyme monoacylglycerol lipase (MGL) [124–126,129,130]. The hydrolysis of TGs results in the release of NEFA and glycerol into the bloodstream, which can then be used as a substrate by other tissues [120]. These by-products can be re-esterified within the adipocyte to form TGs, or released into the circulation to be used as fuel by other tissues. In the latter case, released NEFAs could be consumed by oxidative tissues such as muscle, and glycerol could be used by the liver in the gluconeogenesis process [127].

Another function of WAT, but no less important, is its endocrine activity. To date, more than one hundred factors are known to be produced and released by WAT, known as adipokines [131]. Adipokines play an important role in the regulation of many processes in the organism, such as glucose and lipid metabolism (resistin and adiponectin), inflammation (Tumour Necrosis Factor α (TNFα) and interleukin (IL) -1β), coagulation (Plasminogen Activator Inhibitor-1 (PAI-1)), blood pressure (angiotensinogen and angiotensin II) and food intake (leptin). Many of these factors act locally within the WAT through autocrine/paracrine mechanisms, but others act systemically to influence the function of distant tissues, such as the brain, skeletal muscle, liver, pancreas, blood vessels and heart [132–135]. Together, these hormones function to regulate food intake, the reproductive axis, insulin sensitivity and immune responses [109,110,135–137].

Leptin, is one of the best characterised adipokines. Leptin is secreted almost exclusively by adipocytes and plays a major role in suppressing appetite and promoting energy expenditure. Leptin exerts its effects via the leptin receptor. Activation of leptin receptors in the hypothalamus leads to supress appetite by inducing the synthesis of anorexigenic peptides and blocking that of orexigenic peptides [18,98,110,138].

Obesity is associated with increased leptin levels, which contributes to the development of IR and metabolic syndrome. Leptin also increases fatty acid oxidation and decreases TG

storage in muscle [139]. Low circulating leptin levels may reflect depleted lipid stores in the AT and increased energy requirements [109].

Leptin also mediates responses in peripheral tissues, including WAT, the endocrine pancreas and other insulin-sensitive tissues. Indeed, leptin suppresses insulin signalling in adipocytes and also antagonises hepatic insulin signalling. In the endocrine pancreas, leptin inhibits insulin and glucagon secretion from β-cells, promotes lipid storage and leptin synthesis in adipocytes, creating a bidirectional regulatory loop between β-cells and adipocytes [140].

Another important adipokine that regulates energy balance and insulin sensitivity is adiponectin. It is produced exclusively by adipocytes [141,142]. Adiponectin modulates insulin sensitivity by inhibiting hepatic glucose production, thereby enhancing glucose uptake in muscle and increasing fatty acid oxidation in both liver and muscle [143]. Adiponectin has insulin-sensitising and anti-atherosclerotic properties[132].

Unlike most adipokines, the expression and circulating levels of adiponectin are reduced in obesity and its related comorbidities [141,142]. Abdominal AT can produce large amounts of IL-6, TNFα and IL-1β, which are known for their pro-inflammatory role. A positive correlation between the plasma levels of these cytokines in IR and increased risk of T2D has been observed. Importantly, IL-1β has been suggested to play a role in inflammatory pancreatic β-cell damage and apoptosis [144]. Furthermore, blocking IL-1β may be beneficial in preventing IR and inflammation in obese individuals [145]. Similarly, TNFα has been shown to impair insulin sensitivity both *in vitro* and *in vivo* [146].

1.2.2.2   Brown Adipose Tissue

BAT is mainly formed by brown adipocytes, polygonal cells rather smaller than white, characterised by multiple small LD homogeneously distributed in their cytoplasm. Brown adipocytes are also rich in mitochondria, giving them their reddish colour and a much higher oxidative capacity than WAT [105]. Brown fat is highly innervated by the SNS and densely vascularised to ensure adequate oxygen and nutrient exchange and rapid heat distribution [108].

At molecular level, a unique defining feature of brown adipocytes is that they specifically express Uncoupled Protein 1 (UCP1) [147]. UCP1 is located in the inner mitochondrial

membrane of brown adipocytes and acts as a proton channel [105], allowing proton flux from the intermembrane space into the mitochondrial matrix. This uncouples the oxidation of reducing equivalents from the synthesis of ATP and dissipates the proton gradient generated by the respiratory chain as heat [148,149].

BAT is unique to humans and large mammals. In humans, BAT was initially thought to be present only during fetal and perinatal developmental in large interscapular and peri-renal depots that help maintain core body temperature [66], and that adult humans lack brown fat after neonatal BAT regression. However, recent studies using fluorodeoxyglucose-positron emission tomography in combination with computed tomography have shown that adult humans have identifiable and active BAT. Human BAT depots are mainly located in the cervical, interscapular, axillary, perirenal and periaortic regions [148].

The main function of BAT is to dissipate energy as heat by metabolising fatty acids and glucose in non-shivering thermogenesis through uncoupled mitochondrial respiration and the action of UCP1 [99,105,150] to regulate body temperature and protect mammals from hypothermia [66].

This process is triggered by increased sympathetic tone or by the action of endocrine hormones that stimulate intracellular lipolysis in brown adipocytes. Cold receptors in the skin detect cool ambient temperatures and send a signal to hypothalamic centres that regulate body temperature. The efferent signal to the BAT is carried by the SNS and its transmitter norepinephrine, which activates β3-adrenergic receptors and stimulates intracellular lipolysis [108]. Norepinephrine triggers a signalling cascade that activates UCP1, which uncouples aerobic respiration by dissipating the intermembrane proton motive force, creating an ion cycle that generates heat instead of ATP [147].

BAT protects against obesity by promoting energy expenditure. There is a negative correlation between BAT and BMI. Obese individuals have lower levels of active BAT, suggesting that BAT activation helps to reduce fat mass and improve metabolic health [150]. Furthermore, loss of UCP1 causes both cold intolerance and obesity [151].

1.2.2.3   Beige Adipose Tissue

Beige AT develops within WAT through a preadipocyte subpopulation [99] or through trans-differentiation of existing white adipocytes [152], known as WAT *browning*. These types of adipocytes are able to acquire the brown characteristics according to thermic needs [153,154].

Beige adipocytes have a flexible phenotype with characteristics intermediate between WAT and BAT [100], can have either a large unilocular LD or multiple smaller ones, and their mitochondrial density is intermediate and tends to increase upon stimulation [66,101].

In the basal, unstimulated state, the beige cells express very little of the thermogenic gene programme, such as UCP1, and store energy [99]. When stimulated by exercise, cold exposure or β-adrenergic agonist, beige adipocytes activate the expression of UCP1 and other thermogenic compounds, characteristics of classical brown [100,108,109,155]. This suggests that beige cells are programmed to be bifunctional for energy storage in the absence of thermogenic stimuli, fully capable of switching on heat production when the appropriate signals are received [14].

1.2.3   Adipogenesis

Under certain conditions, when the balance between energy expenditure and caloric intake is leaning towards energy excess, AT is stimulated. AT increases in size by promoting hypertrophy and/or hyperplasia. Hypertrophy is the enlargement of pre-existing adipocytes, whereas hyperplasia is the formation of new adipocytes by differentiation of resident precursors (preadipocytes). Hyperplasia increases the number of adipocytes or the adiposity of the tissue, a process known as adipogenesis.

Adipogenesis is a multi-step process in which MSCs differentiate into mature adipocytes. Adipogenesis can be roughly divided into two steps: the commitment of MSCs to become preadipocytes and the subsequent differentiation of preadipocytes into fully mature adipocytes. The vascular stroma of the AT has a resident population of pluripotent MSCs that have the potential to commit and differentiate into osteocytes (bone), adipocytes (fat), chondrocytes (cartilage) or myocytes (muscle) [156] (**Figure 4A**).
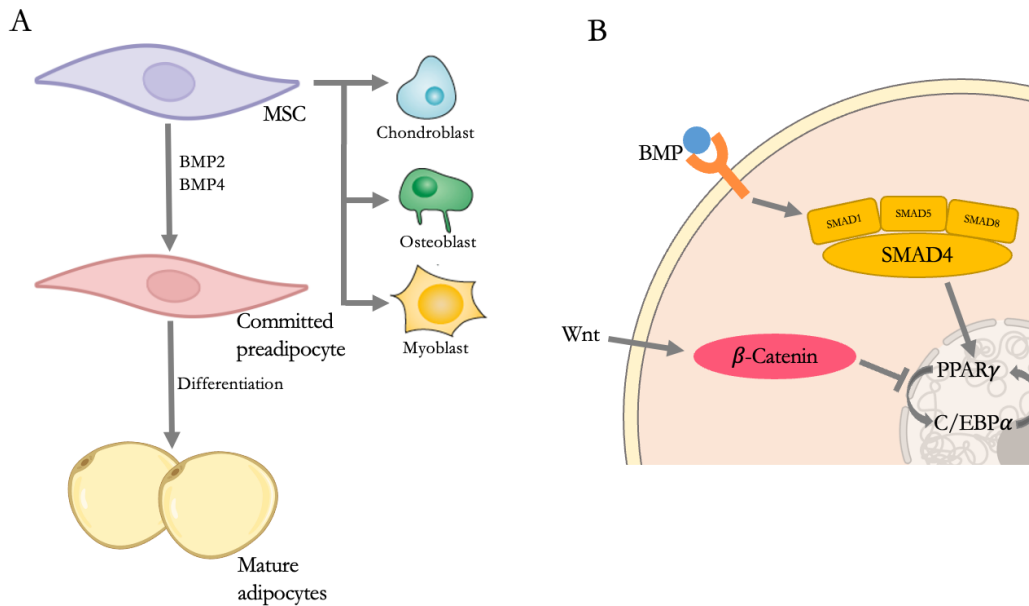
Figure 4 | Adipogenesis. *A.* Multipotent fibroblast-like MSC are adipocytes precursors but also that of chondroblast, osteoblasts and myoblasts. From MSC to mature adipocytes, 2 steps: commitment into preadipocytes and differentiation to adipocytes. **B.** Commitment into preadipocytes, BMP binding to its receptors induce pathway leading to functional synergy between PPARγ and C/EBPα - requirement to achieve fully mature adipocytes. *Figure taken and adapted from Ghaben A. L. (2019)* [18]

The commitment of MSCs to the adipogenic lineage is determined by a network of extracellular signalling factors that often promote one pathway while inhibiting another [18,101,156].

Recruitment to the adipocyte lineage is triggered by excessive energy intake and elevated glucose uptake over a prolonged time period. This metabolic state appears to generate signals that induce MSCs to enter the commitment pathway leading to hyperplasia and the pre-adipocyte phenotype. The main factors that commit or inhibit the conversion of MSCs to the adipocyte lineage are bone morphogenetic protein (BMP), BMP-2 and BMP-4, Wnt and Hedgehog signalling.

BMP-2 and BMP-4 have an activating role, whereas Hedgehog has an inhibitory role. Wnt has an activating role in the commitment step and an inhibitory role in the differentiation step [156]. BMP-2 and BMP-4 bind and signal through their receptors to activate signal molecule of the mother against decapentaplegic (SMAD) -4 by activating its partners SMAD-1, SMAD-5 and SMAD-8. Activated SMAD-4 is translocated to the nucleus where it induces

the transcription of peroxisome proliferator activated receptor gamma (PPARγ). PPARγ is considered to be the master regulator of adipogenesis. Wnt is a family of autocrine and paracrine ligands that leads to the stabilisation of β-catenin, which in pre-adipocytes inhibits the activation of PPARγ and CCAAT / enhancer – binding protein (C/EBP) alfa, another regulator of adipogenic gene transcription. While β-catenin-dependent signalling blocks the adipogenic lineage, it promotes both myogenic and osteogenic lineages. Hedgehog signalling results in the redirection of adipose precursors towards an osteogenic commitment. The Hedgehog family of ligands suppresses adipogenesis by inhibiting BMP signalling pathways [18,156] (**Figure 4B**).

The second step in the formation of new mature adipocytes is the differentiation of committed pre-adipocytes [14,157] and is dependent on the transcription factors PPARγ and C/EBPα. The promoters for the genes of these factors contain C/EBP regulatory elements and require the expression of C/EBPβ and C/EBPδ. Once induced, PPARγ and C/EBPα act synergistically as pleiotropic transcriptional activators to further stimulate adipocyte differentiation. PPARγ and C/EBPα promote and maintain the expression of key adipogenic genes for adipocyte function including insulin receptors, enzymes of fatty acid and TG biosynthesis, GLUT4, and secreted hormones such as leptin and adiponectin [12,18,156,158].

1.2.4   Dysfunction of AT in obesity

AT dysfunction is one of the early abnormalities in the development of obesity. It appears to be an important mechanism in determining an individual's risk of developing obesity-related comorbidities [133,159–162]. AT dysfunction may develop under conditions of continuous positive energy balance in patients with an impaired ability to expand of AT stores [147,163,164]. The inability to store excess calories in healthy fat depots may represent a critical node in ectopic fat accumulation [159,162]. As a result, several mechanisms are activated leading to AT dysfunction, including adipocyte hypertrophy, AT hypoxia, mechanical stress from interactions between enlarged adipocytes and the extracellular matrix, autophagy and inflammation (**Figure 5**).
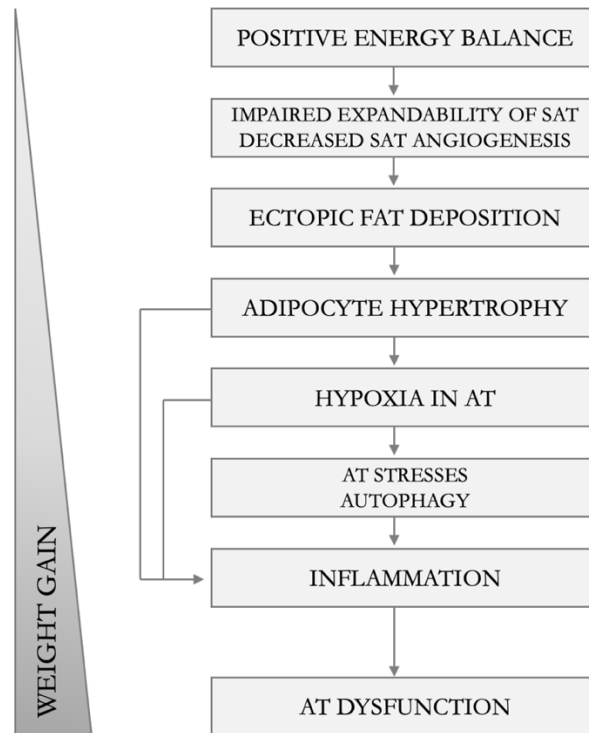
Figure 5 | Adipose tissue dysfunction. A positive energy balance causes expanding fat mass by increasing the average fat cell volume and the number of adipocytes. Potential mechanisms for the development of AT dysfunction include impaired expandability of AT, ectopic fat accumulation, genetic factors, inflammatory processes in AT, hypoxia, and others stresses such as ER, oxidative and metabolic stress. ER: endoplasmic reticulum. *Figure taken and adapted from Bluher M. (2009, 2013)* [137,159]

AT dysfunction is characterised by ectopic fat accumulation, an increased number of AT-infiltrating immune cells, enlarged adipocytes and increased autophagy and apoptosis[137]. Importantly, with the development of AT dysfunction, adipokine secretion is significantly altered and shifts to a pro-inflammatory, atherogenic and diabetogenic pattern [160].

Impaired AT expandability leads to ectopic fat accumulation in liver and muscle, IR, and metabolic disease. AT dysfunction and obesity-related comorbidities may be the consequence of an impaired ability to store fat in healthy fat depots [163,165]. Excessive energy intake promotes fat accumulation in visceral fat depots and, subsequently, contributes to hepatic and peripheral IR [166,167]. SAT plays a protective role in other organs against ectopic fat deposition [163]. In several obese subjects, SAT expandability has been shown to be impaired and the excess lipids are transported to other tissues [163]. However, unimpaired SAT expandability may underline the insulin sensitivity of the healthy obese phenotype [168]. Fat

expansion is dependent on angiogenesis [169]. Under conditions of impaired vascularisation and angiogenesis, AT accumulation is inhibited [170].

Despite having a positive energy balance, not all obese subjects have the same risk of developing obesity-related comorbidities. Subjects with peripheral obesity (distributed subcutaneously) have little or no risk of developing obesity-related complications, whereas individuals with central obesity (fat accumulation in visceral depots) are much more prone to these complications [171].

There is strong evidence for the adverse metabolic and cardiovascular effects of ectopic fat accumulation [172–174]. As noted in *section 1.2.2.1. White Adipose Tissue*, the biology of visceral fat is different from that of subcutaneous fat. VAT adipocytes have higher rates of fatty acid turnover and lipolysis, and are less responsive to the anti-lipolytic effects of insulin than SAT, resulting in greater release of free fatty acids from VAT into the circulation. VAT also produce more IL-6, an inflammatory cytokine that suppresses insulin responsiveness, but less adiponectin and leptin than SAT. There is an association between increased visceral adiposity and IR and inflammation in obesity [18,104]. VAT is characterised by increased secretion of pro-inflammatory cytokines such as IL-6 and TNFα, and increased macrophage infiltration [107,112].

The correct development of AT depends on the balance between adipocyte hypertrophy and hyperplasia [175]. Adipocyte hypertrophy and hyperplasia are associated with intracellular abnormalities in adipocyte function, particularly endoplasmic reticulum (ER) and mitochondrial stress. These processes lead to increased release of adipokines, free fatty acids and inflammatory mediators that cause adipocyte dysfunction and induce adverse effects in the liver, pancreatic β-cells, skeletal muscle, heart and vasculature [176].

Hypertrophic adipocytes show significant changes in their cellular metabolism, inducing hyperplasia, and adipogenesis is stimulated in AT in an attempt at metabolic repair. Impaired adipogenesis in obesity has focused on adipogenic genes, the commitment of MSCs to the adipogenic pathway and the final differentiation into mature adipocytes [12,109,177].

AT contain large and hypertrophic adipocytes that are IR, lose their ability to store TG and have impaired energy expenditure. Fatty acids are released into the circulation and accumulate in other organs, causing cellular stress and metabolic dysregulation, the hallmark of chronic metabolic diseases (T2D, cardiovascular disease and NAFLD). Altered secretion

of endocrine factors from hypertrophic AT contributes to pathological changes in other organs [109].

Hypoxia in the expanding AT in obesity may be a pathogenic factor that causes stress and an inflammatory response within the AT and subsequently leads to its dysfunction. Hypoxia can induce both oxidative and ER stress [178,179]. Hypoxia in the AT increases the expression of pro-fibrotic genes leading to tissue fibrosis [180]. In the fibrotic state, hypertrophic adipocyte stress is increased, but also necrosis, which causes an increase in the infiltration of macrophages and other immune cells [181].

Impaired subcutaneous expandability, ectopic fat accumulation and adipocyte hypertrophy may induce multiple forms of stress in AT. Obesity induces metabolic, inflammatory, oxidative and ER stress in AT [182]. AT responds to these stresses by activating stress-sensing pathways, which may lead to cellular dysfunction and contribute to obesity-related comorbidities [159,182–184]. Stress has been shown to be associated with increased immune cell infiltration into the AT [185].

Autophagy is a process by which intracellular components are targeted for lysosomal degradation through a highly regulated process of vesicle formation and fusion [186]. It is induced in response to conditions of nutrient starvation to increase the release of amino acids, fatty acids, and monosaccharides for energy. Defects in autophagy result in the inability of the cell to synthesise proteins that are required for survival. This process may be a compensatory mechanism in response to stress. Autophagy is important for cellular housekeeping as it removes unnecessary, damaged and/or harmful cellular products and organelles [186].

Autophagy also contributes to carbohydrate and protein degradation and may be involved in the regulation of lipid metabolism [187]. Autophagy has also been shown to be involved in the physiopathology of obesity and its comorbidities [188]. In humans, autophagy is upregulated in the AT of obese and/or T2D patients, predominantly in the VAT, and correlates with the degree of obesity, visceral fat distribution, and adipocyte hypertrophy [187–189].

Activation of autophagy may be associated with the development of IR and may precede the development of obesity-associated morbidities. Furthermore, autophagy may represent a previously unrecognised protective mechanism against obesity-associated AT dysfunction, or it may be a symptom of impaired AT function.

Mechanisms such as adipocyte hypertrophy, nutrient excess, hypoxia and AT stress that cause pro-inflammatory adipokine secretion may lead to the attraction of pro-inflammatory immune cells to the AT and cause chronic, low-grade inflammation. In the majority of obese patients, AT expansion is associated with the increased infiltration of pro-inflammatory immune cells into the AT causing chronic low-grade inflammation [190]. Macrophage infiltration into AT increases proportionally with increased BMI, body fat mass and adipocyte hypertrophy and is a reversible process in obese patients who lose weight [191,192].

In the initial stages, M2 macrophages promote tissular repair and angiogenesis of the AT, with cytokine secretion, reducing hypoxia and cellular stress. It is the result of a balance between pro- and anti-inflammatory signals, developing a healthy expansion [181]. As AT expansion progresses, the adaptive response is not sufficient, involving persistent hypoxia and fibrosis of the extracellular matrix, and secretion of pro-inflammatory cytokines, such as IL-6 and PAI-1 [193,194]. Necrotic adipocytes appear, and circulating macrophages aggregate and form structures around them, changing their pro-inflammatory polarisation with secretion of TNFα and IL-6 [193–195]. This process changes the phenotype of the immune response to a pro-inflammatory state or type 1, which stimulates the infiltration of other cells of the immune response, such as lymphocytes T natural killer, lymphocytes T regulators and activated macrophages [195,196].

Therefore, macrophage infiltration into the AT may be the link between AT dysfunction and systemic IR. An increased number of macrophages in the AT could also cause an increased systemic concentration of pro-inflammatory cytokines [133], such as IL-6, TNFα, PAI-1; and acute phase proteins, such as C-Reactive Protein (CRP) and fibrinogen.

Chronic inflammation begins with a trigger, usually a stressor, that induces an acute adaptive inflammatory response, which is considered a protective response to restore physiological homeostasis [197]. The initial trigger in obesity is a positive energy balance due to overnutrition, which exerts its stressful effect on adipocytes in particular. Although the trigger for this inflammatory state and the causal relationship between inflammation and obesity complications are not fully understood, the degree of inflammation is directly correlated with the severity of systemic IR [87,198].

1.3 OBESITY AND COGNITION

As life expectancy has been increased [199] and the rates of obesity and metabolic syndrome have risen [200], neurological disorders have emerged as a significant global health concern [55].

1.3.1 Brain Domains

The cluster of neurocognitive disorders is characterised by the presence of cognitive deficits that are the most prominent and defining features of a given condition. The neurocognitive cluster is a heterogeneous group of disorders that occur across the lifespan. The Diagnostic and Statistical Manual of Mental Disorders (DSM-5) provides a framework for the diagnosis of neurocognitive disorders based on three syndromes: delirium, mild neurocognitive disorder and major neurocognitive disorder. Each of these syndromes has a range of possible aetiologies [201].

Typical approaches to characterising and classifying cognitive performance in clinical neuropsychology refer to domains of cognitive function. Within each domain, there are typically subdomains that refer to component ability processes within the larger constructs [202]. The DSM-5 classifies neurocognitive disorders into six key domains of cognitive function, which can help determine the aetiology and severity of the neurocognitive disorder. Neurocognitive disorders can include impairments in one or more cognitive domains. These domains are: i) perceptual-motor function; ii) language; iii) learning and memory; iv) social cognition; v) complex attention; and vi) executive function [201] (**Figure 6**).

The origin of these domains has been linked to the areas of the brain where these processes are thought to occur. Domains and subdomains may be involved in different neurodegenerative diseases.
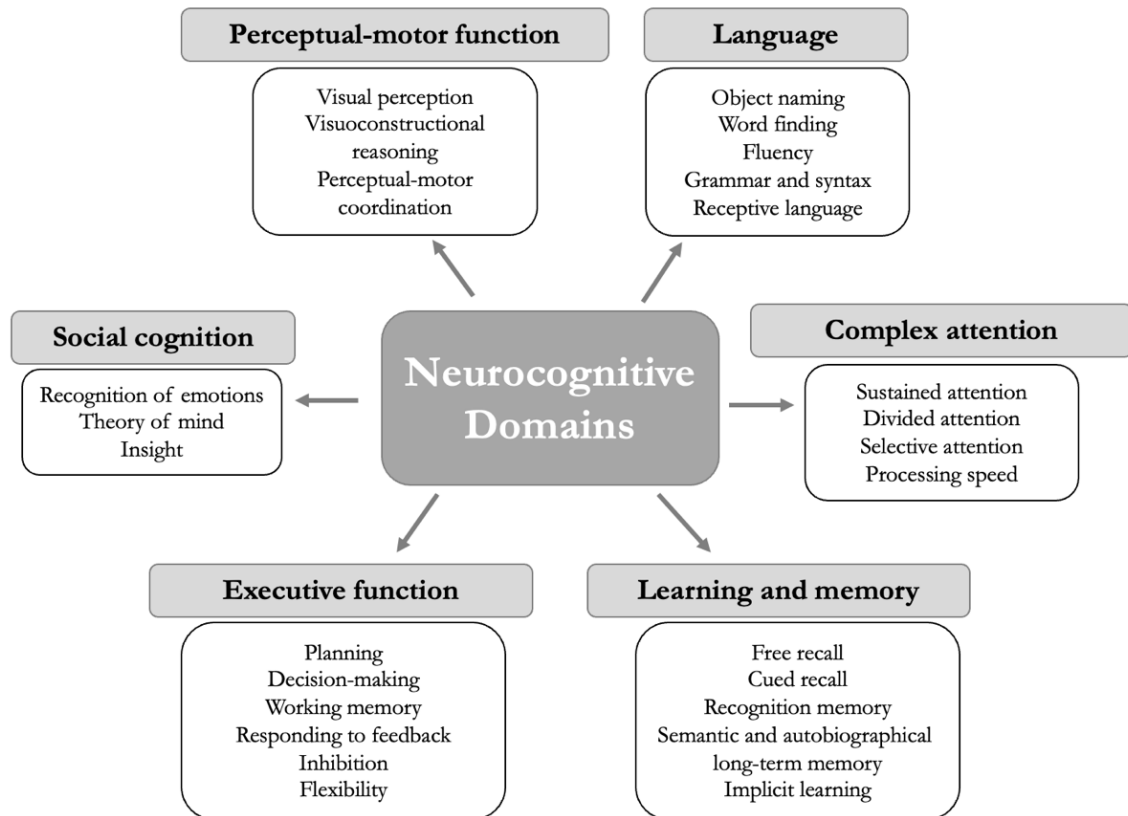
Figure 6 | Neurocognitive domains. The DSM-5 defines six key domains of cognitive function with the respective subdomains. These included, Perceptual-Motor Function, Language, Complex Attention, Learning and Memory, Executive Function, and Social Cognition. *Figure taken and adapted from Sachdev P. S. (2014)* [201]

Delirium is characterised by attentional disturbances that make it difficult for the individual to direct, maintain and shift their focus. In mild and major neurocognitive disorders, there is a decline from a previous level of functioning in one or more of the key cognitive domains. Attention may be impaired in these disorders but, unlike delirium, this is not the central feature and awareness of the environment is generally maintained. Mild neurocognitive disorder is a new framework for the commonly used diagnosis of mild cognitive impairment (MCI), and major neurocognitive disorder is what was previously known as dementia. Both disorders are categorical diagnostic constructs imposed on an underlying continuum of cognitive impairment from normality to severe impairment [201].

MCI is defined as the transitional stage between normal cognition and major cognitive impairment [203,204]. MCI can remain stable or improve if the causes are reversible.

The conversion rate from mild to major neurocognitive impairment has been estimated to be between 3% and 13% per year [205]. Conversion rates can vary depending on the nature of the sample and the standards used for diagnosis, but tend to be higher compared with people of similar age who do not have mild neurocognitive impairment. There are many types of dementia, with AD being the most common, followed by vascular dementia. Frontotemporal degeneration and dementias associated with brain injury, infection and alcohol abuse are less common. There is a strong association between dementia and age [206]. Dementia tends to occur in people over the age of 65 years, when co-morbidity is common [207]. Episodic memory and executive function deficits are strong predictors of conversion to AD [204].

Body fat has been positively associated with cognitive performance [208] and is associated with relative deficits in executive function. Obesity is associated with broad deficits in executive function compared with healthy weight individuals, including poorer cognitive flexibility, inhibition and working memory [209]. Several studies have strengthened the association between midlife obesity and an increased risk of dementia in later life [208,210–213]. Being obese in midlife increased the risk of developing dementia in later life.

Learning and memory, executive function and attention were the neurocognitive domains most vulnerable to impairment in the metabolically dysregulated population. Executive function has also been shown to be the most robust cognitive domain susceptible to impairment specifically in obese populations, while there is also evidence that memory and attention may also be affected [214].

A large battery of neuropsychological tests is now available to characterise cognitive dysfunction across the neurocognitive domains (*see section 3.1.3. Neuropsychological assessment*).

1.3.1.1   *Verbal learning and memory function*

The cognitive domain of learning and memory is a complex structure with different subcomponents that can be structured in different ways. When studying the neurobiological substrates of memory, a distinction has been made between declarative and non-declarative memory function [215].

Declarative memory includes episodic and semantic memory and refers to everyday memory functions that rely on medial temporal lobe structures, including the hippocampus. This type

of memory corresponds to explicit memories that are conscious and verbally communicable [215]. Episodic memory refers to the ability to consciously recall personal episodes or experiences and involves three steps: i) encoding, which describes the direction of cerebral resources to process information via attentional mechanisms; ii) consolidation, which involves the storage of this information in a form that will be mentally accessible in the future; and iii) retrieval, which refers to the act of recalling such information. Semantic memory refers to an individual's acquired knowledge about things in the world, the content of which is abstracted from experience and generalised without reference [216].

Non-declarative memory includes various subcomponents, the most prominent of which is procedural memory or the formation of motor memories, which depend on the striatum, cerebellum and cortical association areas [215]. Procedural memory is an unconscious type of memory based on the ability to acquire automatic skills [216], which also includes associative forms of learning (priming, habituation and learning of perceptual and cognitive routines). Non-declarative memory is an implicit and non-verbal type of memory that is acquired unconsciously [215].

Another important dichotomy distinguishes memory subcomponents along a temporal dimension of duration, short-term memory (STM) and long-term memory (LTM), which depend on different neural substrates. Medial temporal lobe structures are responsible for the establishment of new representations. STM is an essential component of cognition and is defined as the maintenance of information over short periods of time (seconds). STM involves the conscious maintenance of sensory stimuli over a short period of time, after which they are no longer present. LTM refers to the mechanism by which acquired memories become stable or strengthened over time and resistant to interference. LTM involves the reactivation of past experiences that were not consciously available between the time of encoding and retrieval. Two main components of LTM are described as declarative, episodic and semantic memory [215].

Memory is tightly connected to time perception, attention and emotional valence of memory contents, and brain circuits implicated with these functions are overlapping with areas involved in processing of memory functions. Debates over the implication of attention functions to memory and the role of parietal regions to retrieval of episodic memory. Attention to memory model postulates that the dorsal parietal cortex mediates top-down

attention processes guided by retrieval goals while ventral parietal cortex mediates automatic bottom-up attention processes captured by retrieved memory outputs [215].

Although there are many neuropsychological tests to assess learning and memory function, in this thesis the California Verbal Learning Test II (CVLT-II) and the Rey-Osterrieth Complex Figure (ROCF) were used. The CVLT-II is a test that assesses episodic verbal learning and memory (*this method is explained in the section 3.1.3.1. The California Verbal Learning Test II*), whereas the ROCF assesses episodic visual learning and memory (*this method is explained in the section 3.1.3.5. The Rey-Osterrieth Complex Figure Test*).

Obesity is associated with poorer episodic memory as well as other memory parameters such as visual working memory tasks. There are several mechanisms by which obesity may adversely affect episodic memory performance, including morphological brain changes, IR, neuroinflammation, TG, circulating glucocorticoid levels and cerebral metabolite concentrations [217]. In a recent review from 2018, [217] it was found that of the 14 studies, 10 found an inverse association between weight status and hippocampal volume, an indicator of memory function. Higher BMI was negatively associated with memory function and learning [218,219]. Improvements in indices of memory function have been found after bariatric surgery [220]. Others have found no association [221,222].

Age-related cognitive decline in obesity causes atrophy of medial temporal lobe regions involved in memory, such as the hippocampus. Loss of synapses in the hippocampus is characteristic of neurodegenerative disorders [223].

1.3.1.2   *Executive function and attention*

Executive function refers to a constellation of cognitive abilities that enable and drive adaptive, goal-oriented behaviour. These include the ability to generate thoughts and think flexibility, to mentally update and manipulate information, to inhibit what is irrelevant to current goals, to self-monitor, and to plan and adapt behaviour to the current context. Intact executive function is critical to the ability to adapt to an ever-changing world, whereas deficits in executive function led to disproportionate impairments in function and activities of daily living. At anatomical level, executive function is a cognitive domain associated with the frontal lobe structure of the brain, which relies on distributed neural networks including the prefrontal cortex, parietal cortex, basal ganglia, thalamus and cerebellum [224].

From a clinical perspective, executive function can be divided into four components: i) working memory is a limited capacity system that allows us to temporarily process, store and manipulate information within conscious awareness; ii) inhibition of prepotent responses is the ability to inhibit a predominant, automatic or previously learned response that may be inappropriate or irrelevant in the current context; iii) mental set shifting reflects the ability to modify attention and behaviour in response to changing circumstances and demands; and iv) fluency represents the ability to maximise the production of verbal or visual information in a given period of time, avoiding repetitive responses [224,225].

Working memory refers to the temporary, active maintenance and manipulation of stored information necessary for its use it in a complex task of STM. There are two types of working memory: verbal and non-verbal (visual-spatial). Working memory is crucial for making sense of anything that unfolds over time, because it always involves keeping in mind what happened earlier and relating it to what comes later. It is important to note that working memory is different from STM, which only involves holding information in mind. Working memory relies on the dorsolateral prefrontal cortex, whereas holding information in mind but not manipulating it does not require the involvement of the dorsolateral prefrontal cortex. Working memory is highly dependent on top-down processing and selective attention [215,216,225].

The components of executive function work together to enable planning and organisation, which are higher order cognitive constructs that allow an individual to identify, prioritise and appropriately sequence the individual steps required to achieve a goal in an adaptive and efficient manner [224].

The neuropsychological tests used to assess executive function were the Trail Making Test (TMT), the Digit Span Test (DST), the Stroop Colour and Word Test (SCWT) and the ROCF. The TMT is a test that assesses visual attention (*this method is explained in the section 3.1.3.4. The Trail Making Test*), while the SCWT assesses inhibitory control (*this method is explained in the section 3.1.3.3. The Stroop Colour and Word Test*). The DST includes Forward, which is a test that assesses STM, and Backward, which is a test that assesses working memory (*this method is explained in the section 3.1.3.2. The Digit Span Test*).

Executive function is related to the control of food intake and has been studied in relation to BMI [226]. BMI is associated with pathophysiological changes that negatively affect in cognitive function. Obese individuals show poorer attention and executive function

performance on measures that include tasks requiring response inhibition, working memory, planning, and the ability to shift cognitive sets [227].

Cognitive performance appears to improve after bariatric surgery and weight loss. Patients with bariatric surgery have better cognitive test performance on measures of memory and executive function before surgery, predicting greater weight loss [227].

1.3.2   Brain – Adipose tissue axis

AT is controlled by an endocrine loop in which leptin acts on neural circuits in the hypothalamus and elsewhere in the brain to regulate food intake and peripheral metabolism [228]. Leptin increases the sympathetic efferent signal to the BAT [229,230] and it has been suggested that leptin also activates sympathetic efferent signals to the WAT to increase lipolysis in the WAT [231]. It has not been established whether the increased lipolysis in WAT in response to leptin is due to a circulating hormone such as norepinephrine and/or another mediator released centrally or peripherally (adrenal gland or macrophages), or to specific efferent neuronal inputs to WAT mediating central leptin action. The effect of leptin on energy balance does not require the presence of an intact adrenal gland, suggesting that this organ is unlikely to be the source of the lipolytic signal [232].

Macrophages in AT account for 10% of SVF and local catecholamines produced by these cells also contribute to lipolysis in WAT [233,234]. The decrease in AT mass after leptin treatment could be mediated by catecholamines or other mediators produced by neurons. Zheng and colleagues demonstrated that catecholamines released at neuro-adipose junctions mediate the lipolytic effect of leptin, establishing the effector mechanism underlying the reduction of fat mass by leptin, and that local sympathetic activity in WAT is necessary for lipolytic effect of leptin. In addition, β-adrenergic receptors constitute a signalling pathway responsible for the lipolytic effect of leptin. The effect of presynaptic manipulations suggests direct activation of sympathetic inputs to AT as a strategy for induce fat loss [231].

Group 2 innate lymphoid cells (ILC2) contribute to VAT metabolism via type 2 innate cytokine and Met-Enkephalin. The nervous system and ILC2 cooperate to control adipose physiology via higher order brain-body interfaces. Neural circuits and immune cells cooperate to drive inter-organ communications to understand organismal physiology and systemic diseases [235].

Among the most critical functions of the brain is its role in homeostasis, the maintenance of conditions within the internal milieu that support optimal cellular function and life itself. There is a complex relationship between the maintenance of homeostasis and the defence of core body temperature. The preoptic area of the hypothalamus is the primary integrative site in the brain for thermoregulation, in close proximity to hypothalamic regions involved in the regulation of homeostatic variables and associated motivated behaviours [236].

There is increasing awareness that peripheral tissues modulate brain function, shaping different cognitive domains. The ageing brain is vulnerable to inflammation due to the high prevalence of age-related cognitive decline. Circulating pro-inflammatory factors may promote cognitive decline. In ageing mice, myeloid cell bioenergetics is suppressed in response to increased signalling by the lipid messenger prostaglandin E2 (PGE2), which is a modulator of inflammation. In ageing macrophages, PGE2 signalling through its receptor promotes glucose sequestration into glycogen, reducing glucose flux and mitochondrial respiration. Cognitive ageing can be reversed by reprograming myeloid glucose metabolism to restore immune functions [237].

Energy balance and metabolic communication between the gastrointestinal tract and the brain is mediated by the vagus nerve. Neurons in the hippocampus, a brain region associated with learning and memory control and feeding behaviour [238], are activated by direct stimulation of the vagus nerve and by vagally mediated gastrointestinal signals [239,240]. Furthermore, rats with hippocampal lesions are impaired in the use of interoceptive hunger and satiety to control learned anticipatory appetite outcomes [241], suggesting that the hippocampus functionally integrates gastrointestinal cues relevant to energy balance. Gastrointestinal-derived vagal sensory signalling endogenously promotes hippocampal-dependent learning and memory function in rats. Non-selective and sensory selective ablative methods of gastrointestinal vagal disconnection impaired hippocampal-dependent memory processes, including spatial working memory and contextual episodic memory [242].

Food restriction rapidly depletes glycogen stores and induces lipolysis, altering body lipid levels [243], and hypothalamic neurons have been shown to control peripheral lipid metabolism [244,245] and complex behaviours beyond feeding [245–247]. In rodents, depletion of liver glycogen content reduces blood glucose levels and induces liver lipolysis and lipid secretion into the blood [248].

1.3.3   Cognitive impairment

Obesity is detrimental to cognitive impairment and has an impact on dementia [156,249]. Cognitive impairment and dementia are influencing the lives of older people, with the burden of the ageing population growing rapidly [156,249,250]. By 2050, there will be three times as many people with dementia as in 2015 [249]. Evidence suggests that risk factor modification can prevent 30 – 35% of dementia cases [156].

The effect of obesity on cognition may be age-dependent and change over time. Obesity would be associated with poorer performance and greater cognitive decline, which would be attenuated by older age. Greater abdominal obesity, measured by WHR, was associated with poorer cognitive performance and decline at ages below 65 years. Processing speed and executive function were the domains most associated with abdominal obesity, with effects on performance on tasks of attention, intelligence, memory, cognitive flexibility, processing speed and general executive function [250,251].

Specific fat components are associated with different metabolic profiles and have different effects on cognitive impairment and dementia [156]. The relationship between adiposity and cognition may depend on the anthropometric measure of adiposity. Although BMI may be a good measure of adiposity in midlife, it is not an ideal measure in older people because of the concurrent loss of lean body mass and increase in AT in the absence of age-related weight change. Waist circumference and WHR are more reliable measures of adiposity in older people and of abdominal adiposity, which is detrimental to cognition [250].

A number of clinical conditions are characterized by impairments in brain function, particularly memory and cognitive ability [252,253]. Recent studies have shown that obesity exacerbates the progression of neurodegenerative disorders [254,255]. Several mechanisms associated with obesity have been implicated in neurodegeneration, including altered lipid and fatty acid metabolism [256,257], ceramide dysregulation leading to IR and impaired cognitive function [258], as well as mechanisms related to oxidant stress. Although there are certainly differences between the mechanisms by which different neurodegenerative diseases progress, there is some overlap between these disease pathways and those underlying obesity, such as those related to oxidative stress, mitochondrial dysfunction and increased inflammation.

AT secretes hormones, cytokines and growth factors that can cross Blood-Brain Barrier (BBB) and affect brain health [259]. Neurons express receptors for several adipokines,

suggesting that factors released from AT have the potential to communicate directly with the brain [260]. Factors released from AT may interact with blood vessels and contribute to disruption of homeostasis [259]. The increase in inflammatory cytokines, CRP and IL-6, associated with obesity can damage the CNS and affect cognitive function. This metabolic dysfunction can lead to neuronal death and altered synaptic plasticity of neurons, increasing the risk of neurodegenerative disorders [261–263]. Inflammation predicts poorer performance on tests of memory and executive function, which correlates with BMI. Associations between BMI and cognitive function are mediated by inflammatory markers, IL-6 and CRP [251].

Deposition of VAT induces systemic inflammation and promotes the development of metabolic complications in obesity [14,264]. The inflammatory VAT microenvironment leads to the formation of inflammasome complexes that amplify innate immune responses in AT [265,266]. The Nucleotide oligomerization domain (NOD) like receptor family, pyrin domain-containing 3 (NLRP3) is a component of the inflammasome complex, and NLRP3 induction in VAT promotes synthesis and release of the pro-inflammatory cytokine IL-1β in obesity [266]. NLRP3 knock-out mice develop obesity but are protected against High Fat Diet (HFD)-induced AT inflammation and IR [265,266] and are protected against cognitive deficits in aged mice and AD [267,268]. Activation of the NLRP3 inflammasome in VAT impairs cognitive in obesity. These effects were mediated by activation of IL-1R1 in C-X-C motif chemokine receptor 1 (CXCR1)-expressing cells, which detect and amplify IL-1β in the brain. Exposure to IL-1β, as seen in chronic inflammatory diseases, impairs synaptic plasticity and cognition in the hippocampus [269].

Unlike visceral fat, which contains a homogeneous population of white adipocytes, subcutaneous fat contains both white and beige adipocytes, which use energy in a manner analogous to brown fat [270]. Beige adipocytes continuously interact with immune cells, and the acquisition of thermogenic features (*beiging*) requires induction of the anti-inflammatory cytokine IL-4 by leukocytes in SAT [271,272]. Beige adipocytes are essential for the neuroprotective and anti-inflammatory effects of SAT fat and implicate beige fat-stimulated IL-4 production in communication between SAT and CNS. Mice lacking beige adipocytes exhibited stronger pro-inflammatory responses to a HFD in the brain and periphery, and were more susceptible to cognitive deficits and hippocampal synaptic dysfunction [273].

Metabolic dysfunction, and IR in particular, is known to have detrimental effects on the brain vasculature, inflammatory processes and mitochondrial function, among others, which may

alter cognition. In the brain, mitochondrial dysfunction leading to increased reactive oxygen species (ROS) has been linked to early brain ageing [274]. Insulin is known to exert protective effects against oxidative stress in the brain, and thus central IR can act in concert with mitochondrial dysfunction to promote cognitive decline [275].

IR also plays a role in the pathophysiology of neurodegenerative diseases, such as AD. In particular, in AD, IR increases brain amyloidosis and alters clearance of amyloid beta, which can have direct effects on memory [276]. Animal models show that insulin binding sites are highly concentrated in the hippocampus, and thus impaired insulin signalling in this region may directly affect learning and memory, independent of its role in AD pathology [277].

Oxidative stress in adipocytes attributable to Na- and K-dependent adenosine triphosphatase (Na,K-ATPase) signalling, a previously known ion-pumping activity of this complex [278–280]. Signalling through this Na,K-ATPase pathway requires phosphorylation of Src [280–283]. Na,K-ATPase is stimulated by oxidative stress and leads to the generation of ROS. This pathway has been characterised as the Na,K-ATPase oxidant amplification loop (NKAL). The synthetic peptide NaKtide abolishes the NKAL by preventing phosphorylation of Src [284]. Genetically modified mice engineered to release the NaKtide peptide in adipocytes resulted in improved hippocampal memory by inhibiting Na,K-ATPase signalling in adipocytes [223].

1.4 OBESITY AND ENVIRONMENT

1.4.1 Global warming

Climate change is a real global phenomenon [285]. Nowadays, climate change is changing and will continue for the next decades [286] and is the greatest global health threat of the 21st century [287]. Global warming defines current climate change. The term global warming refers to an aspect of climate change characterised by a gradual increase in the Earth's average surface temperature, mainly due to the burning of fossil fuels that increase greenhouse gases [33,139].

Natural greenhouse warming is primarily enhanced by water vapour, which plays a crucial role in keeping the Earth's surface temperature at a level that is habitable for humans, around 15°C. Human activities, particularly the burning of fossil fuels, have disrupted the Earth's natural greenhouse. Atmospheric carbon dioxide levels have increased by more than a third since the industrial revolution [139,288]. Excessive levels of carbon dioxide, methane and nitrous oxide increase the greenhouse effect, trapping heat and causing the Earth's surface temperature to rise [139,289]. One of the goals of the United Nations is to stabilise greenhouse gas concentrations in the atmosphere at a level that would prevent dangerous anthropogenic interference with the climate system [290].

As a result of climate change, outdoor temperatures are likely to increase, reducing the need for heating in winter and increasing the need for cooling in summer [291]. As temperatures rise, more water vapour evaporates from the oceans and other water sources into the atmosphere, causing temperatures to rise further. The Earth's surface temperature has risen by $0.6 - 0.9$ °C, and climate models predict a further increase of around $2 - 6$ °C by the end of the 21st century (**Figure** 7) if we continue to burn more fossil fuels and accumulate greenhouse gases in the Earth's atmosphere [139]. Climate change is likely to exacerbate differences in runoff between wet and dry regions [292]. Among these regions, the Mediterranean basin appears to be particularly vulnerable, with both temperature and drought events are expected to increase further by the end of the century [293].
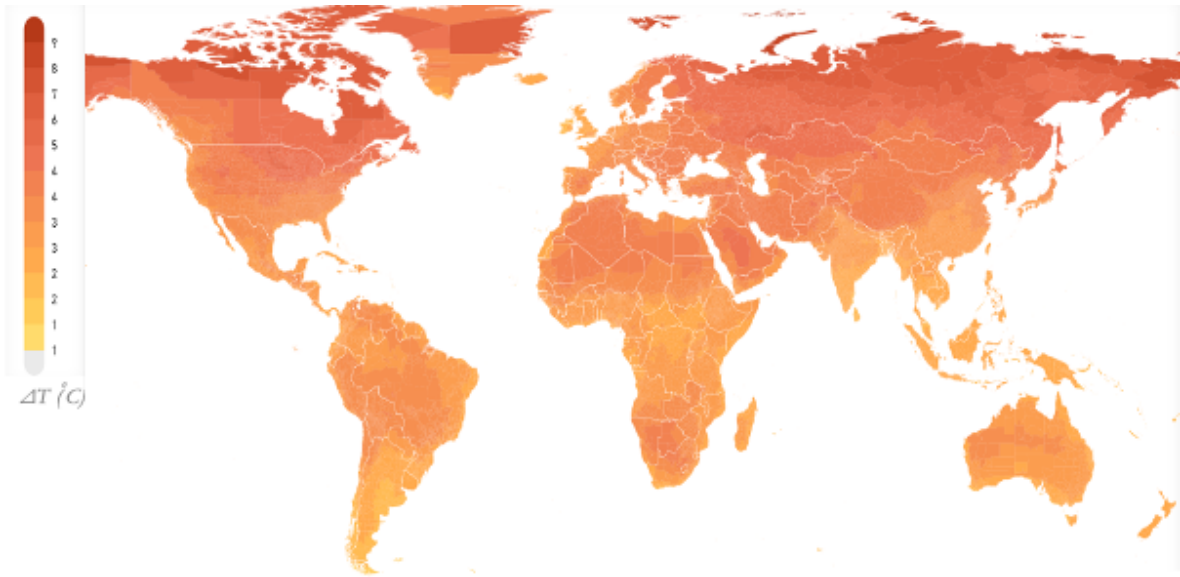
Figure 7 | Map of average annual temperatures predicted by the end of the century (2080 – 2099). The map indicates the increase in the average annual temperature (ºC) of the Earth by the end of the century. *Figure taken and adapted from Climate Impact Lab (2022)* [294]

The consequences of global warming include variable weather, heat waves, heavy precipitation events, floods, droughts, more intense storms, sea level rise and air pollution [33]. Warming is expected to be associated with changes in precipitation, which can affect water supply for humans, agriculture and ecosystems [295]. As the Earth's climate warms, hotter days and nights and heat waves are becoming more frequent and intense. Global warming is pushing the climate temperature curve towards extremes. The number of heat waves has tripled and their duration has increased [139].

Climate change will lead to a range of harmful impacts in different regions and sectors, some of which will occur immediately in association with warming, while others will build up under sustained warming due to the time lags of the processes involved [290]. Urbanisation and mean annual temperature show regional differences [296]. Nowadays, around 55% of the world's population lives in urban areas, and the urban population is expected to increase to as much as 68% [297]. In Spain, around 82% of the population lives in urban areas. Urban areas are an important driver of economic growth, innovation and wealth creation, but have also brought with them a number of negative health effects related to environmental exposures such as air pollution, noise, and lack of green spaces [298].

Characterisation of the exposure to ambient temperature in urban areas typically relies on observations from the nearest meteorological station, although gridded data from climate models can be used to examine local or small-scale mortality effects in large cities or metropolitan areas [299]. Large urban areas are warmer than surrounding rural areas because of loss of vegetation, more pavement and buildings absorbing the sun's energy, reduced airflow in alleyways, and heat generated by vehicles, air conditioners, and factories. Daytime temperatures in cities are higher than in rural areas, and the night-time temperature difference is greater because of the heat retained from the day. Cities are vulnerable to heat waves, often associated with air pollution [139].

Global warming has serious implications for food, water supplies, housing, economic activity and human health [139]. As a result of global warming, the world's population is increasingly exposed to moderate and extreme warm temperatures and less to moderate extreme cold temperatures, with serious implications for various health outcomes [300]. The relationship between weather and human health is heterogeneous, with associations varying by geography and by the point at which both cold- and heat-related risks increase for different diseases, cardiovascular-related mortality and all-cause mortality [295].

Climate change is expected to affect human health directly by increasing exposure to extreme temperatures, and indirectly through a variety of pathways including sea level rise, extreme weather events, migration, and changes in agricultural leading to rural poverty [287,301]. Warmer conditions are expected to contribute to an increase in heat-related morbidity and mortality and a concomitant decrease in cold-related hospitalisations and deaths worldwide [302]. These exposures are projected to increase in frequency and magnitude as the world continues to warm in response to greenhouse gas emissions.

Climate change, particularly rising temperatures and more frequent and prolonged heat waves, is causing injuries, illnesses, and deaths, and the risks are projected to increase with further climate change, threatening the health of many millions of people unless investments in adaptation and mitigation is scaled up rapidly [285,303].

According to the most recent Global Burden Disease study, ambient air pollution is the leading environmental risk factor for mortality and morbidity worldwide. They estimated that air pollution caused 4.2 million deaths (7.6% of total global mortality) and 103.1 million DALYs (4.2% of global DALYs) in 2015 [304]. Air pollution in adults is been associated with

adverse respiratory and cardiovascular diseases, reduced lung function, premature mortality, cancer and diabetes, and also obesity [305,306].

In ageing societies such as Europe, the growing elderly population is expected to increase vulnerability to high ambient temperatures, as the elderly have a reduced psychological capacity to regulate core body temperature under conditions of heat stress [307]. According to the WHO, climate change is expected to cause an additional 250,000 deaths per year between 2030 and 2050, 38,000 of which will be due to heat exposure in older people. Prolonged exposure to heat could also lead to additional illness and death by exacerbating pre-existing chronic conditions such as various cardiovascular and neurological diseases [285].

Even when high ambient temperatures are associated with morbidity and mortality, this association is based on the use of outdoor meteorological data as a proxy for individual exposure, with measurements taken at long distances from actual indoor exposure [308]. However, there is strong evidence of an association between high ambient temperatures and outdoor meteorological data to general morbidity and mortality [286].

In 2019, the Eat and Transition (EAT) Lancet Commission published a report on the definition of a heathy diet from sustainable food systems and what actions can support and accelerate the transformation of food systems in the current era and geological epoch. This report summarises that 820 million people do not have enough or good quality food, contributing to the rising incidence of diet-related obesity. Food production is one of the largest drivers of global environmental change, contributing to climate change, biodiversity loss, freshwater use, disruption of global nitrogen and phosphorus cycles, land system change and chemical pollution [289,309].

Climate change leads to changes in temperature and precipitation, which are expected to reduce global crop productivity, cause changes in food production and consumption, and affect the health of the global population by altering diet composition and the profile of diet- and weight-related risk factors and associated mortality. The impact on food supply and food security could be a consequence of climate change, given the large number of people who could be affected [287]. Climate change could reduce the protein and micronutrient content of plant-based foods, increasing the price of basic food and leading to an increase in nutrient deficiencies and chronic malnutrition among the most vulnerable populations [310].

The food system is responsible for more than a quarter of greenhouse gas emissions, up to 80% of which are linked to livestock production. The choices we make about the food we eat affect our health and have a major impact on the state of the environment. Our overall dietary choices therefore have major impact on climate change. Changing our diets may be a more effective option to avoid climate change and may be essential to avoid negative environmental impacts such as large-scale agricultural expansion and global warming of more than 2 °C [287,311].

1.4.2   Obesity and environment temperatures

The obesity pandemic is one element of a global syndemic, which also includes malnutrition and climate change [310]. Syndemics are two or more diseases with three characteristics: i) they co-occur in time and place; ii) they interact at biological, psychological or social levels; and iii) they share common underlying societal drivers. Although the syndemic concept was originally used to describe the interaction of two or more diseases at the individual level, it provides a useful construct with which to consider the interaction of two or more pandemics, in this case obesity, malnutrition and climate change.

With climate change being accorded pandemic status because of its projected impact on human health. Malnutrition in all its forms, including obesity, undernutrition, and diet-related risks for non-communicable diseases, is already by far the largest cause of health loss worldwide. The increasing health impacts of climate change in the future mean that global syndemics will remain the leading cause of poor health worldwide.

A recent systematic review on the relationship between global warming and the obesity epidemic, which included 50 studies published in or after 2002, attempted to find answers to the questions of whether global warming and the obesity epidemic share common determinants, where one influences the other and/or each other, and what pathways would underlie such a relationship [33]. The authors of this review constructed a conceptual model linking global warming and the obesity epidemic [33,289,312].

Thus, inside this review at least 13 studies have postulated that the obesity epidemic is influenced by global warming [33].

1.4.2.1   Human thermoregulation

Humans are endothermic homeotherms, we generate our own body heat and have the ability to regulate body temperature. Body temperature is influenced by the environment, internal mechanisms (homeostasis) and behavioural adaptations. Humans have thermoregulatory mechanisms that adapt to environmental changes to maintain a normal core body temperature, which is critical for the maintenance of physiological functions such as energy balance [313]. The thermal environment influences energy expenditure and intake in mammals, where an optimal temperature must be maintained consistently. Metabolic heat production is regulated in response to environmental temperature fluctuations, known as adaptive thermogenesis [314]. This specialised form of thermoregulation means that the control of body temperature accounts for a large proportion of the energy expended by endotherms when the environmental temperature deviates from the thermoneutral zone.

The thermoneutral zone is defined as a homogeneous range of comfortable ambient temperatures, 20.3 – 23 ℃ for clothed humans, at which metabolic rates are minimal [313] and no physiological processes need to be initiated to maintain thermal homeostasis [291]. A reduction in air temperature from 22 ℃ to 16 ℃ causes a graded increase in energy expenditure in clothed humans. This additional energy is used to maintain thermal homeostasis through acute shivering and tissue heat production. The extra energy expended at temperatures below the thermoneutral zone may be offset by a compensatory increase in appetite and caloric intake. This food intake contributes to heat production.

Adaptive thermogenic responses, which refers to the generation of heat for homeostatic purposes, result in increased energy expenditure through shivering and non-shivering thermogenesis. Shivering is an acute response to cold exposure that generates heat through involuntary contraction of skeletal muscle fibres. During mild cold exposure, shivering is rapidly reduced by adaptation, although the metabolic increases associated with cold exposure are not reduced, demonstrating that non-shivering thermogenic processes are present in humans. Non-shivering adaptive thermogenesis defends body temperature by generating heat in tissues and is initiated in response to feeding [313]. Thermogenesis plays a role in energy balance. Energy expenditure in humans is negatively associated with the thermal environment over a range of ambient temperatures that includes exposure to daily life temperatures [315]. Non-shivering thermogenesis is mediated by BAT, in which energy is released as heat through the action of UCP1 in mitochondria. In addition to its function in

preventing hypothermia, brown fat has also been implicated as a defence against obesity and diabetes [316]. Changes in ambient temperature could alter a population's risk of obesity [315].

Climate change and the associated warming trend observed in many areas may affect endotherms. Some endotherms may be so thermally specialised that their only option is to increase energy expenditure to maintain a constant body temperature as the environmental temperature increasingly deviates from the animal's thermoneutral zone, reducing the energy available for other basic functions, such as growth and reproduction [314].

Global warming is a public health challenge and there are bidirectional influences on obesity and global warming [312]. Obesogenic food environments are associated with the thermal comfort of Western lifestyles, which may override the natural tendency to reduce food intake in warmer conditions [313]. Obesity may be promoted by impaired thermogenesis and reduced expression of thermogenesis-related genes [289].

Studies in controlled environments have shown that human energy expenditure increases in response to mild cold exposure, and there appears to be a graded relationship between energy expenditure and ambient temperature [291].

There is an association between increased time spent in thermal comfort and increased adiposity in the population [313]. Increased exposure to thermoneutral conditions and associated reduced exposure to mild seasonal cold as part of Western lifestyle may contribute to weight gain [291]. In addition, increased time spent in thermoneutral conditions may lead to loss of BAT and reduced thermogenic capacity, reducing the frequency and/or duration of occasions on which cold-induced energy expenditure is initiated [313].

1.4.2.2 How cold temperature environment affect to obesity

The mechanisms of human responses to cold are of great interest due to the role of BAT in human thermogenesis [313]. Low ambient temperatures can affect the body's ability to maintain energy balance by increasing the capacity for thermogenesis [291,313]. Cold is an environmental signal that activates thermogenesis in vivo [316]. As thermogenic capacity is stimulated by cold exposure, an increase in time spent in thermal comfort leads to reduced thermogenic capacity and loss of BAT [313].

Cold exposure is a potent inducer of beige adipocytes recruitment. Acute and chronic cold exposure can induce browning [317]. Cold is first perceived by sensory nerves in peripheral tissues. This information is then received and processed in the hypothalamus, which controls the activity of the SNS, leading to the release of norepinephrine into brown and beige fat cells. Norepinephrine acts through G protein-coupled B-adrenergic receptors on adipocytes to activate the cAMP/PKA response element-binding protein signalling cascade, which controls transcription of the thermogenic gene program [316].

Energy expenditure in humans is negatively related to the thermal environment [315]; at lower temperatures, energy expenditure increases to maintain body temperature [318]. Exposure to cold is a natural afferent signal for BAT. Association between BAT activity and favourable metabolic profile, and BAT mass and activity associated with BMI, activation of BAT by increasing time spent in cold environment could prevent obesity and its metabolic comorbidities [315]. It has been shown how areas with moderate or cold temperatures have a protective effect against external causes associated with metabolic diseases [301]. The presence of BAT in adults has reignited the hypothesis that the thermogenic potential of BAT could increase energy expenditure and have an anti-obesity effect. Higher exposure to colder outdoor temperatures could be associated with lower prevalence of obesity [315].

1.4.2.3 How warm temperature environment affect to obesity

As heat waves become more frequent, severe and longer, and cold and frost less frequent, more heat-related illnesses and deaths are expected, especially among children, the elderly, people with chronic health conditions, and poor or underserved communities [313].

Environmental influences such as increases in ambient temperature associated with climate change and global warming, together with transport, thermal insulation of buildings and individuals, have reduced the need for people to generate energy by inducing thermogenesis [312]. Increased environmental temperature has been associated with an increased prevalence of obesity and alterations in glucose metabolism [315,319]. As atmospheric temperatures increase, adaptive thermogenesis is expected to be reduced in people with obesity through a reduction in physical activity [310].

Heat stress due to global warming could increase the incidence of neurodegenerative diseases. Stress could induce apoptotic pathways and autophagy in neurons, which could

expose susceptible cells to neurodegeneration. Molecular mechanisms activated by heat play a role in the deterioration of functionality in people suffering from neurodegenerative diseases or in the elderly, whose thermoregulatory outcomes are compromised and play a role in the onset of these diseases [285].

The impact of climate change on mental health is increasingly recognised, with exposure to flooding and other extreme events increasing the risk of depression and anxiety, which may disproportionately affect people with pre-existing mental health problems [303].

2. HYPOTHESIS

1. **Genes in AT have a bidirectional interaction in the cognitive performance of middle-age obese subjects**

Obesity is a chronic multifactorial disease associated with an abnormal accumulation of dysfunctional AT and has been associated to cognitive dysfunction. Cognitive decline is a major health problem exacerbated by metabolic diseases such as obesity, particularly in morbid obesity. We hypothesise that there is a bidirectional interaction between AT and brain function, which would be more pronounced in subjects with morbid obesity.

2. **Cognitive function in animal models is influenced by the expression of genes in the AT**

Cognition has been extensively studied in animal models such as mice or *Drosophila melanogaster*, as well as in animal models of obesity. We hypothesise that cognition is possibly influenced by the expression of genes in AT, demonstrating a bidirectional interaction.

3. **Subjects from colder regions have increased expression of browning markers in WAT and consequently improved insulin sensitivity and AT function.**

The aetiology of obesity is multifactorial, including environmental factors. Nowadays, environmental factors are changing due to global warming which is increasing the temperature of the Earth. *Browning* of WAT is an important process in the physiology of AT, which is enhanced in colder environment. We hypothesise a relationship of environmental temperatures with the expression of genes in AT.

3. OBJECTIVES

1. **To assess the associations involved in the bidirectional interactions between AT gene expression and cognitive function**

1.1.   To analyse the relationship between cognitive tests and the whole genome expression of genes in AT from morbidly obese subjects through Ribonucleic Acid sequencing (RNA-seq) and to validate the results in an independent cohort

1.2.   To analyse the expression level of several genes in peripheral blood mononuclear cells (PBMCs) in association with cognitive traits in humans

2. **To assess the cognitive function in animal models with targeted changes in gene expression in AT**

2.1.   To analyse the cognition of *Drosophila melanogaster,* in which some candidate genes has been altered in the fat body

2.2.   To analyse the memory of mice with a targeted down-regulation of a candidate gene in AT

3. **To examine the effects of outdoor temperature on obese subjects in a large multicentre cohort with participants from different Spanish regions**

3.1.   To analyse the potential associations of metabolic parameters and markers of AT physiology in a cohort of subjects with and without obesity

4. MATERIALS AND METHODS

4.1   STUDY POPULATION

The total study population was recruited at the Endocrinology Department of the Dr. Josep Trueta University Hospital (Girona, Spain) and participants were included in different cohorts of the Nutrition, Eumetabolism and Health Research Group depending on their characteristics. The entire cohort was of Caucasian origin and included obese and non-obese subjects.

In addition, participants from the Endocrinology Department of the University Hospital Virgen de la Victoria (Málaga, Spain), the University Hospital Reina Sofia (Córdoba, Spain), the University Hospital Complex of Santiago (Santiago de Compostela, Spain) and the University Clinic of Navarra (Pamplona, Spain) were included in one of the studies.

To be included in any of the cohorts studied, all subjects had to have a stable body weight for at least three months prior to enrolment and were studied in the post-absorptive state.

The study protocol was revised, validated and approved by the Ethics Committee and the Clinical Investigation Committee (CEIC) of the Dr. Josep Trueta University Hospital. The purpose of each study was explained to the participants, who signed a written informed consent prior to enrolment.

4.1.1   Cohorts Description

The cohorts included in this thesis were named: i) Ironmet; ii) Intestine; iii) Imageomics and; iv) Fatbank. The characteristics of the specific cohort used, the inclusion and exclusion criteria for each study and the biological samples used in each case are explained and described on the following sections (**Table 6**).

Table 6 | Summary of the cohorts used in this thesis. qPCR (quantitative polymerase chain reaction). *N Oliveras-Cañellas (2024)*

Ironmet Cohort	Intestine Cohort	Imageomics Cohort	Fatbank Cohort
Discovery Cohort	**Validation Cohort 1**	**Validation Cohort 2**	**Validation Cohort 3**
17 subjects BMI > 35 kg/m^2 VAT RNA-seq Neuropsychological assessment	22 subjects BMI > 35 kg/m^2 SAT / VAT RNA-seq Neuropsychological assessment 2-3 years later	816 subjects Wide range of BMI PBMC's qPCR Neuropsychological assessment	40 subjects Wide range of BMI VAT qPCR Neuropsychological assessment 4-10 years later
			Adipomit Cohort
			1070 subjects Wide range of BMI SAT qPCR Temperatures collected

4.1.1.1 Ironmet Cohort (Discovery Cohort)

Ironmet cohort consists of a total of 181 participants (31.5 % of male), obese (n = 102 with BMI = 43.8 ± 7.17 kg/m^2) and non-obese (n = 79 with BMI = 25.2 ± 2.72 kg/m^2), aged between 25 and 67 years old, recruited between January 2016 and October 2017. The aim of this project was to assess AT, muscle and brain iron and volume by MRI, as well as their relationships with gut microbiota and the effects of weight loss. Exclusion criteria for inclusion in this cohort are present in **Table 7**.

Table 7 | **Exclusion criteria** of the Ironmet Cohort (Discovery Cohort). *N Oliveras-Cañellas (2024)*

Exclusion criteria of Ironmet Cohort	
Presence of concomitant disease	Type 1 or 2 diabetes Malignant condition Chronic active inflammatory disease (rheumatoid arthritis, *Crohn's* disease or asthma) Chronic kidney or liver conditions
Neuropsychiatric conditions	Neurological or psychiatric diseases History of traumatic brain injury Language disorders Severe eating disorders
Infection in the previous month	
Any of the next treatments in the last 3 months	Antibiotics, antifungal, antiviral, proton pump inhibitors, anti-inflammatory drugs
Use of drugs or alcohol abuse	40g/day for men and 20g/day for women
Pregnancy or lactation	

From the 181 participants available in this cohort, a sub-selection of 17 participants were also recruited for bariatric surgery and had AT available for study. This subset was called the *Discovery Cohort* and they are used for the studies in this thesis. All have morbid obesity (BMI > 35 kg/m²) (11.8 % of male with BMI 48.8 ± 4 kg/m²).

4.1.1.2 Intestine Cohort (Validation Cohort 1)

Intestine cohort consist of a total of 41 consecutive morbidly obese subjects (BMI > 35 kg/m²) aged between 23 and 57 years, recruited between January 2017 and November 2019. These participants have different degrees of insulin action measured using the hyperinsulinemic-euglycaemic clamp (*this method is explained in the subsection 4.1.2.3*). The aim of this project was to evaluate the relationship between obesity-related metabolic diseases and the secretion of the fibroblastic growth factor 15/19 (FGF15/19) in the gut and the lipopolysaccharide-binding protein (LBP) as a therapeutic potential. Exclusion criteria are shown in **Table 8**.

Table 8 | Exclusion criteria of the Intestine Cohort (Validation Cohort 1). *N Oliveras-Cañellas (2024)*

Exclusion criteria of Intestine Cohort	
Presence of concomitant disease	Type 1 or 2 diabetes Malignant condition Chronic active inflammatory disease (rheumatoid arthritis, *Crohn's* disease or asthma) Chronic kidney, liver conditions (tumoral disease or Hepatitis C Virus (HCV) infection) or thyroid dysfunction
Neuropsychiatric conditions	Neurological or psychiatric diseases History of traumatic brain injury Language disorders Severe eating disorders
Infection in the previous month	
Use of drugs or alcohol abuse	40g/day for men and 20g/day for women

Although the 41 available participants in this cohort had AT, only 22 (9.75% of men with BMI of 45.84 ± 5.7 kg/m^2) were used for the study because these 22 were the only ones who had cognitive tests done. This selection was called *Validation Cohort 1*.

4.1.1.3 Imageomics Cohort (Validation Cohort 2)

The Aging Imageomics Study [320] is an observational study that includes 816 participants from two independent cohort studies with their own eligibility criteria of individuals residing in the province of Girona (Northeast Catalonia, Spain): the Maturity and Satisfactory Ageing in Girona study (MESGI50 study) [321] and the Improving intermediate Risk management study (MARK study) [322]. These participants were recruited between November 2017 and June 2019. The MESGI50 study is a population-based cohort linked to the Survey of Health, Ageing and Retirement in Europe project (SHARE), which included a representative sample of the population of the province of Girona aged ≥ 50 years [323]. The MARK study included a random sample of patients aged $35 - 74$ years, with intermediate cardiovascular risk recruited from public primary care centres in the province of Girona [322].

The aim of this project was to combine data from whole-body imaging with data from other fields to develop a panel of biomarkers of biological aging that can identify individuals at high risk of developing age-related diseases or disabilities.

Members of both cohorts were contacted by telephone and invited to participate in the Aging Imageomics Study. During this standardized telephone call, potential candidates were informed about the study and encouraged to request more detailed information if they so desired. Subjects who agreed to participate were asked to select a date and time to complete the enrolment process. To be eligible for the study, potential participants had to meet the criteria listed in **Table 9**.

Table 9 | Inclusion criteria of the Imageomics Cohort (Validation Cohort 2). *N Oliveras-Cañellas (2024)*

Inclusion criteria of Imageomics Cohort	
Age	≥ 50 years old
Dwelling	in the community (not institutionalized)
No history of infection	during the last 15 days
No contraindications of MRI	electronic cardiac implants, cochlear implants, incompatible prosthetic hearth valves, incompatible vascular clips, metallic foreign bodies, or claustrophobia
Consent to be informed	of potential incidental findings

All 816 participants (54% male with an average age of 67.55 years and average BMI of 27.97 kg/m^2) from this cohort were used in the studies and were called *Validation Cohort 2*.

4.1.1.4   *Fatbank Cohort (Validation Cohort 3 / Adipomit Cohort)*

The Fatbank cohort was a multi-role collection promoted by the *Centro de Investigación Biomédica en Red Fisiopatología de la Obesidad y Nutrición* (CIBEROBN) and led by the *Institut d'Investigació Biomèdica de Girona* (IDIBGI) Biobank (B.0000872), which is integrated in the Spanish National Biobanks Network. It involved participants from Dr. Josep Trueta

University Hospital (Girona, Spain), University Hospital Virgen de la Victoria (Málaga, Spain), University Hospital Reina Sofía (Córdoba, Spain), University Hospital Complex of Santiago (Santiago de Compostela, Spain), and, University Clinic of Navarra (Pamplona, Spain). Although this is a multicentre cohort, all centres used the same standard operating procedures.

The aim of this cohort was to create the first biological bank specialized in AT, in order to obtain a collection useful for studying its relationship and incidence in the progression of several diseases.

This cohort started the recruitment in 2010 and is still ongoing, including participants with and without obesity, aged above 18 years old. The exclusion criteria are shown in **Table 10**.

Table 10 | Exclusion criteria of the Fatbank Cohort (Validation Cohort 3 / Adipomit Cohort). *N Oliveras-Cañellas (2024)*

Exclusion criteria of Fatbank Cohort
No systemic disease other than obesity
Acute infection or inflammation in the previous month
Liver conditions (specifically tumoral disease and HCV infection)
Thyroid dysfunction
Be on **oncological treatment**
Pregnancy or breastfeeding women

In the present work, this cohort was used for two different studies. In the first study, 40 subjects (32.5% male) from Girona with several degrees of obesity (n = 12 with BMI < 35 kg/m²; n = 28 with BMI > 35 kg/m²), aged between 40 and 64 years, were selected. This first selection was called *Validation Cohort 3* and was made according to previous results of gene expression in the same participants. In the second study, 1070 participants (28% male), with and without obesity (12%), aged between 18 and 81 years, were selected from all the centres integrated in the Biobanks Network *(Adipomit Cohort)*.

4.1.2 Clinical measurements

4.1.2.1 Anthropometric Characterization

At the first visit to the Endocrinology Department, each participant was asked about their family and medical history, including age, sex, ethnicity, alcohol intake, family history of obesity, cardiovascular disease, or diabetes. A physical examination was also carried out.

BMI was calculated from weight and height (kg/m^2), and waist circumference (cm) was measured by touching around the highest point of the upper edge of the iliac crest, parallel to the ground, without compressing the skin, at the end of a non-forced expiration. The percentage of fat mass was measured by densitometry, an approach that distinguishes fat mass from total fat free mass. In addition to densitometry, the Deurenberg formula [324] and electrical bioimpedance (TANITA® MC-190 Body Composition Analyzer; *Tanita Corporation, Tokyo, Japan*) were used to estimate body fat percentage. Blood pressure was measured by both systolic blood pressure (SBP) and diastolic blood pressure (DBP) in the upper arm.

4.1.2.2 Biochemical parameters

After fasting for at least of eight hours, blood sample were tested using routine clinical laboratory techniques.

Serum fasting glucose concentrations were determined by an oxidation reaction and the resulting colorimetric change, monitored by a Beckman Glucose Analyzer II spectrophotometer (*Beckman Instruments, California, USA*).

Total cholesterol (TC) was also measured by spectrophotometry and the peroxidase-catalysed esterification/oxidation reaction in a BM/Hitachi 747-100 analyser (*Roche Diagnostics, Indianapolis, USA*). HDL and LDL were measured directly in serum by precipitation of apolipoprotein B (ApoB)-containing lipoproteins, and polyethylene glycol-coupled cholesterol esterase and cholesterol oxidase for the HDL cholesterol measurement, whereas LDL is most commonly determined using the "Friedewald formula", which incorporates measurements of total cholesterol, HDL, and TG: LDL = (TC) – (HDL) – (TG/5), where units are mg/dL. TG were analysed by the glycerol phosphate oxidase/peroxidase reaction. Circulating concentrations were measured by spectrophotometric methods in both cases.

Total haemoglobin (Hb) and CRP are also routine biochemical determinations obtained by spectrophotometry in plasma samples with ethylenediaminetetraacetic acid (EDTA) (*Coulter Electronics, Florida, USA*), a common anticoagulant. It is common for Hb to bind free glucose molecules in plasma by covalent attachment. The percentage of these proteins with glucose molecules attached is called HbA1c and is an indicator of glucose concentrations in the bloodstream during the half-life of Hb (from 6 to 8 weeks) and an indirect marker of impaired glucose tolerance (> 6%). HbA1c has been measured in erythrocyte lysate by chromatographic, immunological and electrophoretic methods.

4.1.2.3   Hyperinsulinemic-euglycemic clamp

Insulin action was determined using the hyperinsulinemic-euglycemic clamp [325]. After an overnight fast, two catheters were inserted into an antecubital vein, one for each arm, used to administer constant infusions of glucose and insulin and to obtain arterialized venous blood samples. A 2-hour hyperinsulinemic-euglycemic clamp was initiated by a two-stage primed infusion of insulin (80 mU/m²/min for 5 min, 60 mU/m²/min for 5 min), immediately followed by a continuous infusion of insulin at a rate of 40 mU/m²/min (regular insulin [Actrapid; *Novo Nordisk, Plainsboro, NJ*]). Glucose infusion began at the fourth minute with an initial perfusion rate of 2 mg/kg/min, which was then adjusted to maintain plasma glucose concentration between 88.3 and 99.1 mg/dl. Blood samples were taken every 5 min for the determination of plasma glucose and insulin. Insulin sensitivity was assessed as the mean glucose infusion rate over the last 40 min. At steady-state, the amount of glucose infused (M) equals the glucose taken up by body tissues and is a measure of overall insulin sensitivity.

4.1.3   Neuropsychological assessment

Neuropsychologists have a variety of neuropsychological tests to assess the cognitive domains (**Figure 6**) with the aim to examine the cognitive function of all participants. In this thesis, only three of the six cognitive domains have been studied (complex attention, learning and memory, and executive function).

4.1.3.1   The California Verbal Learning Test

The CVLT-II is one of the most widely used neuropsychological tests for assessing verbal learning and memory in the Wechsler Adult Intelligence Scale-III (WAIS-III) [326–330].

STEP 1						STEP 2				STEP 3	
List A	Trial 1	Trial 2	Trial 3	Trial 4	Trial 5	**Interference List (List B)**		**List A**		**List A**	
Football				x	x	Strawberry		Football	x	Football	x
River	x	x	x	x	x	Hand	x	River	x	River	x
Lemon						Dress		Lemon		Lemon	
Boxing	x	x	x	x		Pineapple	x	Boxing	x	Boxing	x
Dog	x	x	x	x	x	Fish	x	Dog		Dog	
Apple						Head		Apple		Apple	
Lion		x	x	x	x	Shirt		Lion	x	Lion	
Mountain	x	x	x	x	x	Mango		Mountain	x	Mountain	x
Orange	x	x	x	x	x	Trousers	x	Orange	x	Orange	x
Tiger						Arm	x	Tiger		Tiger	
Island				x	x	Penguin		Island	x	Island	
Tennis			x	x	x	Socks	x	Tennis	x	Tennis	x
Cat						Leg	x	Cat		Cat	
Beach				x		Delfin		Beach		Beach	
Banana				x		Peach		Banana		Banana	
Baseball						Bear		Baseball		Baseball	
	5	6	7	9	10				8		6
	37										

→ 20 minutes

IMMEDIATE FREE RECALL — **SHORT DELAYED RECALL** — **LONG DELAYED FREE RECALL**

Figure 8 | An example of the CVLT-II test. In the first step, the examinee presents a list of words (List A) and the participant has to remember as many words as possible in 5 different trials. In a second step, the examinee reads another list of words, called Interference List, and the participant has to remember not only this Interference List but also List A for the first step. The last step consists of waiting for 20 min, with no-word exchange, and then the participant must remember List A for the first step. *N Oliveras-Cañellas (2024)*

The CVLT-II consists of three distinct parts (**Figure 8**). In step 1, the participant is presented with a list of 16 words from 4 different semantic categories, called List A. Immediately after each presentation, the subject has 5 trials to remember and say as many words as possible in any order. The result of these five trials is the CVLT Immediate Recall score and provides information about learning process. In the second step, the participant is presented with an interference list, called List B, which shares two semantic categories with List A, and is asked to recall this interference list immediately, as well as List A, free (CVLT Short Delayed Free Recall, CVLT-SDFR) or with semantic facilitation (CVLT Short Delayed Cued Recall, CVLT-SDCR). Step 3 takes place 20 min after Step 2, but non-verbal tasks are carried on

during this waiting period. In this step, subjects are asked to repeat a list of words previously presented (List A) without semantic facilitation (CVLT Long Delayed Free Recall, CVLT-LDFR) to assesses LTM. The final score is proportional to memory function; higher score indicates better memory function.

4.1.3.2 The Digit Span Test

The Digit Span Test (DST) is an executive task that is particularly dependent on working memory and is a subtest of the WAIS-III [327,331].

Forward Digit Span Task		Backward Digit Span Task	
(1)	5 – 8 – 2	(1)	2 – 4
	6 – 9 – 4		5 – 8
(2)	6 – 4 – 3 – 9	(2)	6 – 2 – 9
	7 – 2 – 8 – 6		4 – 1 – 5
(3)	4 – 2 – 7 – 3 – 1	(3)	3 – 2 – 7 – 9
	7 – 5 – 8 – 3 – 6		4 – 9 – 6 – 8
(4)	6 – 1 – 9 – 4 – 7 – 3	(4)	1 – 5 – 2 – 8 – 6
	3 – 9 – 2 – 4 – 8 – 7		6 – 1 – 8 – 4 – 3
(5)	5 – 9 – 1 – 7 – 4 – 2 – 8	(5)	5 – 3 – 9 – 4 – 1 – 8
	4 – 1 – 7 – 9 – 3 – 8 – 6		7 – 2 – 4 – 8 – 5 – 6
(6)	5 – 8 – 1 – 9 – 2 – 6 – 4 – 7	(6)	8 – 1 – 2 – 9 – 3 – 6 – 5
	3 – 8 – 2 – 9 – 5 – 2 – 7 – 4		4 – 7 – 3 - - 9 – 1 – 2 – 8
(7)	2 – 7 – 5 – 8 – 6 – 2 – 5 – 8 – 4	(7)	9 – 4 – 3 – 7 – 6 – 2 – 5 – 8
	7 – 1 – 3 – 9 – 4 – 2 – 5 – 6 – 8		7 – 2 – 8 – 1 – 9 – 6 – 5 – 3

Figure 9 | An example of the DST test. In the first part (Forward), the participant has to repeat the numbers said by the examinee in the same order. In the second part (Backward), the participant has to repeat the numbers the examinee says, but in reverse order. Each part ends when the participant is unable to repeat some of the sequences or repeats one of them incorrectly. *N Oliveras-Cañellas (2024).*

This test consists of two subtests involving numbers (**Figure 9**). In the DST Forward, the subject has to repeat a sequence of numbers in the same order as presented by the examinee. The length of the sequence is increased until the participant cannot longer repeat the sequence correctly. This test is useful for working memory but also for attention. In the DST

Backward, the subject has to repeated a sequence of numbers in reverse order to the sequence as presented, which becomes progressively longer.

Total DST was the sum of the two previous tests. A higher score reflected better working memory.

4.1.3.3 The Stroop Colour Word Test (Golden's version)

The Golden's version of the SCWT assesses the ability to inhibit cognitive interference, which occurs when the processing of one stimulus feature interferes with the simultaneous processing of another feature of the same stimulus. It also assesses executive function, cognitive flexibility, selective attention, and information of processing speed [332,333].

It consists of three parts, all of which require the subject to read the tables as quickly as possible (**Figure 10**). In the first part, the paper given to the subject contains 100 colour names printed in black ink. The subject has to read the colour name that is written. In the second part, the paper contains 100 "XXX" printed in colour ink. The subject must name the colour. Finally, on the last page there are 100 colour names (from the first part) printed in coloured ink (from the second part), but the colour name and the ink colour do not match. The subject has to name the ink colour (and not read the colour name). 45 seconds were given for each of the three tasks. After this time, the last item completed was recorded, giving three scores (one for each part, Word (W), Colour (C) and Colour – Word (CW), respectively).

The interference index (I) was also obtained from by subtracting CW – CW' (CW' = (W * C) / (W + C)). Higher scores represent a better cognitive test and therefore a greater ability to inhibit cognitive interferences.

STEP 1				
GREEN	YELLOW	RED	BLUE	YELLOW
GREEN	RED	BLUE	GREEN	BLUE
RED	YELLOW	BLUE	GREEN	RED
YELLOW	YELLOW	GREEN	BLUE	RED
GREEN	YELLOW	BLUE	RED	RED
BLUE	YELLOW	GREEN	YELLOW	RED
GREEN	BLUE	RED	GREEN	BLUE
YELLOW	YELLOW	BLUE	RED	GREEN

STEP 2				
XXX	XXX	XXX	XXX	XXX
XXX	XXX	XXX	XXX	XXX
XXX	XXX	XXX	XXX	XXX
XXX	XXX	XXX	XXX	XXX
XXX	XXX	XXX	XXX	XXX
XXX	XXX	XXX	XXX	XXX
XXX	XXX	XXX	XXX	XXX
XXX	XXX	XXX	XXX	XXX

STEP 3				
BLUE	YELLOW	BLUE	RED	BLUE
GREEN	YELLOW	RED	GREEN	YELLOW
GREEN	RED	GREEN	YELLOW	YELLOW
YELLOW	RED	YELLOW	GREEN	BLUE
BLUE	RED	YELLOW	YELLOW	GREEN
RED	BLUE	GREEN	YELLOW	GREEN
RED	YELLOW	BLUE	RED	GREEN
BLUE	GREEN	YELLOW	YELLOW	YELLOW

Figure 10 | An example of the SCWT test. In the first step, the subject has to read the colour names written on the paper. In the second step, the subject has to say the names of the colours printed on the paper. In the last step, the participant has to say the colour names, but they are printed in an ink that does not match the real colour. *N Oliveras-Cañellas (2024)*

4.1.3.4   The Trail Making Test

The TMT assesses visual attention and executive function [334,335].

This test consists of two parts (**Figure 11**). TMT part A assesses visual attention and consists of a standardized page on which numbers from 1 to 25 are printed in circles in a random order. The subject was asked to match the numbers in order as quickly as possible. The second part, TMT Part B, assesses executive function. The structure is similar to Part A, but the standardized page contains both numbered and lettered circles in a random order.

Subjects have to connect the numbers and letters alternately. Before starting, a 6-item practice test was given to the subject to ensure that they understand both tasks.
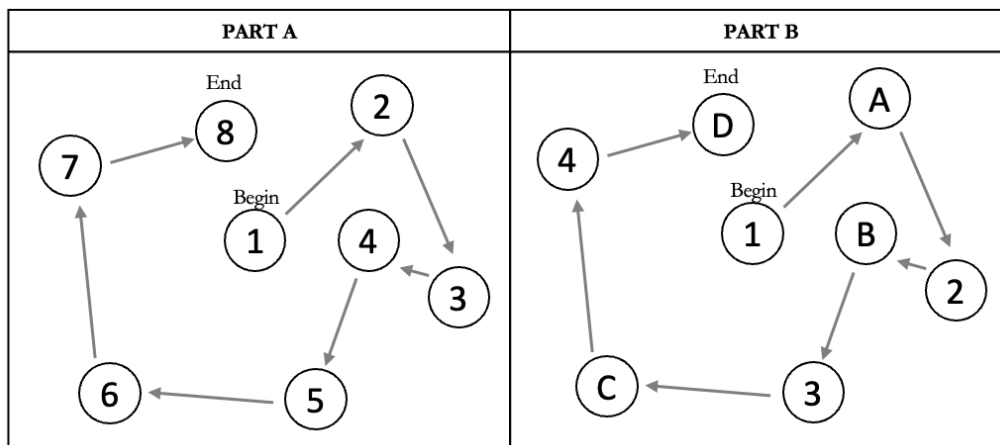
The examinee will time the participant and if the participant makes a mistake, the time will not stop. Each part ends when the participant has completed the connection between the numbers or when the time exceeds 300 seconds. The score is the time taken to complete each part of the test. In both tests, shorter times indicates better performance.

4.1.3.5   *The Rey-Osterrieth Complex Figure Test*

The ROCF Test [336–338] is one of the most widely used neuropsychological tests for assessing visuospatial constructional ability, visual memory and executive function. The ROCF is a complex cognitive task involving the ability to organize the figure into a meaningful perceptual unit.

The first part of the test consists of copying a complex geometric figure (**Figure 12**), which requires attention and concentration as well as planning and organizational abilities. This part provides information about executive function. The second part, called immediate recall, consists of reproduce the same figure from memory immediately after the first part. Finally,

the third part, the participant has to reproduce the same figure from memory after a longer delay of 20 – 30 min. These two parts provide information about memory function.
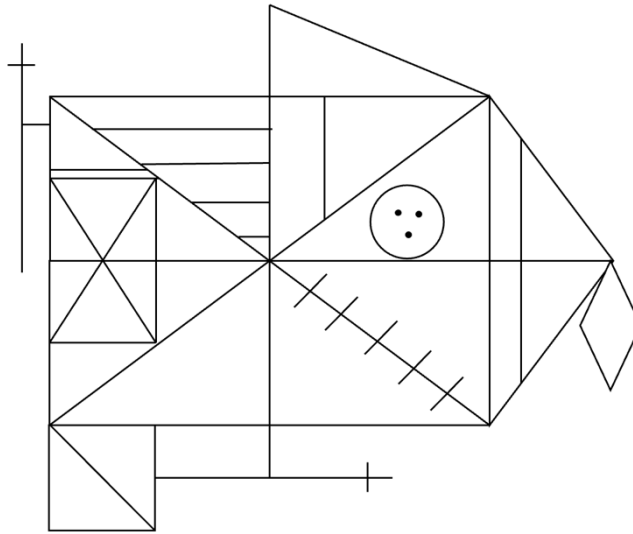
Figure 12 | An example of the Geometric figure included in the ROCF test. The participants must copy and reproduce it. *N Oliveras-Cañellas (2024)*

4.1.4   Adipose tissue collection and handling

All samples included in this thesis, regardless of the origin, used the same procedure for collecting and preserving AT samples.

AT samples were obtained from SAT or VAT of non-consecutive participants, following elective surgical (cholecystectomy, surgery of abdominal hernia and gastric bypass surgery) using standard procedures.

AT samples were immediately transported to the laboratory (5 – 10 min). Tissue handling was performed under strict aseptic conditions. AT samples were washed in sterile Phosphate Buffered Saline (PBS), cut off into small pieces (100 mg) with forceps and scalpel, and immediately flash-frozen in liquid nitrogen before storage at -80 °C.

4.1.5 Temperature data

The *Spanish National Meteorological Agency* (AEMET) provided us with the daily atmospheric temperature in Celsius degrees (ºC) for 10 years, from 2010 to 2020, for all the meteorological stations managed by AEMET. Post-processing was carried out to obtain the average, maximum and minimum monthly temperatures (**Figure 13**).

The data had to be processed with the aim of associating the place of residency of each participant with the nearest weather station, in order to obtain the monthly temperature (average, minimum and maximum) for the month in which the AT sample was obtained and of the previous month.

Figure 13 | Map of Spain with the annual average temperature (ºC) between 1988 and 2017, with the five Biobank Network of study. *N Oliveras-Cañellas (2024)*

4.2   ANIMAL MODELS

The animal models used in this thesis were *Drosophila melanogaster* and *Mus musculus*. *Drosophila melanogaster* experiments were carried out in the "Drosophila, Fly Room" platform belonging to IDIBGI. *Mus musculus* experiments were carried out in the Neuropharmacology-Neurophar Laboratory, belonging to the University Pompeu Fabra, Barcelona.
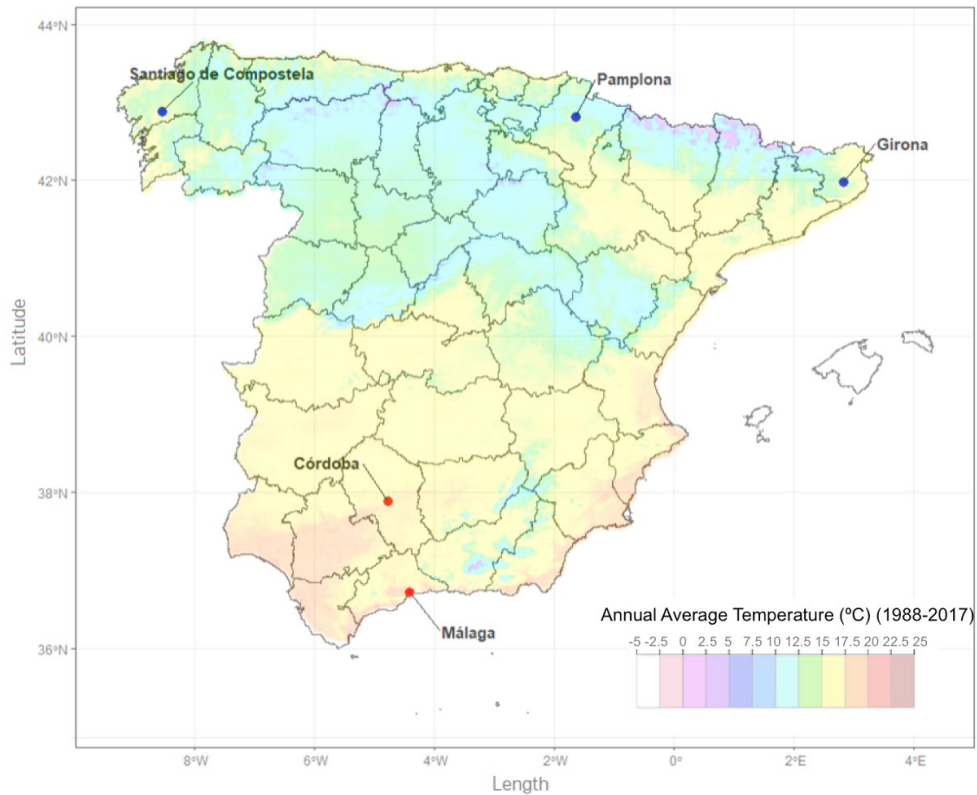
4.2.1   *Drosophila melanogaster*

Drosophila melanogaster has been used as a model organism since the beginning of the last century, when it was first used for genetic studies by Thomas H. Morgan, and its use has allowed the understanding of many important biological processes and mechanisms of human health research [339–341].

4.2.1.1   *Advantages to use Drosophila melanogaster as an animal model*

The use of *Drosophila* has many advantages over other animal models (**Figure 14**). They are easy and inexpensive to maintain. Due to its short generation cycle (10 days) and exponential growth (a single female can lay more than 100 eggs), flies are easy to breed in large numbers. They are small, which makes it easy to analyse whole flies or tissues in large numbers and at high resolution under the microscope [341,342]. Additionally, there are no legal restrictions on the production or experimental use of these animals [339–343].

Drosophila provides research with a large battery of genetic tools, molecular assays and behavioural test. The generation of *Drosophila* mutants is relatively easier and faster than in any other model organism. Moreover, comprehensive collections of *Drosophila* stocks, facilitating gene expression manipulation through Interference Ribonucleic Acid (RNAi), are readily accessible at stock centres for an affordable price.

Finally, the adult fly has organs that are functionally similar to mammalian organs, so *Drosophila* provides a complex model organism that is similar to mammals. Flies and humans share common evolutionary roots and show striking similarities at the levels of their genes, cells, tissues and the biological processes. Homologues have been identified for almost 75%

of human disease-related genes, making it an excellent model for studying human genes and biological pathways [341,342].
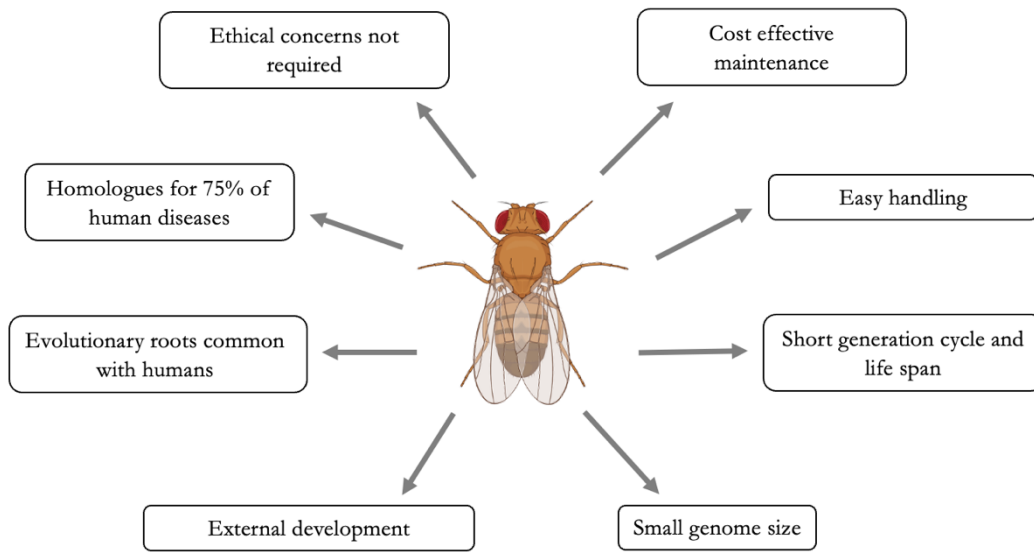
Figure 14 | Advantages of using Drosophila melanogaster as an animal model. Summary of the main advantages of using Drosophila as an animal model in the laboratory. *N Oliveras-Cañellas (2024)*

4.2.1.2   Upstream Activating Sequence – Galactosidase 4 system

The Upstream Activating Sequence (UAS) – Galactosidase 4 system (GAL4) system is a powerful tool for precisely targeting the down regulation by RNAi or the overexpression of any gene of interest in a tissue-specific manner [344,345].

The UAS-GAL4 system consists of two genetic elements combined by crossing of individual fly strains (**Figure 15**). The so-called driver line expresses GAL4, a yeast transcriptional activator, under the control of a specific promoter, while the reporter line carries the UAS followed by the element of interest. When the driver and reporter lines are crossed and the offspring inherit both genetic elements, GAL4 binds to its target UAS sequence and drives expression of the gene of interest, which is restricted to GAL4-expressing tissues. This system can be used to overexpress (**Figure 15 A**) the gene of interest or to downregulate (**Figure 15 B**) genes by RNAi. In the latter case, when GAL4 binds to the UAS, it activates the RNAi insert following the UAS to express a short hairpin Ribonucleic Acid (shRNA). This shRNA is cleaved by the enzyme Dicer (Dcr-2) into short interference Ribonucleic Acid (siRNAs), which assemble by complementarity with the target Messenger Ribonucleic Acid

(mRNA). The Ribonucleic Acid (RNA)-induced silencing complex (RISC) leads to the cleavage of the mRNA, which down-regulates the expression of the gene of interest.
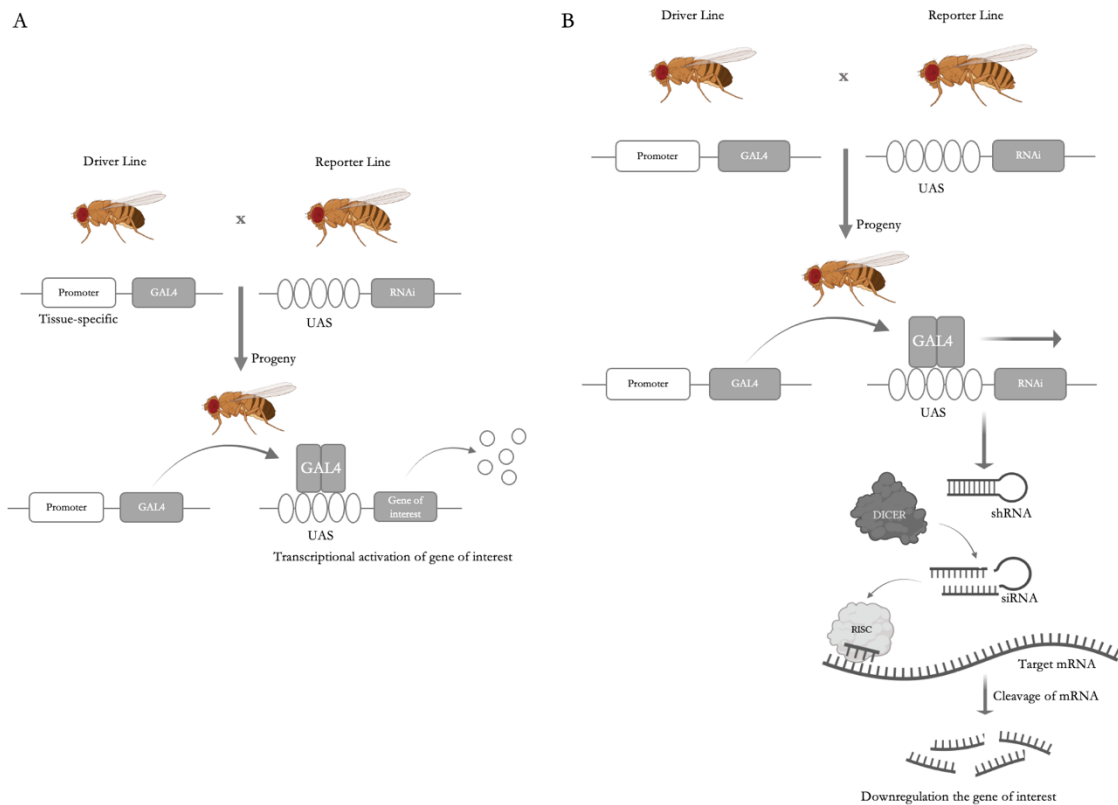
Figure 15 | A. UAS-GAL4 system. Method used in Drosophila melanogaster to overexpress the gene of interest. Flies carrying GAL4 with a specific promoter are crossed with flies carrying UAS with the gene of interest. The offspring inherit both elements, and GAL4 is linked to the UAS, which promotes transcription of the gene of interest. *Figure taken and adapted from Brand 1993* [344] **B. UAS GAL4 RNAi**. System used in Drosophila to generate downregulation of the gene of interest. Flies carrying GAL4 with a specific promoter were crossed with flies carrying UAS-RNAi transgene targeting the gene of interest. The offspring inherit both elements and GAL4 is linked to UAS, which promotes transcription of the RNAi in which UAS express shRNA. These are cleaved by Dcr-2 into siRNAs, which assemble with the target mRNA. Finally, RISC leads to cleavage of the mRNA, which down-regulates the expression of the target gene. *Figure taken and adapted from Diezl 2007* [345].

There are several public stock centres that provide different collections of transgenic *Drosophila* (libraries) stocks at relatively low price, allowing rapid acquisition of *Drosophila* stocks. The three main stock centres are: i) Vienna *Drosophila* RNAi Centre (VDRC); ii) National Institute of Genetics in Japan (NIG-FLY); and iii) Bloomington *Drosophila* stock centre in Indiana (BDSC).

Currently, in the VDRC stock centre has the highest coverage of the genome, targeting approximately 89% of the protein-coding genes. This stock centre consists of two releases, the Georg Dietzl (GD) and Krystyna Keleman (KK) libraries. The insertion site of each GD line is made using P-element-mediated transposition, resulting in a random integration site. In the KK library, however, the transgenes have been integrated using a site-specific integration. The NIG-FLY stock centre covers approximately 45% of protein-coding genes. The RNAi constructs contain long inverted repeats in a UAS vector and were inserted into the genome by random P-element integration. Finally, the BDSC, covers about 70% of protein-coding genes and works in a similar way to VDRC KK, whose lines were made by targeted integration, and comprises the transgenic RNAi project (TRiP)

4.2.1.3 *Drosophila melanogaster stocks and maintenance*

Flies were raised on standard medium, the components of which are listed in **Table 11**, and cultured according to standard procedures at 28 ºC on a 12:12 hours light-dark cycle.

Table 11 | Fly food. Proportions of each of components for the composition of fly feed for 1 litre of total standard feed. *N Oliveras-Cañellas (2024)*

Components	For 1L of food
Agar	5 g
Cornmeal	52 g
Sugar	110 g
Yeast	27.2 g
0.1% Methyl paraben	5 ml
Propionic Acid	5 ml

RNAi expression was induced in the fat body (equivalent to human AT) using the *w; C7-GAL4; UAS-Dcr-2* driver line, which carries a fat tissue-specific promoter (*C7*) that drives GAL4 expression specifically on *Drosophila* fat body, and was kindly provided by Marek Jindra [346].

Conditional RNAi lines targeting the genes of interest and the corresponding genetic background controls, (v60000, Control 1; and v60100, Control 2) for KK and GD RNAi line collections, respectively, were obtained from VDRC (http://stockcenter.vdrc.at/control/main). The *Rim* overexpression line (UAS-Rim) and the corresponding genetic background control (BL36304, Control 3) were obtained from the BDSC. (http://fllystocks.bio.indiana.edu/).

The RNAi lines were crossed with the *w; C7-GAL4; UAS-Dcr-2* promoter line to knock down gene expression in the fat body. In addition, the *UAS-Rim* line was crossed with the same promoter line to drive overexpression of *Rim*. *UAS-Rim* was then isomerized into the genetic background for 6 generation.

We downregulated or overexpressed *Vmat, Rim, Amph, Datp, Oat, Moe, Hr38, Timp* and *Unc-5* (**Table 12**), the well conserved orthologues of *SLC18A2, RIMS1, AMPH, NUDT2, OAT, EZR, NR4A2, TIMP1* and *UNC5B*, respectively, specifically in the fat body.

Table 12 | Conditional RNAi lines targeting the genes of interest. Information of the RNAi lines used in the experiments of this thesis. *Table taken from Oliveras-Cañellas N (2023)* [347]

Line name	Genotype	Stock Center	Order number	Target gene	Human Orthologue
Vmat-RNAi1	w; P{KK112993}VIE-260B	VDRC	104072	Vmat	SLC18A2
Vmat-RNAi2	w1118; P{GD1982}v4856	VDRC	4856		
Rim-RNAi1	w1118; P{GD15273}v39384	VDRC	39384	Rim	RIMS1
Rim-RNAi2	w118; P{GD15273}v39385/TM3, Tb, Sb	VDRC	39385		
UAS-Rim	w*; P{UAS-Rim.G}3	BDSC	78050		
Amph-RNAi1	w1118; P{GD1311}v9264	VDRC	9264	Amph	AMPH
Amph-RNAi1	w1118; P{GD1311}v7190	VDRC	7190		
Datp-RNAi1	w1118; P{GD15139}v39150	VDRC	39150	Datp	NUDT2
Datp-RNAi2	w; P{KK111614}VIE-260B	VDRC	102412		
Oat-RNAi1	w; P{KK107991}VIE-260B	VDRC	107178	Oat	OAT
Oat-RNAi2	w1118; P{GD14026}v28952	VDRC	28952		
Moe-RNAi	w; P{KK108480}VIE-260B	VDRC	110654	Moe	EZR
Hr38-RNAi	w; P{KK107365}VIE-260B	VDRC	104178	Hr38	NR4A2
Timp-RNAi	w; P{KK108268}VIE-260B	VDRC	109427	Timp	TIMP1
Unc-5-RNAi	w; P{KK102074}VIE-260B	VDRC	110155	Unc-5	UNC5B

4.2.1.4   *Drosophila courtship conditioning*

The courtship conditioning paradigm measures associative learning and memory capabilities and has been used to assess cognition in *Drosophila* [348–350].

The *Drosophila* courtship is an innate and stereotypic behaviour presented by male flies, which is characterized by orienting towards and following the female, tapping, extending and vibrating the wing, licking, and attempting to copulate (**Figure 16**). As this is an innate behaviour of the males, they will court all females. Male flies can learn to distinguish between

receptive virgin and non-receptive mated females, using specific pheromones, and after sexual rejection, they show reduced courtship behaviour towards non-receptive females. This natural behaviour can be used to study learning, short- and LTM.
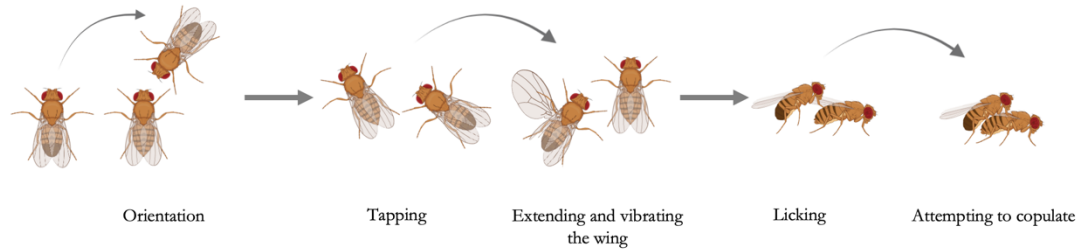
Figure 16 | Stereotypical male courtship behaviour towards a female fly. Different stages of courtship behaviour are shown: orientation, tapping, wing vibration and extension, licking, and attempted copulation. *Figure taken and adapted from Koemans T. S. (2017)* [350]

During courtship conditioning, both sexes exchange stimuli of different modalities, such as visual, chemosensory and auditory [351]. This behaviour depends on the presence of a pheromone, cis-vaccenyl acetate (cVA), on the female abdomen, which is deposited by the male during copulation. The detection of cVA on the female abdomen naturally reduces courtship behaviour, and when coupled with the act of rejection by the female, the effect of cVA on reducing male courtship is enhanced [350].

In the courtship conditioning assay learning and memory captivities are assessed by measuring the reduction in courtship behaviour of male flies upon the exposure to mated females in comparison to naïve males [350] (**Figure 17**). We assessed learning and STM. First, males were collected at eclosion and kept in isolation at 25ºC until 7 days of age, when they were randomly assigned to either trained or naïve groups. Depending on whether we want to assess learning or STM, male courtship rates can be assessed at different times after training periods with premated females.
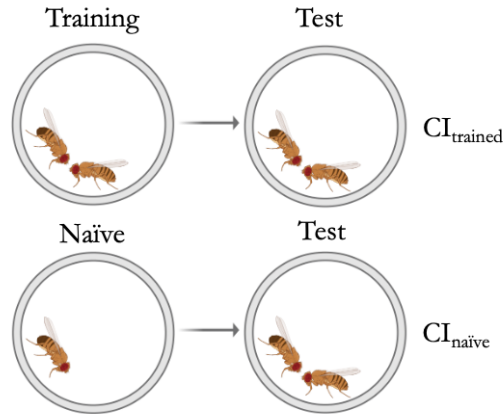
Figure 17 | Courtship conditioning paradigm. Males were divided into training and naïve group. In the training group, males were trained with a premated female for a specific period of time (depending on whether we wanted to assess learning or STM). In the naïve group, males were kept alone the same length of time as in the training group. For the test, males from both groups were placed with a premated female to assess learning or STM. *Figure taken and adapted from Koemans T. (2017)* [350]

Learning was assessed by pairing individual males with a single premated wild-type female for 2.5 hours during the training period. Immediately after training, the males were tested to assess learning.

STM was assessed by pairing individual males with a single premated wild-type female for 6 hours during the training period, and subsequently, the male was individually isolated for 1-hour prior testing. Testing was performed by transferring the male to a 1-cm-diameter chamber in the presence of a premated female and filming for 8 min. The courtship behaviour of male toward females was manually quantified from the videos.

Mean courtship indices (CI) were defined as the percentage of time that male spent in courtship during the first 8 min interval of the testing period, for each individual male fly. The CI of trained males and socially naïve males were used to calculated the learning index (LI), defined as the percentage reduction in mean courtship activity in trained males compared to naïve males; $LI = (CI_{naïve} - CI_{trained}) / CI_{trained}$. For all conditions, male-female pairs were analysed on at least three different test days and the data were pooled. A higher LI indicates better learning or STM.

Nonparametrical statistical bootstrapping analysis was performed to assess differences in LI (learning and STM) between RNAi knockdown or overexpression lines and their

corresponding genetic background controls. The R script provided by Koemans *et al.* [350] was used to perform the bootstrapping analysis. Briefly, CI values were randomly sampled with replacement to generate 10,000 hypothetical Lis, which were used to determine the 95% confidence interval of the difference between the index of the control and the index of the knockdown and the probability that this difference is >0. T test or one-way analysis of variance (ANOVA) was performed to assess statistical differences in CI of the compared conditions.

4.2.2 Mice models

4.2.2.1 Animals

A total of 48 male wild-type C57BL/6J (*Charles River, France*) 8-week-old mice were individually housed under controlled conditions (21 ± 1 ºC, 55 ± 10% humidity, 12 hours light/dark cycle). Some mice were free fed for 8 weeks either with a normal chow diet (ND (~ 3.512 kcal/kg: 10% fat, 66% carbohydrate and 24% protein); n = 23) or a high-fat diet (HFD (~5.228 kcal/kg: 60% fat, 16% carbohydrate and 24% protein); n = 25). ND (C1090-10) and HFD (C-1090-60) were obtained from Altromin Spezialfutter, GmbH & Co. (*KG, Large, Germany*).

Three days after the start of the diet, weight-matched mice of each group (ND or HFD) were divided into two groups and injected intravenously via the tail vein with 200 μL of either the AAV8-RSV-GFP-Adp-miRNASLC18A2 (AAV) vector (**Figure 18**) containing $1 \cdot 10^{12}$ Genome Copies (GC) in PBS or with saline. The AAV vector was produced by the Viral Product ion Unit in the Universitat Autònoma de Barcelona http://sct.uab.cat/upv). This vector expresses Green Fluorescence Protein (GFP) and a microRNA to selectively down-regulate *Slc18a2* in AT.
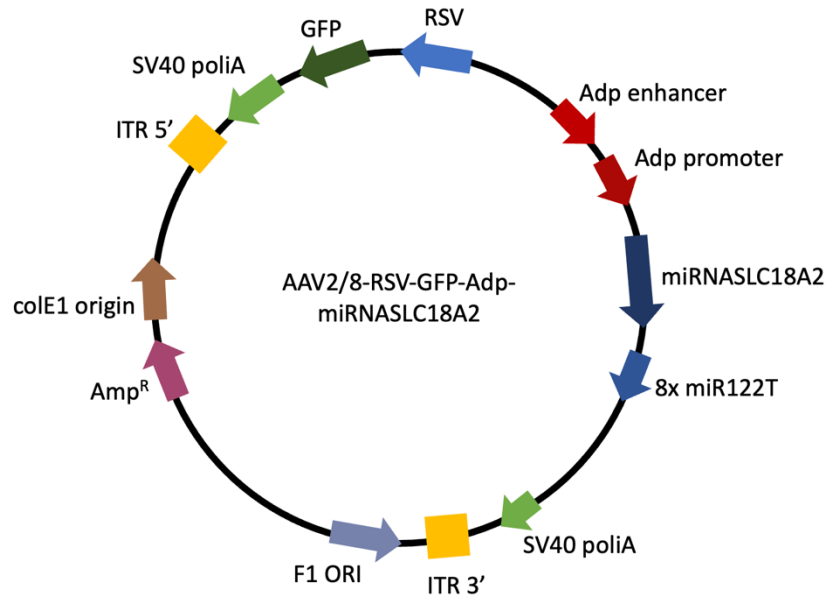
Figure 18 | AAV vector. Schematic of the AAV packaging plasmid used to down-regulate SLC18A2 gene expression. *Figure taken from Oliveras-Cañellas N (2023)* [347]

Body weight and food intake were monitored weekly throughout the protocol. All experiments were performed in the light phase. All procedures were performed in strict accordance with the guidelines of the European Comminities Directive 86/609/EEC on animal experimentation and were approved by the local ethical committee (Comitè Ètic d'Experimentació Animal – Parc de Recerca Biomèdica de Barcelona, CEEA – PRBB, agreement Nº 9687).

4.2.2.2 Experimental procedure

The time-course of the experiment was shown in **Figure 19**. Viral expression was estimated to occur for the next 4 weeks after AAV injection, in which behavioural tasks were then performed. Behavioural tasks to assess short- and LTM (Novel Object Recognition (NOR) in V-maze) and locomotor activity (horizontal and vertical activity assessment) were performed using standardized tests.
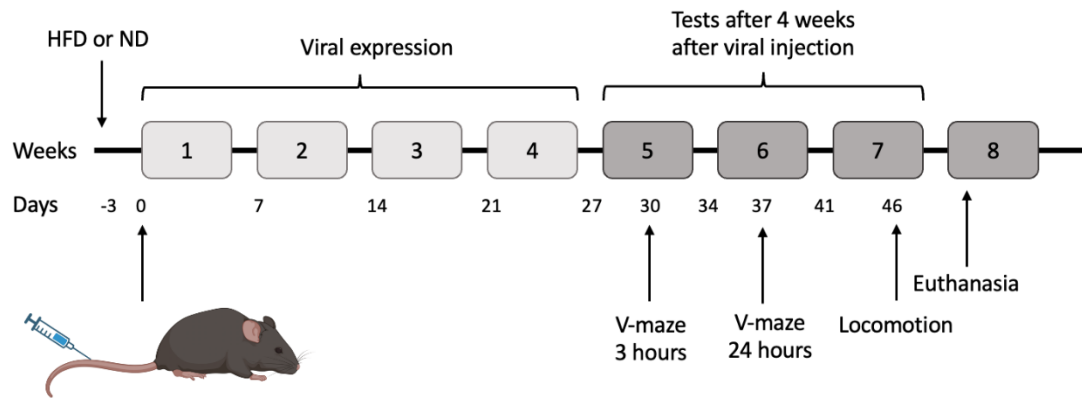
Figure 19 | Timeline of events and cognitive testing of mice. On day 0, mice were injected with AAV or saline. After 4 weeks, mice were started to done the cognitive test to assess short- and LTM, and locomotion. *Figure taken from Oliveras-Cañellas N (2023)* [347]

NOR memory was tested in a V-shaped maze (30 cm long x 4.5 cm wide x 15.3 cm heigh per corridor). On day 1 of the test, mice were habituated to the empty maze for 9 min. On the second day, mice were returned to the maze for 9 min, where 2 identical objects were presented, one at the end of each corridor, and the time the mice spent exploring each object was recorded. In the test phase, the mice were returned to the maze 3 hours after the training phase (30 days after the AAV injection) for STM, or 24 hours later (37 days after the AAV injection) for LTM, for 9 min, with one of the familiar objects was replaced by a novel object. The total time spent exploring each of the two objects (novel and familiar) was recorded. A discrimination index was calculated as the difference between the time spent exploring the novel object divided by the total time spent exploring both objects. A higher discrimination index is considered to reflect greater memory retention for the familiar object [352,353].

Locomotion activity was assessed using individual locomotor activity boxes (10.8 x 20.3 x 18.6 cm, Imetronic, Pessac, France) equipped with infrared sensors to detect horizontal activity and an infrared plane to detect rearing. Mice were placed in the boxes on day 46 after AAV injection. Horizontal activity (number of beam breaks) and rearing were recorded for 1 hour [354,355].

Mice were sacrificed by decapitation, and mesenteric WAT (mWAT) and inguinal AT (iWAT) were collected, and frozen with dry ice.

4.3 GENE EXPRESSION ANALYSIS

4.3.1 RNA extraction

Total RNA can be easily purified from animal (mouse or *Drosophila*) or human tissues or blood samples using an appropriate kit. The used RNeasy® Mini Kit (*QIAgen, Hilden, Germany*) was used for mouse and human tissues samples, the Tempus™ Spin RNA isolation Kit (*Applied Biosystems, California, USA*) for blood samples and the Arcturus™ PicoPure™ RNA Isolation Kit (*Applied Biosystems, California, USA*) for *Drosophila* samples. The procedure represents a well-established technology for RNA purification, combining phenol/guanidine-based sample lysis, silica-membrane-based and the speed of microspin technology.

4.3.1.1 *Human and Mice Adipose Tissue RNA Extraction*

Frozen AT samples (30 mg) were first lysed and homogenized in 1 mL of QIAzol® Lysis Reagent (*QIAgen, Hilden, Germany*) using a tissueLyser (*QIAgen, Hilden, Germany*) prior to RNA extraction. QIAzol Lysis Reagent is a monophasic solution of phenol and guanidine thiocyanate designed to facilitate lysis of AT and to inhibit ribonucleases (RNase). After homogenization, 0.2 mL of chloroform was added and the homogenate was separated into aqueous and organic phases by centrifugation (12,000 rpm, 15 min, 4 °C). RNA partitions to the upper aqueous phase, while DNA partitions to the interphase and proteins to the lower, organic phase. The upper, aqueous phase was extracted to a new RNase-free tube and a 1:1 volume of 100% ethanol was added to create a suitable condition to promote selective binding of RNA to the RNeasy membrane. The sample was then applied to the RNeasy Mini Spin column (*QIAgen, Hilden, Germany*), where the total RNA bound to the membrane. Phenol and other contaminants were efficiently washed away using wash buffers with reduced alcohol concentrations. Finally, high-quality RNA is eluted in RNase-free water.

In general, Deoxyribonuclease I (DNase) digestion is not required with the RNeasy Kit because the silica membrane technology efficiently removes most of the DNA without DNase treatment. However, for certain RNA applications, such as RNA-seq, further DNA removal may be required. In this case, residual DNA was removed by a DNase digestion using RNAse-Free DNase Set (*QIAgen, Hilden, Germany*). After one of the wash steps, the

RNA is treated with DNase I while bound to the RNeasy membrane. The DNase I is removed by subsequent washing steps.

4.3.1.2 Drosophila RNA Extraction

Heads or fat body of *Drosophila melanogaster* were collected and stored with RNA later (*Sigma, Misuri, USA*) while RNA extraction was not done. RNA later is an aqueous tissue storage reagent that rapidly permeates most tissues to stabilize and protect RNA in fresh tissues.

Total RNA from samples from *Drosophila melanogaster's* heads or fat body was purified using Arcturus™ PicoPure™ RNA Isolation Kit (*Applied Biosystems, California, USA*), which is designed to recover high-quality total RNA from pico-scale samples without compromising quality. RNA later was removed under microscope and whole heads or fat body were pestled into Eppendorf tubes containing 0.1 mL Extraction Buffer. The samples were immediately incubated in a water bath at 42 °C for 30 min. This was followed by a centrifugation step at 3,000 $x g$ for 2 min and 4 °C to spin down debris. A 1:1 volume of 70% ethanol was added to create a suitable condition for RNA to bind to the membrane. The sample was applied to the conditioned column, where the total RNA bound to the membrane thanks to a centrifugation step (100 $x g$ for 2 min, follow by a 16,000 $x g$ for 30 sec).

The sample was washed in several consecutive steps. Between washing steps 1 and 2, the sample was incubated at 25 °C with DNase I for 15 min to remove traces of bound DNA. Finally, elution buffer was added to elute the total RNA.

4.3.1.3 Peripheral blood mononuclear cell RNA Extraction

Total RNA from PBMC can be easily purified from 3 mL of human blood using the Tempus™ Spin RNA isolation Kit (*Applied Biosystems, California, USA*), which is collected directly into a Tempus™ Blood RNA Tube containing a proprietary reagent composition based on a patented RNA Stabilization Technology. This reagent composition protects RNA molecules from degradation by RNases and minimizes ex vivo changes in gene expression. Immediately after filling the tube, it is necessary to shake the tube vigorously for 10 seconds to ensure that the stabilizing reagent is mixed with the sample.

3 mL of blood sample were first mixed vigorously with the same volume of 1X PBS Calcium / Magnesium – free and centrifuge at 3,000 $x\,g$ for 30 min and 4 °C. After decanting the supernatant, the pellet was resuspended with 0.4 mL of RNA Purification Resuspension Solution and added to the purification filter, followed by a centrifugation step at 16,000 $x\,g$ for 30 seconds. Several washing steps were performed to remove contaminants and washed samples. Finally, the RNA was incubated with 0.1 mL of Nucleic Acid Purification Elution Solution for 2 min at 70 °C and centrifugated at 16,000 $x\,g$ for 2 min to elute the RNA.

4.3.2 RNA concentration, purity and integrity

The purity and concentration of the obtained RNA, independent of its origin, were estimated using the NanoDrop™ ND-Spectrophotometer (*ThermoFisher Scientific, Massachusetts, USA*). Nucleic acids absorb at 260 nm (A_{260}), proteins at 280 nm (A_{280}), and chemical substances, such as ethanol or salts at 230 nm (A_{230}). The $A_{260/230}$ and $A_{260/280}$ ratios are used to represent the relative abundance of different contaminants in the RNA sample. The accepted ranges of these ratios are within 1.7 and 2.0 for most common applications.

RNA integrity was checked using the Nano lab-on-a-chip assay for total eukaryotic RNA using bioanalyzer 2100 (*Agilent Technologies, California, USA*). It is useful for quantifying the degree of degradation of genomic material by measuring the major ribosomal subunits, 18S Ribosomal RNA and 28S Ribosomal RNA, measured by the RNA integrity number.

4.3.3 RNA sequencing

Samples were quantified using the Qubit® RNA Broad Range Assay Kit (*ThermoFisher Scientific, Massachusetts, USA*) and RNA integrity was estimated using the RNA 6000 Nano bioanalyzer 2100 Assay (*Agilent, California, USA*). RNA-seq libraries were prepared using Illumina® TruSeq® Stranded Total RNA Sample Preparation Kit according to the manufacturer's recommendations. Depending on availability (100 to 500 ng of total RNA), ribosomal RNA (rRNA) was removed from total RNA using the Ribo-Zero Magnetic Gold Kit. The remaining RNA was purified and fragmented into small pieces using divalent cations at an elevated temperature. The cleaved RNA fragments were then copied into first-strand cDNA using reverse transcriptase and random primers, followed by second-strand synthesis

in the presence of Deoxyuridine Triphosphate. The complementary DNA (cDNA) was adenylated by adding an adenine ('A') nucleotide to the 3' ends of the blunt fragments to prevent ligation during adapter ligation. The corresponding thymine ('T') nucleotide at the 3' end of the adapter provides a complementary overhang. cDNA was then ligated to Illumina platform-compatible, IDT, dual-index adapters with unique molecular identifiers (integrated DNA Technologies) for paired-end sequencing. The ligation products were enriched with 15 cycles of Polymerase Chain Reaction (PCR) and the final library was validated on an Agilent 2100 Bioanalyzer using the DNA 7500 assay (*Agilent, California, USA*).

Libraries were sequenced on NovaSeq 6000 (Illumina) in a fraction sequencing flow cell with a read length of 2 x 101 base pair following the manufacturer's protocol for dual indexing. Image analysis, base calling and run quality scoring were performed using the manufacturer's Real Time Analysis (RTA v3.4.4) software, followed by generation of FASTQ sequences files.

RNA-seq reads were mapped to the human reference genome (GRCh38) using Spliced Transcripts Alignment to a Reference (STAR) software version 2.5.3a [356] with ENCODE parameters. Genes were quantified using RNA-seq by Expectation Maximization (RSEM) version 1.3.0. [357] with default parameters and using the GENCODE version 29 annotation file. Only protein-coding genes expressed > 1CPM in at least 10 samples were considered for the association of gene expression with clinical variables.

4.3.4   Reverse Transcription

Total RNA was reverse transcribed (RT) to cDNA using the High-Capacity cDNA® Reverse Transcription Kit (*Applied Biosystems, California, USA*) according to the manufacturer's protocol. The kit contains all the reagents (10X RT Buffer, 10X RT Random Primers, 25X Deoxynucleotides Triphosphate (dNTP) Mix 100mM, MultiScribe™ Reverse Transcriptase 50 U/ μL and RNase Inhibitor) required to reverse transcribe up to 2 μg of total RNA to single-stranded cDNA in a 20 μL reaction. When these reagents are combined, the 2X Reverse Transcription Master Mix is ready for use (**Table 13**).

Table 13 | 2X Reaction Mix for cDNA synthesis. *N Oliveras-Cañellas (2024)*

RT Reaction Mix Components	Volume for One Sample (μL)
10X RT Buffer	2.0
25X dNTPs Mix (100mM)	0.8
10X RT Random Primers	2.0
MultiScribe™ Reverse Transcriptase	1.0
RNase Inhibitor	1.0
Nuclease-free H_2O	3.2
Total	**10.0**

The random primer method is used to initiate cDNA synthesis and to ensure that first strand synthesis is efficient with all types of RNA molecules present, including mRNA and rRNA. The retrotranscription reaction consists of two steps, one of melting or association of complementary sequences (primers with mRNAs molecules) for 10 min at 25 °C, and another of elongation of the sequences and degradation of the mRNA molecules, controlled by the action of the enzyme retrotranscriptase, for 120 min at 37 °C (**Table 14**). The last step consists of incubation at 85 °C for 5 min to stop the reaction. The cDNA obtained was stored at -20 °C until use.

Table 14 | Thermal cycling conditions for cDNA synthesis. *N Oliveras-Cañellas (2024)*

	Step 1	Step 2	Step 3	Step 4
Temperature	25 °C	37 °C	85 °C	4 °C
Time	10 min	120 min	5 min	∞

4.3.5 Quantitative Polymerase Chain Reaction

Using sequence-specific primers and DNA polymerases, the target cDNA can be amplified by quantitative Polymerase Chain Reaction (qPCR). The amount of cDNA is measured after each cycle using fluorescent dyes that give an increasing fluorescent signal proportional to the number of molecular PCR products produced, called amplicons. qPCR consists of three main steps:

The first step of qPCR consists of a denaturation phase in which high temperature incubation is used to convert double-stranded DNA into single-stranded DNA, which loses its secondary structure. The highest temperature the DNA polymerase can withstand without losing efficiency is around 95 ºC. In the second step, complementary sequences of single-stranded DNA and primers are hybridized. An appropriate temperature is used based on the melting temperature of the primers (usually 5 ºC below the melting temperature of the primers). The final step is primer extension at rates of up to 100 bases per second, with optimal DNA polymerase activity at 70 – 72 ºC.

The double-stranded DNA intercalating agent SYBR Green® and the TaqMan® hydrolysis probes are two chemistries used to detect the qPCR product. The SYBR Green® method is based on the binding of a fluorescent dye to double-stranded DNA. During qPCR amplification, SYBR Green dye binds to all double-stranded amplicons and produces fluorescence signal. As qPCR progresses, more qPCR product is produced, resulting in an increase in fluorescence intensity proportional to the amount of qPCR product produced accumulating fluorescent signal.

Otherwise, TaqMan method is based on 5' nuclease chemistry and each assay contain a primer and probe set for each target of interest. The hydrolysis probe is constructed with a fluorescent dye at 5' and a suppressor dye at 3'. While the probe is intact, before qPCR begins, the proximity of the suppressor dye blocks the fluorescence emitted by the fluorescence dye by fluorescence resonance energy transfer. The first step of qPCR takes place at higher temperatures to denature the double-stranded cDNA. Immediately after this, the temperature is lowered to allow primers and probes to anneal to their target sequences and DNA polymerase synthesize a complementary strand of DNA. If the TaqMan probe is annealed to the correct target sequence, the polymerase's 5' endonuclease activity cleaves the probe, releasing a fragment containing the fluorescent dye, which anneals to the suppressor dye. This results in an increase in fluorescence intensity proportional to the amount of cDNA accumulate in each qPCR cycle.

Both methods were used for gene expression analysis using LightCycler® Real Time PCR System (*Roche Diagnostics, Barcelona, Spain*), with pre-validated TaqMan gene probe sets (*ThermoFisher Scientific, Massachusetts, USA*) or gene-specific primers pairs (*Sigma-Aldrich, Missouri, USA*).

TaqMan (**Table 15**) and SYBR Green (**Table 16**) LightCycler® Master Mixes are ready-to-use reaction mix specially designed for hydrolysis probe-based assays and SYBR Green detection to be run in multiwell plates on the LightCycler® 480 instrument. Both contain FastStart Taq DNA Polymerase for hot start PCR, which significantly improves the specificity and sensitivity of qPCR by minimizing the formation of non-specific amplification products at the beginning of the reaction.

Table 15 | Reaction Mix for Taqman qPCR. *N Oliveras-Cañellas (2024)*

Mix Components	Volume for One Well (µL)
LightCycler® Taqman® Master	3.3
Taqman® hydrolysis probe	0.3
Nuclease-free water	1.3
cDNA	2.0
Total	**7.0**

Table 16 | Reaction Mix for SYBR Green qPCR. *N Oliveras-Cañellas (2024)*

Mix Components	Volume for One Well (µL)
LightCycler® SYBR® Green I Master	5.0
Primers (Forward + Reverse)	0.8
Nuclease-free water	3.2
cDNA	1.0
Total	**9.0**

Relative expression values are given for each gene and each sample as the number of times the target gene is expressed relative to an endogenous control. An endogenous control, also known as a housekeeping reference gene, is defined as a gene whose expression is not altered by the parameters under study. As endogenous controls, Glyceraldehyde-3-phosphate Dehydrogenase (GAPDH) and Peptidylprolyl isomerase A (PPIA or cyclophilin) were used

for human samples (circulating and AT, respectively); β-actin (*Actb*) for mice samples; and RNA polymerase II (*RNApol2*) and γ-tubulin23 (*1tub23cf*) for *Drosophila* samples [358].

During qPCR, each sample produces a sigmoidal curve for all the genes studied and a level of fluorescence determined for each Ct at over the 45 amplification cycles (**Table 17** for TaqMan qPCR and **Table 18** for SYBR Green qPCR). From the curves, we can determine the threshold, which are the number of cycles required to achieve an arbitrary fluorescence value. The Ct value is defined as the number of cycles in which the fluorescent signal from the reaction crosses the threshold and is inversely proportional to the number of copies of the original transcript. Therefore, the greater the number of copies, the fewer Ct values are required to reach the threshold.

Table 17 | Thermal cycling conditions for running quantitative qPCR Taqman. *N Oliveras-Cañellas (2024)*

Stage	Temperature	Time
Pre-incubation	95 °C	10 min
Amplification (45 cycles)	95 °C	10 sec
	60 °C	30 sec
Cooling	40 °C	30 sec

Table 18 | Thermal cycling conditions for running qPCR SYBR Green. *N Oliveras-Cañellas (2024)*

Stage	Temperature	Time
Pre-incubation	95 °C	10 min
Amplification (45 cycles)	95 °C	10 sec
	60 °C	10 sec
	72 °C	10 sec
Melting Curve	95 °C	5 sec
	65 °C	
	97 °C	1 min
Cooling	40 °C	30 sec

Differential gene expression was calculated using the $2^{-\Delta\Delta Ct}$ method ($\Delta\Delta Ct = \Delta Ct$ sample – ΔCt endogenous control) [359] and indicates the number of times the target gene is expressed relative to an endogenous control. The mean Ct value for each sample was calculated from the geometric mean Ct value of the corresponding reference gene to calculate the ΔCt value.

The commercially available and pre-validated TaqMan primer/probe sets used and the pre-designed KiCqStart® primers are listed in **Table 20** and **Table 21** Annex I. For *Drosophila* samples, a minimum of 5 biological replicates and two technical replicates were analysed.

4.4 PROTEIN ANALYSIS

4.4.1 Protein Extraction

Frozen mice AT samples (100 mg) were homogenized with Ultraturrax using Radioimmunoprecipitation lysis buffer system (sc-24948, *Santa Cruz Biotechnology, CA*) with a 1:100 dilution of phenylmethylsulfonyl fluoride, protease inhibitor cocktail and sodium orthovanadate at 4 ℃ for 30 min. Cellular debris was removed by centrifugation at 13,000 *x g* for 15 min at 4 ℃. Protein concentrations were then measured from the supernatants using the reducing agent and detergent compatible protein assay (RC/DC™ Protein Assay) (*Bio-Rad Laboratories, Hercules, CA*). This is a colorimetric assay based on the Lowry protocol that measures the total protein concentration at 750 nm in comparison with a known concentration of bovine serum albumin (BSA, *Sigma-Aldrich, Missouri, USA*).

4.4.2 Western blot analysis

Equal amounts of total proteins were subjected to electrophoresis on 4-20% precast polyacrylamide gels (#4568096, *Bio-Rad Laboratories, Hercules, CA*), which separate proteins according to their molecular weight. After separation, proteins were transferred from the polyacrylamide gel to a 0.45 µm Low Fluorescence polyvinylidene fluoride membrane (*Bio-Rad Laboratories, Hercules, CA*).

The membrane was blocked with 5% of BSA in Tris-Buffered Saline (TBS) for 1 h, followed by an overnight incubation at 4 ℃ with primary antibody Vesicle monoamine transporter member 2 (VMAT2) / Synaptic Vesicle Monoamine Transporter (SLC18A2) at a 1:250 dilution (EB06558, *VWR International EuroLab, SL*) diluted in 2% BSA – 1x TBS containing 0.1% Tween-20, according to the manufacturer's recommendations. After incubation with secondary antibody (Anti-Goat horsedish peroxidase (HRP), HAF019, *R&D Systems, Minneapolis, USA*), the blot signal was detected using enhanced chemiluminescence HRP substrate (*Millipore, Massachussetts, USA*) and analysed with a luminescent image analyser ChemiDoc MP Imaging System (*Bio-Rad Laboratories, California, USA*). Tris-Glycine eXtended Stain-Free gels (#4568096, *Bio-Rad laboratories, California, USA*) were used as a protein loading control. Signals were quantified using Image J software (*https://imagej.nih.gov/ij/*).

4.4.3 Enzyme-Linked ImmunoSorbent Assay

Enzyme-linked immunosorbent assays (ELISA) is an immunological test based on the interaction between antigens and antibodies. It is used to measure antibodies, antigens, proteins, hormones and glycoproteins in biological samples. There are several variations of an ELISA assay, depending on whether antibodies or antigens are being tested, but they all share the same basic elements.

First, a surface plate is coated with a known amount of capture antibody raised against the antigen of interest. After an overnight incubation at 4 ℃, the plate was washed to remove any excess of unbound antibody and blocked with BSA to cover any unsaturated surface-binding sites.

Samples were added to the plate and any antigen present in the samples will bind to the capture antibody already coated on the plate. After incubation, excess sample is washed off the plate. Detection antibody labelled with an enzyme, usually HRP, has been added and will bind to any target antigen already bound to the plate. After incubation with the antibody, its excess was washed off the plate.

The final steps involved the addition of a substrate, usually 3,3',5,5'-Tetramethylbenzidine (TMB), which the enzyme uses to convert into a coloured product. This product can be measured using a plate reader to obtain the absorbance and determine the presence and amount of antigen.

To determine the concentration of antigen in a sample, a standard curve must be constructed using antigens of known concentration. The standard curve is then plotted from serial dilution data with concentration on the x-axis using a logarithmic scale and absorbance on the y-axis using a linear scale to obtain the concentrations of unknown samples.

The incubation time of each step depends on the type of ELISA and the manufacturer's protocol.

Plasma EDTA samples from the FATBANK cohort and Ironmet cohort were used to measured concentrations of Adiponectin (ADIPOQ), IL-6, IL-4, α-synuclein, Amyloid β (aa 1-42) (Aβ42) and Tau (**Table 19**) according to the manufacturer's instructions.

Table 19 | Commercial information of the ELISA's used. *N Oliveras-Cañellas (2024)*

Marker	Kit Name	Cohort used	Trading House
Adiponectin	Human Adiponectin ELISA Kit	Adipomit	RD191023100 (*BioVendor, Brno, Czech Republic*)
IL- 6	Human IL-6 Quantikine HS ELISA Kit	Ironmet	RND-HS600C (*R&D Systems, Minneapolis, USA*)
IL- 4	Human IL-4 Quantikine HS ELISA Kit	Ironmet	RND-HS400 (*R&D Systems, Minneapolis, USA*)
α-Synuclein	Human α-synuclein DuoSet ELISA	Ironmet	RND-DY1338-05 (*R&D Systems, Minneapolis, USA*)
Aβ 42	Human Aβ (amino acids 1 to 42) Quantikine ELISA Kit	Ironmet	RND-DAB142 (*R&D Systems, Minneapolis, USA*)
Tau	Human Tau ELISA Kit	Ironmet	NBP2-62749 (*Novus Biologicals, Centennial, USA*)

4.5   METABOLOMICS ANALYSIS

High Performance Liquid Chromatography (HPLC) – Electrospray Ionization (ESI-) – Tandem Mass Spectrometry (MS/MS) and Plasma Proton Nuclear Magnetic Resonance (^{1}H NMR) were used to analysed metabolites present in plasma samples from the Ironmet cohort. HPLC – ESI – MS/MS and ^{1}H NMR are complementary techniques; both provide information on metabolic intermediate and/or end products.

4.5.1   HPLC – ESI – MS/MS

Metabolites were extracted from plasma samples using methanol with phenylalanine-C13 as internal standard, as previously described by Wikoff et colleagues [360]. Briefly, 30 µL of cold methanol was added to 10 µL of each sample, vortexed for 1 min and incubated for 1 h at 20 ºC. Samples were homogenized using FastPrep-24 (*MP Biomedicals, California, USA*) and incubated o/n in a rocker at 4 ºC. All samples were then centrifugated at 12,000 g for 3 min and the supernatant was collected and filtered through a 0.2 µm Eppendorf filter. 2 µL of the extracted sample was applied to a reversed-phase column (Zorbax SB-Aq 1.8 µm, 2.1 x 50 mm; *Agilent Technologies, California, USA*) equipped with a precolumn (Zorbax – SB – C8 Rapid Resolution Catridge 2.1 x 30 mm; 3.5 µm; *Agilent Technologies, Califrornia, USA*) at a column temperature of 60 ºC. The flow rate was 0.6 mL/min. Solvent A was water containing 0.2% acetic acid and solvent B was methanol containing 0.2% acetic acid. The gradient started at 2% B, increased to 98% B in 13 min and was maintained at 98% B for 6 min, with a post-time of 5 min.

Data were collected in positive and negative electrospray time-of-flight modes operated in full scan mode from 50 to 3000 mass/charge ratio in an extended dynamic range (2GHz) using N2 as the nebulizer gas (5 liters/min at 350 ºC). The capillary voltage was 3500 V with a scan rate of 1 scan/s. The ESI source used a separate nebulizer for continuous low-level (10 liters/min) introduction of reference mass compounds 121.050873 and 922.009798, which were used for continuous online mass calibration. MassHunter Data Analysis software (*Agilent Technologies, Barcelona, Spain*) was used to collect the results, and MassHunter Qualitative Analysis software (*Agilent Technologies, Barcelona, Spain*) was used to obtain the molecular features of the samples, representing different ionic species of a given molecular entity, using the Molecular Feature Extractor algorithm (*Agilent Technologies, Barcelona, Spain*).

Samples with a minimum of two ions were selected. Multiple charge states were not allowed. Compounds from different samples were aligned using a retention time window of 0.1% ± 0.25 min and a mass window of 20.0 parts per million ± 2.0 mDa. Only those present in at least 50% of the samples in a group were selected and corrected for individual bias.

4.5.2 ^{1}H NMR

Plasma samples were thawed at room temperature. For each sample, 400 μL of plasma was combined with 200 μL of phosphate buffer [9% (w/v) NaCl and 100% D_2O] containing 10 mM of 3-trimethyl-silyl-1-[2,2,3,3,-^{2}H4] (TSP) (cell, cell host). Samples were mixed by vortexing and centrifuged at 10,000 g for 10 min. After which a 550 μL aliquot was transferred to a 5 mm NMR tube for NMR analysis.

^{1}H spectra of low-molecular weight metabolites were acquired using a Carr-Purcell-Meiboom-Gill (CPMG) sequence (RD-90º-[t-180º-t]$_n$-ACQ-FID) with a spin-echo delay of 400 μs (for a total T2 filter of 210 ms), which allows efficient attenuation of the lipid NMR signals. The CPMG sequence produces spectra processed by T2 relaxation times, reducing broad resonances from high-molecular weight compounds and facilitating the observation of low-molecular weight metabolites. The total acquisition time was 2.73 s with a Recycling Delay (RD) of 2s, and the 90º pulse length was automatically calibrated for each sample at approximately 11.1 μs. For each sample, 8 dummy scans were followed by 256 scans and collected in 64,000 points over a spectral width of 20 ppm. TSP was used as a general reference for NMR samples as it does not introduce any additional signals apart from the sharp methylsilyl resonance at 0 ppm. In addition, a high concentration of TSP was used to release low-weight metabolites with high affinity for serum proteins by binding competition with TSP.

All ^{1}H NMR spectra were recorded at 300 K on an Avance III 600 spectrometer (*Bruker, Germany*) operating at a proton frequency of 600.20 MHz using a 5 mm Broad Band Multinuclear gradient probe and an automatic sample loader with a cooling rack at 4 ºC.

4.6 STATISTICAL ANALYSIS

Normal distribution and homogeneity of the variances were first assessed using Kolmogorov-Smirnov test and Levene's test, respectively. For normally distributed continuous variables, results were presented as mean ± standard error of the mean (SEM); for non-normal distributed continuous variables, results were presented as median ± interquartile range.

The unpaired T-test was used to determine whether the means of two sets of data were significantly different. ANOVA for multiple comparisons was used to compare groups with respect to continuous variables, with post hoc by Bonferroni or Newman-keuls least significant difference (LSD) procedures for two-by-two comparisons.

Bivariate model using the Spearman test were used to determine the lineal relationship between quantitative variables. Multiple regression is a statistical technique that uses multiple explanatory variables to predict the outcome of a response variable. The aim was to model the linear relationship between the explanatory (independent) variables and the response (dependent) variables. Here we used multiple linear regression to assess the contribution of environmental temperatures to the variance in the expression of several genes, taking into account the effect of age, gender, BMI, etc.

Level of significance was set at p-value < 0.05. Statistical analyses were performed using SPSS (*SPSS v21 Inc., Illinois, USA),* GraphPad Prism 8.0 (*Graphpad Software, California, USA*) and R Statistical Software (http://www.rproject.org/).

4.6.1 Specific statistical procedures

4.6.1.1 *RNA-Seq analysis*

Differential expression gene (DEG) analysis was performed on gene counts using the "limma" R package [361]. First, low expressed genes were filtered to select only genes with more than 10 reads in at least two samples. The RNA-seq data were then normalized for RNA composition using the trimmed mean of the *M*-value, as implemented in the edgeR package [362]. The normalized counts were then converted to $\log_2$ count per million (CPM) with associated precision weights to account for variation in precision between different

observations using the "voom" function with donor age, BMI, sex and years of education as covariates.

A robust linear regression model adjusted for the previous covariates was then fitted to the data using the "lmFit" function with the method = "robust" option to limit the influence of outlying samples. Finally, an empirical Bayes method was applied to borrow information between genes with the function "eBayes".

P values were adjusted for multiple comparisons using the False Discovery Rate (pFDR) procedure and statistical significance was set at pFDR of < 0.05.

The functional roles of differentially expressed genes were characterized using over-representation analyses based on the Reactome and WikiPathways databases using ConsensusPathDB [363]. Pathway significance was assessed using a hypergeometric test, and a Storey procedure (q value) was applied to correct for multiple testing. Statistical significance was set at a q value < 0.1.

For differentially expressed genes simultaneously in different samples, data were further analyzed using functional gene-gene interaction networks, in which genes were mapped to the Search Tool for Retrieval of Interacting Proteins/Genes (STRING) database (which integrates known and predicted protein/gene interaction) [364]. Functional local clusters in the interaction network were then determined using a Markov cluster algorithm with an inflation parameter =1.4. Active interacting sources, including text mining, experiments, databases, co-expression and co-occurrence, and an interaction score of >0.4 were used to construct the interaction networks. In addition, we integrated the information provided by differential expression analysis, gene-gene interaction networks, and pathway overrepresentation analysis using the R package "pathfinder" with default parameters [365].

After mapping significant genes onto a STRING gene-gene interaction network, active subnetworks of connected genes (including genes that are not significant themselves but connect significant genes) were identified in this gene-gene interaction network. Finally, separate pathway over-representation analyses based on the Reactome databases were performed for each active subnetwork, using the significant genes in each of the active subnetworks and genes in the Protein-protein Interaction Network as background genes. Statistical significance of pathways was set at the pFDR <0.05. Significantly enriched pathways were clustered using hierarchical clustering. Genes in each pathway were used to

calculate the pairwise kappa statistic, a chance-corrected measure of co-occurrence between pathways. The distance matrix 1 - kappa statistic was used for agglomerative hierarchical clustering, and a threshold of 0.35 for the kappa statistic was used to define a strong relationship.

Partial Spearman's correlation analysis, controlling for age, BMI, sex, and education level, was used to determine the correlation between circulating levels of genes and the neurocognitive tests scores. As it works by obtaining the residuals of the ranked variables after removing the effect of the ranked covariates, scatter plots and violin plots were generated with the ranked residuals of the model adjusted for selected covariates. Nonparametric monotonic trends according to the gene tertiles or quintiles for the selected cognitive tests were assessed using the Mann-Kendall trend test.

4.6.1.2   Machine Learning Algorithm (Boruta)

We used machine learning (ML) algorithm to identify the most relevant clinical variables related to metabolic variables and AT gene expression markers, and to analyse the metabolomics data. Specifically, an all-relevant ML variable selection strategy was adopted using a random forest (RF)-based methods as implemented in the Boruta algorithm [366].

The Boruta algorithm is a wrapped algorithm that performs feature selection based on the learning performance of the model [366]. It has recently been proposed as one of the two best-performing variable selection methods use of RF. It performs variable selection in several steps:

i) Randomization, which is based on creating a duplicate copy of the original features that are randomly permutate across the observations to remove their correlation with the response.

ii) Model building. To add the shadow feature to the original predictor feature dataset, an RF is built with the extended dataset, and the normalized permutation importance (Z) scores for each predictor and shadow feature are compute.

iii) Statistical testing to find the maximum normalized importance among shadow attributes (MZSA) and compare it to each original predictor feature using a Bonferroni-corrected two-tailed binomial test. Predictor features with significantly higher, significantly lower or nor

significantly different Z-scores than expected by chance compared to the MZSA are considered important, unimportant, or tentative, respectively.

iv) Iteration, unimportant and shadow features are removed, and the previous steps are repeated until the status of all features is decided or a predefined number of iterations have been performed.

We run the Boruta algorithm with a maximum of 1000 iterations, a confidence level cut-off of 0.005 for the Bonferroni adjusted p-values, 5000 trees to grow the forest (ntree), and several features randomly sampled at each split given by one third of the number of features (the mtry recommended for regression analysis). The ranger's choice on "respect unordered factors" was set to true in order to include both quantitative and categorical variables as predictors in the model.

5. RESULTS

The results of this thesis are included in the following publications:

Manuscript I

<u>Oliveras-Cañellas N</u>*, Castells-Nobau A*, de la Vega-Correa L*, Latorre-Luque J, Motger-Albertí A, Arnoriaga-Rodriguez M, Garre-Olmo J, Zapata-Tona C, Coll-Martínez C, Ramió-Torrentà L, Moreno-Navarrete JM, Puig J, Villarroya F, Ramos R, Casadó-Anguera V, Martín-García E, Maldonado R, Mayneris-Perxachs J, Fernández-Real JM. **Adipose tissue coregulates cognitive function.** Sci Adv. 2023 Aug 11; 9(32):eadg4017. doi: 10.1126/sciadv.adg4017

Impact factor (JCR 2022): 13.6 (D1, 7/73 Multidisciplinary Sciences)

Manuscript II

<u>Oliveras-Cañellas N</u>, Moreno-Navarrete JM, Lorenzo PM, Garrido-Sánchez L, Becerril S, Rangel O, Latorre J, de la Calle Vargas E, Pardo M, Valentí V, Romero-Cabrera JL, Oliva-Olivera W, Silva C, Diéguez C, Villarroya F, López M, Crujeiras AB, Seoane LM, López-Miranda J, Frühbeck G, Tinahones FJ, Fernández-Real JM. **Downregulated adipose tissue expression of browning genes with increased environmental temperatures.** J Clin Endocrinol Metab. 2023 Dec 21; 109(1):e145-e154. doi: 10.1210/clinem/dgad469

Impact factor (JCR 2022): 5.8 (Q1, 31/145 Endocrinology & Metabolism)

5.1 ORIGINAL PAPER I

Adipose tissue coregulates cognitive function

Oliveras-Cañellas N*, Castells-Nobau A*, de la Vega-Correa L*, Latorre-Luque J, Motger-Albertí A, Arnoriaga-Rodriguez M, Garre-Olmo J, Zapata-Tona C, Coll-Martínez C, Ramió-Torrentà L, Moreno-Navarrete JM, Puig J, Villarroya F, Ramos R, Casadó-Anguera V, Martín-García E, Maldonado R, Mayneris-Perxachs J, Fernández-Real JM.

NEUROSCIENCE

Adipose tissue coregulates cognitive function

Núria Oliveras-Cañellas[1,2,3,4]†, Anna Castells-Nobau[1,2,3,4]†, Lisset de la Vega-Correa[1,2,3,4]†, Jessica Latorre-Luque[1,2,3,4], Anna Motger-Albertí[1,2,3], Maria Arnoriaga-Rodriguez[1,2,3], Josep Garre-Olmo[5], Cristina Zapata-Tona[1,2], Clàudia Coll-Martínez[6], Lluís Ramió-Torrentà[4,6,7], José Maria Moreno-Navarrete[1,2,3], Josep Puig[8], Francesc Villarroya[3,9], Rafel Ramos[4,10], Verònica Casadó-Anguera[11,12], Elena Martín-García[11,12], Rafael Maldonado[11,12], Jordi Mayneris-Perxachs[1,2,3]‡*, José Manuel Fernández-Real[1,2,3,4]‡*

Obesity is associated with cognitive decline. Recent observations in mice propose an adipose tissue (AT)–brain axis. We identified 188 genes from RNA sequencing of AT in three cohorts that were associated with performance in different cognitive domains. These genes were mostly involved in synaptic function, phosphatidylinositol metabolism, the complement cascade, anti-inflammatory signaling, and vitamin metabolism. These findings were translated into the plasma metabolome. The circulating blood expression levels of most of these genes were also associated with several cognitive domains in a cohort of 816 participants. Targeted misexpression of candidate gene ortholog in the *Drosophila* fat body significantly altered flies memory and learning. Among them, down-regulation of the neurotransmitter release cycle–associated gene *SLC18A2* improved cognitive abilities in *Drosophila* and in mice. Up-regulation of *RIMS1* in *Drosophila* fat body enhanced cognitive abilities. Current results show previously unidentified connections between AT transcriptome and brain function in humans, providing unprecedented diagnostic/therapeutic targets in AT.

INTRODUCTION

There is an increased awareness that peripheral tissues modulate brain function shaping different cognitive domains. Recent studies in rodents revealed that restoring glucose metabolism of myeloid cells reversed cognitive decline in aging (*1*), whereas selective gastrointestinal vagal afferent ablation impaired hippocampus-dependent episodic and spatial memory in rats (*2*). The liver has also been proposed to play a major role in regulating feeding behavior in mice (*3*).

Obesity is associated with increased risk of cognitive impairment (*4*, *5*). An increased fatness in middle-aged adults (<65 years) predicts decreased cognitive abilities in late life, mainly memory, executive functioning, and learning (*6–8*). However, the precise mechanisms involved remain largely unknown.

The brain regulates adipose tissue performance. For instance, sympathetic neuroadipose connections mediate lipolysis (*9*) and cytokine production (*10*), while neuroimmune interactions are involved in thermoregulation (*11*). Recent observations in rodents show that adipose tissue also regulates brain function. Genetically modified mice engineered to release the peptide NaKtide in adipocytes led to improved hippocampal memory through the inhibition of Na- and K-dependent adenosine triphosphatase (Na,K-ATPase) signaling in adipocytes (*12*). Visceral adipose NLR family Pyrin Domain Containing 3 (NLRP3) was linked to impaired memory in obese mice via interleukin-1R1 (IL-1R1) on CX3CR1+ cells, leading to microglial activation (*13*). An increased abundance of beige adipocytes in subcutaneous fat restored hippocampal synaptic plasticity in mice through induction of anti-inflammatory cytokine IL-4, protecting from obesity-induced cognitive impairment (*14*).

We have investigated in humans and animal models the mechanisms involved in the bidirectional interactions between adipose tissue gene expression and cognitive abilities. An RNA sequencing (RNA-seq) analysis of adipose tissue identified genes associated with different cognitive domains in discovery and different validation human cohorts. The gene expression of those genes most consistently associated with a battery of neuropsychological tests was then targeted in the fat body of *Drosophila* and in adipose tissue of mice to evaluate the possible functional implications. Last, we studied the expression of several of these genes in peripheral blood mononuclear cells (PBMCs) in association with cognitive traits in humans.

RESULTS

Adipose tissue gene expression is linked to several cognitive domains

To gain insights into the fat-brain axis, we performed a transcriptomics analysis (RNA-seq) of visceral adipose tissue (VAT) from 17

[1]Department of Diabetes, Endocrinology and Nutrition, Dr. Josep Trueta University Hospital, Girona, Spain. [2]Nutrition, Eumetabolism and Health Group, Girona Biomedical Research Institute (IdibGi), Girona, Spain. [3]CIBER Fisiopatología de la Obesidad y Nutrición (CIBERobn), Instituto de Salud Carlos III, Madrid, Spain. [4]Department of Medical Sciences, School of Medicine, University of Girona, Girona, Spain. [5]Department of Nursing (Serra-Hunter Professor), University of Girona, Girona, Spain. [6]Neuroimmunology and Multiple Sclerosis Unit, Department of Neurology, Dr. Josep Trueta University Hospital, Girona, Spain. [7]Girona Neurodegeneration and Neuroinflammation Group, Girona Biomedical Research Institute (IdibGi), Girona, Spain. [8]Department of Radiology (IDI), Girona Biomedical Research Institute (IdIBGi), Dr. Josep Trueta University Hospital, Girona, Spain. [9]Department of Biology, University of Barcelona, Barcelona. Spain. [10]Vascular Health Research Group of Girona (ISV-Girona), Jordi Gol Institute for Primary Care Research (Institut Universitari per a la Recerca en Atenció Primària Jordi Gol I Gorina -IDIAPJGol), Girona, Spain. [11]Laboratory of Neuropharmacology-Neurophar, Department of Medicine and Life Sciences, Universitat Pompeu Fabra (UPF), Barcelona, Spain. [12]Hospital del Mar Medical Research Institute (IMIM), Barcelona, Catalonia, Spain.

*Corresponding author. Email: jmayneris@idibgi.org (J.M.-P.); jmfreal@idibgi.org (J. M.F.-R.)

†These authors contributed equally to this work.

‡These authors contributed equally to this work.

subjects with severe obesity [body mass index (BMI) > 35 mg/kg^2] aged 28 to 60 years (table S1). Ten different cognitive tests assessed the functional performance of three cognitive domains: memory, executive function, and attention. The tests and their interpretation are shown in Materials and Methods.

Following normalization by trimmed mean of M value and calculating weights to account for variations in precision between observations, we fitted robust linear regression models with empirical Bayes moderation of the standard errors to identify gene transcripts associated with each cognitive test score controlling for age, sex, BMI, and years of education, all confounding factors know to affect cognitive function. There are other lifestyle-related factors known to cause or contribute to cognitive function such as physical activity, diet, or alcohol use (15). However, we found no significant associations of any of the 10 cognitive tests with physical activity (table S2), macronutrients, alcohol intake, glycemia, or hemoglobin A1c (fig. S1). Note that all subjects had morbid obesity (table S1).

We observed significant associations with gene transcripts in all cognitive tests at Benjamini-Hochberg procedure for false discovery rate (pFDR) of <0.05 (Fig. 1; fig. S2, A and B; and tables S3 to S12). Among these genes, *NUDT2*, *AMPH*, *UNC5B*, and *OAT* were those with most significant associations across the different cognitive domains (significant in seven, six, six, and eight cognitive tests at pFDR of <0.05, respectively). The attributed action of the proteins encoded by these genes was concordant with their function in the central nervous system (CNS), but their expression in adipose tissue in association with cognition is unprecedented. Variants in the *NUDT2* gene have been recently associated with intellectual disability (16, 17). *AMPH* encodes for a protein highly concentrated in presynaptic terminals (18) and is one of the six proteins altered in the cerebrospinal fluid of patients with mild cognitive impairment and Alzheimer's disease (19). *Amph* in *Drosophila* is an important postsynaptic protein that regulates the location of key components of glutamatergic signaling and dendrite dynamics, maturation, and synaptogenesis (20, 21). *OAT* is the gene that encodes for the enzyme ornithine aminotransferase (OAT), which plays a key role in transforming ornithine and arginine into glutamate and γ-aminobutyric acid as well as major excitatory and inhibitory neurotransmitters, respectively (22). In addition, genes involved in tryptophan metabolism such as *KYNU*, *QPRT*, and *INMT* were among the most significant genes associated with inhibitory control (Fig. 1A), attention (fig. S2A), and executive function (Fig. 1B). Consistently, subjects with obesity had impaired memory and inhibitory control through alterations in tryptophan metabolism (23, 24).

To facilitate interpretation and identify relevant adipose tissue pathways associated with cognitive function, we next performed overrepresentation analyses mapping significant genes to the Reactome and WikiPathways databases included in the ConsensusPathDB. We found an overrepresentation of pathways with important role in the CNS associated with measurements of inhibitory control, working memory, immediate memory, and attention (Fig. 1, D to F; fig. S2, C to F; and tables S13 to S17). Executive function was associated with axon guidance, nervous system development, synaptic vesicle pathway, and signaling by receptor tyrosine kinases (Fig. 1D). The neuronal system and the serotonin and dopamine neurotransmitter release cycles were the most significant pathways associated with immediate memory (Fig. 1E) and attention. The axon guidance and the nervous system development

were also overrepresented in the inhibitory control (Fig. 1F) and attention domains (fig. S2C). Semaphorin signaling and interactions (Fig. 1F), which play an important role in adult neuronal plasticity (25), were associated with inhibitory control, while alterations in complement activation were linked to executive function. We also found an overrepresentation of pathway involved in inflammation associated with the different cognitive domains. Hence, alterations in both notch signaling and complement activation were significantly associated with working memory (Fig. 1D).

Adipose tissue gene expression was associated with several cognitive functions later in life

We next sought to validate these results performing an RNA-seq of both VAT and subcutaneous adipose tissue (SAT) in an independent longitudinal cohort of 22 subjects with severe obesity aged 23 to 57 years that underwent the same battery of cognitive tests (table S1). Patients from this cohort underwent the same battery of cognitive tests that patients in the discovery cohort. However, in this case, the cognitive testing was performed 2 to 3 years after the collection of adipose tissue samples. Once more, we did not find any significant association of physical activity, diet, alcohol intake, glucose, or hemoglobin A1c levels (fig. S1). Thus, models were adjusted for age, sex, BMI, and education years. We again found significant genes associated with all cognitive test at a pFDR of <0.05 both in VAT (Fig. 2, A to C, and tables S18 to S28) and in SAT (fig. S3 and tables S29 to S37). Consistent with the previous results, enrichment analyses highlighted an overrepresentation of pathways with important roles in the CNS (tables S38 to S40). Axon guidance, nervous system development, neuronal system, and tryptophan (Fig. 2, D and E) were replicated as the pathways most significantly associated with attention (Fig. 2, D and E), while semaphorin signaling was associated with inhibitory control (Fig. 2F). The activation of the complement system in VAT was again strongly associated with the performance in several cognitive domains (Fig. 2, D to F). In SAT (tables S41 to S43), pathways related to synaptic transmission, neuronal system, and one-carbon metabolism were associated with both long-term (fig. S3, D and E) and short-term memory (fig. S3, F and G). Complement activation in SAT was again among the pathways most significantly linked to attention (fig. S3, H and I).

The gene encoding for Ezrin (*EZR*) was one with most associations across the different cognitive domains in VAT (significant in four tests at a pFDR of <0.05), being the most significantly associated gene with the digit span forward score (Fig. 2C and table S22). In line with previous findings, complement-related genes were particularly and strongly associated with inhibitory control (Fig. 2A). This cognitive function was also associated with early immediate genes from the orphan nuclear receptor 4A family (*NR4A1* and *NR4A2*). In particular, *NR4A2* was the most significant gene associated with the STROOPI test (which evaluates inhibitory control), while *NR4A1* was among the top genes associated with trail making test part B (TMTB) (executive function). In SAT, *NR4A1* and *NR4A2* were negatively associated with long-term memory (fig. S3A), while the complement genes were particularly associated with attention (fig. S3C). A gene from the NR4A (*NR4A3*) had again the strongest negative association with inhibitory control (table S35). Last, *AMPH* was the gene most significantly associated with digit span forward test (table S31) and the total digit span test (table S33).

Fig. 1. Associations of VAT gene expression and cognitive domains in the discovery cohort. Volcano plots of differentially expressed genes in the VAT associated with (**A**) the STROOP Interference tests, (**B**) the trail making test part B (TMTB), and (**C**) California verbal learning test immediate recall (CVLT_IR) scores in discovery cohort (IRONMET, $n = 17$) identified by limma-voom analysis controlling for age, BMI, sex, and education years. The $\log_2$ fold change associated with a unit change in the cognitive test score and the $\log_{10} P$ values adjusted for multiple testing (pFDR) are plotted for each gene. Differentially expressed genes (pFDR < 0.05) are colored in red and green indicating down-regulation and up-regulation, respectively. (**D**) Manhattan-like plot of pathways significantly associated ($q < 0.1$) with the TMTB in the VAT identified from a pathway overrepresentation analysis mapping significant genes to the Reactome and WikiPathways databases. (**E**) Dot plot of pathways significantly associated ($q < 0.1$) with the CVLT_IR in the VAT identified from a pathway overrepresentation analysis mapping significant genes to the Reactome database. Dots are colored by the q value. (**F**) Manhattan-like plot of pathways significantly associated ($q < 0.1$) with the STROOP Interference in the VAT identified from a pathway overrepresentation analysis mapping significant genes to the Reactome and WikiPathways databases. In the Manhattan-like plots, the bubble size represents the ratio of input genes that are annotated in a pathway (GeneRatio). CREB, adenosine 3′,5′-monophosphate response element–binding protein; tRNA, transfer RNA; NCAM1, Neural Cell Adhesion Molecule 1; TP53, Tumor Protein 53; PKA, Protein Kinase CAMP-Activated Catalytic Subunit Alpha.
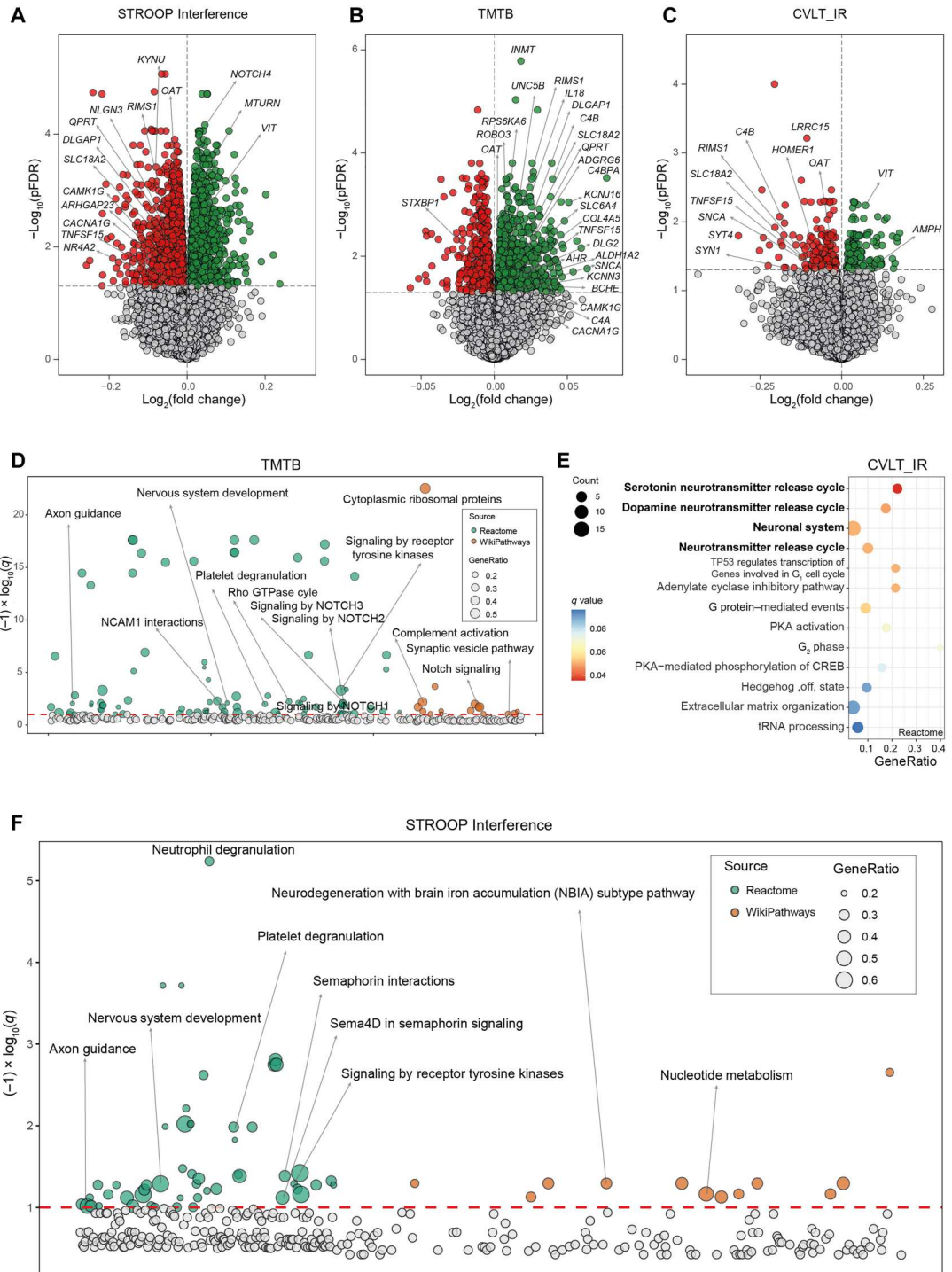
Adipose tissue genes linked to cognitive function are involved in neuronal system and synaptic formation

To gain further insights into the coincident associations between both cohorts, we performed an enrichment analysis considering only those genes significantly associated with at least one cognitive test in all three tissues (VAT from discovery and VAT and SAT from validation cohorts), and a total of 188 coincident genes were found (Fig. 3A and table S44). The most overrepresented pathways from the subset of genes included mostly pathways with key roles in synaptic function (Fig. 3, B and C; fig. S4, A and B; and table S45) and inflammation (tryptophan metabolism and complement activation). Mapping these genes to the Search Tool for the Retrieval of Interacting Proteins/Genes (STRING) database to construct a gene-gene interaction network, a cluster of highly interconnected genes mainly involved in neuronal system and synapse formation and maintenance (26) (*DLG4*, *DLGAP1*, *DLG2*, *ATP1B1*, *HOMER1*,
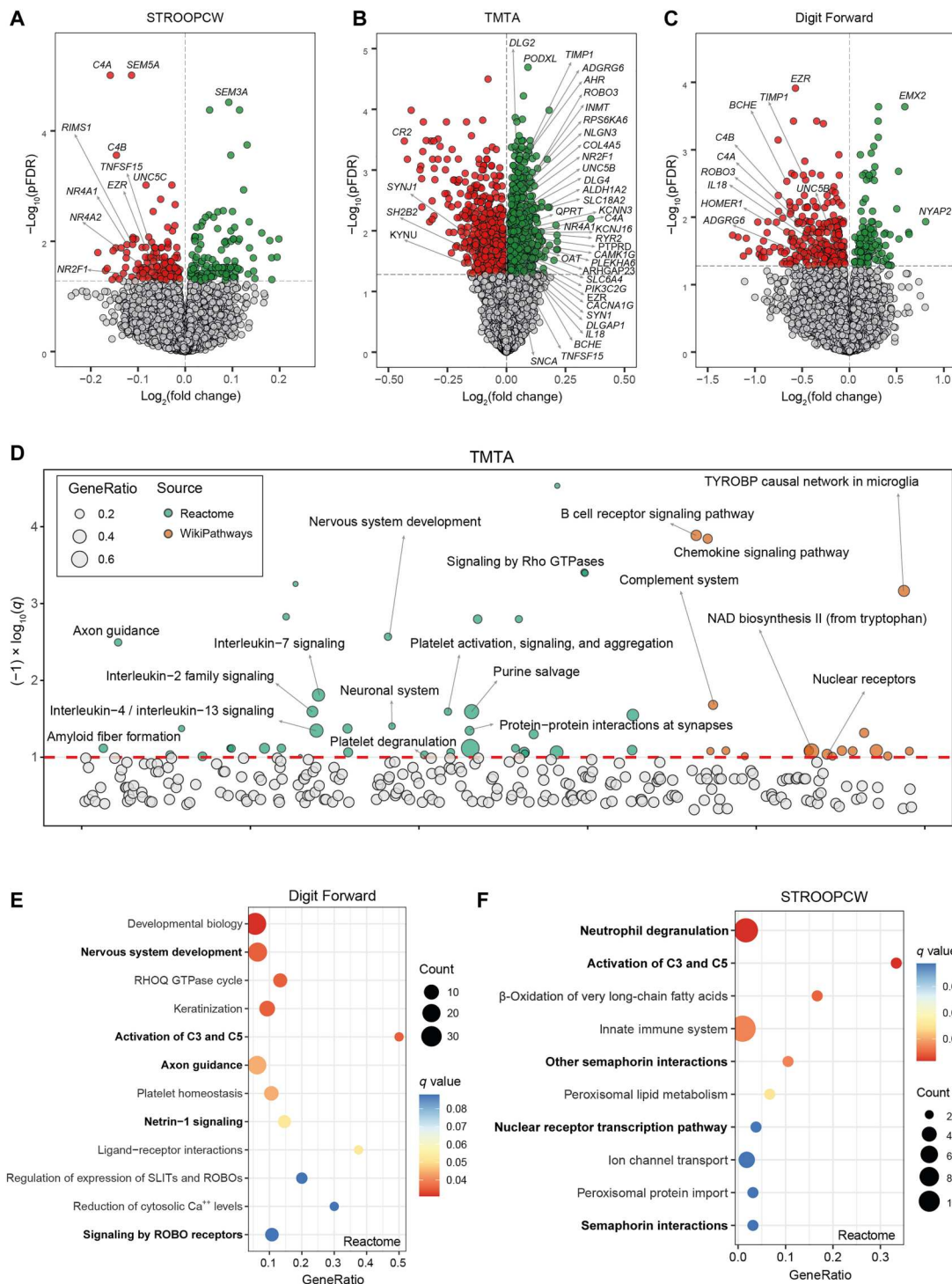
Fig. 2. Longitudinal associations of VAT gene expression at baseline and the scores in different cognitive domains later in life. Volcano plots of differentially expressed genes in the VAT at baseline associated with (**A**) the STROOP color word tests (STROOPCW), (**B**) the TMTA, and (**C**) the Forward Digit Span scores 2 to 3 years later in the validation cohort (INTESTINE, $n = 22$) identified by limma-voom analysis controlling for age, BMI, sex, and education years. The $\log_2$ fold change associated with a unit change in the cognitive test score and the $\log_{10} P$ values adjusted for multiple testing (pFDR) are plotted for each gene. Differentially expressed genes (pFDR < 0.05) are colored in red and green indicating down-regulation and up-regulation, respectively. (**D**) Manhattan-like plot of pathways significantly associated ($q < 0.1$) with the TMTA in the VAT identified from a pathway overrepresentation analysis mapping significant genes to the Reactome and WikiPathways databases. (**E**) Dot plot of pathways significantly associated ($q < 0.1$) with the STROOPCW and (**F**) the Forward Digit Span in the VAT identified from a pathway overrepresentation analysis mapping significant genes to the Reactome database. The x axis in the dot plots and the bubble size in the Manhattan-like plots represent the ratio of input genes that are annotated in a pathway (GeneRatio). Dots are colored by the q value. NAD, nicotinamide adenine dinucleotide; TYROBP, Transmembrane Immune Signaling Adaptor TYROBP; SLIT, Slit Guidance Ligand; ROBO, Roundabout Guidance Receptor.

Fig. 3. Pathway analysis of differentially expressed genes in common among the VAT and SAT in the discovery and validation cohorts (n = 188). (**A**) Venn diagram representing the overlap of significant genes associated with at least one cognitive test in VAT of the discovery cohort, the VAT of the validation cohort, and the SAT of the validation cohort. (**B**) Dot plot of significantly overrepresented pathways (q < 0.1) mapping common differentially expressed genes (n = 188) to the WikiPathways and (**C**) Reactome databases. The x axis in the dot plots represents the ratio of input genes that are annotated in a pathway (GeneRatio). Dots are colored by the q value. (**D**) Gene-gene interaction network constructed using common differentially expressed genes via the STRING database. The network nodes are genes, and the edges represent the predicted functional interactions. The thickness indicates the degree of confidence prediction of the interaction. Functional gene clusters are colored on the basis of the Markov cluster algorithm (MCL) with an inflation parameter of 1.4. Only connected nodes are shown. A highly connected functional cluster (in red) was detected comprising genes with important roles in the CNS. (**E**) Enrichment map of the interrelation of significant pathways identified using an active subnetwork oriented approach. Each color displays a cluster of related pathways using a threshold for kappa statistics = 0.35. The size of the nodes corresponds to its $-\log_{10}(pFDR)$. The thickness of the edges between nodes corresponds to the kappa statistic between the two nodes. IP_3, inositol 1,4,5-trisphosphate; IP_4, inositol 1,4,5,6-tetrakisphosphate; PI, phosphatidylinositol; TNF, tumor necrosis factor; NMDA, N-methyl-D-aspartate; CNV, copy number variations; L1CAM, L1 Cell Adhesion Molecule.
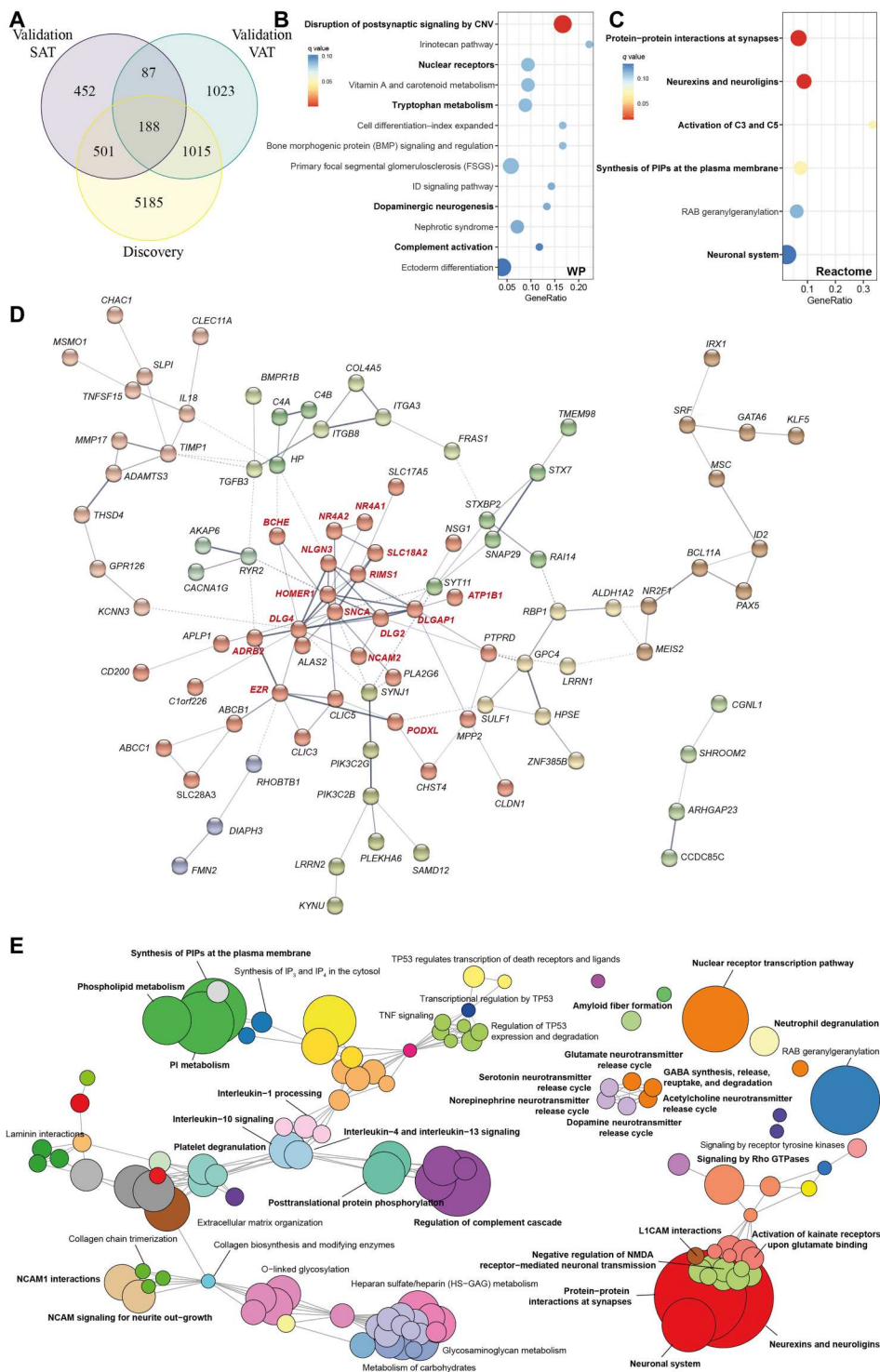
NLGN3, SNCA, BCHE, RIMS1, SLC18A2, ADRB2, EZR, PODXL, and *NCAM2)* was disclosed (Fig. 3D).

To obtain a better picture of the associated pathways, we leveraged the interaction information from the gene-gene interaction network to identify distinct active subnetwork and then performed an active subnetwork–oriented enrichment analysis on these subnetworks. Using this approach, we identified a total of 120

overrepresented Reactome pathways (pFDR < 0.05). To reduce complexity derived from this large number of pathways, we performed a hierarchical clustering to collapse redundant pathways and ease the identification of mechanisms relevant to cognition (table S46). Figure 3E shows the functional network of the clustered pathways. Of 53 clusters, the most significant one included pathways related to the neuronal system and synaptic function

(*RIMS1*, *SLC18A2*, *DLG2*, *DLG4*, *DLGAP1*, *HOMER1*, *NLGN3*, *PTPRD*, *BCHE*, and *KCNN3*) (Fig. 4A). This cluster was strongly connected with three other cluster involved in the synthesis and metabolism of phospholipids, particularly phosphatidylinositols (PIPs) (*PIK3C2B*, *PIK3C2G*, *SYNJ1*, and *PLEKHA6*), the signaling by Rho guanosine triphosphatase (GTPases) (*ARHGAP23*,

DIAPH3, *DLG4*, *RHOBTB1*, *SGO2*, and *SRF*), and the release of neurotransmitters (*RIMS1* and *SLC18A2*) (Fig. 4B).

To gain better insights into potential mechanisms linking adipose tissue to cognition, we next performed a multiblock Partial Least Squares (PLS) analysis to integrate these 188 adipose tissue genes with the plasma levels of metabolites measured by nuclear magnetic resonance (NMR), high-performance liquid

Fig. 4. Selected clusters from active subnetwork oriented pathway analysis of common significant genes among the VAT and SAT in the discovery and validation cohorts (*n* = 188) and integration with circulating metabolites. (**A**) Dot plot of enrichment analysis results performed on active subnetworks grouped by selected clusters. The *x* axis represents the fold enrichment defined as the ratio of the frequency of input genes annotated in a pathway to the frequency of all genes annotated to that pathway. The dot size indicates the number of differentially expressed genes in a given pathway. Dots are colored by the −log₁₀(pFDR), with red indicating high significance. (**B**) Gene-concept network depicting significant genes involved in enriched pathways from selected clusters. The dot size of the pathways represents the −log₁₀(pFDR). Pathways with the same color correspond to the same cluster. (**C**) Correlation circle plot for the integration of the adipose tissue genes, metabolites (NMR, HPLC-ESI-MS/MS in positive and negative mode), and cytokines and neurotoxic proteins using a multiblock PLS model in canonical mode. Strongly positively associated variables or groups of variables are projected close to one another on the correlation circle (<0° angle). The variables or groups of variables strongly negatively associated are projected diametrically opposite (<180° angle) on the correlation circle. Variables not correlated are situated <90° from one another.
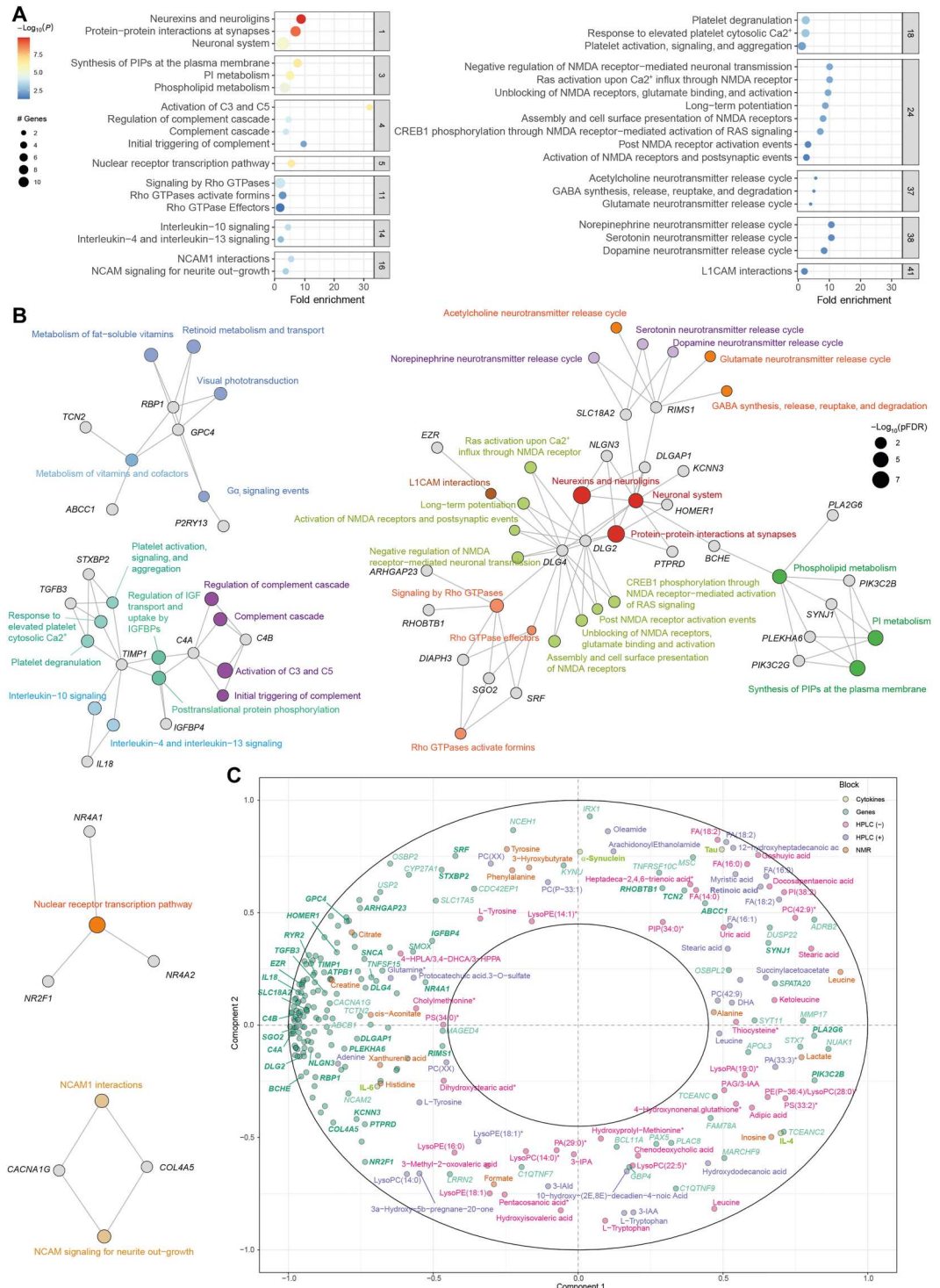
chromatography–electrospray ionization tandem mass spectrometry (HPLC-ESI-MS/MS) in positive and negative modes and the circulating levels of cytokines and neurotoxic proteins [IL-6, IL-4, Tau, α-synuclein, and amyloid-β42 (Aβ42)]. The expression levels of adipose tissue genes involved in phospholipid metabolism, such as *PIK3C2B*, *PLA2G6*, or *SYNJ1*, had a strong association with several circulating phospholipids and lysophospholipids (Fig. 4C). Although lipids are essential to brain function and, in particular, phospholipids are crucial for synaptic plasticity, neurotransmission, and memory (*27*), the brain can synthesize a limited number of lipids. However, plasma fatty acids can cross the Blood-Brain Barrier (BBB) as nonesterified free fatty acids or esterified in lysophospholipids such as lysophosphatidylcholine (LPC) (*28*, *29*). Notably, some of the genes from the phospholipid metabolism cluster codified for phospholipase A2 (*PLA2G6*), which catalyzes the hydrolysis of the sn-2 position of glycerophospholipids to yield nonesterified fatty acids and lysophospholipids. Hence, these phospholipids could be mediating the effects of adipose tissue on cognition.

We also identified three highly interconnected clusters of genes related to inflammatory response that included the complement cascade (*C4A* and *C4B*) and the IL-4, IL-10, IL-13 interleukin signaling (*IL18* and *TIMP1*). Chronic low-grade inflammation is a hallmark of obesity, and the association between obesity and cognitive decline has recently been shown to be mediated by inflammation (*30*, *31*). In addition, a complement-dependent synapse elimination has been recently identified as a mechanism for memory loss (*32*). In line with our findings, NLRP3 from the VAT has recently shown to impair cognition in mice by activating microglial IL-1 receptor (*7*), whereas IL-4 has shown to mediate the protective effects of beige fat on obesity-induced cognitive impairment by restoring synaptic plasticity in the hippocampus (*14*). Consistent with recent findings that inhibition of Na,K-ATPase signaling resulted in improved cognitive function (*12*), we also identified a cluster containing the Na$^+$/K$^+$ ATPase transporting subunit beta 1 gene (*ATP1B1*). Notably, the Na,K-ATPase signaling pathway requires the activation of PIP 3-kinase, and we identified a cluster of pathways involved in PIP metabolism strongly associated with cognition (Fig. 4B). Last, the genes involved in the inflammatory cluster (*C4A*, *C4B*, *IL18*, and *TIMP1*) had a strong positive association with the circulating levels of IL-6 and a strong negative association with the IL-4 levels in plasma (Fig. 4C). Therefore, these adipokines could be released by the adipose tissue and mediate its effects on cognition. Accumulating evidence indicates that peripheral inflammation contributes to increased neuroinflammation (*33*) and could be a potential causal mechanisms involved in the obesity-related cognitive impairment (*34*, *35*).

Other significant clusters included the nuclear receptor transcription (*NR4A1*, *NR4A2*, and *NR2F1*) and the metabolism of vitamins (*ABCC1*, *TCN2*), particularly vitamin A (*RBP1* and *GPC4*). Recent studies have shown that *NR4A2* activation enhances long-term memory in young mice and ameliorates age-related memory impairments in old mice (*36*). Several studies have also suggested that water-soluble vitamins (C, E, and Bs) may affect cognitive performance by reducing reactive oxygen species generation and proinflammatory mediators such as NLRP3 inflammasome (*37*). Retinoic acid, the active form of vitamin A, is essential for regulating synaptic plasticity in regions of the brain involved in memory and learning (*38*). Notably, we found a strong positive association

between the expression levels of genes involved in the metabolism of vitamins in the adipose tissue, particularly *TCN2* and *ABCC1*, and the circulating levels of retinoic acid (Fig. 4C). Notably, *RBP1*, which encodes for cellular retinol binding protein 1 involved in the transport of retinol, had a strong negative association with the plasma levels of retinoic acid. Together, these results suggest that the adipose tissue could modulate cognitive performance through the metabolism of vitamin A.

From the identified cluster of genes in Fig. 4B, *SLC18A2* and *RIMS1* (regulating synaptic exocytosis 1) were those with the largest number of significant associations across the different cognitive domains in the three tissues analyzed. *SLC18A2* encodes for VMAT2 (vesicle monoamine transporter member 2), a protein that transports cytoplasmic monoamine neurotransmitters (dopamine, norepinephrine, histamine, and serotonin) into presynaptic vesicles and has been linked to the pathophysiology of different neuropsychiatric and neurological disorders (*39*). The *Drosophila* and mouse *RIMS1* orthologues have shown to be a central component in the regulation of synaptic vesicle exocytosis and the neurotransmitter release (*40*). Mice lacking *Rim1α* show severely impaired learning and memory (*41*), and *RIMS1* has recently been identified as the highest-ranked candidate gene in autism spectrum disorder (*42*).

Morbid obesity modulates the direction of the associations between adipose tissue genes and cognition

We sought to further validate these results using an additional cohort. Hence, we measured the expression levels of *EZR*, *UNC5B*, *NUDT2*, and *NR4A2* in the VAT from a third independent validation cohort (ADIPOBRAIN cohort) consisting of n = 40 patients with and without obesity aged 40 to 64 years old (Fig. 5A and table S1) who underwent the Rey-Osterrieth complex figure (ROCF) test 4 to 10 years later. The ROCF is one of the top 10 tests used by neuropsychologists for the evaluation of visuospatial constructional ability, visual memory, and executive function (*43*). Consistent with our findings in the discovery cohort (including only patients with morbid obesity), the expression of *EZR* (Fig. 5B) and *UNC5B* (Fig. 5C) at baseline was strongly negatively associated with the ROCF copy scores in subjects with morbid obesity (BMI > 35 kg/m^2). Conversely, the expression of these genes was positively associated with executive function in subjects with a BMI of <35 kg/m^2 (Fig. 5, F and G). The expression of *NUDT2* was positively associated with the ROCF copy performance in subjects with morbid obesity (Fig. 5D) but not in subjects with a BMI of <35 kg/m^2 (Fig. 5H), whereas we did not find any significant association with the expression of *NR4A2* (Fig. 5, E and I).

Blood expression levels of key genes linked to cognitive performance

To further validate these findings and provide noninvasive biomarkers of cognitive function as an alternative to adipose tissue biopsies, we measured the expression of some of the most promising genes in the circulation of n = 816 individuals from the general population aged ≥50 years taking part in the Aging Imageomics study (Fig. 5J and table S1). Initially, we validated those genes with the largest number of associations across the different neuropsychological tests in the discovery cohort (*NUDT2*, *AMPH*, *UNC5B*, and *OAT*) and validation cohort 1 (*EZR* and *NR4A2*). In agreement with our findings, the circulating levels of *NUDT2* were negatively associated with executive function (Fig. 5K), while the circulating

Fig. 5. Associations of expression levels of selected genes with cognition in a validation cohort, the Aging Imageomics cohort, and *D. melanogaster*. (**A**) Main baseline characteristics of the validation cohort 3 (ADIPOBRAIN). Scatter plots of the partial Spearman's rank correlations (adjusted for age, BMI, sex, and education years) between ROCF copy scores and the VAT expression levels of (**B**) *EZR*, (**C**) *UNC5B*, (**D**) *NUDT2*, and (**E**) *NR4A2* in patients with a BMI of >35 kg/m^2 from the ADIPOBRAIN cohort. (**F** to **I**) The same associations but in patients with a BMI of <35 kg/m^2. (**J**) Main baseline characteristics of the validation cohort 2 (Imageomics). Violin plots of the score in several cognitive tests and the tertiles (T1, T2, and T3) of the circulating expression levels of selected genes: (**K**) normalized STROOP color word test–color word (SCWT CW) versus *NUDT2*; (**L**) symbol digit test (SDT) versus *AMPH*; (**M**) total paired recall (TFP) versus *OAT*; (**N**) normalized digit span test (DST) backward versus *UNC5B*; and (**O**) normalized DST backward versus *EZR*. The ranked residuals after controlling for age, BMI, gender, and education level are plotted. Overall significance was assessed using a Mann-Kendall trend test. (**P**) Scheme of the RNA interference via the UAS-GAL4 system. (**Q**) Courtship conditioning paradigm. (**R** to **W**) The graphs display courtship conditioning paradigm results of fat body promoter line *w; C7-GAL4; UAS-Dcr-2* crossed with RNAi lines targeting (R) *unc-5*, (S) *Datp*, (T) *Moe*, (U) *Hr38*, (V) *Amph*, (W) *Oat*, and their corresponding genetic background controls (controls 1 and 2). Boxplots represent the CI of naïve (N) and trained (T) males. Significance of courtship suppression upon training was assessed with Kruskal-Wallis nonparametrical test and post hoc Dunn's multiple comparison test. LI statistical significance was determined with the nonparametrical bootstrap analysis with 10,000 iterations. *$P < 0.05$, **$P < 0.01$, ***$P < 0.001$, and ****$P < 0.0001$. ns, not significant.
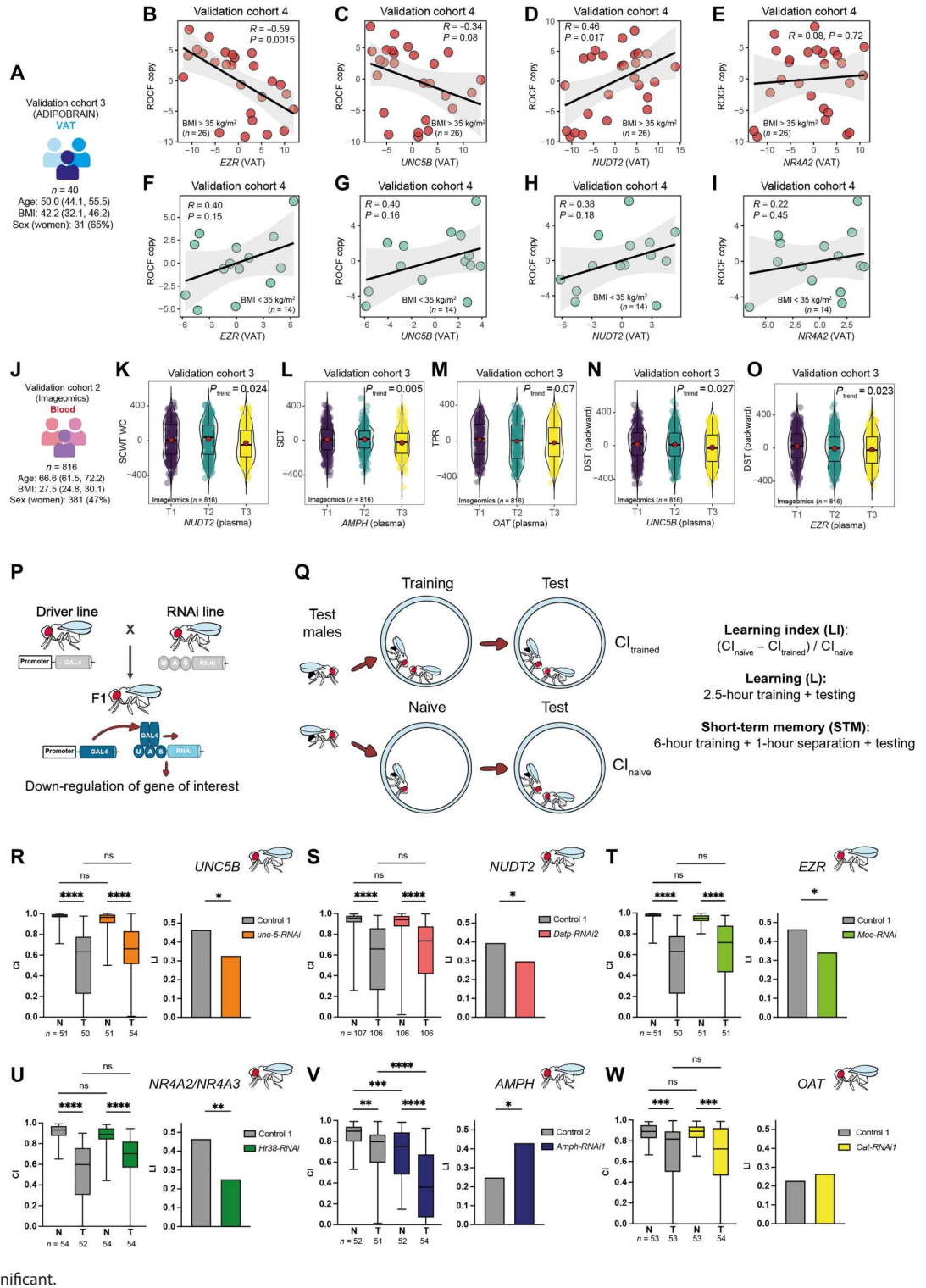
expression of *AMPH* was negatively associated with processing speed (Fig. 5L) and memory (assessed by the total free recall; P_{trend} = 0.02). Increased levels of *OAT* and *UNC5B* tended to be associated with delayed memory (Fig. 5M) and executive function (Fig. 5N). Last, we also found consistent negative associations between the circulating expression of *EZR* and executive functioning (Fig. 5O) and the quintiles of *NR4A2* with memory (P_{trend} = 0.027).

Down-regulation of candidate genes in the fat body of *Drosophila melanogaster* improves cognition

We next assessed the causal effect of the adipose tissue expression of these candidate genes (*AMPH*, *UNC5B*, *NUDT2*, *OAT*, *NR4A2*, *NR4A3*, and *EZR*) on cognitive function using the model organism *D. melanogaster* (fruit flies). A main advantage of *Drosophila* is the possibility of manipulating gene expression in a tissue-specific manner by means of the UAS-GAL4 system (Fig. 5P) (*44*). To evaluate *Drosophila* cognition, we used the courtship conditioning paradigm to measure associative learning and memory capabilities (*45*). Male courtship behavior is conditioned by the exposure to nonreceptive premated females resulting in a suppression of courtship after a learning process. Male courtship rates can be assessed at different times after training periods with premated females. Learning is assessed immediately after the training period, and short-term memory is typically assessed 1 hour after training. The courtship index (CI; the percentage of time spent on courtship during an 8-min interval) of trained and of socially naïve male is used to calculate the learning index (LI). A higher LI is indicative of a better learning or short-term memory (Fig. 5Q).

We down-regulated *Amph*, *unc-5*, *Datp*, *Oat*, *Hr38*, and *Moe* (the well-conserved orthologues of *AMPH*, *UNC5B*, *NUDT2*, *OAT*, *NR4A2/NR4A3*, and *EZR*, respectively) specifically in the fat body of *Drosophila*, which is the equivalent of the adipose tissue in humans. The fat body promoter line *w; C7-GAL4; UAS-Dcr-2* was crossed with at least one RNA interference (RNAi) line targeting each gene of interest (table S47). Learning capabilities were assessed immediately after training using the courtship conditioning assay. Down-regulation of *unc-5*, *Datp*, *Hr38*, and *Moe* lead to a significant decrease in learning capabilities compared to their corresponding genetic background controls in at least one of the RNAi lines tested (Fig. 5, R to U). Conversely, down-regulation of *Amph* lead to an improvement of learning capabilities for one RNAi line (Fig. 5V). Down-regulation of *Oat* in the fat body was lethal for one RNAi line or did not affect learning captivities when using a second RNAi line (Fig. 5W). Our findings demonstrate that specific down-regulation of some of these genes in the fat body of *Drosophila* modulates learning, thereby suggesting a direct effect on cognition uniquely depending on its expression and/or function in fat body.

Neurotransmitter release cycle–associated genes *SLC18A2* and *RIMS1* modulate cognition in mice adipose tissue or *Drosophila* fat body

Among the genes associated with cognition in both VAT and SAT from the discovery and validation cohort 1, the cluster of genes involved in the release of neurotransmitters (*RIMS1* and *SLC18A2*) (Fig. 4B) had the largest number of significant associations across different cognitive domains. Therefore, we also validated these associations in the third validation cohort (ADIPOBRAIN). Again,

we found that in subjects with morbid obesity (Fig. 6A), the expression of *SLC18A2* at baseline was strongly negatively associated with the ROCF copy performance 4 to 10 years later, whereas it was positively associated in subjects with a BMI of <35 kg/m^2 (Fig. 6B).

To demonstrate a possible causal effect of adipose tissue *SLC18A2* on cognition, we studied two preclinical models. In a mice model, we used an AAV2/8-RSV-GFP-Adp-miRNASLC18A2 vector that expresses a miRNA to selectively down-regulate *slc18a2* gene expression in adipose tissue (Fig. 6C). Eight-week-old mice were fed a normal chow diet (ND; *n* = 23) or a high-fat diet (HFD; *n* = 25) for 8 weeks (Fig. 6D). Three days after the start of the diet, each dietary group was divided into two groups and injected intravenously via tail vein either with the AAV2/8-RSV-GFP-Adp-miRNASLC18A2 vector or with saline. The expression levels of green fluorescent protein (GFP) contained in the vector as a reporter gene was significantly increased in both inguinal and mesenteric white adipose tissue (iWAT and mWAT) of mice from the vector-injected groups compared to the saline groups (fig. S5, A and B), thereby indicating that the vector was able to reach the adipose tissue. We also found a significant decrease in the solute carrier family 18 member A2 (slc18a2) protein levels in the mWAT of virus-injected mice fed an HFD compared to their respective controls (fig. S5, C and D). Four weeks after injection, we assessed short- and long-term memory and locomotor activity. As expected, mice fed an HFD gained more weight in parallel to food intake compared with those fed an ND (Fig. 6E and fig. S6, A and B). There is good evidence that obesity affects cognition in rodents (*35*). Consistently, mice fed an HFD had lower short- and long-term memory than mice fed an ND (Fig. 6, F and G). Down-regulation of *slc18a2* in the mice adipose tissue reversed the memory impairment induced by an HFD (Fig. 6, F and G). We observed no differences in the exploration time between groups (fig. S6, C and D). Although we found a diet effect on locomotion, down-regulation of *slc18a2* had no substantial effect (fig. S6, E to H).

To further assess the role of adipose tissue *SLC18A* mRNA on cognition, we performed RNAi-mediated knockdown of *Vmat* (the orthologue in *Drosophila*) using the *w; C7-GAL4; UAS-Dcr-2* promoter line for specific knockdown in the fat body (the equivalent of adipose tissue in humans). The courtship-conditioning paradigm was performed, and short-term memory was assessed 1 hour after training. Males of *Vmat-RNAi1* were able to suppress courtship significantly better than the corresponding genetic background control flies (Fig. 6H). Consequently, the LI was significantly increased (*Vmat-RNAi1*: LI = 0.577, control 2: LI = 0.366, *P* = 0.0064), indicating that *Vmat-RNAi1* presented more short-term memory (Fig. 6H). Next, we performed real-time polymerase chain reaction (RT-PCR) to prove that *Vmat* was specifically knocked down in the fat body but not in the fly head (Fig. 6I), indicating that when decreasing *Vmat* expression exclusively in the fat body flies are able to learn better. To unravel a potential mechanism through which *Vmat* expression in the fat body could influence cognition, we performed RT-PCR to evaluated the expression of *rutabaga* (*rut*), *dunce* (*dnc*), *amnesiac* (*amn*), *homer*, *CAMKll*, and *orb2* in *Drosophila* heads. These genes are part of the cyclic adenosine 5′-monophosphate pathway, which have been demonstrated to influence learning and short-term memory in the courtship-conditioning assay (*46*). RNAi-mediated knockdown of *Vmat* in the fat body lead to a significant increase in memory related genes (*rut*, *dnc*, *caMKll*, and *orb*) in the fly head (Fig. 6J). To further validate our
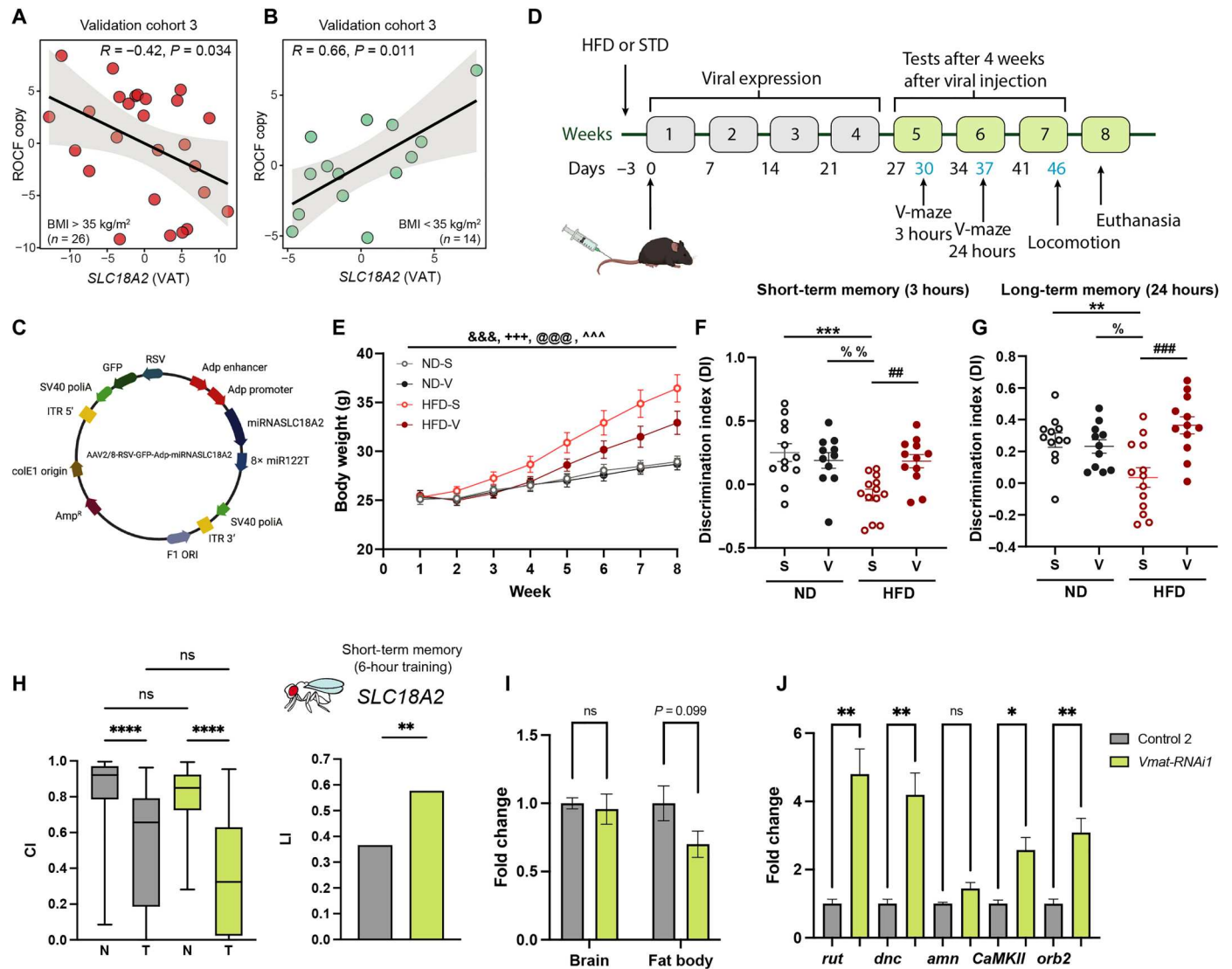
Fig. 6. Associations of *SLC18A2* with cognition in the validation cohort 3 and altered expression in preclinical models. Scatter plots of the partial Spearman's correlations (adjusted for age, BMI, sex, and education years) between the *SLC18A2* VAT expression and the ROCF copy scores in (**A**) morbid obese patients (BMI > 35 kg/m^2) and (**B**) patients with a BMI of <35 kg/m^2 (ADIPOBRAIN cohort, $n = 40$). (**C**) Schematic representation of the AAV packaging plasmid used to down-regulate *SLC18A2* gene expression. (**D**) Timeline of events and mice cognitive testing. Arrows indicate punctual events such as virus injection, tests, and euthanasia. (**E**) Weekly body weight (in grams). Means ± SEM; $n = 12$ normal diet + saline (ND-S), $n = 11$ normal diet + virus (ND-V), $n = 13$ high fat diet + saline (HFD-S), $n = 12$ high fat diet + virus (HFD-V). &&&$P < 0.001$ week effect; +++$P < 0.001$ diet effect, @@@$P < 0.001$ week × diet interaction, and ^^^$P < 0.001$ week × treatment interaction (three-way ANOVA). (**F** and **G**) Short-term (3 hours) and long-term (24 hours) memory using the novel object recognition test. Dots with the means ± SEM. **$P < 0.01$, ***$P < 0.001$ ND-S versus HFD-S, %$P < 0.05$, %%$P < 0.01$ ND-V versus HFD-S, and ##$P < 0.01$, ###$P < 0.001$ HFD-S vs HFD-V (two-way ANOVA). (**H**) Male short-term memory in the courtship-conditioning paradigm. Control 2 (*w; C7-GAL4/+; UAS-Dcr-2/+*) and Vmat-RNAi1 fat body–specific knockdown flies (*w; C7-GAL4/+; UAS-Dcr-2/Vmat-RNAi*). (**I**) Relative gene expression of Vmat in fly heads and fat body and (**J**) *rutabaga* (*rut*), *dunce* (*dnc*), *amnesiac* (*amn*), *homer, CAMKll*, and *orb2* in fly heads of Vmat-RNAi1 fat body–specific knockdown flies and its corresponding genetic background control. Means ± SEM. (*t* test: *$P < 0.05$, **$P < 0.01$, and ****$P < 0.0001$). Data are based on a minimum of five biological and two technical replicates. (C) and (D) were created with BioRender.com.

results, we used an independent RNAi line against *Vmat* (Vmat-RNAi2). When down-regulating Vmat in the fat body with RNAi2, we observed a significant increase in short-term memory (*Vmat-RNAi2*: LI = 0.650, control 1: LI = 0.437, $P = 0.002$) (fig. S7A) and a significant overexpression of *dnc*, *CAMKll*, and *orb2* in the fly head (fig. S7B), confirming our previous data.

In the third validation cohort, VAT *RIMS1* mRNA was also evaluated. In line with the results obtained for *SLC18A2*, the expression

of *RIMS1* was negatively associated with ROCF in subjects with severe obesity (Fig. 7A) but positively in subjects with a BMI of <35 kg/m^2 (Fig. 7B). To prove a possible causal effect, we assessed learning in *Drosophila* after down-regulation or overexpression of *Rim* (the well-conserved orthologue of *RIMS1*) in the fat body. A significant decrease in CI after learning was observed in two independent RNAi lines and corresponding genetic background controls, but we did not observe significant differences in the LI (fig.

Fig. 7. Associations of *RIMS1* with cognition in the validation cohort 3 and Rim overexpression in *Drosophila* fat body effects in learning and gene expression profiles. (**A** and **B**) Scatter plots of the partial Spearman's rank correlations (adjusted for age, BMI, sex, and education years) between the VAT expression levels of *RIMS1* and the ROCF copy scores in (A) morbid obese patients (BMI > 35 kg/m²) and (B) patients with a BMI of <35 kg/m² from the ADIPO-BRAIN cohort (*n* = 40). (**C**) Rim overexpression in the *Drosophila* fat body and associations with learning. Differences in CI between naïve and trained males were assessed with Kruskal-Wallis nonparametrical test and post hoc Dunn's multiple comparison test. LIs to assess either short-term memory (for *Vmat*) or learning (for *Rim*) were calculated from CIs as specified in Materials and Methods. Statistical significance was determined with the nonparametrical bootstrap analysis with 10,000 replicates. ****P < 0.0001. (**D**) *Rim* relative expression assessed by quantitative RT-PCR (qRT-PCR) in fly brain or fat body in *UAS-Rim* fat body–specific overexpression flies and its corresponding genetic background control. Data are derived from a minimum of five biological and two technical replicates. (**E**) Dot plot of significantly (*q* < 0.1) overrepresented Reactome pathways, (**F**) GO biological processes (GO-BP), and (**G**) GO molecular functions (GO-MF) associated with the miss expressed genes in the fat body of *UAS-Rim* flies. (**H** and **I**) Gene-concept network depicting significant genes involved in enriched Reactome pathways [from (E)] and GO-GO-BP [from (F)]. (**J**) Overrepresentation analysis of pathways (*q* > 0.1) associated with differentially expressed gene transcript in *UAS-Rim* fly heads based on the Reactome database. (**K**) Gene-concept network associated with significant genes involved in Reactome pathways of (J). (**L**) Significantly overrepresented GO molecular functions of significant gene transcripts in fly heads (*q* > 0.1). HDL, high-density lipoprotein; HSF1, heat shock factor 1; IGF, insulin-like growth factor; IGFBP, insulin-like growth factor binding protein; NADP⁺, nicotinamide adenine dinucleotide phosphate; PCNA, proliferating cell nuclear antigen.
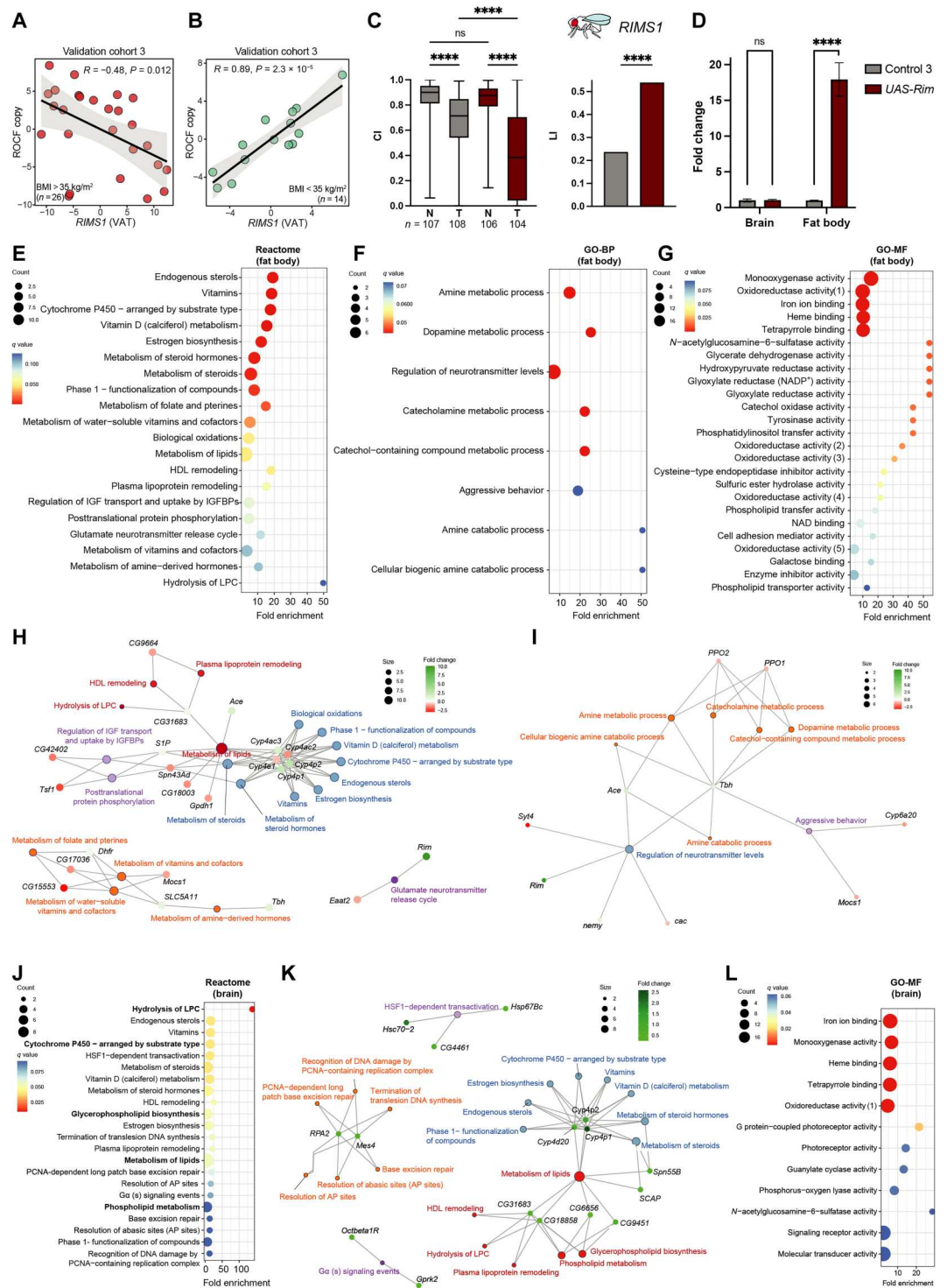
S7, C and D). However, when *Rim* was overexpressed (*UAS-Rim*) in the fat body, males were able to suppress courtship significantly better than the corresponding genetic background control flies (Fig. 7C), resulting in a significant increase in the LI (*UAS-Rim*: LI = 0.539, control 3: LI = 0.237, *P* = 0.0001) (Fig. 7D). Our results indicate that flies that overexpress *Rim* exclusively in the fat body are able to learn better. Next, we used RT-PCR to prove that *Rim* was uniquely targeted in the fat body but not in the brain (Fig. 7D). Again, learning improvement was exclusively promoted by *Rim* altered expression in the fat body and not due to a "leakage" of the RNAi in the brain.

To elucidate the potential mechanisms underlying the overexpression of *Rim* in learning, we performed an mRNA-seq in the fat body and fly heads of *UAS-Rim* flies that overexpressed *Rim* specifically in the adipocytes. We identified the differentially expressed genes between the flies overexpressing *Rim* and the corresponding genetic backgrounds in the fat body (table S48) and fly heads (table S49). In the fat body, consistent with our results in humans, an enrichment analysis based on Reactome identified an overrepresentation of pathways involved in vitamin metabolism and lipid metabolism, including the hydrolysis of LPC and the glutamate neurotransmitter release cycle (Fig. 7, E and H). It also identified genes involved in other pathways involved in biological oxidations and cytochrome P450 (*Cyp4e1*, *Cyp4ac2*, *Cyp4ac3*, *Cyp4p1*, and *Cyp4p2*). Notably, a gene ontology (GO) enrichment analysis identified mainly biological processes participating in neurotransmitter regulation, in particular, the metabolism of biogenic amines (dopamine, serotonin, and norepinephrine), which is strongly consistent with our findings in humans (Fig. 7, F and I). At the molecular function level, we identified several functions involved in monooxygenase and oxidoreductase activity (Fig. 7G). Notably, we also identified several functions involved in the PIP transfer and phospholipid transfer and transport. These results were replicated in the fly heads. We found again an overrepresentation of pathways involved in the metabolism of lipids (particularly phospholipids and the hydrolysis of LPC), vitamins, and biological oxidations (table S50). An analysis based only on up-regulated genes also identified alterations in DNA metabolism (Fig. 7, J and K), while a GO analysis identified once more molecular functions related to monooxygenase and oxidoreductase activity (Fig. 7L).

Oxidative damage and reduction of antioxidants are associated with a decline in cognitive function due to neurodeterioration (*47*). Vitamins can act as potent antioxidant molecules protecting neurons from oxidative stress and improving overall neuronal functioning (*48*). Reducing oxidative stress in *Drosophila* has been associated with an increase in lifespan (*49*) and improves age-related memory impairment (*47*). Similarly, monooxygenase and oxidoreductase enzymes are contributing to the cellular levels of oxygen reactive species, and cytochrome P450 family members have been found to be up-regulated in the presence of oxidative stress having a detoxification and antioxidant function in *Drosophila* (*50*). Notably, low-grade inflammation is also associated with cellular oxidative imbalance and one of the physiopathological mechanisms behind obesity-associated syndromes (*51*). Phospholipids are also abundant molecules in *Drosophila* brain, where they play essential roles in cognition, by both supplying energy for brain activity and particip4ating in membrane trafficking and neurotransmission (*52*). Similar to mammals, main source of phospholipids in *Drosophila* are lipid droplets inside fat body cells (*53*). In *Drosophila*,

phospholipid homeostasis has been found to be important for the regulation of dendrite morphogenesis (*54*), and lipid imbalance is used as a target to protect against Aβ42-induced cytotoxicity in Alzheimer's disease (AD) fly model (*55*).

Overall, we have demonstrated that overexpression of *Rim* uniquely in *Drosophila* fat body is sufficient to promote an increment in learning and that the effect of *Rim* overexpression in the fat body can mediate changes at the transcriptional level in the adipose tissue itself and in peripheral tissues as the brain modulating pathways associated with neuronal functioning, cellular oxidative balance and detoxification, and genes from the phospholipid metabolism. Together, these results suggest that altering *Vmat* or *Rim* expression in the fat body mediates changes in gene expression in the head (brain) throughout a putative fat body-to-brain axis.

DISCUSSION

While the brain regulates adipose tissue performance, here, we show that the reverse is also plausible. We found that the expression of genes linked to axon guidance, nervous system development, neuronal system, tryptophan, and inflammation activity in human adipose tissue were all linked to cognition in three different cohorts of subjects.

SLC18A2 expression in the brain has been linked to the pathophysiology of different neuropsychiatric and neurological disorders (*39*). Similarly, decreased expression of *Rim1*α in the brain of mice led to impaired learning and memory (*41*) . For this reason, and given the associations of both *SLC18A2* and *RIMS* mRNA in the adipose tissue with cognitive function, we selected these neurotransmitter release cycle–associated genes to test their possible functional relevance. Knockdown of *slc18A2* exclusively in adipose tissue reversed the memory impairment induced by an HFD in mice (Fig. 6, F and G). Down-regulation of *Vmat* in the fat body of two different lines of *Drosophila* also led to improved short-term memory. Overexpressing *Rim* [the orthologue of regulating synaptic membrane exocytosis 1 (Rims1)] exclusively in the fat body also led to an increment in learning abilities in *Drosophila*. The altered expression of other genes linked to cognition in humans (*AMPH*, *UNC5B*, *NUDT2*, *NR4A2/NR4A3*, and *EZR*) in the fat body of *Drosophila* again modified cognition of the latter.

In the search of more accessible biomarkers, we evaluated the expression of most of these genes in PBMCs. PBMC mRNA levels of adipogenic genes decreased after weight loss in subjects with obesity (*56*), while an HFD-induced cognitive disruption led to alterations in the PBMC transcriptome in rats (*57*). Here, we show that the expression of genes in PBMCs that were most associated with cognition in adipose tissue (*NUDT2*, *AMPH*, *UNC5B*, *OAT*, *EZR*, and *NR4A2*) were also linked to cognitive traits in a cohort of 816 subjects.

The main limitation of the current study is that it is only focused on morbid obese subjects (BMI > 35 mg/kg^2); hence, our results may not be generalizable to other populations. Findings should be confirmed in longitudinal, larger samples of subjects to generalize these results to the general population.

Together, these findings suggest a systemic developmental program that changes in parallel in different tissues and cells, being reflected in neuronal networks. Current findings hint at potential therapeutic targets: Peripheral administration of miRNAs targeting the adipose tissue and influencing cognition seems far

safer than targeting the brain. Current observations also provide information about useful biomarkers in predicting cognitive decline and in monitoring response to therapy using accessible sources.

MATERIALS AND METHODS
Clinical cohorts
In discovery cohort (IRONMET, *n* = 17) (*58, 59*), from January 2016 to October 2017, a cross-sectional case-control study was undertaken in the Endocrinology Department of Dr. Josep Trueta University Hospital (Girona, Spain). In 17 morbidly obese patients (BMI > 35 mg/kg^2) aged 28 to 60 years old, adipose tissue–stranded RNA-seq was analyzed. In validation cohort 1 (INTESTINE, *n* = 22) (*58*), consecutively, 22 morbidly obese (BMI > 35 kg/m^2) subjects with different degrees of insulin action (measured using hyperinsuline-mic-euglycaemic clamp) were recruited at the Endocrinology Service of the Dr. Josep Trueta University Hospital to validate adipose tissue RNA-seq analysis.

In both cohorts, all subjects were of Caucasian origin and reported a body weight stable for at least 3 months before the study. Subjects were studied in the postabsorptive state. Exclusion criteria were previous type 2 diabetes mellitus, chronic inflammatory systemic diseases, and acute or chronic infections in the previous month; severe disorders of eating behavior or major psychiatric antecedents; neurological diseases, history of trauma or injured brain, language disorders; and excessive alcohol intake (≥40 g of OH/day in women or 80 g of OH/day in men). Body fat composition was estimated using bioelectrical impedance analysis (BC-418, Tanita Corporation of America, Illinois, USA).

This protocol was revised, validated, and approved by the ethics committee of the Dr. Josep Trueta University Hospital. The purpose of the study was explained to participants, and they signed written informed consent before being enrolled in the study.

In validation cohort 2 (Imageomics, *n* = 816) (*58, 59*), the Aging Imageomics study is an observational study including participants from two independent cohort studies (MESGI50 and MARK). Detailed description of the cohorts can be found elsewhere (*60*). Briefly, the MESGI50 cohort included a population aged ≥50 years old, while the MARK cohort included a random sample of patients aged 35 to 74 years with intermediate cardiovascular risk. Eligibility criteria included ages of ≥50 years, dwelling in the community, no history of infection during the past 15 days, no contraindications for magnetic resonance imaging, and consent to be informed of potential incidental findings. The Aging Imageomics study protocol was approved by the ethics committee of the Dr. Josep Trueta University Hospital.

In validation cohort 3 (ADIPOBRAIN, *n* = 40), all the samples and data of the participants included in this study were provided by the FATBANK (platform promoted by the CIBEROBN and coordinated by the IDIBGI Biobank) and integrated in the Spanish National Biobank Network. A total of 40 patients, ages 40 to 64 years, were included. From these, 26 subjects had morbid obesity (BMI > 35 mg/kg^2), aged between 40 and 63. Patients had no systemic disease other than obesity, and all were free of any infection in the month before the study. Liver disease [specifically tumor disease and Hepatitis C Virus (HCV) infection] and thyroid dysfunction were specifically excluded. Adipose tissue samples were obtained from VAT depots during elective surgical procedures.

Neuropsychological assessment
The primary end point in all these cohorts was the study of cognitive function. In these subjects, the following tests were collected (*58, 59*).
Digit span tests
The digit span is a subtest of the Wechsler Adult Intelligence Scale-III (*61*). It is based on numbers and includes the forward and the backward digit span tests. In the forward digit span test, the examinee repeats a number sequence in the same order as presented. This constitutes a measure not only of working memory but also of attention. In the backward digit span task, the examinee repeats in reverse order series of digits that became gradually longer. This is an executive task particularly dependent on working memory. A higher score reflects a better working memory. In a standardization sample of 394 participants (aged 16 to 89 years), the reliability coefficient was very high, ranging from 0.94 to 0.97 (*62*).
Trail making test
The TMT is composed by two parts: TMTA and TMTB. The TMTA (greater focus on attention) consisted of a standardized page in which numbers 1 to 25 are scattered within the circles, and participants were asked to connect the numbers in order as quickly as possible. Before starting the test, a six-item practice test was administered to the participants to make sure they understood both tasks. A maximum time of 300 s was allowed before suspending the test. The direct scores of TMTA were the time in seconds taken to complete each task. In the same way, the TMTB (greater focus on executive function) consisted of an alternating sequence of numbered circles and letters (*63, 64*). In both tests, shorter times to completion indicate better performance.
California verbal learning test-II
The California verbal learning test-II (CVLT) is used to assess verbal learning and memory (*65*). It consists of five learning tests in which a list of words (list A) is presented and the subject is asked, immediately after each presentation, to recall as much words as possible. Then, an interference list (list B) is presented, and the subject is asked to repeat the same task. CVLT immediate recall score is a result of the first five tests and provides information about the learning process. In the short delay test, the patient is asked to recall list A, free (CVLT short-delayed free recall) or with semantic facilitation (CVLT short-delayed cued recall). After 20 min, in which nonverbal tasks are carried on, the subjects are asked to repeat a list of words that the examinee has previously presented without semantic facilitation (the CVLT long-delayed free recall) to assess long-term memory. A higher score reflects a better memory function. About 50 min are necessary to administrate this test, and its reliability ranges from 0.78 to 0.94 (*66*).
STROOP test (Golden's version)
The STROOP test was used to assess cognitive flexibility, selective attention, inhibition, and information-processing speed. This version consists of three different parts: (i) 100 words (color names) are printed in black ink, and the subject is asked to read them as fast as possible; (ii) 100 "XXX" are printed in color ink (green, blue, and red), and the subject is asked to name as fast as possible the ink color; and (iii) 100 color names (from the first page) were printed in color ink (from the second page), the color name and the ink color do not match, and the subject is asked to name the ink color (and not to read the color name). The subject is given 45 s for each task. After the 45 s, the last item completed is noted, obtaining three scores: one for each part of the test ("W," "C,"

and "CW"). The interference ("I") index was also obtained from the subtraction CW − CW′, where CW′ = (C × W)/(C + W). Standard administration procedures were followed as indicated in the test manual (*67*).

Memory binding test
The memory binding test consists of 16 category cues two word lists containing 16 word items in each list. Both lists are learned and recalled by controlled learning and cued and paired recall. The memory binding test produces four principal measures, the total paired recall, total free recall, total delayed free recall, and total delayed paired recall.

Symbol digit test
The symbol digit test is a subtest of the Wechsler Adult Intelligence Scale-III. It includes a coding key that shows nine abstract symbols, each paired with a number, and below the key, series of symbols were presented. The participants were asked to write down the corresponding numbers associated with the abstract symbols as quickly as possible. This task is a measure of information processing speed. The number of correct substitutions during a 90-s interval was scored, and higher numbers indicate better performance.

General cognition
A composite cognitive score was computed as the sum of the standardized scores of each individual for each test included in the Aging Imageomics cohort.

Adipose tissue collection and handling
Adipose tissue samples were obtained from SAT and VAT during elective surgical procedures (cholecystectomy, surgery of abdominal hernia, and gastric bypass surgery) (*68*). Both SAT and VAT samples were collected from the abdomen, following standard procedures. Samples of adipose tissue were immediately transported to the laboratory (5 to 10 min). The handling of tissue was carried out under strictly aseptic conditions. Adipose tissue samples were washed in phosphate-buffered saline, cut off with forceps and scalpel into small pieces (100 mg), and immediately flash-frozen in liquid nitrogen before stored at −80°C.

VAT- and SAT-stranded RNA-seq (discovery IRONMET; validation cohort 1 INTESTINE)
VAT and SAT RNA purification was performed using RNeasy-Tissue Mini-Kit (QIAGEN). Total RNA was quantified by Qubit RNA BR Assay kit (Thermo Fisher Scientific), and the integrity was checked by using the RNA Kit (15NT) on 5300 Fragment Analyzer System (Agilent Technologies) (*68*).

The RNA-seq libraries were prepared with Illumina TruSeq Stranded Total RNA Sample Preparation kit following the manufacturer's recommendations with some modifications. Briefly, in function of availability, 100 to 500 ng of total RNA was ribosomal RNA depleted using the RiboZero Magnetic Gold Kit and fragmented by divalent cations. The strand specificity was achieved during the second-strand synthesis performed in the presence of deoxyuridine triphosphate. The cDNA was adenylated and ligated to Illumina platform compatible IDT adaptors with unique dual indexes with unique molecular identifiers (Integrated DNA Technologies) for paired-end sequencing. The ligation products were enriched with 15 PCR cycles, and the final library was validated on an Agilent 2100 Bioanalyzer with the DNA 7500 assay (Agilent Technologies). The libraries were sequenced on NovaSeq 6000 (Illumina) in a fraction of sequencing flow cell with a read length of 2 × 101 base pairs

following the manufacturer's protocol for dual indexing. Image analysis, base calling, and quality scoring of the run were processed using the manufacturer's software Real Time Analysis (RTA v3.4.4) and followed by generation of FASTQ sequence files.

RNA-seq reads were mapped against human reference genome (GRCh38) using STAR software version 2.5.3a (*69*) with ENCODE parameters. Genes were quantified using RSEM version 1.3.0 (*70*) with default parameters and using the annotation file from GENCODE version 29. Only protein-coding genes that were expressed >1 count per million (cpm) in at least 10 samples were considered for the association of gene expression with clinical variables.

Circulating gene expression analysis (validation cohort 2, Aging Imageomics)
Total RNA was purified from blood using PAXgene Blood RNA Kit (QIAGEN, Gaithersburg, MD). RNA concentrations were assessed with Nanodrop ND-1000 Spectrophotometer (Thermo Fisher Scientific, Wilmington, DE). Total RNA was reverse-transcribed to cDNA using High Capacity cDNA Archive Kit (Applied Biosystems, Darmstadt, Germany). Gene expression was assessed by RT-PCR using the LightCycler 480 Real-Time PCR System (Roche Diagnostics SL, Barcelona, Spain), using SYBR green technology suitable for relative genetic expression quantification. Glyceraldehyde-3-phosphate dehydrogenase (GAPDH) was used as endogenous control.

The commercially predesigned KiCqStart primers used were as follows: NR4A2, 5′-GACTATCAAATGAGTGGAGATG-3′ (forward) and 5′-GACCTGTATGCTAATCGAAG-3′ (reverse); OAT, 5′-CAGACCTGATATAGTCCTCC-3′ (forward) and 5′-CTTCTTCTA AAACCTCAAGGG-3′ (reverse); amphiphysin (AMPH), 5′-CCTGACATAAAGAATCGCATC-3′ (forward) and 5′-CAAACACTTTCTGTGCTTTC-3′ (reverse); nudix hydrolase 2 (NUDT2), 5′-TTCTGCTTCGGTCCTTAG-3′ (forward) and 5′-AACTCAATTGCATTGTTGTC-3′ (reverse); Unc-5 netrin receptor B (UNC5B), 5′-AGGACAGTTACCACAACC-3′ (forward) and 5′-GGGGATCTCCTGGTATTTG-3′ (reverse); EZR, 5′-TGACTTTGTGTTTTATGCCC-3′ (forward) and 5′-CTCCTTTTCTT CTCTGTTTCC-3′ (reverse); GAPDH, 5′-ACAGTTGCCATGTAGACC-3′ (forward) and 5′-TTGAGCA CAGGGTACTTTA-3′ (reverse).

VAT expression of candidate genes by RT-PCR (validation cohort 3 ADIPOBRAIN)
Total RNA was purified from VAT using RNeasy Lipid Tissue Mini Kit (QIAGEN, Izasa, SA). RNA concentrations were assessed with Nanodrop ND-1000 Spectrophotometer (Thermo Fisher Scientific, Wilmington, DE), and the integrity was checked by Agilent Bioanalyzer (Agilent Technologies, Palo Alto, CA). Total RNA was reverse-transcribed to cDNA using High Capacity cDNA Archive Kit (Applied Biosystems, Darmstadt, Germany). Gene expression was assessed by RT-PCR using a LightCycler 480 Real-Time PCR System (Roche Diagnostics SL, Barcelona, Spain), using TaqMan technology suitable for relative genetic expression quantification. Peptidylprolyl isomerase A (PPIA) and GAPDH were used as endogenous control. The commercially available and prevalidated TaqMan primer/probe sets used were as follows: SLC18A2 (Hs00996835_m1); RIMS1 (Hs01112189_m1), PPIA (Hs99999904_m1), and GAPDH (4352934). The commercially

predesigned KiCqStart primers used were as follows: NUDT2, EZR, UNC5B, NR4A2, and PPIA.

Plasma HPLC-ESI-MS/MS metabolomics (discovery IRONMET)

Metabolites were extracted from plasma samples with methanol (containing phenylalanine-C13 as an internal standard) according to previously described methods (*58, 59, 71*). Briefly, samples (30 μl) of cold methanol were added to 10 μl of each sample, vortexed for 1 min, and incubated for one hour at −20°C. Samples were homogenized using FastPrep-24 (MP Biomedicals) and were incubated overnight in a rocker at 4°C. Then, all samples were centrifuged for 3 min at 12,000*g*, and the supernatant was recovered and filtered with a 0.2 μm Eppendorf filter. Two microliters of the extracted sample were applied onto a reversed-phase column (Zorbax SB-Aq 1.8 μm, 2.1 × 50 mm; Agilent Technologies) equipped with a precolumn (Zorbax-SB-C8 Rapid Resolution Cartridge 2.1 × 30 mm, 3.5 μm; Agilent Technologies) with a column temperature of 60°C. The flow rate was 0.6 Ml/min. Solvent A was composed of water containing 0.2% acetic acid, and solvent B was composed of methanol containing 0.2% acetic acid. The gradient started at 2% B, increased to 98% B in 13 min, and held at 98% B for 6 min. Posttime was established in 5 min.

Data were collected in positive and negative electrospray modes time of flight operated in full-scan mode at 50 to 3000 mass/charge ratio in an extended dynamic range (2 GHz), using N2 as the nebulizer gas (5 liters/min at 350°C). The capillary voltage was 3500 V with a scan rate of 1 scan/s. The ESI source used a separate nebulizer for the continuous, low-level (10 liters/min) introduction of reference mass compounds 121.050873 and 922.009798, which were used for continuous, online mass calibration. MassHunter Data Analysis software (Agilent Technologies, Barcelona, Spain) was used to collect the results, and MassHunter Qualitative Analysis software (Agilent Technologies, Barcelona, Spain) was used to obtain the molecular features of the samples, representing different, comigrating ionic species of a given molecular entity using the Molecular Feature Extractor algorithm (Agilent Technologies, Barcelona, Spain). We selected samples with a minimum of two ions. Multiple charge states were forbidden. Compounds from different samples were aligned using a retention time window of 0.1% ± 0.25 min and a mass window of 20.0 parts per million (ppm) ± 2.0 mDa. We selected only those present in at least 50% of the samples of one group and corrected for individual bias.

Plasma ^{1}H NMR metabolomics (discovery IRONMET)

Plasma samples were thawed at room temperature. For each sample, 400 μl of plasma were combined with 200 μl of phosphate buffer [9% (w/v) NaCl and 100% D$_2$O] that contained 10 mM of 3-trimethyl-silyl-1-[2,2,3,3-^{2}H4] (TSP) (*58, 59*). Samples were mixed with the use of a vortex and centrifuged (10,000*g*) for 10 min. Then, a 550 μl aliquot was transferred into a 5 mm NMR tube before NMR analysis. ^{1}H spectra of low–molecular weight metabolites were performed using a Carr-Purcell-Meiboom-Gill (CPMG) sequence (RD–90°–[t–180°– t]$_n$–ACQ-FID) with spin-echo delay of 400 μs (for a total T2 filter of 210 ms) allowing an efficient attenuation of the lipid NMR signals. The CPMG sequence generates spectra edited by T2 relaxation times, reducing broad resonances from high–molecular weight compounds facilitating the observation of low–molecular weight metabolites. The total acquisition time was

2.73 s with a Recycling Delay (RD) of 2 s, and the 90° pulse length was automatically calibrated for each sample at around 11.1 μs. For each sample, eight dummy scans were followed by 256 scans and collected in 64,000 points over a spectral width of 20 ppm. TSP was used a general reference for NMR samples because it does not introduce any additional signals apart from the sharp methylsilyl resonance at 0 ppm. In addition, a high concentration of TSP was used to release low–weight metabolites with high affinity for serum proteins by binding competition with TSP.

All ^{1}H NMR spectra were recorded at 300 K on an Avance III 600 spectrometer (Bruker, Germany) operating at a proton frequency of 600.20 MHz using a 5 mm Broad Band Multinuclear (PABBO) gradient probe and automatic sample changer with a cooling rack at 4°C.

Plasma cytokines and neurotoxic proteins

Commercially available enzyme-linked immunosorbent assay (ELISA) kits were used to measure the plasma of IL-6 (RND-HS600C, human IL-6 Quantikine HS ELISA kit, R&D Systems), IL-4 (RND-HS400, human IL-4 Quantikine HS ELISA kit, R&D Systems), α-synuclein (RND-DY1338-05, human α-synuclein DuoSet ELISA, R&D Systems), Aβ42 [RND-DAB142, human Aβ (amino acids 1 to 42) Quantikine ELISA kit, R&D Systems], and tau (NBP2-62749, human tau ELISA kit, Novus Biologicals) following the manufacturer's protocol.

D. melanogaster experiments
D. melanogaster stocks and maintenance

Flies were raised on standard medium (cornmeal, sugar, and yeast) and cultured according to standard procedures at 28°C in a 12:12-hour light-dark cycle.

Conditional RNAi lines targeting the genes of interest are summarized in table S47. v60000 (control 1) and v60100 (control 2) were obtained from Vienna *Drosophila* RNAi Centre (http://stockcenter.vdrc.at/control/main) and used as the corresponding genetic background controls for KK and GD RNAi line collections, respectively. The *Rim* overexpression line (UAS-Rim), stock BL78050, referred to as *UAS-Rim* and the corresponding genetic background control (BL36304; control 3) were obtained from the Bloomington *Drosophila* Stock Centre (http://flystocks.bio.indiana.edu/). *UAS-Rim* was subsequently isomerized for six generations into the (BL36304; control 3) genetic background.

RNAi expression in the fat body was induced by *w; C7*-GAL4*; UAS-Dcr-2* driver line, which carries a fat tissue–specific promoter, driving the expression of GAL4 specifically on *Drosophila* adiposities, was provided by M. Jindra (*72*).

Drosophila courtship conditioning

Drosophila courtship conditioning was used to assess *Drosophila* learning and memory capabilities. Courtship conditioning was performed as described previously (*45*). RNAi and overexpression lines together with their corresponding genetic background controls (table S47) were crossed with *w; C7*-GAL4*; UAS-Dcr-2* driver line and raised at 28°C to down-regulate or overexpress the corresponding targeted genes in the adipose tissue. Males were collected at eclosion.

and kept in isolation until 7 days of age at 25°C. Males were randomly assigned to either trained or naïve groups. Learning capabilities were assessed by pairing individual males with a single premated wild-type female for 2.5 hours during the training

period. Immediately after training, the males were tested to assess learning. Short-term memory was assessed by pairing individual males with a single premated wild-type female for 6 hours during the training period, and, subsequently, the male was individually isolated for 1 hour before testing. Testing was performed by transferring male to a 1-cm-diameter chamber with in the presence of a premated female and filmed for 8 min. The courtship behavior of male flies toward females was quantified manually from videos. The mean CIs (defined as the percentage of time spent on courtship during an 8-min interval) of trained males and naïve males were used to calculate the LI, which is defined as the per cent reduction in mean courtship activity in trained males compared with naïve males; $LI = (CI_{naïve} - CI_{trained})/CI_{naïve}$. For all conditions, male-female pairs were analyzed on a minimum of three different test days, and the data were pooled.

Nonparametrical statistical bootstrapping analysis was preformed to assess differences in LI (learning and short-term memory) between RNAi knockdown or overexpression lines and their corresponding genetic background controls. The R script provided by Koemans et al. (45) was used to perform the bootstrapping analysis. Briefly, CI values were randomly sampled with replacement to generate 10,000 hypothetical LIs, which were used to determine the 95% confidence interval of the difference between the index of the control and the index of the knockdown and the probability that this difference is >0. t test or one-way analysis of variance (ANOVA) was performed to assess statistical differences in CI of the compared conditions.

mRNA extraction and cDNA synthesis
Seven-day-old male were selected for quantitative RT-PCR (qRT-PCR) or RNA-seq. A total of 10 adult heads or 10 fat bodies were collected per sample and transferred to RNAlater solution (Sigma-Aldrich). Total RNA was extracted using the Arcturus PicoPure RNA Purification kit (Thermo Fisher Scientific). To avoid amplification from genomic DNA, deoxyribonuclease treatment was performed using the DNA-free Ambion kit, and RNA was reverse-transcribed into cDNA using the High-Capacity cDNA reverse transcription (Applied Biosystems) according to the manufacturers' procedures.

Quantitative real-time polymerase chain reaction
Quantitative PCRs were performed using the LightCycler 480 SYBR Green Master (Roche) in a LightCycler 480 II machine (Roche). Primer sequences and the reference genes RNApol2 and 1tub23cf are provided in table S51. For each condition, a minimum of five biological replicates and two technical replicates were analyzed. Differential gene expression was calculated using the $2^{\Delta\Delta Ct}$ method. The average threshold cycle (C_t) value for each sample was calculated and subtracted from the geometric mean C_t value of the reference genes RNApol2 and 1tub23cf to calculate the ΔC_t value. t test (GraphPad Prism version 5.00 for Windows) was used for calculations of P values.

mRNA sequencing of fat body and fly heads
The starting material for sequencing library preparation was total RNA. The samples were quantified using the Qubit RNA BR Assay kit (Thermo Fisher Scientific), and RNA integrity was estimated with the RNA 6000 Nano Bioanalyzer 2100 Assay (Agilent Technologies). The RNA-seq libraries were constructed using the KAPA Stranded mRNA-Seq Illumina Platforms Kit (Roche), following the manufacturer's recommendations. The size and

quality of the libraries were assessed using a High Sensitivity DNA Bioanalyzer assay (Agilent Technologies). The libraries were sequenced on a NovaSeq 6000 (Illumina) in paired-end mode, with a read length of 2 × 51 base pairs, following the manufacturer's protocol for dual indexing. Image analysis, base calling, and quality scoring of the run were processed using the manufacturer's software, Real Time Analysis (RTA 3.4.4). RNA-seq reads were mapped D. melanogaste reference genome (BDGP6.32) with STAR/2.7.8a (ref1) with ENCODE parameters (69) with ENCODE parameters. Gene quantification was performed with RSEM/1.3.0 (70) with default parameters and using ensembl109 annotation. Only protein-coding genes that were expressed >1 cpm in at least 10 samples were considered.

Mice experiment
Animals
Male wild-type C57BL/6J (Charles River, France) 8-week-old mice were housed individually in controlled laboratory conditions (21° ± 1°C, 55 ± 10%) with illumination at 12-hour cycles (lights on at 7:30 a.m. and off at 7:30 p.m.). Animals were fed ad libitum for 8 weeks either with an ND (~3.514 kcal/kg: 10% fat, 66% carbohydrate, and 24% protein; n = 23) or an HFD (~5.228 kcal/kg: 60% fat, 16% carbohydrate, and 24% protein; n = 25). ND and HFD were obtained from Altromin Spezialfutter GmbH & Co. (KG, Lage, Germany), references C1090-10, and C1090-60, respectively. Three days after the start of the diet, weight-matched mice of each group (ND or HFD) were divided into two groups and injected intravenously via tail vein with 200 μl of either the AAV8-RSV-GFP-Adp-miR-NASLC18A2 vector containing 1 × 10^12 Genome Copies (GC) (Fig. 6C) in phosphate-buffered saline or with saline. Adeno-associated virus (AAV) vector was produced by the Viral Production Unit, UAB (www.viralvector.eu/). The AAV2/8-RSV-GFP-Adp-miRNASLC18A2 vector expresses the GFP and an miRNA designed to down-regulate SLC18A2 gene expression. It has a recombinant AAV2/8 serotype that has been demonstrated to be effective at targeting adipose tissue (73). Adipose selectivity was enhanced by incorporating a proximal promoter and distal enhancer of the adiponectin gene into the AAV vector. To decrease vector expression in the liver, this AAV incorporates eight copies of the liver-specific miR-122T into the 3′ untranslated region of the expression cassette (Fig. 6C) (73). Bodyweight and food intake were monitored weekly for the entire protocol. All experiments were performed during the light phase. Mice were euthanized by decapitation, and mWAT was collected and frozen with dry ice. All procedures were conducted in strict accordance with the guidelines of the European Communities Directive 86/609/EEC regulating animal experimentation and were approved by the local ethical committee (Comitè Ètic d'Experimentació Animal-Parc de Recerca Biomèdica de Barcelona, CEEA-PRBB, agreement no. 9687).

Experimental procedure
Behavioral tasks aimed to assess short- and long-term memory (novel object recognition in V-maze), and locomotor activity (horizontal and vertical activity assessment) was performed chronologically as indicated in (Fig. 6D) using standardized tests.

Novel object recognition test (V-MAZE)
Object-recognition memory was assayed in a V-shaped maze (30 cm long × 4.5 cm wide × 15 3 cm height each corridor) (74, 75). On day 1 of the test, mice were habituated for 9 min to the maze. Then, 24 hours later, mice were put back in the maze for 9 min, two

identical objects were presented, and the time that the mice spent exploring each object was recorded. The mice were again placed in the maze 3 hours (30 days after the AAV injection to assess short-term memory) or 24 hours (37 days after the AAV injection to assess long-term memory) later for 9 min, with one of the familiar objects replaced with a novel object. The total time spent exploring each of the two objects (novel and familiar) was computed. A discrimination index was calculated as the difference between the times spent exploring the novel object divided by the total time exploring both objects. A higher discrimination index is considered to reflect greater memory retention for the familiar object (76, 77).

Locomotion
On day 46 after AAV injection, mice underwent a 1-hour locomotion test in individual locomotor activity boxes (10.8 × 20.3 × 18.6 cm; Imetronic, Pessac, France) equipped with infrared sensors to detect locomotor activity and an infrared plane to detect rearing (76, 77).

Statistical analysis
The number of animals (n) in each experimental condition is indicated in figure legends. All graphs and statistical comparisons were performed using GraphPad Prism software version 8.0 for Mac (GraphPad Software, San Diego, CA, USA). To test whether the data were normally distributed, the Kolmogorov-Smirnov test was applied. Comparison of means between different groups was performed using two-way ANOVA, followed by Newman-Keuls multiple comparisons test as post hoc test. Three-way ANOVA was performed when required to test the evolution over time. Results are expressed as individual values with the means ± SEM, specified in the figure legend. A $P < 0.05$ was used to determine statistical significance.

RNA expression
RNA purification was performed using RNeasy Lipid Tissue Mini Kit (QIAGEN, Hilden, Germany), and concentrations were measured using a Nanodrop ND-1000 Spectrophotometer (Thermo Fisher Scientific, Waltham, MA). Integrity was checked by Agilent Bioanalyzer (Agilent Technologies, Palo Alto, CA). Total RNA was reversed transcribed to cDNA using High Capacity cDNA Archive Kit (Applied Biosystems, Darmstadt, Germany). Gene expression was assessed by RT-PCR using a LightCycler 480 Real-Time PCR System (Roche Diagnostics SL, Barcelona, Spain), using SYBR Green technology suitable for relative genetic expression quantification. The RT-PCR reaction was performed in a final volume of 10 μl. The cycle program consisted of an initial denaturing of 10 min at 95°C and then 40 cycles of 15 s denaturizing phase at 95°C and 1 min annealing and extension phase at 60°C. A C_t value was obtained for each amplification curve and then a ΔC_t was first calculated by subtracting the C_t value for endogenous control from the C_t value for each sample. Fold changes compared with the endogenous control were then determined by calculating $2 - \Delta C_t$. β-Actin (Actb) was used as housekeeping. Actb and GFP were analyzed by SYBR green technology using the following primer sets: Actb, 5′-GATGTATGAAGGCTTTGGTC-3′ (forward) and 5′-TGTGCACTTTTATTGGTCTC-3′ (reverse); GFP, 5′-CAACAGCCACAACGTCTATATCATG-3′ (forward) and 5′-ATGTTGTGGCGGATCTTGAAG-3′ (reverse).

Protein analysis
Adipose tissue samples (100 mg) were homogenized using radioimmunoprecipitation lysis buffer system (sc-24948, Santa Cruz Biotechnology, CA) at 4°C for 30 min. Cellular debris were eliminated by centrifugation at 13,000g for 15 min (4°C). Protein concentration was determined using the RC/DC Protein Assay (Bio-Rad Laboratories, Hercules, CA). For Western blot analysis, samples were resolved by SDS–polyacrylamide gel electrophoresis and transferred to a polyvinylidene difluoride membrane (Bio-Rad Laboratories, Hercules, CA). Membrane was exposed overnight at 4°C to primary antibody VMAT2/SLC18A2 (EB06558) at 1:250 dilution (VWR International EuroLab, SL) diluted in 2% bovine serum albumin–1× tris-buffered saline containing 0.1% Tween 20, following the recommendations of the manufacturer. After secondary antibody incubation (anti-goat horseradish peroxidase), signal was detected using enhanced chemiluminescence horseradish peroxidase substrate (Millipore) and analyzed with a luminescent image analyzer ChemiDoc MP Imaging System (Bio-Rad Laboratories, Hercules, CA). TGX Stain-Free gels (#4568096, Bio-Rad Laboratories, Hercules, CA) were used as protein loading control.

Statistical analysis
Differential expression gene analyses were performed on gene counts using the "limma" R package (78). First, low expressed genes were filtered, so that only genes with more than 10 reads in at least two samples were selected. RNA-seq data were then normalized for RNA composition using the trimmed mean of M value as implemented in edgeR package (79). Normalized counts were then converted to $\log_2$ count per million with associated precision weights to account for variations in precision between different observations using the "voom" function with donor's age, BMI, sex, and education years as covariates. A robust linear regression model adjusted for the previous covariates was then fitted to the data using the "lmFit" function with the option method = "robust," to limit the influence of outlying samples. Last, an empirical Bayes method was applied to borrow information between genes with the "eBayes" function. P values were adjusted for multiple comparisons using the pFDR. A cutoff for the pFDR of <0.05 was used a threshold for statistical significance. The functional roles of differentially expressed genes were characterized using overrepresentation analyses based on the Reactome and WikiPathways databases using ConsensusPathDB (80). Pathway significance was assessed using a hypergeometric test, and a Storey procedure (q value) was applied for multiple testing corrections. Statistical significance was set at $q < 0.1$. For differentially expressed genes simultaneously in the VAT and SAT of the discovery and validation cohorts, data were further analyzed using functional gene-gene interaction networks mapping genes to the STRING database (which integrates known and predicted protein/gene interactions) (81). Then, functional local clusters in the interaction network were determined using a Markov cluster algorithm (MCL) with an inflation parameter = 1.4. Active interacting sources including text mining, experiments, databases, coexpression, and cooccurrence and an interaction score of >0.4 were used to construct the interaction networks. In addition, we integrated the information provided from differential expression analysis, gene-gene interaction networks, and pathway overrepresentation analysis using the R package "pathfinder" with default parameters (82). First, significant genes were mapped onto a STRING gene-gene interaction network. Then, active subnetworks of interconnected genes (including genes that are not significant themselves but connect significant genes) in this gene-gene interaction network were identified. Last, separate pathway overrepresentation analyses based on the Reactome

databases were performed for each active subnetwork using the significant genes in each of the active subnetworks and genes in the Protein-protein Interaction Network (PIN) as the background genes. Pathway statistical significance was set at the pFDR of <0.05. Significantly enriched pathways were clustered via hierarchical clustering. Genes in each pathway were used to calculate the pairwise kappa statistics, a chance-corrected measure of cooccurrence between pathways. The distance matrix 1-kappa statistic was used for agglomerative hierarchical clustering and a threshold of 0.35 for the kappa statistics was used to define strong relation. Partial Spearman's correlation analysis controlling for age, BMI, sex, and education level was used to determine the correlation between circulating levels of genes and the neurocognitive tests scores. As it works by obtaining the residuals of the ranked variables after removing the effect of the ranked covariates, scatter and violin plots were generated with the ranked residuals of the model adjusting for selected covariates. Nonparametric monotonic trends according to the gene tertiles or quintiles for the selected cognitive tests were assessed by the Mann-Kendall trend test.

Supplementary Materials

This PDF file includes:
Figs. S1 to S7
Legends for tables S1 to S51

Other Supplementary Material for this manuscript includes the following:
Tables S1 to S51

REFERENCES AND NOTES

1. P. S. Minhas, A. Latif-Hernandez, M. R. McReynolds, A. S. Durairaj, Q. Wang, A. Rubin, A. U. Joshi, J. Q. He, E. Gauba, L. Liu, C. Wang, M. Linde, Y. Sugiura, P. K. Moon, R. Majeti, M. Suematsu, D. Mochly-Rosen, I. L. Weissman, F. M. Longo, J. D. Rabinowitz, K. I. Andreasson, Restoring metabolism of myeloid cells reverses cognitive decline in ageing. *Nature* **590**, 122–128 (2021).

2. A. N. Suarez, T. M. Hsu, C. M. Liu, E. E. Noble, A. M. Cortella, E. M. Nakamoto, J. D. Hahn, G. De Lartigue, S. E. Kanoski, Gut vagal sensory signaling regulates hippocampus function through multi-order pathways. *Nat. Commun.* **9**, 2181 (2018).

3. H. Endle, B. Horta, B. Stutz, M. Muthuraman, I. Tegeder, Y. Schreiber, I. F. Snodgrass, R. Gurke, Z.-W. Liu, M. Sestan-Pesa, K. Radyushkin, N. Streu, W. Fan, J. Baumgart, Y. Li, F. Kloss, S. Groppa, N. Opel, U. Dannlowski, H. J. Grabe, F. Zipp, B. Rácz, T. L. Horvath, R. Nitsch, J. Vogt, AgRP neurons control feeding behaviour at cortical synapses via peripherally derived lysophospholipids. *Nat. Metab.* **4**, 683–692 (2022).

4. Y. Qu, H. Y. Hu, Y. N. Ou, X. N. Shen, X. Wu, Z. T. Wang, Q. Dong, L. Tan, J. T. Yu, Association of body mass index with risk of cognitive impairment and dementia: A systematic review and meta-analysis of prospective studies. *Neurosci. Biobehav. Rev.* **115**, 189–198 (2020).

5. X. Tang, W. Zhao, M. Lu, X. Zhang, P. Zhang, Z. Xin, R. Sun, W. Tian, M. A. Cardoso, J. Yang, R. Simó, J. B. Zhou, C. D. A. Stehouwer, Relationship between central obesity and the incidence of cognitive impairment and dementia from cohort studies involving 5,060,687 participants. *Neurosci. Biobehav. Rev.* **130**, 301–313 (2021).

6. A. K. Dahl, L. B. Hassing, E. I. Fransson, M. Gatz, C. A. Reynolds, N. L. Pedersen, Body mass index across midlife and cognitive change in late life. *Int. J. Obes. (Lond)* **37**, 296–302 (2013).

7. H. Gardener, M. Caunca, C. Dong, Y. K. Cheung, T. Rundek, M. S. V. Elkind, C. B. Wright, R. L. Sacco, Obesity measures in relation to cognition in the Northern Manhattan study. *J. Alzheimers Dis.* **78**, 1653–1660 (2020).

8. M. C. Farruggia, D. M. Small, Effects of adiposity and metabolic dysfunction on cognition: A review. *Physiol. Behav.* **208**, 112578 (2019).

9. W. Zeng, R. M. Pirzgalska, M. M. A. Pereira, N. Kubasova, A. Barateiro, E. Seixas, Y. H. Lu, A. Kozlova, H. Voss, G. G. Martins, J. M. Friedman, A. I. Domingos, Sympathetic neuro-adipose connections mediate leptin-driven lipolysis. *Cell* **163**, 84–94 (2015).

10. F. Cardoso, R. G. J. Klein Wolterink, C. Godinho-Silva, R. G. Domingues, H. Ribeiro, J. A. da Silva, I. Mahú, A. I. Domingos, H. Veiga-Fernandes, Neuro-mesenchymal units control ILC2 and obesity via a brain–adipose circuit. *Nature* **597**, 410–414 (2021).

11. S. F. Morrison, K. Nakamura, Central mechanisms for thermoregulation. *Annu. Rev. Physiol.* **81**, 285–308 (2019).

12. K. Sodhi, R. Pratt, X. Wang, H. V. Lakhani, S. S. Pillai, M. Zehra, J. Wang, L. Grover, B. Henderson, J. Denvir, J. Liu, S. Pierre, T. Nelson, J. I. Shapiro, Role of adipocyte Na,K-ATPase oxidant amplification loop in cognitive decline and neurodegeneration. *iScience* **24**, 103262 (2021).

13. D. H. Guo, M. Yamamoto, C. M. Hernandez, H. Khodadadi, B. Baban, A. M. Stranahan, Visceral adipose NLRP3 impairs cognition in obesity via IL-1R1 on CX3CR1⁺ cells. *J. Clin. Investig.* **130**, 1961–1976 (2020).

14. D. H. Guo, M. Yamamoto, C. M. Hernandez, H. Khodadadi, B. Baban, A. M. Stranahan, Beige adipocytes mediate the neuroprotective and anti-inflammatory effects of subcutaneous fat in obese mice. *Nat. Commun.* **12**, 4623 (2021).

15. M. Kivipelto, F. Mangialasche, T. Ngandu, Lifestyle interventions to prevent cognitive impairment, dementia and Alzheimer disease. *Nat. Rev. Neurol.* **14**, 653–666 (2018).

16. S. Anazi, S. Maddirevula, E. Faqeih, H. Alsedairy, F. Alzahrani, H. E. Shamseldin, N. Patel, M. Hashem, N. Ibrahim, F. Abdulwahab, N. Ewida, H. S. Alsaif, H. Al Sharif, W. Alamoudi, A. Kentab, F. A. Bashiri, M. Alnaser, A. H. Alwadei, M. Alfadhel, W. Eyaid, A. Hashem, A. Al Asmari, M. M. Saleh, A. Alsaman, K. A. Alhasan, M. Alsughayir, M. Al Shammari, A. Mahmoud, Z. N. Al-Hassnan, M. Al-Husain, R. Osama Khalil, N. Abd Elmeguid, A. Masri, R. Ali, T. Ben-Omran, P. Elfishway, A. Hashish, A. Ercan Sencicek, M. State, A. M. Alazami, M. A. Salih, N. Altassan, S. T. Arold, M. Abouelhoda, S. M. Wakil, D. Monies, R. Shaheen, F. S. Alkuraya, Clinical genomics expands the morbid genome of intellectual disability and offers a high diagnostic yield. *Mol. Psychiatry* **22**, 615–624 (2017).

17. F. Diaz, S. Khosa, D. Niyazov, H. Lee, R. Person, M. M. Morrow, M. Signer, N. Dorrani, A. Zheng, M. Herzog, R. Freundlich, J. B. Birath, Y. Cervantes-Manzo, J. A. Martinez-Agosto, C. Palmer, S. F. Nelson, B. L. Fogel, S. K. Mishra, Novel NUDT2 variant causes intellectual disability and polyneuropathy. *Ann. Clin. Transl. Neurol.* **7**, 2320–2325 (2020).

18. K. Takei, V. I. Slepnev, V. Haucke, P. De Camilli, Functional partnership between amphiphysin and dynamin in clathrin-mediated endocytosis. *Nat. Cell Biol.* **1**, 33–39 (1999).

19. S. Bergström, J. Remnestål, J. Yousef, J. Olofsson, I. Markaki, S. Carvalho, J. C. Corvol, K. Kultima, L. Kilander, M. Löwenmark, M. Ingelsson, K. Blennow, H. Zetterberg, B. Nellgård, F. Brosseron, M. T. Heneka, B. Bosch, R. Sanchez-Valle, A. Månberg, P. Svenningsson, P. Nilsson, Multi-cohort profiling reveals elevated CSF levels of brain-enriched proteins in Alzheimer's disease. *Ann. Clin. Transl. Neurol.* **8**, 1456–1470 (2021).

20. Y. Yu, T. Niccoli, Z. Ren, N. S. Woodling, G. Aleyakpo, L. Szabadkai, L. Partridge, PICALM rescues glutamatergic neurotransmission, behavioural function and survival in a Drosophila model of Aβ42 toxicity. *Hum. Mol. Genet.* **29**, 2420–2434 (2020).

21. C. Sheng, U. Javed, M. Gibbs, C. Long, J. Yin, B. Qin, Q. Yuan, Experience-dependent structural plasticity targets dynamic filopodia in regulating dendrite maturation and synaptogenesis. *Nat. Commun.* **9**, 3362 (2018).

22. A. Ginguay, L. Cynober, E. Curis, I. Nicolis, Ornithine aminotransferase, an important glutamate-metabolizing enzyme at the crossroads of multiple metabolic pathways. *Biology (Basel)* **6**, 18 (2017).

23. M. Arnoriaga-Rodríguez, J. Mayneris-Perxachs, O. Contreras-Rodríguez, A. Burokas, J. A. Ortega-Sanchez, G. Blasco, C. Coll, C. Biarnés, A. Castells-Nobau, J. Puig, J. Garre-Olmo, R. Ramos, S. Pedraza, R. Brugada, J. C. Vilanova, J. Serena, J. Barretina, J. Gich, V. Pérez-Brocal, A. Moya, X. Fernández-Real, L. Ramio-Torrentà, R. Pamplona, J. Sol, M. Jové, W. Ricart, M. Portero-Otin, R. Maldonado, J. M. Fernández-Real, Obesity-associated deficits in inhibitory control are phenocopied to mice through gut microbiota changes in one-carbon and aromatic amino acids metabolic pathways. *Gut* **70**, 2283–2296 (2021).

24. M. Arnoriaga-Rodríguez, J. Mayneris-Perxachs, A. Burokas, O. Contreras-Rodríguez, G. Blasco, C. Coll, C. Biarnés, R. Miranda-Olivos, J. Latorre, J. M. Moreno-Navarrete, A. Castells-Nobau, M. Sabater, M. E. Palomo-Buitrago, J. Puig, S. Pedraza, J. Gich, V. Pérez-Brocal, A. Moya, X. Fernández-Real, L. Ramió-Torrentà, R. Pamplona, J. Sol, M. Jové, M. Portero-Otin, R. Maldonado, J. M. Fernández-Real, Obesity impairs short-term and working memory through gut microbial metabolism of aromatic amino acids. *Cell Metab.* **32**, 548–560.e7 (2020).

25. D. Carulli, F. de Winter, J. Verhaagen, Semaphorins in adult nervous system plasticity and disease. *Front. Synaptic Neurosci.* **13**, 672891 (2021).

26. T. C. Südhof, Neuroligins and neurexins link synaptic function to cognitive disease. *Nature* **455**, 903–911 (2008).

27. V. García-Morales, F. Montero, D. González-Forero, G. Rodríguez-Bey, L. Gómez-Pérez, M. J. Medialdea-Wandossell, G. Domínguez-Vías, J. M. García-Verdugo, B. Moreno-López, Membrane-derived phospholipids control synaptic neurotransmission and plasticity. *PLOS Biol.* **13**, e1002153 (2015).

28. R. W. Mitchell, G. M. Hatch, Fatty acid transport into the brain: Of fatty acid fables and lipid tails. *Prostaglandins Leukot. Essent. Fatty Acids* **85**, 293–302 (2011).

29. L. N. Nguyen, D. Ma, G. Shui, P. Wong, A. Cazenave-Gassiot, X. Zhang, M. R. Wenk, E. L. K. Goh, D. L. Silver, Mfsd2a is a transporter for the essential omega-3 fatty acid do-cosahexaenoic acid. *Nature* **509**, 503–506 (2014).

30. K. Bourassa, D. A. Sbarra, Body mass and cognitive decline are indirectly associated via inflammation among aging adults. *Brain Behav. Immun.* **60**, 63–70 (2017).

31. Y. Yang, G. S. Shields, Q. Wu, Y. Liu, H. Chen, C. Guo, The association between obesity and lower working memory is mediated by inflammation: Findings from a nationally repre-sentative dataset of U.S. adults. *Brain Behav. Immun.* **84**, 173–179 (2020).

32. C. Wang, H. Yue, Z. Hu, Y. Shen, J. Ma, J. Li, X. D. Wang, L. Wang, B. Sun, P. Shi, L. Wang, Y. Gu, Microglia mediate forgetting via complement-dependent synaptic elimination. *Science* **367**, 688–694 (2020).

33. R. Dantzer, J. C. O'Connor, G. G. Freund, R. W. Johnson, K. W. Kelley, From inflammation to sickness and depression: When the immune system subjugates the brain. *Nat. Rev. Neu-rosci.* **9**, 46–56 (2008).

34. A. A. Miller, S. J. Spencer, Obesity and neuroinflammation: A pathway to cognitive im-pairment. *Brain Behav. Immun.* **42**, 10–21 (2014).

35. O. Guillemot-Legris, G. G. Muccioli, Obesity-induced neuroinflammation: Beyond the hy-pothalamus. *Trends Neurosci.* **40**, 237–253 (2017).

36. S. Chatterjee, E. N. Walsh, A. L. Yan, K. P. Giese, T. Safe, T. Abel, Pharmacological activation of Nr4a rescues age-associated memory decline. *Neurobiol. Aging* **85**, 140–144 (2020).

37. H. Shah, F. Dehghani, M. Ramezan, R. B. Gannaban, Z. F. Haque, F. Rahimi, S. Abbasi, A. C. Shin, Revisiting the role of vitamins and minerals in Alzheimer's disease. *Antioxidants (Basel)* **12**, 415 (2023).

38. M. U. Wołoszynowska-Fraser, A. Kouchmeshky, P. McCaffery, Vitamin A and retinoic acid in cognition and cognitive disease. *Annu. Rev. Nutr.* **40**, 247–272 (2020).

39. J. Ng, A. Papandreou, S. J. Heales, M. A. Kurian, Monoamine neurotransmitter disorders - Clinical advances and future perspectives. *Nat. Rev. Neurol.* **11**, 567–584 (2015).

40. P. S. Kaeser, L. Deng, M. Fan, T. C. Südhof, RIM genes differentially contribute to organizing presynaptic release sites. *Proc. Natl. Acad. Sci. U.S.A.* **109**, 11830–11835 (2012).

41. C. M. Powell, S. Schoch, L. Monteggia, M. Barrot, M. F. Matos, N. Feldmann, T. C. Südhof, E. J. Nestler, The presynaptic active zone protein RIM1α is critical for normal learning and memory. *Neuron* **42**, 143–153 (2004).

42. N. Krumm, T. N. Turner, C. Baker, L. Vives, K. Mohajeri, K. Witherspoon, A. Raja, B. P. Coe, H. A. Stessman, Z. X. He, S. M. Leal, R. Bernier, E. E. Eichler, Excess of rare, inherited trun-cating mutations in autism. *Nat. Genet.* **47**, 582–588 (2015).

43. M. S. Shin, S. Y. Park, S. R. Park, S. H. Seol, J. S. Kwon, Clinical and empirical applications of the Rey-Osterrieth complex figure test. *Nat. Protoc.* **1**, 892–899 (2006).

44. A. H. Brand, N. Perrimon, Targeted gene expression as a means of altering cell fates and generating dominant phenotypes. *Development* **118**, 401–415 (1993).

45. T. S. Koemans, C. Oppitz, R. A. T. Donders, H. Van Bokhoven, A. Schenck, K. Keleman, J. M. Kramer, Drosophila courtship conditioning as a measure of learning and memory. *J. Vis. Exp.* **2017**, 55808 (2017).

46. N. Raun, S. Jones, J. M. Kramer, Conditioned courtship suppression in *Drosophila mela-nogaster*. *J. Neurogenet.* **35**, 154–167 (2021).

47. M. Haddadi, S. R. Jahromi, B. K. C. Sagar, R. K. Patil, T. Shivanandappa, S. R. Ramesh, Brain aging, memory impairment and oxidative stress: A study in *Drosophila melanogaster*. *Behav. Brain Res.* **259**, 60–69 (2014).

48. D. Wang, L. Qian, H. Xiong, J. Liu, W. S. Neckameyer, S. Oldham, K. Xia, J. Wang, R. Bodmer, Z. Zhang, Antioxidants protect PINK1-dependent dopaminergic neurons in Drosophila. *Proc. Natl. Acad. Sci. U.S.A.* **103**, 13520–13525 (2006).

49. S. Bahadorani, P. Bahadorani, J. P. Phillips, A. J. Hilliker, The effects of vitamin supple-mentation on Drosophila life span under normoxia and under oxidative stress. *J. Gerontol. A Biol. Sci. Med. Sci.* **63**, 35–42 (2008).

50. W. G. Roeterdink, K. E. Strecker, C. C. Hayden, M. H. M. Janssen, D. W. Chandler, Imaging the rotationally state-selected NO(A,n) product from the predissociation of the A state of the NO-Ar van der Waals cluster. *J. Chem. Phys.* **130**, 134305 (2009).

51. T. Kawai, M. V. Autieri, R. Scalia, Adipose tissue inflammation and metabolic dysfunction in obesity. *Am. J. Physiol. Cell Physiol.* **320**, C375–C391 (2021).

52. Z. Liu, X. Huang, Lipid metabolism in *Drosophila*: Development and disease. *Acta Biochim. Biophys. Sin (Shanghai)* **45**, 44–50 (2013).

53. R. P. Kühnlein, The contribution of the Drosophila model to lipid droplet research. *Prog. Lipid Res.* **50**, 348–356 (2011).

54. S. Meltzer, J. A. Bagley, G. L. Perez, C. E. O'Brien, L. DeVault, Y. Guo, L. Y. Jan, Y. N. Jan, Phospholipid homeostasis regulates dendrite morphogenesis in Drosophila sensory neurons. *Cell Rep.* **21**, 859–866 (2017).

55. J. Muffat, D. W. Walker, S. Benzer, Human ApoD, an apolipoprotein up-regulated in neu-rodegenerative diseases, extends lifespan and increases stress resistance in Drosophila. *Proc. Natl. Acad. Sci. U.S.A.* **105**, 7088–7093 (2008).

56. A. Costa, B. Reynés, J. Konieczna, M. Martín, M. Fiol, A. Palou, D. Romaguera, P. Oliver, Use of human PBMC to analyse the impact of obesity on lipid metabolism and metabolic status: A proof-of-concept pilot study. *Sci. Rep.* **11**, 18329 (2021).

57. M. Cifre, A. Palou, P. Oliver, Cognitive impairment in metabolically-obese, normal-weight rats: Identification of early biomarkers in peripheral blood mononuclear cells. *Mol. Neu-rodegener.* **13**, 14 (2018).

58. J. Mayneris-Perxachs, A. Castells-Nobau, M. Arnoriaga-Rodríguez, M. Martin, L. de la Vega-Correa, C. Zapata, A. Burokas, G. Blasco, C. Coll, A. Escrichs, C. Biarnés, J. M. Moreno-Nav-arrete, J. Puig, J. Garre-Olmo, R. Ramos, S. Pedraza, R. Brugada, J. C. Vilanova, J. Serena, J. Gich, L. Ramió-Torrentà, V. Pérez-Brocal, A. Moya, R. Pamplona, J. Sol, M. Jové, W. Ricart, M. Portero-Otin, G. Deco, R. Maldonado, J. M. Fernández-Real, Microbiota alterations in proline metabolism impact depression. *Cell Metab.* **34**, 681–701.e10 (2022).

59. J. Mayneris-Perxachs, A. Castells-Nobau, M. Arnoriaga-Rodríguez, J. Garre-Olmo, J. Puig, R. Ramos, F. Martínez-Hernández, A. Burokas, C. Coll, J. M. Moreno-Navarrete, C. Zapata-Tona, S. Pedraza, V. Pérez-Brocal, L. Ramió-Torrentà, W. Ricart, A. Moya, M. Martínez-García, R. Maldonado, J. M. Fernández-Real, Caudovirales bacteriophages are associated with improved executive function and memory in flies, mice, and humans. *Cell Host Microbe* **30**, 340–356.e8 (2022).

60. J. Puig, C. Biarnes, S. Pedraza, J. C. Vilanova, R. Pamplona, J. M. Fernández-Real, R. Brugada, R. Ramos, G. Coll-de-Tuero, L. Calvo-Perxas, J. Serena, L. Ramió-Torrentà, J. Gich, L. Gallart, M. Portero-Otin, A. Alberich-Bayarri, A. Jimenez-Pastor, E. Camacho-Ramos, J. Mayneris-Perxachs, V. Pineda, R. Font, A. Prats-Puig, M.-L. Gacto, G. Deco, A. Escrichs, B. Clotet, R. Paredes, E. Negredo, B. Triaire, M. Rodríguez, A. Heredia-Escámez, R. Coronado, W. de Graaf, V. Prevost, A. Mitulescu, P. Daunis-I-Estadella, S. Thió-Henestrosa, F. Miralles, V. Ribas-Ripoll, M. Puig-Domingo, M. Essig, C. R. Figley, T. D. Figley, B. Albensi, A. Ashraf, J. H. C. Reiber, G. Schifitto, U. Md Nasir, C. Leiva-Salinas, M. Wintermark, K. Nael, J. Vilalta-Franch, J. Barretina, J. Garre-Olmo, The aging imageomics study: Rationale, design and baseline characteristics of the study population. *Mech. Ageing Dev.* **189**, 111257 (2020).

61. D. Wechsler, WAIS-IV. Escala de inteligencia de Wechsler para adultos-IV, in *Manual técnico y de interpretación* (NCS Pearson, Madrid, Inc. Edici., 2012).

62. E. Strauss, E. M. S. Sherman, O. Spreen, *A Compendium of Neuropsychological Tests: Ad-ministration, Norms, and Commentary* (Oxford Univ. Press, 3rd Oxfo., 2006).

63. J. D. Corrigan, N. S. Hinkeldey, Relationships between parts A and B of the trail making test. *J. Clin. Psychol.* **43**, 402–409 (1987).

64. M. D. Lezak, Neuropsychological assessment in behavioral toxicology - Developing techniques and interpretative issues. *Scand. J. Work Environ. Health* **10 (suppl. 1)**, 25–29 (1984).

65. D. C. Delis, J. H. Kramer, E. Kaplan, B. A. Ober, *Manual for the California Verbal Learning Test, (CVLT-II)* (The Psychological Corporation, 2000).

66. A. M. Paolo, A. I. Tröster, J. J. Ryan, Test-retest stability of the California verbal learning test in older persons. *Neuropsychology* **11**, 613–616 (1997).

67. C. Golden, A manual for the clinical and experimental use of the Stroop color and word test, in Faculty Books and Book Chapters. Stoelting Company, 751–758 (1978).

68. J. Latorre, J. Mayneris-Perxachs, N. Oliveras-Cañellas, F. Ortega, F. Comas, J. M. Fernández-Real, J. M. Moreno-Navarrete, Adipose tissue cysteine dioxygenase type 1 is associated with an anti-inflammatory profile, impacting on systemic metabolic traits. *EBioMedicine* **85**, 104302 (2022).

69. A. Dobin, C. A. Davis, F. Schlesinger, J. Drenkow, C. Zaleski, S. Jha, P. Batut, M. Chaisson, T. R. Gingeras, STAR: Ultrafast universal RNA-seq aligner. *Bioinformatics* **29**, 15–21 (2013).

70. B. Li, C. N. Dewey, RSEM: Accurate transcript quantification from RNA-seq data with or without a reference genome. *BMC Bioinformatics* **12**, 323 (2011).

71. W. R. Wikoff, G. Pendyala, G. Siuzdak, H. S. Fox, Metabolomic analysis of the cerebrospinal fluid reveals changes in phospholipase expression in the CNS of SIV-infected macaques. *J. Clin. Investig.* **118**, 2661–2669 (2008).

72. J. Rynes, C. D. Donohoe, P. Frommolt, S. Brodesser, M. Jindra, M. Uhlirova, Activating transcription factor 3 regulates immune and metabolic homeostasis. *Mol. Cell. Biol.* **32**, 3949–3962 (2012).

73. S. M. O'neill, C. Hinkle, S. J. Chen, A. Sandhu, R. Hovhannisyan, S. Stephan, W. R. Lagor, R. S. Ahima, J. C. Johnston, M. P. Reilly, Targeting adipose tissue via systemic gene therapy. *Gene Ther.* **21**, 653–661 (2014).

74. E. Puighermanal, G. Marsicano, A. Busquets-Garcia, B. Lutz, R. Maldonado, A. Ozaita, Cannabinoid modulation of hippocampal long-term memory is mediated by mTOR sig-naling. *Nat. Neurosci.* **12**, 1152–1158 (2009).

75. A. Busquets-Garcia, E. Puighermanal, A. Pastor, R. De La Torre, R. Maldonado, A. Ozaita, Differential role of anandamide and 2-arachidonoylglycerol in memory and anxiety-like responses. *Biol. Psychiatry* **70**, 479–486 (2011).

76. M. Gomis-González, L. Galera-López, M. Ten-Blanco, A. Busquets-Garcia, T. Cox, R. Maldonado, A. Ozaita, Protein kinase C-gamma knockout mice show impaired

hippocampal short-term memory while preserved long-term memory. *Mol. Neurobiol.* **58**, 617–630 (2021).

77. A. Escudero-Lara, D. Cabañero, R. Maldonado, Kappa opioid receptor modulation of endometriosis pain in mice. *Neuropharmacology* **195**, 108677 (2021).

78. M. E. Ritchie, B. Phipson, D. Wu, Y. Hu, C. W. Law, W. Shi, G. K. Smyth, Limma powers differential expression analyses for RNA-sequencing and microarray studies. *Nucleic Acids Res.* **43**, e47 (2015).

79. M. D. Robinson, D. J. McCarthy, G. K. Smyth, edgeR: A Bioconductor package for differential expression analysis of digital gene expression data. *Bioinformatics* **26**, 139–140 (2010).

80. A. Kamburov, U. Stelzl, H. Lehrach, R. Herwig, The ConsensusPathDB interaction database: 2013 update. *Nucleic Acids Res.* **41**, D793–D800 (2013).

81. D. Szklarczyk, A. L. Gable, D. Lyon, A. Junge, S. Wyder, J. Huerta-Cepas, M. Simonovic, N. T. Doncheva, J. H. Morris, P. Bork, L. J. Jensen, C. von Mering, STRING v11: Protein-protein association networks with increased coverage, supporting functional discovery in genome-wide experimental datasets. *Nucleic Acids Res.* **47**, D607–D613 (2019).

82. E. Ulgen, O. Ozisik, O. U. Sezerman, PathfindR: An R package for comprehensive identification of enriched pathways in omics data through active subnetworks. *Front. Genet.* **10**, 858 (2019).

Science Advances

VAAAS

Supplementary Materials for

Adipose tissue coregulates cognitive function

Núria Oliveras-Cañellas *et al.*

Corresponding author: Jordi Mayneris-Perxachs, jmayneris@idibgi.org;
José Manuel Fernández-Real, jmfreal@idibgi.org

The PDF file includes:

Figs. S1 to S7
Legends for tables S1 to S51

Other Supplementary Material for this manuscript includes the following:

Tables S1 to S51
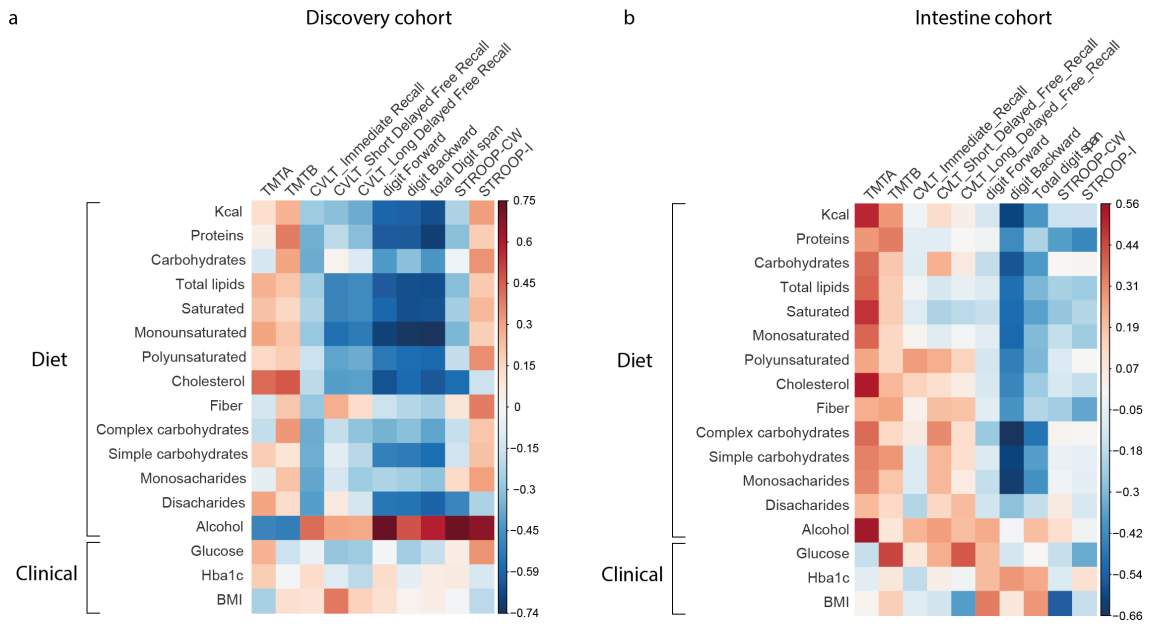
Figure Supplemental 1. Associations between dietary, clinical parameters and cognitive test. Heat map of Spearman's correlations among dietary and clinical parameters and cognitive test after correcting for multiple comparisons (FDR) **a)** in the discovery cohort and **b)** in the intestine cohort.
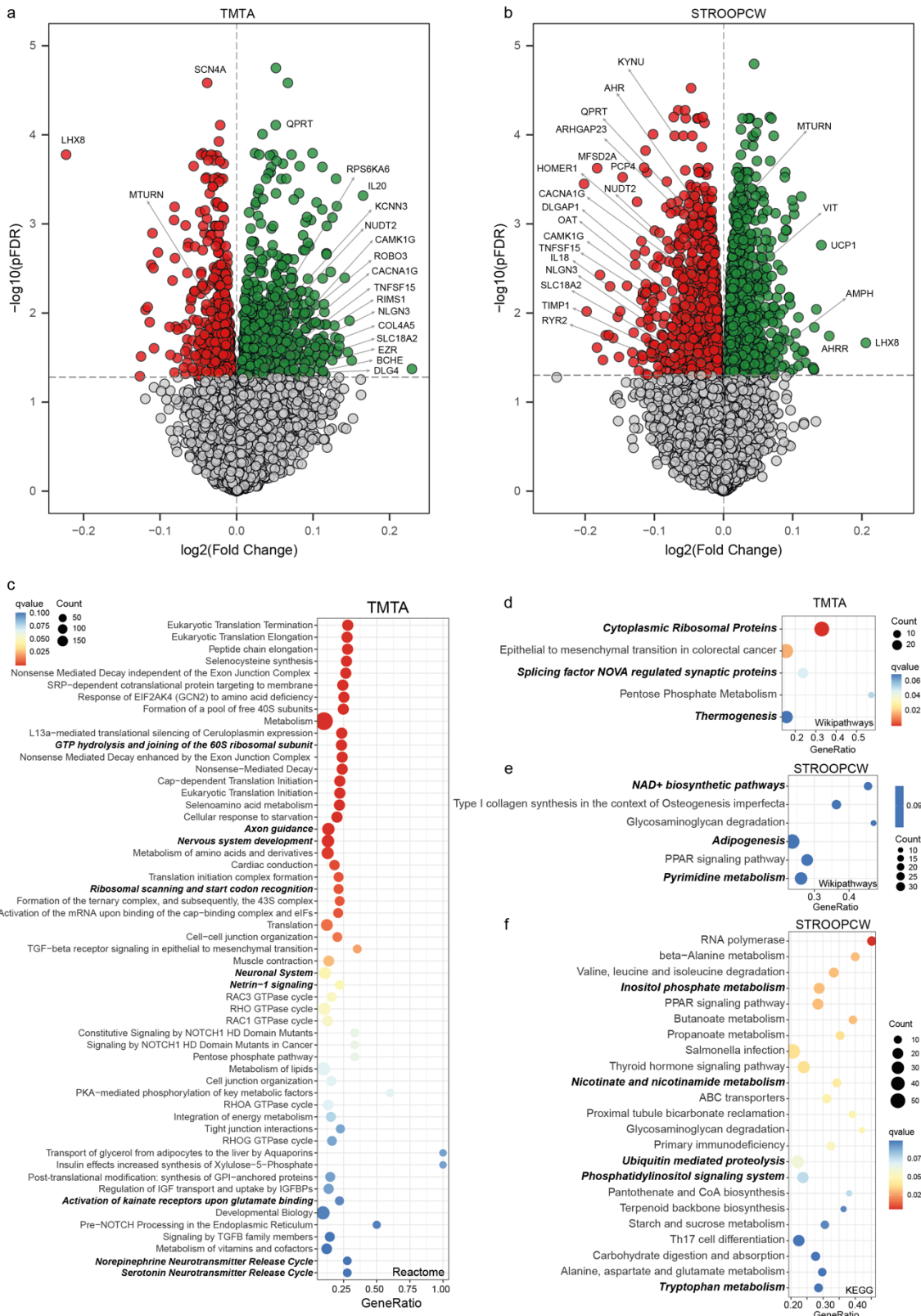
Figure Supplemental 2. Associations of visceral adipose tissue gene expression and other cognitive domains in the discovery cohort. Volcano plots of differentially expressed genes in the visceral adipose tissue associated with **a)** the Trail Making Test

Part A (TMTA), **b)** THE STROOP Colour Word test (STROOPCW) scores in discovery cohort (IRONMET, *n*=17) identified by limma-voom analysis controlling for age, BMI, sex, and education years. The log2 fold change associated with a unit change in the cognitive test score and the log10 *p*-values adjusted for multiple testing (pFDR) are plotted for each gene. Differentially expressed genes (pFDR<0.05) are coloured in red and green indicating down- and up-regulation, respectively. **c)** Dot plot of pathways significantly associated (qvalue<0.1) with the TMTA in the visceral adipose tissue identified from a pathway over-representation analysis mapping significant genes to the Reactome database and **d)** the Wikipathways database. **e)** Dot plot of pathways significantly associated (qvalue<0.1) with the STROOPCW test in the visceral adipose tissue identified from a pathway over-representation analysis mapping significant genes to the Wikipathways database and **f)** the KEGG database. The x-axis in the dot plots and the bubble size in the Manhattan-like plots represents the ratio of input genes that are annotated in a pathway (GeneRatio). Dots are coloured by the qvalue.
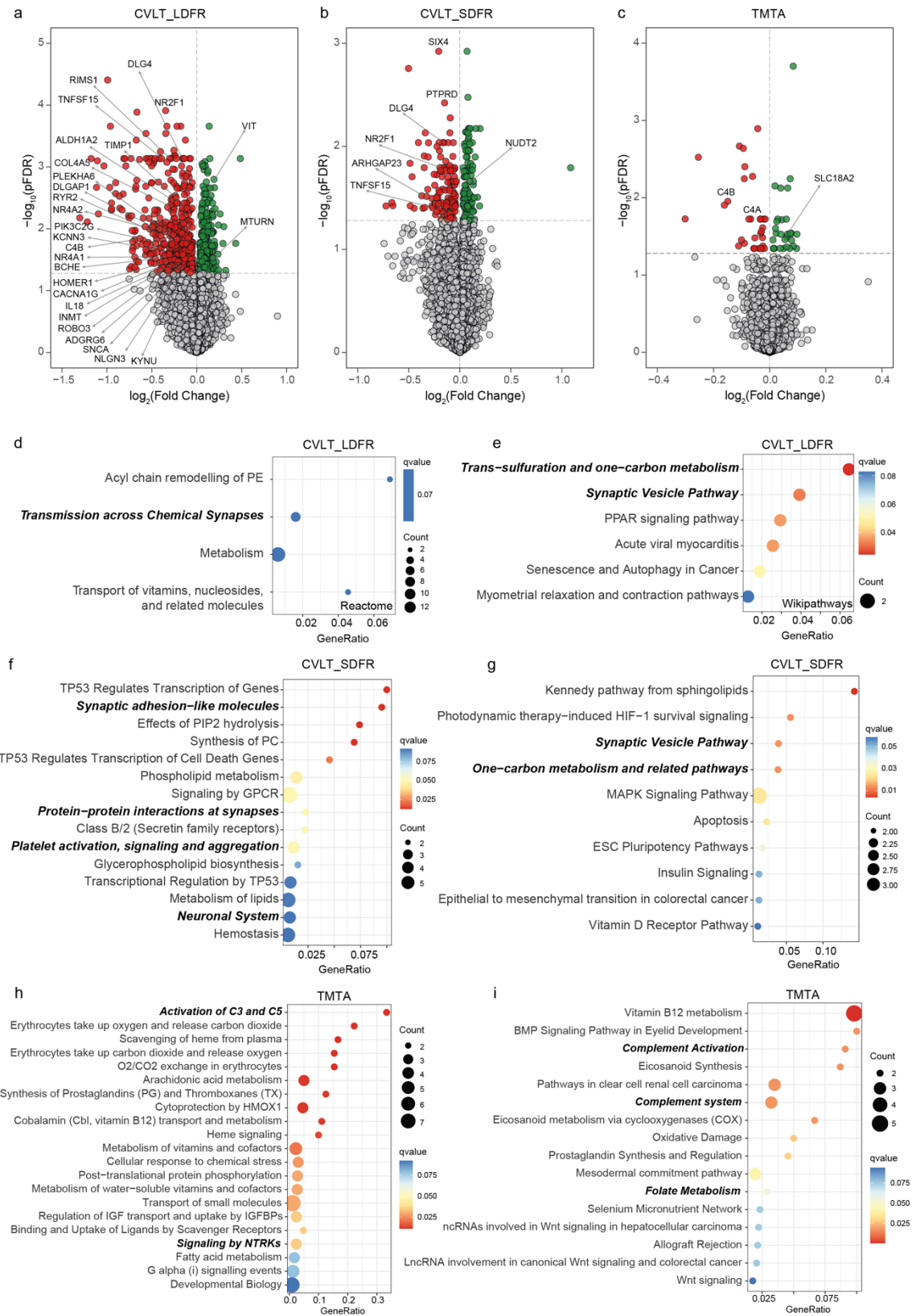
Figure Supplemental 3. Longitudinal associations of subcutaneous adipose tissue (SAT) gene expression at baseline and the scores in different cognitive domains later

in life. Volcano plots of differentially expressed genes in the SAT at baseline associated with **a)** the California Verbal Learning Test Long Delayed Free Recall (CVLT_LDFR), **b)** the California Verbal Learning Test Short Delayed Free Recall (CVLT_SDFR), and **c)** the Trail Making Test part A (TMTA) scores two to three years later in the validation cohort (INTESTINE, *n*=22) identified by limma-voom analysis controlling for age, BMI, sex, and education years. The log2 fold change associated with a unit change in the cognitive test score and the log10 *p*-values adjusted for multiple testing (pFDR) are plotted for each gene. Differentially expressed genes (pFDR<0.05) are coloured in red and green indicating down- and up-regulation, respectively. **d)** Dot plot of pathways significantly associated (qvalue<0.1) with the CVLT_LDFR in the SAT identified from a pathway over-representation analysis mapping significant genes to the Reactome and **e)** Wikipathways databases. **f)** Dot plot of pathways significantly associated (qvalue<0.1) with the CVLT_SDFR in the SAT identified from a pathway over-representation analysis mapping significant genes to the Reactome and **g)** Wikipathways databases. **h)** Dot plot of pathways significantly associated (qvalue<0.1) with the TMTA in the SAT identified from a pathway over-representation analysis mapping significant genes to the Reactome and **i)** Wikipathways databases. The x-axis in the dot plots represents the ratio of input genes that are annotated in a pathway (GeneRatio). Dots are coloured by the qvalue.
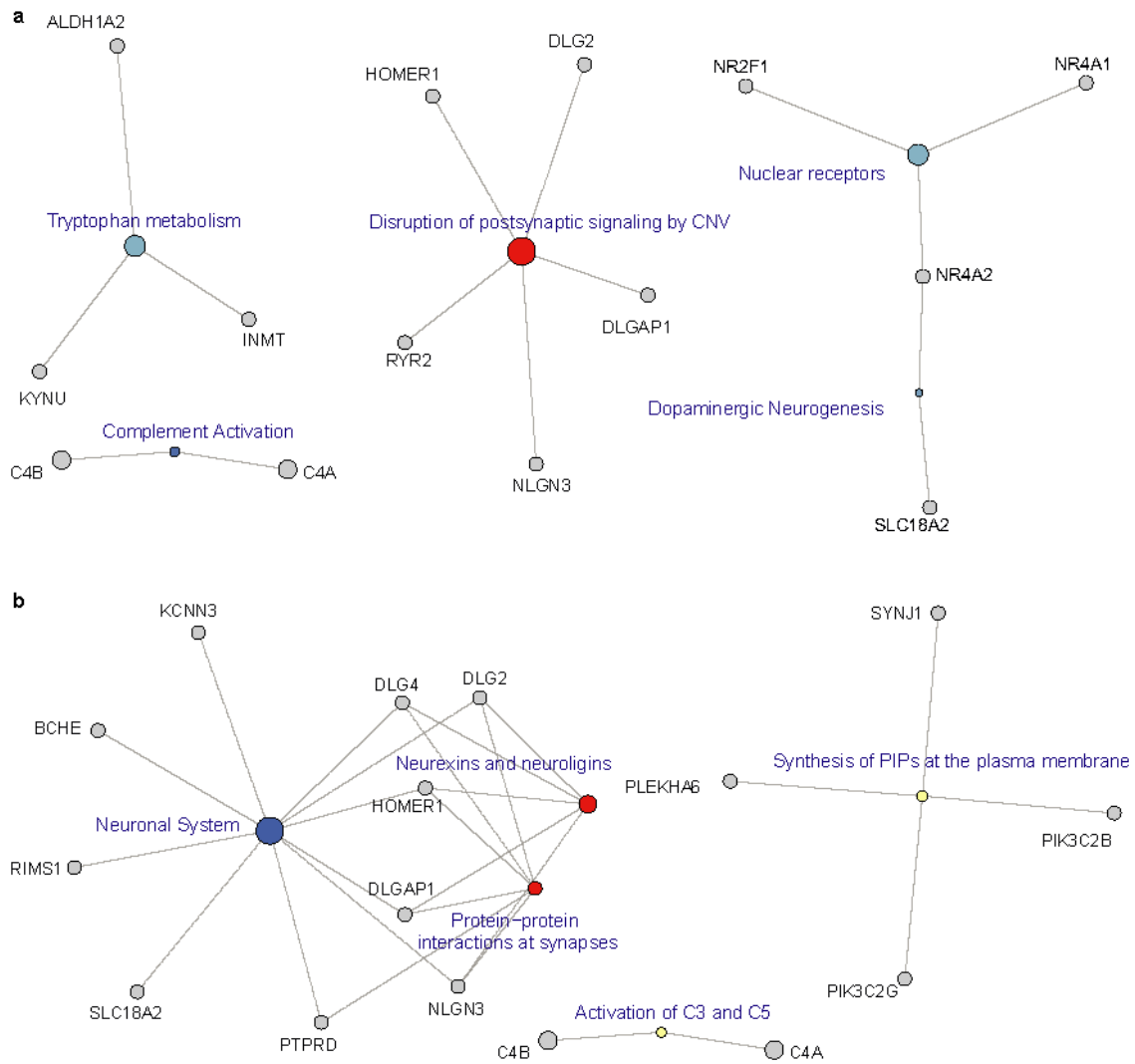
Figure Supplemental 4. Gen-concept networks depicting pathways and genes with key roles in synaptic function a) Gene-concept network depicting significant genes involved in selected enriched pathways from the Wikipathways and b**)** Reactome databases.
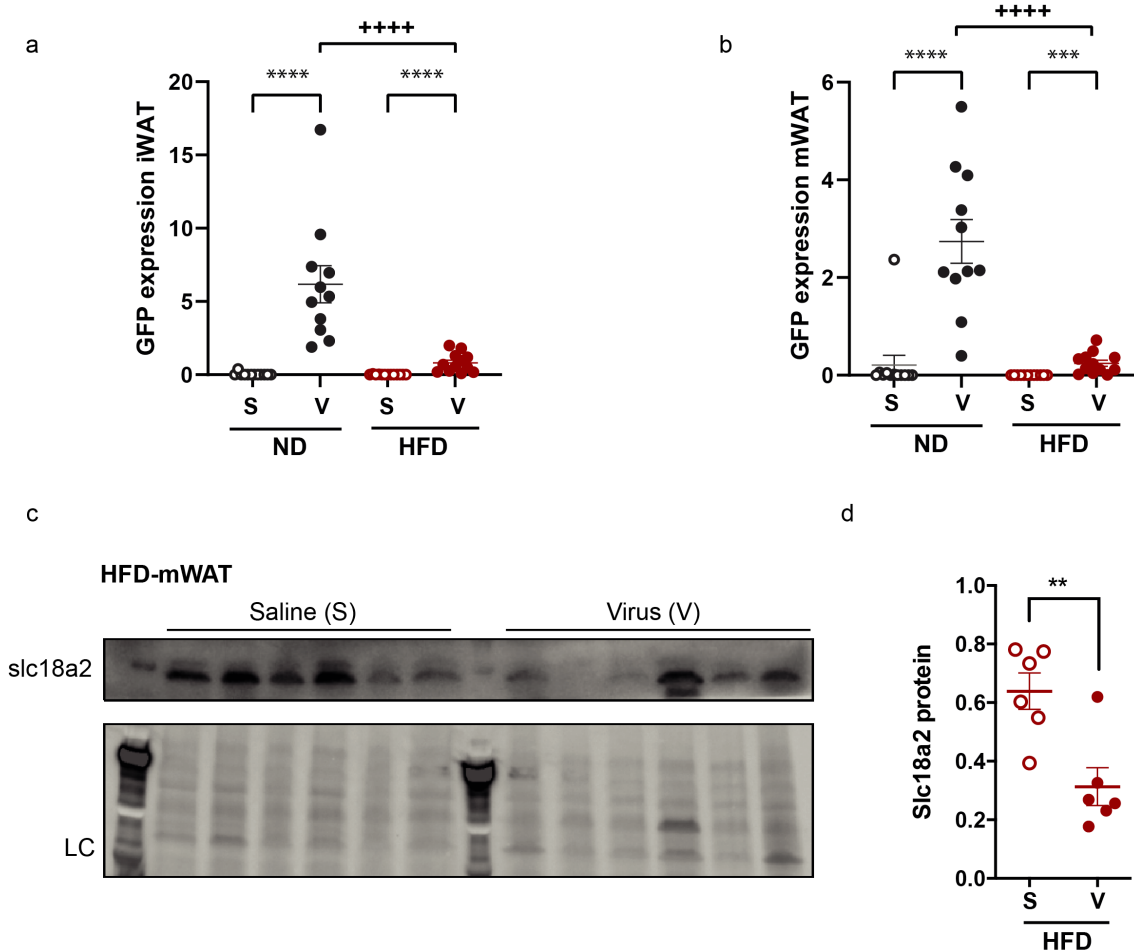
Figure Supplemental 5. Validation of downregulation of *slc18a2* in adipose tissue. a) Expression of green fluorescence protein (GFP) in the inguinal white adipose tissue (iWAT) and **b)** the mesenteric white adipose tissue (mWAT). **c)** Western-Blot for the protein levels of slc18a2 in the mWAT of mice fed a HFD. **d)** slc18a2 protein levels of the groups fed a HFD. Data is shown as dots with the mean ± SEM; n=12 normal diet + saline (ND-S), n=11 normal diet + virus (ND-V), n=13 high fat diet + saline (HFD-S), n=12 high fat diet + virus (HFD-V). ** $P < 0.01$, *** $P < 0.001$, **** $P < 0.0001$ for the comparison S *vs* V; ++++ $P < 0.0001$ diet effect. Calculated with two-way ANOVA.
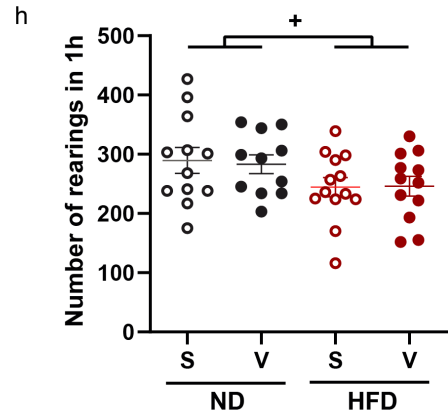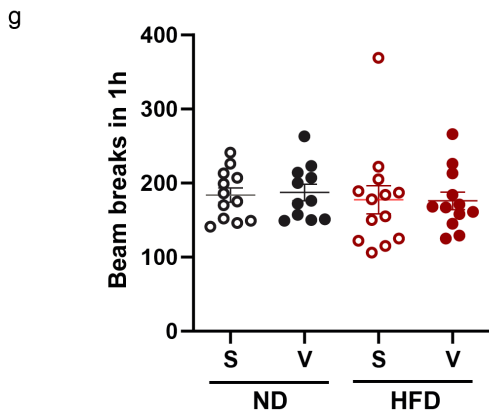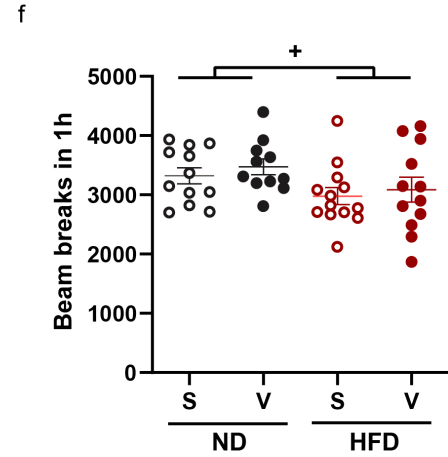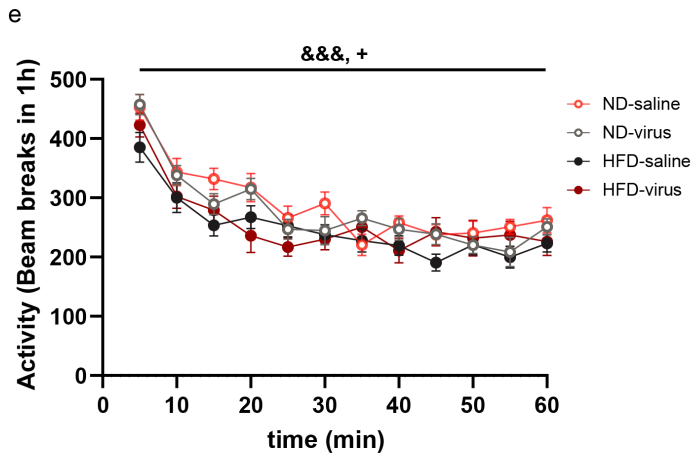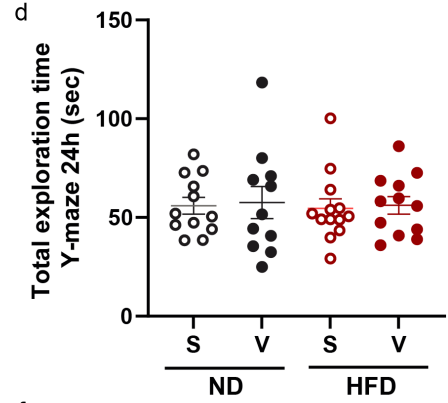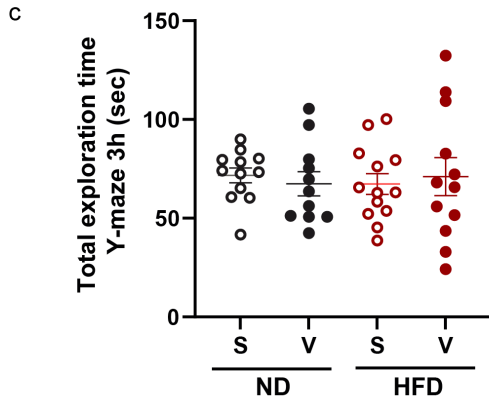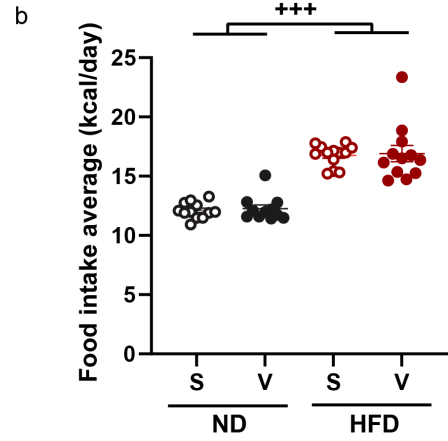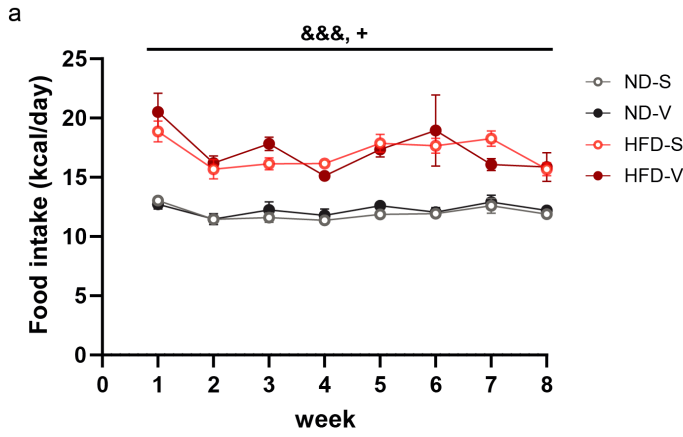
Figure Supplemental 6. Effect of diet and *slc18a2* downregulation in the adipose tissue of mice on food intake, exploration time and locomotion. a) Food intake (kcal/day) was monitored weekly during the entire protocol (8 weeks). **b)** Average of food intake in kcal/day. **c,d)** Exploration time on the short-term (3h) and long-term (24h) novel object-recognition tests. **e)** Kinetics of total activity measured as beam breaks in activity chambers for 1 hour. **f)** Total horizontal activity, **g)** back or forth movements, and **h)** rearings measured in 1 hour. In **a,e** individual data is shown as the mean ± SEM and in **b-d,f-h** as dots with the mean ± SEM; .n=12 normal diet + saline (ND-S), n=11 normal diet + virus (ND-V), n=13 high fat diet + saline (HFD-S), n=12 high fat diet + virus (HFD-V). ^{&&&} P < 0.001 week effect; **** P < 0.0001 ND-S *vs* ND-V or HFD-S *vs* HFD-V; ⁺ P < 0.05, ⁺⁺⁺ P < 0.001 diet effect; $ P < 0.05 treatment effect; ^{@@@} P < 0.001 week x diet interaction; ^{^^^} P < 0.001 week x treatment interaction; **a,e** calculated with three- or **b-d,f-h** two-way ANOVA.
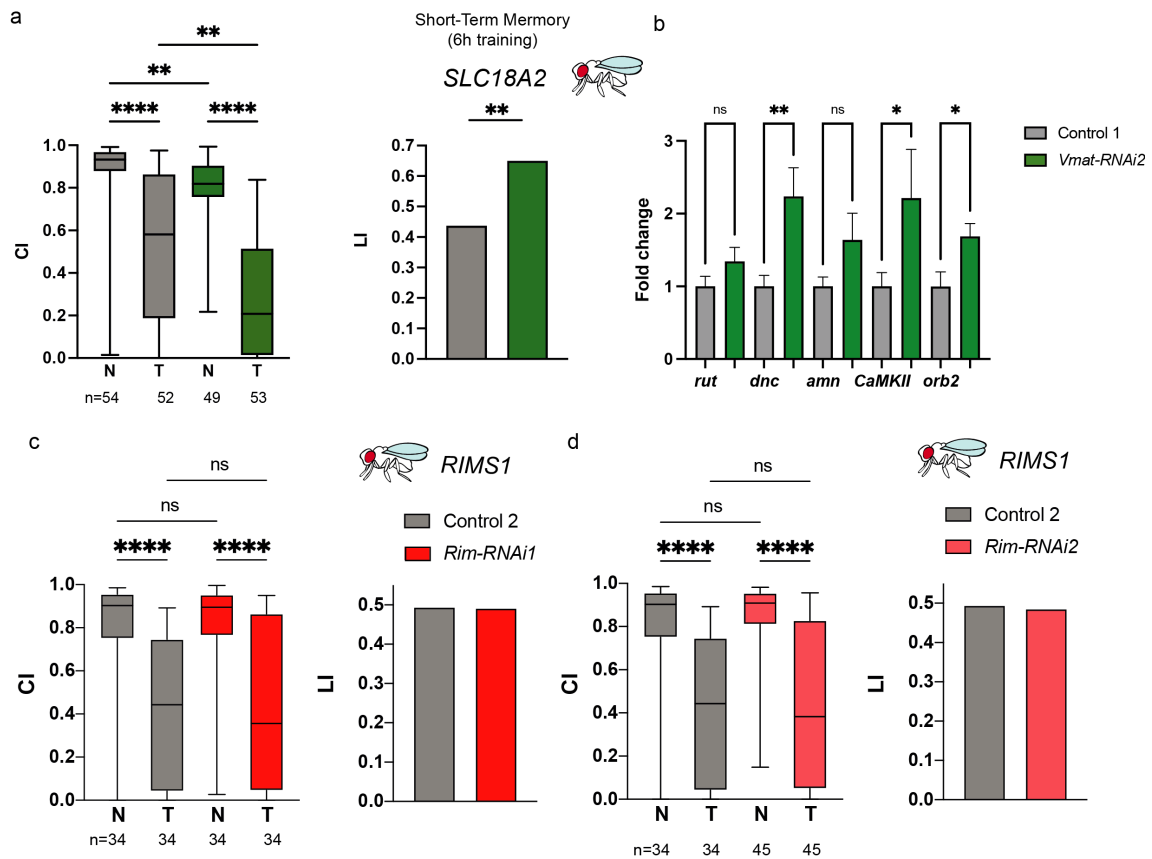
Figure Supplemental 7. Courtship and learning indexes of flies of with SLC18A2 and Rim knockdown in fat body. a) *Vmat* downregulation in the *Drosophila* fat body and associations with short-term memory. Results display male short-term memory in the courtship conditioning paradigm performed 6h after training and 1 hour of isolation. Control-1 (*w; C7*-GAL4/+) and *Vmat-RNAi2* fat body-specific knockdown flies (*w; C7-GAL4/+; UAS-Dcr-2/ Vmat -RNAi2*). **b)** Relative gene expression assessed by qRT-PCR of *rutabaga(rut), dunce (dnc), amnesiac (amn), homer, CAMKll,* and *orb2* in fly brains of *UAS-Rim* fat body-specific overexpression flies and their corresponding genetic background control. Error bars represent normalized S.E.M. *P*-values were determined using the *t*-test (* *P*<0.05, ** *P* <0.01, *** *P* <0.001, **** *P* <0.0001). Data are derived from a minimum of five biological and two technical replicates. **c,d)** *Rim* downregulation in the *Drosophila* fat body and associations with learning. Results display male learning in the courtship conditioning paradigm performed immediately after 2.5h training.

Control-1 and 2 (*w; C7*-GAL4/+*; UAS-Dcr-2/+*) and *Rim-RNAi1 and Rim-RNAi2* fat body-specific knockdown flies (*w; C7*-GAL4/*Rim-RNAi1; UAS-Dcr-2/+* and *w; C7*-GAL4/+*; UAS-Dcr-2/ Rim-RNAi2*). Error bars represent normalized S.E.M. *P*-values were determined using the *t*-test (* *P*<0.05, ** *P* <0.01, *** *P* <0.001, **** *P* <0.0001). Data are derived from a minimum of five biological and two technical replicates.

Table S1. General lineal model, controlling by age, sex and years of education (ANCOVA) depicting the efects of physical exercise in the 10 cognitive test

Table S2. Cohorts clinical and neuropsychological characteristics.

Table S3. Gene transcripts associated with the **CVLT Immediate Recall** fitting a robust linear regression model controlling for age, BMI, sex and education years in the **Discovery cohort (IRONMET, n=17)**

Table S4. Gene transcripts associated with the **CVLT Long Delayed Free Recall** fitting a robust linear regression model controlling for age, BMI, sex and education years in the Discovery cohort (IRONMET, n=17)

Table S5. Gene transcripts associated with the **CVLT Short Delayed Free Recall** fitting a robust linear regression model controlling for age, BMI, sex and education years in the Discovery cohort (IRONMET, n=17)

Table S6. Gene transcripts associated with the **Backaward Digit Span** fitting a robust linear regression model controlling for age, BMI, sex and education years in the Discovery cohort (IRONMET, n=17)

Table S7. Gene transcripts associated with the **Forward Digit Span** fitting a robust linear regression model controlling for age, BMI, sex and education years in the Discovery cohort (IRONMET, n=17)

Table S8. Gene transcripts associated with the **Total Digit Span** fitting a robust linear regression model controlling for age, BMI, sex and education years in the Discovery cohort (IRONMET, n=17)

Table S9. Gene transcripts associated with the **STROOPCW** fitting a robust linear regression model controlling for age, BMI, sex and education years in the Discovery cohort (IRONMET, n=17)

Table S10. Gene transcripts associated with the **STROOPI** fitting a robust linear regression model controlling for age, BMI, sex and education years in the Discovery cohort (IRONMET, n=17)

Table S11. Gene transcripts associated with the **TMTA** fitting a robust linear regression model controlling for age, BMI, sex and education years in the Discovery cohort (IRONMET, n=17)

Table S12. Gene transcripts associated with the **TMTB** fitting a robust linear regression model controlling for age, BMI, sex and education years in the Discovery cohort (IRONMET, n=17)

Table S13. Over-representation analysis (**REACTOME**) of the **VAT genes** significantlly associated with the **CVLT Immediate Recall** in the **discovery cohort (IRONMET, n=17)**

Table S14. Over-representation analysis (**REACTOME, WIKIPATHWAYS**) of the **VAT genes** significantlly associated with the **TMTB** in the **discovery cohort (IRONMET, n=17)**

Table S15. Over-representation analysis (**REACTOME, WIKIPATHWAYS**) of the **VAT genes** significantlly associated with the **STROOPI** in the **discovery cohort (IRONMET, n=17)**

Table S16. Over-representation analysis (**REACTOME, WIKIPATHWAYS**) of the **VAT genes** significantlly associated with the **TMTA** in the **discovery cohort (IRONMET, n=17)**

Table S17. Over-representation analysis (**WIKIPATHWAYS, KEGG**) of the **VAT genes** significantlly associated with the **STROOPCW** in the **discovery cohort (IRONMET, n=17)**

Table S18. **VAT G**ene transcripts associated with the **CVLT Immediate Recall** fitting a robust linear regression model controlling for age, BMI, sex and education years in the **Validation cohort (INTESTINE, n=22)**

Table S19. VAT Gene transcripts associated with the **CVLT Long Delayed Free Recall** fitting a robust linear regression model controlling for age, BMI, sex and education years in the **Validation cohort (INTESTINE, n=22)**

Table S20. **VAT**Gene transcripts associated with the **CVLT Short Delayed Free Recall** fitting a robust linear regression model controlling for age, BMI, sex and education years in the **Validation cohort (INTESTINE, n=22)**

Table S21. **VAT**Gene transcripts associated with the **Backward Digit Span** fitting a robust linear regression model controlling for age, BMI, sex and education years in the **Validation cohort (INTESTINE, n=22)**

Table S22. VAT Gene transcripts associated with the **Forward Digit Span** fitting a robust linear regression model controlling for age, BMI, sex and education years in the **Validation cohort (INTESTINE, n=22)**

Table S23. VAT Gene transcripts associated with the **Total Digit Span** fitting a robust linear regression model controlling for age, BMI, sex and education years in the **Validation cohort (INTESTINE, n=22)**

Table S24. VAT Gene transcripts associated with the **STROOPCW** fitting a robust linear regression model controlling for age, BMI, sex and education years in the **Validation cohort (INTESTINE, n=22)**

Table S25. VAT Gene transcripts associated with the **STROOPI** fitting a robust linear regression model controlling for age, BMI, sex and education years in the **Validation cohort (INTESTINE, n=22)**

Table S26. VAT Gene transcripts associated with the **TMTA** fitting a robust linear regression model controlling for age, BMI, sex and education years in the **Validation cohort (INTESTINE, n=22)**

Table S27. VAT Gene transcripts associated with the **TMTB** fitting a robust linear regression model controlling for age, BMI, sex and education years in the **Validation cohort (INTESTINE, n=22)**

Table S28. **SAT** Gene transcripts associated with the **CVLT Immediate Recall** fitting a robust linear regression model controlling for age, BMI, sex and education years in the **Validation cohort (INTESTINE, n=22)**

Table S29. **SAT** Gene transcripts associated with the **CVLT Long Delayed Free Recall** fitting a robust linear regression model controlling for age, BMI, sex and education years in the **Validation cohort (INTESTINE, n=22)**

Table S30. **SAT** Gene transcripts associated with the **CVLT Short Delayed Free Recall** fitting a robust linear regression model controlling for age, BMI, sex and education years in the **Validation cohort (INTESTINE, n=22)**

Table S31. **SAT** Gene transcripts associated with the **Forward Digit Span** fitting a robust linear regression model controlling for age, BMI, sex and education years in the **Validation cohort (INTESTINE, n=22)**

Table S32. **SAT** Gene transcripts associated with the **Backward Digit Span** fitting a robust linear regression model controlling for age, BMI, sex and education years in the **Validation cohort (INTESTINE, n=22)**

Table S33. **SAT** Gene transcripts associated with the **Total Digit Span** fitting a robust linear regression model controlling for age, BMI, sex and education years in the **Validation cohort (INTESTINE, n=22)**

Table S34. **SAT** Gene transcripts associated with the **STROOPCW** fitting a robust linear regression model controlling for age, BMI, sex and education years in the **Validation cohort (INTESTINE, n=22)**

Table S35. **SAT** Gene transcripts associated with the **STROOPI** fitting a robust linear regression model controlling for age, BMI, sex and education years in the **Validation cohort (INTESTINE, n=22)**

Table S36. **SAT** Gene transcripts associated with the**TMTA** fitting a robust linear regression model controlling for age, BMI, sex and education years in the **Validation cohort (INTESTINE, n=22)**

Table S37. **SAT** Gene transcripts associated with the**TMTB** fitting a robust linear regression model controlling for age, BMI, sex and education years in the **Validation cohort (INTESTINE, n=22)**

Table S38. Over-representation analysis (**REACTOME,WKIPATHWAYS**) of the **VAT genes** significantlly associated with the **TMTA** in the **validation cohort (INTESTINTE, n=22)**

Table S39. Over-representation analysis (**REACTOME**) of the **VAT genes** significantlly associated with the Digit Forwards Span in the **validation cohort (INTESTINTE, n=22)**

Table S40. Over-representation analysis (**REACTOME**) of the **VAT genes** significantlly associated with the STROOPCW in the **validation cohort (INTESTINTE, n=22)**

Table S41. Over-representation analysis (**REACTOME, WIKIPATHWAYS**) of the S**AT genes** significantlly associated with the CVLT Long Delayed Free Recall in the **validation cohort (INTESTINTE, n=22)**

Table S42. Over-representation analysis (**REACTOME, WIKIPATHWAYS**) of the S**AT genes** significantlly associated with the CVLT Short Delayed Free Recall in the **validation cohort (INTESTINTE, n=22)**

Table S43. Over-representation analysis (**REACTOME, WIKIPATHWAYS**) of the S**AT genes** significantlly associated with the TMTA in the **validation cohort (INTESTINTE, n=22)**

Table S44. Genes form the Veen Diagram associated at least with one cognitive test.

Table S45. Over-representation analysis (**REACTOME, WIKIPATHWAYS**) of the **common significant genes (n=188)** assocaited with at least one tests in the **VAT and SAT from the discovery (IRONMET, n=17) and validation cohort (INTESTINTE, n=22).**

Table S46. Results from network-oriented over-representation analysis after hierarchial clustering of redundant terms

Table S47. Resume results of learning capabilities assessed with the courtship conditioning paradigme

Table S48. FAT BODY Gene transcripts for the comparison CONTROL vs RIM overexpression in Drosophila fat body

Table S49. BRAIN Gene transcripts for the comparison CONTROL vs RIM overexpression in Drosophila heats

Table S50. Over-representation analysis (**REACTOME**) of differentially expressed BRAIN genes for the comparison CONTROL vs RIM overexpression in Drosophila fat body

Table S51. Primer sequences for the Drosophila qRT-PCR analyses

5.2 ORIGINAL PAPER II

Downregulated adipose tissue expression of browning genes with increased environmental temperatures

Oliveras-Cañellas N, Moreno-Navarrete JM, Lorenzo PM, Garrido-Sánchez L, Becerril S, Rangel O, Latorre J, de la Calle Vargas E, Pardo M, Valentí V, Romero-Cabrera JL, Oliva-Olivera W, Silva C, Diéguez C, Villarroya F, López M, Crujeiras AB, Seoane LM, López-Miranda J, Frühbeck G, Tinahones FJ, Fernández-Real JM.

ENDOCRINE
SOCIETY

OXFORD

Downregulated Adipose Tissue Expression of Browning Genes With Increased Environmental Temperatures

Núria Oliveras-Cañellas,[1,2,3,4] José María Moreno-Navarrete,[1,2,3,4] Paula M. Lorenzo,[4,5] Lourdes Garrido-Sánchez,[4,6] Sara Becerril,[4,7] Oriol Rangel,[4,8] Jèssica Latorre,[1,2,3,4] Elena de la Calle Vargas,[1,2,3] Maria Pardo,[4,9] Victor Valentí,[4,7] Juan L. Romero-Cabrera,[4,8] Wilfredo Oliva-Olivera,[6] Camilo Silva,[4,7] Carlos Diéguez,[4,10] Francesc Villarroya,[4,11] Miguel López,[4,10] Ana B. Crujeiras,[4,5] Luisa-Maria Seoane,[4,12] José López-Miranda,[4,8] Gema Frühbeck,[4,7] Francisco José Tinahones,[4,6] and José-Manuel Fernández-Real[1,2,3,4]

[1]Department of Diabetes, Endocrinology and Nutrition, Dr. Josep Trueta University Hospital, Girona 17007, Spain
[2]Nutrition, Eumetabolism and Health Group, Girona Biomedical Research Institute (IDIBGI), Girona 17190, Spain
[3]Department of Medical Sciences, School of Medicine, University of Girona, Girona 17003, Spain
[4]Instituto de Salud Carlos III, Centro de Investigación Biomédica en Red de Fisiopatología de la Obesidad y Nutrición (CIBEROBN), Madrid 28029, Spain
[5]Epigenomics in Endocinology and Nutrition Group, Epigenomics Unit, Instituto de Investigación Sanitaria de Santiago de Compostela (IDIS), Complejo Hospitalario Universitario de Santiago de Compostela (CHUS/SERGAS), Santiago de Compostela 15706, Spain
[6]Servicio de Endocrinología y Nutrición, Instituto de Investigación Biomédica de Málaga (IBIMA), Hospital Virgen de la Victoria, Universidad de Málaga, Málaga 29590, Spain
[7]Obesity Area, Clínica Universidad de Navarra, University of Navarra, Pamplona 31009, Spain
[8]Nutrigenomics, Metabolic Syndrome Department, Servicio de Medicina Interna, Hospital Universitario Reina Sofía, Instituto Maimónides de Investigación Biomédica de Córdoba (IMIBIC), Universidad de Córdoba, Córdoba 14004, Spain
[9]Grupo Obesidómica, Área de Endocrinología, Instituto de Investigación Sanitaria de Santiago de Compostela (IDIS), Xerencia de Xestión Integrada de Santiago (IDIS/SERGAS), Santiago de Compostela 15706, Spain
[10]Department of Physiology, CIMUS, University of Santiago de Compostela-Instituto de Investigación Sanitaria, Santiago de Compostela 15782, Spain
[11]Department of Biochemistry and Molecular Biomedicine, Insitut de Biomedicina (IBUB), University of Barcelona, Barcelona 08028, Spain
[12]Endocrine Physiopathology Group, Instituto de Investigación Sanitaria de Santiago de Compostela (IDIS), Complejo Hospitalario Universitario de Santiago (CHUS/SERGAS), Santiago de Compostela 15706, Spain

Correspondence: José-Manuel Fernández-Real, MD, PhD, Department of Diabetes, Endocrinology and Nutrition, Dr. Josep Trueta University Hospital, Avinguda de França s/n, Girona 17007, Spain. Email: jmfreal@idibgi.org; or Francisco José Tinahones, MD, PhD, Servicio Endocrinología y Nutrición, Instituto de Investigación Biomédica de Málaga (IBIMA), Hospital Virgen de la Victoria, Universidad de Málaga, Calle Severo Ochoa, 35, Málaga 292590, Spain. Email: fjtinahones@uma.es.

Abstract

Context: Climate change and global warming have been hypothesized to influence the increased prevalence of obesity worldwide. However, the evidence is scarce.

Objective: We aimed to investigate how outside temperature might affect adipose tissue physiology and metabolic traits.

Methods: The expression of genes involved in thermogenesis/browning and adipogenesis were evaluated (through quantitative polymerase chain reaction) in the subcutaneous adipose tissue (SAT) from 1083 individuals recruited in 5 different regions of Spain (3 in the North and 2 in the South). Plasma biochemical variables and adiponectin (enzyme-linked immunosorbent assay) were collected through standardized protocols. Mean environmental outdoor temperatures were obtained from the National Agency of Meteorology. Univariate, multivariate, and artificial intelligence analyses (Boruta algorithm) were performed.

Results: The SAT expression of genes associated with browning (*UCP1*, *PRDM16*, and *CIDEA*) and *ADIPOQ* were significantly and negatively associated with minimum, average, and maximum temperatures. The latter temperatures were also negatively associated with the expression of genes involved in adipogenesis (*FASN*, *SLC2A4*, and *PLIN1*). Decreased SAT expression of *UCP1* and *ADIPOQ* messenger RNA and circulating adiponectin were observed with increasing temperatures in all individuals as a whole and within participants with obesity in univariate, multivariate, and artificial intelligence analyses. The differences remained statistically significant in individuals without type 2 diabetes and in samples collected during winter.

Conclusion: Decreased adipose tissue expression of genes involved in browning and adiponectin with increased environmental temperatures were observed. Given the North-South gradient of obesity prevalence in these same regions, the present observations could have implications for the relationship of the obesity pandemic with global warming.

The obesity pandemic is well recognized as one of the most severe health problems around the world, linked to cardiovascular and metabolic disease. An imbalance between energy intake and energy expenditure promotes storage of excess fuel in white adipose tissue (WAT) and fat mass accumulation, leading to the current increased prevalence of obesity (1-4). The restriction of calorie intake, pharmacological treatments, and bariatric surgery are clearly insufficient to prevent this increased prevalence, so knowledge about the possible influence of additional actors is imperative (5-7).

AT is among the most prominent in the human body, influencing almost every aspect of our physiology (1). WAT acts as an energy depot, storing lipids that are constantly released into the circulation (8). Brown AT (BAT), representing 1.5% of total body mass, uses the stored fat to generate heat for defending body temperature and thermogenesis (8, 9). A third type of adipocytes interspersed with the WAT has been characterized in the last decades, the beige adipocytes: Directly involved in thermogenesis, these cells express uncoupling protein 1 (*UCP1*) and other genes described later have multiple and small lipid droplets and more developed mitochondria than WAT. The term *WAT browning* defines the enrichment of WAT depots with beige cells in response to cold exposure or pharmacological agents (8). This process is dependent on the transcriptional regulator PRD1-BF1-RIZ1 homologous domain containing 16 (*PRDM16*) (10), which leads to increased expression of proteins enriched in typical BAT or beige adipocytes, including *UCP1*, cell death–inducing DFFA-like effector A (*CIDEA*), and peroxisome proliferator activated receptor gamma coactivator 1 alpha (*PPARGC1α*) (11). In fact, the simplest definition of browning has been proposed as "any significantly increased *UCP1* expression at the [messenger RNA] mRNA level occurring in what are normally considered as white adipose tissue depots" (12).

The increase in BAT metabolic activity on cold exposure varies with age, sex, and fatness (8). Detectable BAT is inversely associated with body mass index (BMI) (1-3). In a study using positron emission tomography, a strong seasonal variation in the activity of BAT was observed. BAT activity negatively correlated with average monthly temperatures and positively with night length (13). However, retrospective studies mainly used positron emission tomography scan–based data of BAT activity in patients undergoing cancer diagnosis procedures, and therefore the data could have been influenced by the reported altered BAT activity associated with some types of cancer (1-3).

Increased environmental temperature has been associated with a raised prevalence of obesity and alterations of glucose metabolism, suggesting that an increased time spent in a cold environment could prevent the development of obesity and its metabolic comorbidities (14, 15). However, the possible effect of outside temperature on AT physiology has not been systematically investigated. Here, we aimed to investigate how outside temperature might affect AT physiology and metabolic traits. For this purpose, different regions of the same country were compared, exploring associations between environmental temperature and metabolic/AT parameters. This would be the first large, multicenter study exploring the associations of environmental temperature with AT gene expression markers of browning and functionality.

Materials and Methods

Participant Recruitment

All samples and data from participants included in this study were provided by the FATBANK platform promoted by the Centro de Investigación Biomédica en Red Fisiopatología de la Obesidad y Nutrición (CIBEROBN) and coordinated by the IDIBGI Biobank (B.00000872), integrated in the Spanish National Biobanks Network, and they were processed following standard operating procedures with the appropriate approval of the ethics, external scientific, and FATBANK internal scientific committees. All participants gave written informed consent.

A total of 1083 participants (780 women and 303 men) with several degrees of obesity were recruited, 750 from cold regions (Santiago de Compostela, Navarra, and Girona, average outdoor temperature 12.4-13.4 °C), and 333 from warm regions (Córdoba and Málaga, average outdoor temperature 14.4-17.25 °C) (Tables 1 and 2 and (Supplementary Fig. S1) (16).

Participants were studied in the postabsorptive state. BMI was calculated as weight (in kilograms) divided by height (in meters) squared. Liver diseases and thyroid dysfunction were specifically excluded by biochemical workup. Clinical and biochemical variables were collected using a common, standardized protocol, including the month and year in which the AT sample was collected and the specific geographical location of each participant's residence. Metabolic parameters such as fasting plasma glucose, glycated hemoglobin A$_{1c}$, fasting triglycerides, high-density lipoprotein (HDL), low-density lipoprotein (LDL), and total cholesterol, and ultrasensitive C-reactive protein (CRP) were also analyzed at each center.

Adipose Tissue Handling

AT samples were obtained from subcutaneous depots during elective surgical procedures (cholecystectomy, surgery of abdominal hernia, and gastric bypass surgery). Samples of AT were immediately transported to the laboratory (5-10 minutes). The handling of tissues was carried out under strict aseptic conditions. AT samples were washed in phosphate-buffered saline, cut off with forceps and scalpel into small pieces (100 mg), and immediately flash-frozen in liquid nitrogen before being stored at −80 °C.

Gene Expression Analysis

Total RNA was purified from the subcutaneous AT (SAT) using the RNeasy Lipid Tissue Mini Kit (QIAgen, Izasa, SA). RNA concentrations were assessed with the Nanodrop ND-100 Spectrophotometer (Thermo Fisher Scientific), and the integrity

Table 1. Anthropometrical and clinical characteristics of the whole cohort

	Girona	Pamplona	Santiago	Malaga	Cordoba	P
n	216	179	214	191	142	—
Sex (men | women)	51	165	60	119	48	166	68	123	51	91	.015
Age, y	48.17 ± 10.251	48.26 ± 11.868	46.36 ± 10.727	45.56 ± 9.027	45.54 ± 9.809	—
Body mass index	42.533 ± 7.085	43.718 ± 7.8049	48.742 ± 7.090[a,b]	48.849 ± 7.069[a,b]	49.353 ± 8.781[a,b]	$6.56E^{-28}$
Waist circumference, cm	122.213 ± 14.781	129.142 ± 16.2866[a]	131.121 ± 13.244[a]	136.147 ± 16.496[a,b]	145.656 ± 16.751[a,b,c,d]	$2.02E^{-21}$
Fasting glucose, mg/dL	105.54 ± 33.446	106.43 ± 20.929	106.88 ± 37.384	112.24 ± 33.568	109 ± 35.544	.293
Glycated hemoglobin, %	5.891 ± 0.994	6.32 ± 1.1175	5.961 ± 1.444	6.223 ± 1.365	6.275 ± 1.455	.016
Cholesterol, mg/dL	191.94 ± 33.868	190.91 ± 35.992	148.11 ± 43.927[a,b]	179.46 ± 35.714[a,c]	173.31 ± 40.28[a,b,c]	$1.05E^{-32}$
HDL cholesterol, mg/dL	49.82 ± 13.961	54.72 ± 39.245	45.11 ± 31.17[b]	42.65 ± 10.957[a,b]	39.72 ± 9.48[a,b]	$1.16E^{-06}$
LDL cholesterol, mg/dL	117.00 ± 28.584	113.03 ± 30.624	89.86 ± 33.45[a,b]	108.98 ± 30.956[c]	115.62 ± 30.564[c]	$4.82E^{-18}$
Fasting triglycerides (mg/dL)[e]	111 (82-156.5)	115 (82.75-158.25)	119 (96-147)	130 (102-165)	110 (91.5-151)	.142
Ultrasensitive CRP (mg/dL)[e]	0.66 (0.33-1.35)	0.765 (0.347-5.385)	0.7 (0.361-1.245)	9.85 (5.74-16.475)[a,c]	14.215 (6.407-28.677)[a,b,c,d]	$1.50E^{-33}$
Minimum temperature (°C)[e]	8.2 (4.2-11.9)	8.7 (4.3-13.6)	8 (6.225-11.1)	13.7 (10.7-18.2)[a,d]	8.3 (6.25-15.325)[a,d]	$1.63E^{-39}$
Maximum temperature (°C)[e]	18.75 (15.6-23.4)	19.1 (13.4-25)	16.9 (14.2-20.9)[a,b]	21.6 (19.025-27.025)[a,b,c]	21.55 (18.675-30.4)[a,b,c]	$3.37E^{-30}$
Average temperature (°C)[e]	13.4 (9.725-17.775)	13.9 (8.9-18.9)	12.4 (10.5-15.9)	17.25 (14.975-22.675)[a,b,c]	14.4 (12.7-23.05)[a,b,c,d]	$1.31E^{-30}$
Minimum temperature MB (°C)[e]	8.55 (4.1-12.65)	8.5 (3.9-13.6)	8.2 (6.1-11.3)	13.45 (10.7-18.2)[a,b,c]	7.2 (3.9-13.825)[d]	$3.10E^{-36}$
Maximum temperature MB (°C)[e]	19.05 (14.925-23.775)	19 (13.2-26.1)	17.1 (14-21.75)[a]	22.3 (18.7-27) a, b, c	20.3 (16.35-28.775)[a,b,c]	$8.05E^{-19}$
Average temperature MB (°C)[e]	13.6 (9.5-18)	13.7 (8.6-19.8)	12.4 (10.1-16.35)	17.7 (14.975-22.9)[a,b,c]	13.55 (10.35-21.225)[a,c,d]	$3.28E^{-23}$
UCP1 mRNA (RU)[e]	6.05E−04 (4.14E−04-1.11E−04)	4.95E−04 (2.48E−04-9.9E−04)	4.816E−04 (2.79E−04-1.07E−04)	4.04E−04 (2.391E−04-7.987E−04)	7.5E−04 (3.3E−04-2.1E−04)[a,b,c,d]	$1.37E^{-04}$
PRDM16 mRNA (RU)[e]	5.26E−04 (4.03E−04-7.13E−04)	5.53E−04 (4.04E−04-7.34E−04)	4.31E−04 (2.71E−04-6.917E−04)	5.455E−04 (3.7E−04-7.413E−04)	3.77E−04 (2.62E−04-5.455E−04)	.440
PPARGC1α mRNA (RU)[e]	3.52E−03 (2.44E−03-4.978E−03)	3.93E−03 (2.98E−03-5.26E−03)[b]	3.09E−03 (2.13E−03-4.27E−03)[b]	3.67E−03 (2.649E−03-5.29E−03)[c]	3.4E−03 (2.30E−03-4.987E−03)[c]	$1.28E^{-04}$
ADIPOQ mRNA (RU)[e]	2.403 (1.948-3.031)	2.234 (1.569-2.969)	2.488 (1.862-3.160)	2.25 (1.753-2.867)	2.143 (1.487-2.804)	.013
ADIPOQ plasma, ng/mL	10.809 ± 4.707	8.597 ± 3.318[a]	11.25 ± 4.683[b]	10.677 ± 4.626[b]	9.969 ± 3.761	$1.02E^{-06}$

Unless otherwise indicated, data are expressed as mean ± SD. One-factor analysis of variance was used to perform comparisons among groups. P less than .05 indicates statistically significant differences between the groups with obesity. Bold values highlight statistically significant P values.

Abbreviations: CRP, C-reactive protein; HDL, high-density lipoprotein; LDL, low-density lipoprotein; MB, month before; mRNA, messenger RNA; *PPARGC1α*, peroxisome proliferator activated receptor gamma coactivator 1 alpha; *PRDM16*, PRD1-BF1-RIZ1 homologous domain containing 16; UCP1, uncoupling protein 1.

[a]P less than .05 indicates statistically significant differences when comparing Pamplona, Santiago, Malaga, and Cordoba with Girona participants (Bonferroni post hoc test).
[b]P less than .05 indicates statistically significant differences when comparing Santiago, Malaga, and Cordoba with Pamplona participants (Bonferroni post hoc test).
[c]P less than .05 indicates statistically significant differences when comparing Malaga and Cordoba with Santiago participants (Bonferroni post hoc test).
[d]P less than .05 indicates statistically significant differences when comparing Cordoba with Malaga participants (Bonferroni post hoc test).
[e]Median (interquartile range).

Table 2. Anthropometrical and clinical characteristics of the whole cohort

	Girona		*P*
	Without obesity	With obesity	
n	121	216	—
Sex (men | women)	15 | 106	51 | 165	—
Age, y	47.24 ± 10.958	48.17 ± 10.251	.435
Body mass index	24.623 ± 3.068	42.533 ± 7.085	**2.54E^{-102}**
Waist circumference, cm	86.545 ± 9.831	122.213 ± 14.781	**2.53E^{-76}**
Fasting glucose, mg/dL	96.75 ± 35.552	105.54 ± 33.446	.026
Glycated hemoglobin, %	5.502 ± 0.656	5.891 ± 0.994	**2.43E^{-05}**
Cholesterol, mg/dL	203.2 ± 41.272	191.94 ± 33.868	.011
HDL cholesterol, mg/dL	61 ± 15.936	49.82 ± 13.961	**5.71E^{-10}**
LDL cholesterol, mg/dL	121.94 ± 36.8	117.00 ± 28.584	.205
Fasting triglycerides (mg/dL)[a]	87 (60-115)	111 (82-156.5)	**4.66E^{-04}**
Ultrasensitive CRP (mg/dL)[a]	0.34 (0.11-0.685)	0.66 (0.33-1.35)	.001
Minimum temperature (°C)[a]	8.6 (4.6-13.3)	8.2 (4.2-11.9)	.180
Maximum temperature (°C)[a]	20.65 (17.25-26.125)	18.75 (15.6-23.4)	.003
Average temperature (°C)[a]	14.55 (11.2-19.6)	13.4 (9.725-17.775)	.025
Minimum temperature MB (°C)[a]	8.25 (4.025-13)	8.55 (4.1-12.65)	.665
Maximum temperature MB (°C)[a]	19.7 (16.3-26.4)	19.05 (14.925-23.775)	.019
Average temperature MB (°C)[a]	13.95 (10.125-19.7)	13.6 (9.5-18)	.145
UCP1 mRNA (RU)[a]	8.9E^{-04} (5.8E^{-04}-1.5E^{-04})	6.05E^{-04} (4.14E^{-04}-1.11E^{-04})	.034
PRDM16 mRNA (RU)[a]	6.3E^{-04} (4.2E^{-04}-8.8E^{-04})	5.26E^{-04} (4.03E^{-04}-7.13E^{-04})	.011
PPARGC1α mRNA (RU)[a]	4.6E^{-03} (2.9E^{-03}-6E^{-03})	3.52E^{-03} (2.44E^{-03}-4.978E^{-03})	.002
ADIPOQ mRNA (RU)[a]	3.052 (2.38-3.719)	2.403 (1.948-3.031)	**4.64E^{-07}**
ADIPOQ plasma, ng/mL	13.551 ± 5.109	10.809 ± 4.707	**1.01E^{-06}**

Unless otherwise indicated, data are expressed as mean ± SD. Unpaired *t* test was used to compare participants with and without obesity in the Girona subcohort. *P* less than .05 indicates statistically significant differences between participants with and without obesity in the subcohort of Girona. Bold values highlight statistically significant *P* values.
Abbreviations: CRP, C-reactive protein; HDL, high-density lipoprotein; LDL, low-density lipoprotein; MB, month before; mRNA, messenger RNA; *PPARGC1α*, peroxisome proliferator activated receptor gamma coactivator 1 alpha; *PRDM16*, PRD1-BF1-RIZ1 homologous domain containing 16; *UCP1*, uncoupling protein 1.
[a]Median (interquartile range).

was checked by Agilent Bioanalyzer (Agilent Technologies). Total RNA was reverse-transcribed to complementary DNA using the High Capacity cDNA Archive Kit (Applied Biosystems). Gene expression was assessed by real-time polymerase chain reaction (PCR) using a LightCycler 480 Real-Time PCR System (Roche Diagnostics SL), using SYBR green technology suitable for relative genetic expression quantification. Peptidylprolyl isomerase A (PPIA) was used as an endogenous control. The commercially predesigned KiCqStart primers used are shown in Supplementary Table S1 (16).

Circulating Adiponectin Analysis

Levels of *ADIPOQ* in plasma EDTA samples were measured using the human Adiponectin ELISA Kit, High Sensitivity (No. RD191023100, BioVendor) according to the manufacturer's instructions (RRID: AB_2941668). Intra-assay and interassay coefficients of variation for these determinations were between 3.9% and 6%, respectively. The level of detection was 0.47 ng/mL.

Temperature Data of the Participants

The temperatures in the closest meteorological station to the participant place of residence in the month of sample collection and of the immediate previous month were obtained from the National Meteorological Agency of Spain (AEMET) in degrees Celsius (°C). Average mean temperatures, and the average minimum and maximum temperatures, were extracted from the AEMET for each participant.

Statistical Analyses

Statistical analyses were performed using SPSS 21.0 software (SPSS). The relationship between variables were analyzed by simple correlation (Spearman test) and multiple regression analyses in a stepwise manner. In multiple regression analyses, multicollinearity was checked using the variance inflation factor. One-factor analysis of variance with post hoc Bonferroni test and unpaired *t* test were used to compare clinical variables and gene expression relative to obesity status, geographical region, and season. The levels of statistical significance were set at *P* less than .05.

Machine learning analyses

In addition to using multivariate logistic regression models, we also applied a machine learning algorithm (Boruta) to identify the most relevant clinical variables related to metabolic variables and AT gene expression markers. The Boruta
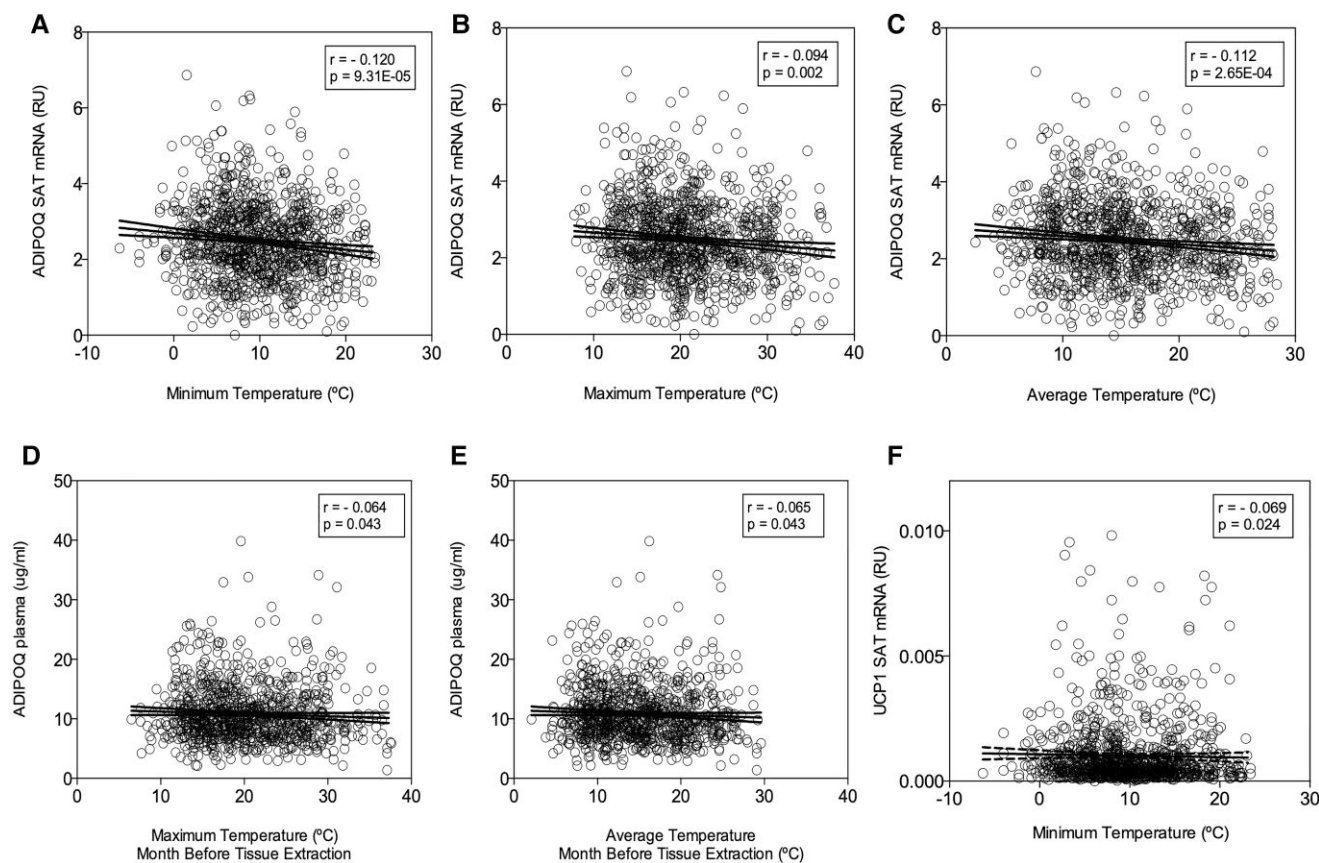
Figure 1. A to C, Association of environmental outdoor temperatures with *ADIPOQ* gene expression; bivariate correlations between *ADIPOQ* gene expression and A, minimum temperature; B, maximum temperature; and C, average temperature. D and E, Bivariate correlations between ADIPOQ plasma and D, maximum temperature of the month before tissue sample was obtained, and E, average temperature of month before tissue sample was obtained. F, Bivariate correlation between *UCP1* gene expression and minimum temperature.

algorithm is a wrapper algorithm that performs feature selection based on the learning performance of the model. It has been recently proposed as one of the two best-performing variable selection methods making use of random forests (17). It performs variables selection in 4 steps: a) randomization, to create a duplicate copy of the original features randomly permutated across the observations (the so-called shadow features) to remove their correlation with the response; b) model building, to add the shadow feature to the original predictor feature data set, build a RF with the extended data set, and compute the normalized permutation importance (Z) scores for each predictor and shadow feature; c) statistical testing, to find the maximum normalized importance among the shadow attributes (MZSA) and compare it with each original predictor feature using a Bonferroni corrected 2-tailed binomial test. Predictor features with significantly higher than, significantly lower than, or nonsignificantly different Z scores from that expected at random compared to the MZSA are deemed important, unimportant, or tentative, respectively; d) iteration, unimportant and shadow features are removed and the previous steps are repeated until the status of all features is decided or a predefined number of iterations have been performed. We ran the Boruta algorithm with a maximum of 1000 iterations, a confidence level cutoff of .005 for the Bonferroni adjusted P values, 5000 to grow the forest (ntree), and several features randomly sampled at each split given by one third of the number of features (the mtry recommended for regression analysis). Ranger's choice on "respect.unordered.factors" was set to true to account for both quantitative and categorical variables as predictors in the model.

Results

Anthropometrical and clinical parameters and variables of AT expression from the participants of the studied cohort are shown in Tables 1 and 2. Participants with glycated hemoglobin A_{1c} equal to or higher than 6.5 and/or undergoing treatment with oral hypoglycemic agents were diagnosed as type 2 diabetes (195 participants, 18% of the total) and were also included. As expected, marked differences in environmental temperature were observed, being highest in the South nodes (Málaga and Córdoba) compared with the North nodes. The average of the minimum temperatures across the year in the South nodes was between 8.3 °C and 13.7 °C, while in the North nodes the average environmental temperatures was between 8.2 °C and 8.7 °C. on the other hand, the average of the maximum temperatures in the South was 21.5 °C, while in the North the average of the maximum temperatures was between 16.9 °C and 20.65 °C (P values between $1.63E^{-39}$ and $3.37E^{-30}$). All nodes included AT samples from individuals with morbid obesity while the Girona node also included samples from individuals without obesity (see Table 2).

Table 3. Multiple regression analyses evaluating the contribution of temperatures on relative gene expression variance in the whole cohort

	ADIPOQ all cohort[b]		ADIPOQ obese[b]		UCP1 all cohort[b]		UCP1 obese[b]		PRDM16 all cohort[b]		PRDM16 obese[b]		CIDEA all cohort[b]		CIDEA obese[b]	
	β	P	β	P	β	P	β	P	β	P	β	P	β	P	β	P
Age[a]	.009	.804	.050	.205	−.008	.824	−.023	.561	−.012	.744	−.015	.712	−.047	.164	.050	.219
Sex[a]	.228	**2.42E−10**	.241	**1.84E−09**	−.104	**.005**	−.094	**.018**	−.068	.076	−.069	.096	−.054	.119	−.069	.090
Body mass index[a]	−.162	**1.84E−04**	−.044	.308	−.141	**.002**	−.123	**.004**	−.091	**.048**	−.080	.077	−.376	**1.76E−18**	−.127	**.004**
Sample origin[a]	−.007	.888	−.008	.868	.040	.406	.039	.417	.084	.094	.076	.130	−.061	.182	−.080	.103
Fasting glucose[a]	.017	.643	.019	.657	.044	.263	.051	.233	−.014	.725	−.017	.712	−.035	.333	−.055	.209
Fasting triglycerides[a]	−.078	**.044**	−.069	.104	−.043	.277	−.041	.337	−.023	.576	−.025	.579	−.092	**.013**	−.063	.148
HDL cholesterol[a]	.085	**.021**	.071	.077	.004	.917	.005	.908	−.013	.750	−.010	.806	.054	.125	.013	.751
Ultrasensitive CRP[a]	.089	**.026**	.092	**.038**	.267	**1.81E−10**	.267	**3.14E−09**	.034	.434	.036	.438	.126	**.001**	.170	**1.933E−04**
Minimum temperature	−.088	**.016**	−.082	**.047**	−.072	.056	−.084	**.044**	−.041	.295	−.045	.303	−.023	.513	−.038	.369
Adjusted R^2	.130		.088		.076		.079		.002		.001		.183		.040	
P (model)		**1.06E−19**		**1.62E−10**		**8.30E−11**		**2.20E−09**		.311		.378		**6.53E−29**		**1.10E−04**
Age[a]	.007	.836	.050	.204	−.007	.838	−.021	.593	−.012	.760	−.014	.735	−.049	.152	.048	.239
Sex[a]	.228	**2.65E−10**	.240	**2.13E−09**	−.103	**.005**	−.094	**.019**	−.068	.077	−.069	.098	−.054	.115	−.071	.077
Body mass index[a]	−.175	**6.18E−05**	−.050	.244	−.146	**.001**	−.129	**.003**	−.093	**.046**	−.083	.066	−.384	**6.30E−19**	−.130	**.003**
Sample origin[a]	−.013	.776	−.014	.770	.029	.546	.025	.601	.077	.125	.067	.177	−.058	.198	−.071	.141
Fasting glucose[a]	.017	.643	.019	.663	.044	.261	.051	.236	−.014	.728	−.017	.709	−.036	.330	−.055	.204
Fasting triglycerides[a]	−.078	**.043**	−.069	.103	−.045	.256	−.043	.318	−.025	.551	−.026	.561	−.091	**.015**	−.061	.161
HDL cholesterol[a]	.084	**.021**	.070	.078	.006	.882	.007	.863	−.011	.775	−.009	.836	.053	.135	.009	.826
Ultrasensitive CRP[a]	.092	**.022**	.094	**.033**	.266	**2.51E−10**	.265	**4.62E−09**	.032	.451	.035	.457	.129	**.001**	.178	**9.70E−05**
Maximum temperature	−.091	**.010**	−.085	**.034**	−.039	.286	−.040	.321	−.015	.703	−.013	.751	−.052	.129	−.107	**.009**
Adjusted R^2	.131		.089		.073		.074		.001		−4.63E−04		.185		.049	
P (model)		**1.15E−19**		**1.27E−10**		**2.58E−10**		**8.57E−09**		.388		.465		**2.65E−29**		**9.00E−06**
Age[a]	.008	.829	.050	.207	−.008	.824	−.022	.575	−.012	.749	−.015	.722	−.048	.159	.049	.233
Sex[a]	.228	**2.57E−10**	.240	**2.04E−09**	−.104	**.005**	−.094	**.018**	−.068	.076	−.069	.096	−.054	.117	−.070	.083
Body mass index[a]	−.169	**9.75E−05**	−.047	.276	−.145	**.001**	−.127	**.003**	−.093	**.044**	−.082	.069	−.380	**1.07E−18**	−.127	**.004**
Sample origin[a]	−.008	.858	−.009	.845	.035	.474	.032	.506	.080	.110	.071	.155	−.058	.201	−.072	.138
Fasting glucose[a]	.017	.644	.019	.660	.044	.262	.051	.235	−.014	.726	−.017	.710	−.036	.331	−.055	.207
Fasting triglycerides[a]	−.077	**.044**	−.069	.104	−.044	.267	−.042	.328	−.024	.564	−.025	.570	−.091	**.014**	−.061	.157
HDL cholesterol[a]	.084	**.021**	.070	.079	.005	.904	.006	.890	−.012	.760	−.010	.819	.053	.131	.010	.798
Ultrasensitive CRP[a]	.091	**.023**	.094	**.034**	.267	**2.00E−10**	.267	**3.57E−09**	.033	.439	.036	.443	.128	**.001**	.174	**1.34E−04**
Average temperature	−.093	**.009**	−.088	**.031**	−.056	.128	−.063	.125	−.028	.471	−.029	.500	−.040	.246	−.079	.060
Adjusted R^2	.131		.089		.074		.077		.001		1.32E−04		.184		.044	
P (model)		**1.06E−19**		**1.18E−10**		**1.52E−10**		**4.68E−09**		.357		.431		**4.20E−29**		**3.60E−05**

The median and interquartile range of variance inflation factor was 1.200 (1.073-1.315). Levels of statistical significance were set at *P* less than .05. Bold values mean that *P* values reached statistical significance. Levels of statistical significance were set at *P* less than .05. Adjusted R^2 compares the explanatory power of regression models that contain different numbers of predictors. Bold values mean that *P* values reached statistical significance. β Corresponds to the standardized β coefficient of the multiple regression analyses.

Abbreviations: CRP, C-reactive protein; HDL, high-density lipoprotein; LDL, low-density lipoprotein; *UCP1*, uncoupling protein 1.

[a]Predictor variable.

[b]Indicates the dependent variable.
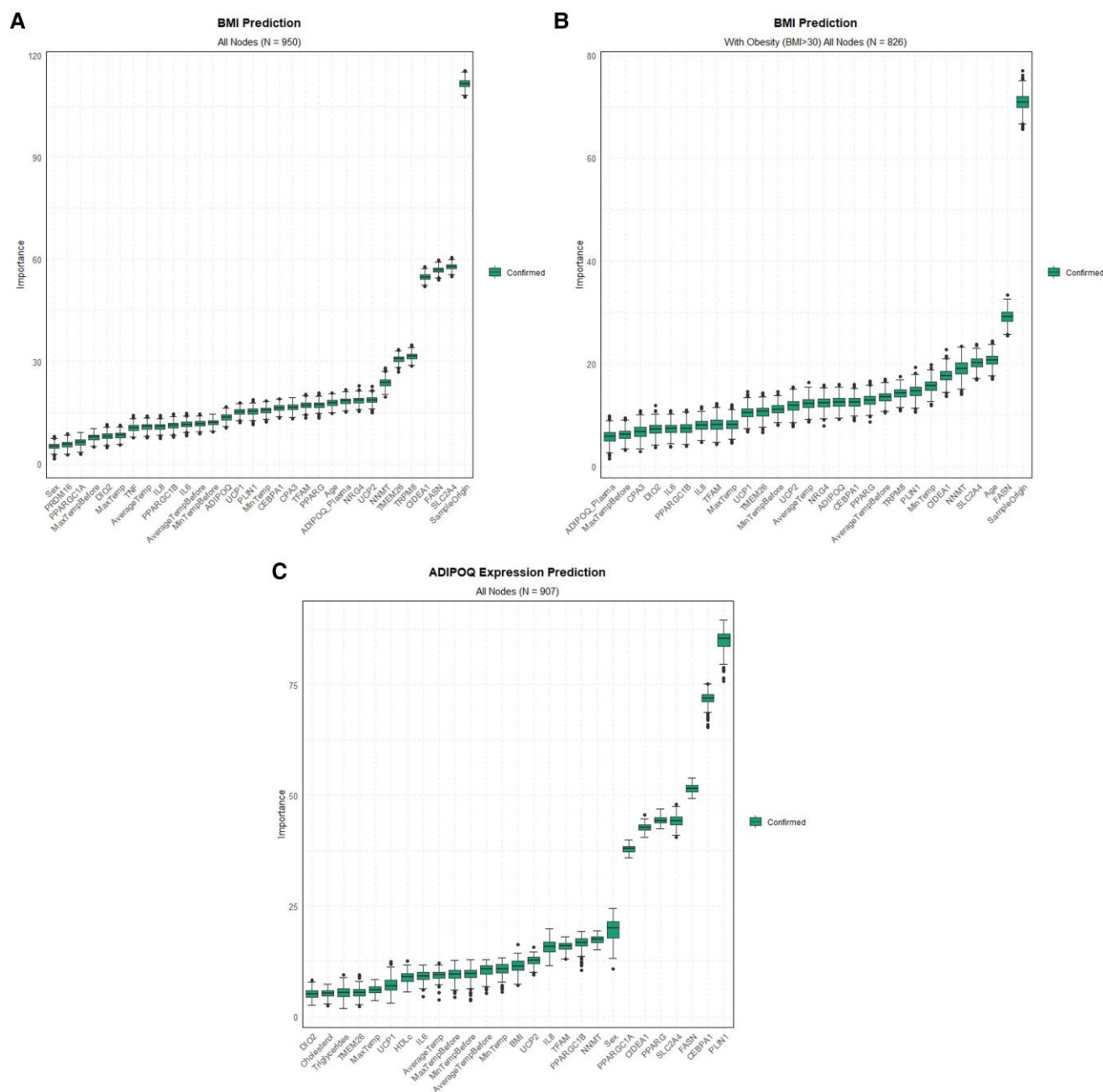
Figure 2. Results from machine learning (Boruta) analyses modeling body mass index (BMI) as the dependent variable in A, all participants, and B, within participants with obesity, with gene expression markers and environmental temperatures as independent variables. C, Modeling *ADIPOQ* gene expression as the dependent variable and clinical/anthropometrical parameters, gene expression markers, and environmental temperatures as independent variables. Box plots show the estimated importance of confirmed features, colored according to the direction of the relationship evaluated with Spearman correlation.

Impaired thermogenesis and decreased expression of thermogenesis-related genes are thought to contribute to the development of obesity (18). In the present study, inverse correlations between BMI and *UCP1* (Fig. 1F), *PRDM16*, and *CIDEA* expression (*P* values between .002 and .001; for the minimum, maximum, and average temperatures, respectively) (Supplementary Table S2) (16) were observed. The monthly temperatures used in the present study are an average of the measured day data of the place of residency of every participant, or the minimum or maximum temperature data of the month analyzed. In the samples obtained in winter, *UCP1* gene expression inversely correlated with mean minimum temperatures suggesting that cold exposure increases the expression of this browning marker in WAT in agreement with the observations seen in a previous study with a small number of participants (n = 27) (19).

Environmental temperatures also negatively correlated with *ADIPOQ* gene expression (*P* values between $9.31E^{-05}$ and .002) and with genes involved in adipogenesis (*PLIN1* [*P* values between .028 and .001], *FASN* [*P* values between .019 and $2.63E^{-07}$], and *SLC2A4* [*P* values between .03 and $2.36E^{-07}$]).

We next performed multivariate linear regression analyses considering those variables linked to environmental

temperatures in univariate comparisons. Minimum ($\beta=-.088$; $P = .016$), maximum ($\beta=-.091$; $P = .010$), and average temperature ($\beta=-.093$; $P = .009$) contributed independently to *ADIPOQ* mRNA variance after controlling for age, sex, BMI, sample origin, glucose, triglycerides, HDL cholesterol, and ultrasensitive CRP (Table 3).

Within participants with obesity, the minimum ($\beta=-.082$; $P = .047$), maximum ($\beta=-.085$; $P = .034$), and average ($\beta -.088$; $P = .031$) temperature also contributed independently to *ADIPOQ* mRNA variance after controlling for the same parameters. The minimum temperature ($\beta=-.084$; $P = .044$) contributed independently to adjusted *UCP1* mRNA variance in individuals with obesity (see Table 3). Furthermore, within participants with obesity, the maximum temperature contributed independently to adjusted *CIDEA* ($\beta=-.107$; $P = .009$), *CEBPA* ($\beta=.093$; $P = .016$), and *NNMT* ($\beta=-.124$; $P = .003$) mRNA variance after controlling for the same parameters. No statistically significant associations were found with the other genes analyzed.

All these analyses were performed using the mean temperatures of the same month in which the samples were obtained. We also explored the temperature of the immediate previous month of the sample collection. Only the minimum temperature contributed independently to *UCP1* mRNA variance in all participants ($\beta=-.086$; $P = .020$) and in individuals with obesity ($\beta=-.093$; $P = .022$) (Supplementary Table S3) (16).

When the participants with type 2 diabetes were excluded from the analysis, the associations remained statistically significant and additional associations emerged: The minimum temperature contributed independently to adjusted *UCP1* mRNA variance in the whole cohort ($\beta=-.073$; $P = .048$); and the maximum temperature contributed independently to adjusted *PLIN1* mRNA ($\beta=-.083$; $P = .045$), *PPARG* mRNA ($\beta=-.087$; $P = .035$), and *NNMT* mRNA ($\beta=-.096$; $P = .023$) in the whole cohort and within participants with obesity ($\beta=-.100$; $P = 0032$; $\beta=-.099$; $P = .036$; $\beta=-.156$; $P = .001$; respectively).

Given the significant and consistent associations with *ADIPOQ* gene expression and its known associations with healthy metabolic traits (Fig. 1A-1C), we also analyzed circulating adiponectin, which was negatively and significantly associated with the maximum and average temperature of the immediate previous month before tissue collection in all participants ($r = -0.064$; $P = .043$; $r = -0.065$; $P = .043$, respectively) (Fig. 1D and 1E) and with the maximum temperature within individuals with obesity ($r = -0.068$; $P = .048$).

When the analyses were stratified according to the season in which the samples were obtained, *UCP1* mRNA was negatively linked to environmental minimum temperature in winter ($r = -0.12$; $P = .003$); and *ADIPOQ* mRNA was negatively associated with the minimum temperature of the immediate previous month of the sample collection in summer ($r = -0.095$; $P = .04$). Within individuals with obesity, the association of *UCP1* remained statistically significant ($r = -0.095$; $P = .028$). Mean *ADIPOQ* mRNA in the samples collected in winter was significantly higher than in those obtained in summer (2.554 ± 1.027 vs 2.375 ± 0.946; $P = .003$) and within participants with obesity (2.472 ± 0.983 vs 2.296 ± 0.923; $P = .005$).

Additionally, when comparing *UCP1* and *ADIPOQ* transcripts from participants with obesity living in the South (Córdoba and Málaga) with those living in the North (see Table 1), the differences were very marked, suggesting that

lower temperatures could be a protective factor in this context. This is in line with the results of a previous study in the same regions evaluated here in which increasing time spent in a cold environment was found to be associated with a decreased prevalence of obesity in the North of Spain compared with the South (14). Furthermore, the mean *ADIPOQ* gene expression was higher in individuals living in the North than in those who lived in the South (2.445 ± 0.941 vs 2.307 ± 0.993, $P = .036$). The mean *ADIPOQ* gene expression in the North was also higher during the summer compared with those in the South (2.377 ± 0.891 vs 2.156 ± 0.963; $P = .020$) in parallel to raised temperatures in the South.

Machine Learning Results

We further analyzed the data applying a machine learning variable selection strategy based on multiple random forests as implemented in the Boruta algorithm to identify the most important outcome predictive variables. In line with previous analyses, BMI was independently predicted by environmental temperatures, in addition to several clinical variables, and the expression of genes associated with beiging or browning (*CIDEA*, *TMEM26*, *TRPM8*, *UCP2*) in all participants as a whole and within individuals with obesity (Fig. 2A and 2B).

Importantly, when *ADIPOQ* gene expression was considered the dependent variable, environmental temperatures and several thermogenic genes (*UCP1*, *DIO2*, *TMEM26*, *PPARGC1α*) also contributed as predictive variables to the model (Fig. 2C), in addition to the adipogenic genes *PLIN1*, *CEBPA*, *FASN*, and *SLC2A4*.

Discussion

We have shown positive associations between environmental temperature, obesity, and associated metabolic complications. In addition, our country appears to be especially suitable to show differences between the North, where BAT would be stimulated in the winter (with average minimum temperatures <10 °C) and the South, with temperatures between 10 °C and 20 °C. This could not be observed in other countries with uniformly low or high temperatures across territories.

ADIPOQ gene expression and circulating adiponectin concentrations are well known to be inversely associated with adiposity (20, 21). *ADIPOQ* also seems to play an important role in thermoregulation given the findings observed in *Adipoq*$^{-/-}$ mice under energy-deficient and cold-challenged conditions (22). Experimental studies have identified adiponectin as a key efferent signal secreted by AT in response to adaptive thermogenesis (23). The findings observed in the present study suggest that adiponectin could be related to the thermogenic regulation in humans. *ADIPOQ* mRNA expression inversely correlated with all measured temperatures in all participants and within individuals with obesity.

In at least 13 studies, the obesity epidemic has been postulated to influence global warming (24). Global warming is defining the current climate change characterized by a gradual increase in the overall temperature of the earth's atmosphere (24). This global change has an effect on food, water supplies, housing, economic activities, and human health. Humans are endothermic, with thermoregulatory mechanisms that adapt to environmental changes to defend normal core body temperature being critical to sustain physiological functions

such as energy balance (25). These mechanisms are influenced by the fluctuating environment (26). Importantly, there are recent observations describing how areas with moderate or cold temperature exhibit a protective effect on external causes associated with metabolic disease (27).

In recent years, at least 4 pandemics have emerged—obesity, undernutrition, climate change, and the COVID-19 pandemic, representing what has been named the global Syndemic (a synergy of epidemics) that affects most people in every country and region worldwide (28). It has been stated that, if no actions are taken urgently, substantial increases in morbidity and mortality are expected in association with a range of health outcomes over the coming decades (29).

It is possible that decreased environmental temperature in individuals without obesity could lead to increased thermogenesis thus preventing weight gain. In people with obesity, given that their AT would play an insulating effect, the decrease in temperature would have a less marked effect and therefore they would remain obese. In keeping with this hypothesis, previous studies have shown that individuals with obesity exhibited a lower response when exposed to cooling than those without obesity as assessed by heat loss (30). It could be speculated that the expression of genes associated with browning might provide relevant information about the optimal temperature to prevent obesity at individual/populations level.

Limitations and Strengths

Some limitations need to be acknowledged. We used the mean outside temperatures in the meteorological stations closest to the places of residence of the study participants. Indoor temperatures where participants lived or worked were not controlled for. The complexities of measuring indoor temperature exposure have been explored in previous articles (31), and these are likely to remain a barrier in accessing robust exposure data. It is also important to note that we focused only on outdoor temperature but other metric variables, such as humidity and air velocity, and therefore thermic sensation, were not included in this study. However, there is strong evidence linking high environmental temperatures and outdoor meteorological data to general morbidity and mortality (32). Another considerable limitation was that dietary patterns and physical activity were not systematically collected, and data analysis was not standardized or taken into account for these parameters. In addition, this study lacks a case-control element in part because of the complexity of obtaining AT samples in the same patients in 2 different seasons during the same year.

However, even bearing in mind these limitations, the observed relationships were remarkably significant and in the expected direction in a large cohort of participants. As to strengths, this is a multicenter study in which all nodes used the same clinical protocols (inclusion and exclusion criteria) for AT sampling and conservation in the centralized Fat Bank, a biobank specializing in AT (www.ciberobn.es/en/platforms/fatbank). The RNA extraction of all AT samples and analyses were all performed in a single laboratory and by the same person (N.O.C.). Notably, to add robustness to the results, analyses were performed not only using univariate or multivariate methods but also artificial intelligence algorithms to control for potential confounders.

In summary, the AT expression of genes involved in thermogenic regulation is negatively associated with environmental temperatures and metabolic traits. The associations were more marked in winter and when excluding individuals with type 2 diabetes. The important potential implications of these findings for obesity epidemics with global warming need to be further considered.

Author Contributions

N.O.C. carried out the extraction and PCR of all the samples. J.M.M.N., P.M.L., L.G.S., S.B., O.R., J.L., E.C.V., M.P., V.V., J.L.R.C., W.O.O., C.S., C.D., F.V., M.L., A.B.C., and L.M.S. analyzed the data. J.L.M., G.F., F.J.T., and J.M.F.R. contributed to the discussion and carried out the conception and coordination of the study and wrote the manuscript. All authors participated in the final approval of the version to be published.

Disclosures

The authors declare no conflicts of interest.

Data Availability

Original data generated and analyzed during this study are included in this published article.

References

1. Cypess AM, Lehman S, Williams G, *et al.* Identification and importance of brown adipose tissue in adult humans.pdf. *N Engl J Med.* 2009;360(15):1509-1517.
2. Becher T, Palanisamy S, Kramer DJ, *et al.* Brown adipose tissue is associated with cardiometabolic health. *Nat Med.* 2021;27(1):58-65.
3. Wibmer AG, Becher T, Eljalby M, *et al.* Brown adipose tissue is associated with healthier body fat distribution and metabolic benefits independent of regional adiposity. *Cell Rep Med.* 2021;2(7):100332.
4. Barquissau V, Léger B, Beuzelin D, *et al.* Caloric restriction and diet-induced weight loss do not induce browning of human subcutaneous white adipose tissue in women and men with obesity. *Cell Rep.* 2018;22(4):1079-1089.

5. LeBlanc ES, Patnode CD, Webber EM, Redmond N, Rushkin M, O'Connor EA. Behavioral and pharmacotherapy weight loss interventions to prevent obesity-related morbidity and mortality in adults updated evidence report and systematic review for the US Preventive Services Task Force. *JAMA*. 2018;320(11):1172-1191.

6. Panagiotou OA, Markozannes G, Adam GP, *et al.* Comparative effectiveness and safety of bariatric procedures in Medicare-eligible patients: a systematic review. *JAMA Surg*. 2018;153(11):e183326.

7. Catalán V, Avilés-Olmos I, Rodríguez A, *et al.* Time to consider the "exposome hypothesis" in the development of the obesity pandemic. *Nutrients*. 2022;14(8):1597.

8. Barneda D, Frontini A, Cinti S, Christian M. Dynamic changes in lipid droplet-associated proteins in the "browning" of white adipose tissues. *Biochim Biophys Acta Mol Cell Biol Lipids*. 2013;1831(5):924-933.

9. Leitner BP, Huang S, Brychta RJ, *et al.* Mapping of human brown adipose tissue in lean and obese young men. *Proc Natl Acad Sci U S A*. 2017;114(32):8649-8654.

10. Seale P, Conroe HM, Estall J, *et al.* Prdm16 determines the thermogenic program of subcutaneous white adipose tissue in mice. *J Clin Invest*. 2011;121(1):96-105.

11. Cohen P, Levy JD, Zhang Y, *et al.* Ablation of PRDM16 and beige adipose causes metabolic dysfunction and a subcutaneous to visceral fat switch. *Cell*. 2014;156(1-2):304-316.

12. Nedergaard J, Cannon B. The browning of white adipose tissue: some burning issues. *Cell Metab*. 2014;20(3):396-407.

13. Au-Yong ITH, Thorn N, Ganatra R, Perkins AC, Symonds ME. Brown adipose tissue and seasonal variation in humans. *Diabetes*. 2009;58(11):2583-2587.

14. Valdés S, Maldonado-Araque C, García-Torres F, *et al.* Ambient temperature and prevalence of obesity in the Spanish population: the Di@bet.es study. *Obesity*. 2014;22(11):2328-2332.

15. Valdés S, Doulatram-Gamgaram V, Lago A, *et al.* Ambient temperature and prevalence of diabetes and insulin resistance in the Spanish population: Di@bet.es study. *Eur J Endocrinol*. 2019;180(5):275-282.

16. Oliveras-Cañellas N, Moreno-Navarrete JM, Lorenzo P, *et al.* Supplementary material for "Downregulated adipose tissue expression of browning genes with increased environmental temperatures." Zenodo. Deposited August 4, 2023. https://zenodo.org/record/8215517

17. Kursa MB, Rudnicki WR. Feature selection with the Boruta package. *J Stat Softw*. 2010;36(11):1-13.

18. Turner JB, Kumar A, Koch CA. The effects of indoor and outdoor temperature on metabolic rate and adipose tissue—the Mississippi perspective on the obesity epidemic. *Rev Endocr Metab Disord*. 2016;17(1):61-71.

19. Kern PA, Finlin BS, Zhu B, *et al.* The effects of temperature and seasons on subcutaneous white adipose tissue in humans: evidence for thermogenic gene induction. *J Clin Endocrinol Metab*. 2014;99(12):E2772-E2779.

20. Hu E, Liang P, Spiegelman BM. Adipoq is a novel adipose-specific gene dysregulated in obesity. *J Biol Chem*. 1996;271(18):10697-10703.

21. Arita Y, Kihara S, Ouchi N, *et al.* Paradoxical decrease of an adipose-specific protein, adiponectin, in obesity. *Biochem Biophys Res Commun*. 1999;257(1):79-83.

22. Wei Q, Lee JH, Wang H, *et al.* Adiponectin is required for maintaining normal body temperature in a cold environment. *BMC Physiol*. 2017;17(1):8.

23. Hui X, Gu P, Zhang J, *et al.* Adiponectin enhances cold-induced browning of subcutaneous adipose tissue via promoting M2 macrophage proliferation. *Cell Metab*. 2015;22(2):279-290.

24. An R, Ji M, Zhang S. Global warming and obesity: a systematic review. *Obes Rev*. 2018;19(2):150-163.

25. Johnson F, Mavrogianni A, Ucci M, Vidal-Puig A, Wardle J. Could increased time spent in a thermal comfort zone contribute to population increases in obesity? *Obes Rev*. 2011;12(7):543-551.

26. Ahima RS. Global warming threatens human thermoregulation and survival. *J Clin Invest*. 2020;130(2):559-561.

27. Burkart KG, Brauer M, Aravkin AY, *et al.* Estimating the cause-specific relative risks of non-optimal temperature on daily mortality: a two-part modelling approach applied to the Global Burden of Disease Study. *Lancet*. 2021;398(10301):685-697.

28. Swinburn BA, Kraak VI, Allender S, *et al.* The global syndemic of obesity, undernutrition, and climate change: the Lancet Commission report. *Lancet*. 2019;393(10173):791-846.

29. Haines A, Ebi K. The imperative for climate action to protect health. *N Engl J Med*. 2019;380(3):263-273.

30. Bittel JHM. Heat debt as an index for cold adaptation in men. *J Appl Physiol (1985)*. 1987;62(4):1627-1634.

31. Tham S, Thompson R, Landeg O, Murray KA, Waite T. Indoor temperature and health: a global systematic review. *Public Health*. 2020;179(1):9-17.

32. Nguyen JL, Schwartz J, Dockery DW. The relationship between indoor and outdoor temperature, apparent temperature, relative humidity, and absolute humidity. *Indoor Air*. 2014;24(1):103-112.

6. DISCUSSION

6.1 MECHANISMS INVOLVED IN THE BIDIRECTIONAL INTERACTIONS BETWEEN AT GENE EXPRESSION AND COGNITIVE FUNCTION

6.1.1 Adipose tissue gene expression is linked to several cognitive domains involved in neuronal system and synaptic formation

Transcriptomic analysis of AT and cognitive tests to assess cognitive domains were performed in subjects with severe obesity to gain insights into the fat-brain axis. Two independent cohorts were used to study AT gene expression in relation to cognitive domains. The first cohort used was the *Discovery Cohort*, which included VAT from 17 subjects who underwent ten different cognitive tests to assess memory, executive function and attention. The second cohort was the *Validation Cohort 1*, which included VAT and SAT from 22 subjects who underwent the same cognitive tests as the *Discovery Cohort,* but 2 to 3 years after the AT samples were collected (**Table 5**).

There are lifestyle-related factors, such as physical activity, diet or alcohol consumption, that are known to cause or contribute to cognitive function [367]. After controlling for age, sex, BMI and years of education, confounders known to affect cognitive function, we found no significant associations of any of the ten cognitive tests with physical activity, macronutrients, alcohol intake, glycemia or HbA1c in either cohort.

We observed significant associations with gene transcripts in all cognitive tests. Among these genes, *Nudix hydrolase 2 (NUDT2), Amphiphysin (AMPH), Unc-5 Netrin Receptor B (UNC5B)* and *Ornithine Aminotransferase (OAT)* were those with the most significant associations across cognitive domains in the *Discovery Cohort*. The effect of the proteins encoded by these genes was concordant with their function in the CNS, but their expression in the AT in relation to cognition is unprecedented. Variants in the *NUDT2* gene have been associated with intellectual disability [368,369]. *AMPH* encodes a protein that is highly concentrated in presynaptic terminals [370] and is one of the proteins altered in the cerebrospinal fluid of patients with MCI and AD [371]. *Amph* in *Drosophila* is a postsynaptic protein that regulates the location of key components of glutamatergic signalling and dendritic dynamics, maturation, and synaptogenesis [372,373]. *OAT* encodes the enzyme ornithine aminotransferase, which plays a key role in the conversion of ornithine and arginine to glutamate and γ-aminobutyric acid,

as well as key excitatory and inhibitory neurotransmitters [374]. In addition, genes involved in tryptophan metabolism such as *Kynureninase (KYNU), Quinolinate phosphoribosyltransferase (QPRT)* and *Indolethylamine N-methyltransferase (INMT)* were among the most significant genes associated with inhibitory control, attention, and executive function in the *Discovery Cohort*. Consistently, subjects with obesity had impaired memory and inhibitory control due to alterations in tryptophan metabolism [375,376].

In *Validation Cohort 1*, the gene encoding for *Ezrin (EZR)* was one of the genes with most associations across the different cognitive domains in VAT, being the gene most significantly associated gene with DST Forward score. In line with previous findings, inhibitory control was strongly associated with complement-related genes and with the early immediate genes of the orphan nuclear receptor 4A family (*NR4A1* and *NR4A2*). In particular, *NR4A2* was the most significant gene associated with the SCWT test (which assesses inhibitory control), while *NR4A1* was among the top genes associated with the TMT part B (which assesses executive function). In the SAT, *NR4A1* and *NR4A2* were negatively associated with LTM, while the complement genes were particularly associated with attention. A gene from the NR4A (*NR4A3*) again had the strongest negative association with inhibitory control. Finally, *AMPH* was the gene most significantly associated with the DST Forward test and the total DST.

To facilitate interpretation and identify relevant AT pathways associated with cognitive function, we next performed overrepresentation analyses mapping significant genes to the Reactome and WikiPathways databases included in the Consensus-PathDB. We found an over-representation of pathways with an important role in the CNS associated with measures of inhibitory control, working memory, immediate memory and attention in both cohorts used. Specifically, in the *Discovery cohort*, executive function was associated with axon guidance, nervous system development, synaptic vesicle signalling, receptor tyrosine kinase signalling and changes in complement activation. Immediate memory and attention were associated with pathways involved in the neuronal system and serotonin and dopamine neurotransmitter release cycles. Inhibitory control and attention were over-represented in axon guidance and nervous system development. Inhibitory control was associated with semaphoring signalling and interaction, which play an important role in adult neuronal plasticity [377]. We also found an over-representation of the inflammatory signalling pathways associated with the different cognitive domains.

In VAT of the *Validation Cohort 1,* attention was again significantly associated with pathways involved in axon guidance, nervous system development, neuronal system and tryptophan. Inhibitory control was associated with semaphoring signalling. The activation of the complement system was again strongly associated with performance in several cognitive domains. In the SAT, both LTM and STM were associated with pathways related to synaptic transmission, the neuronal system and one-carbon metabolism. Attention was significantly associated with complement activation.

To gain further insight in coincident associations between the two cohorts, an enrichment analysis was performed considering only those genes significantly associated with at least one cognitive test in all tissues (VAT from *Discovery Cohort*, VAT and SAT from *Validation Cohort 1*). A total of 188 common genes were found. The most overrepresented pathways included had key roles in synaptic function and inflammation (tryptophan metabolism and complement activation). We construct a gene-gene interaction network mapping these genes to the STRING database, which revealed a cluster of highly interconnected genes mainly involved in the neuronal system and synapse formation and maintenance [378] (*Discs large MAGUK scaffold protein 4 (DLG4), DLG associated protein 1 (DLGAP1), Discs large MAGUK scaffold protein 2 (DLG2), ATPase Na⁺ / K⁺ transporting subunit β1 (ATP1B1), Homer scaffold protein 1 (HOMER1), NLR family pyrin domain containing 3 (NLGN3), Synuclein α (SNCA), Butylcholinesterase (BCHE), Regulating synaptic membrane exocytosis 1 (RIMS1), SLC18A2, Adrenoceptor β2 (ADRB2), EZR, Podocalyxin like (PODXL)* and *Neural cell adhesion molecule 2 (NCAM2)*).

To get a better picture of the associated pathways, we used the interaction information from the gene-gene interaction network to identify active subnetwork and then performed an active subnetwork-oriented enrichment analysis on these subnetworks. In total, 120 over-represented Reactome pathways were identified. To reduce the complexity of this large number of pathways, we performed hierarchical clustering to collapse redundant pathways and facilitate the identification of mechanisms relevant to cognition. Of the 53 clusters, the most significant included pathways related to the neuronal system and synaptic function (*RIMS1, SLC18A2, DLG2, DLG4, DLGAP1, HOMER1, NLGN3, Protein tyrosine phosphatase receptor type D (PTPRD), BCHE,* and *Potassium calcium-activated channel subfamily N member 3 (KCNN3)*). This cluster was strongly connected with three other cluster involved in the synthesis and metabolism of phospholipids, in particular phosphatidylinositols (PIPs) (*Phosphatidylinosiltol-4-phsosphate 3-kinase catalytic subunit type 2 β (PIK3C2B)* and *γ (PIK3C2G),*

Synpasin I (SYNJ1) and *Pleckstrin homology domain containing A6 (PLEKHA6))*, Rho guanosine triphosphatase (GTPases) signalling (Rho GTPase activating protein 23 (*ARHGAP23*), *Diaphanous related formin 3 (DIAPH3), DLG4, Rho related BTB domain containing 1 (RHOBTB1), Shugoshin 2 (SG02)* and *Serum response factor (SRF))*, and neurotransmitters release (*RIMS1* and *SLC18A2*).

Multiblock Partial Least Square analysis were performed to integrate 188 AT genes with plasma levels of metabolites measured by ^{1}H NMR, HPLC-ESI-MS/MS and circulating levels of IL-6, IL-4, Tau, α-synuclein and Aβ42; to gain insight into potential mechanisms linking AT to cognition. Expression levels of AT genes involved in phospholipid metabolism (*PIK3C2B, Phospholipase A2 group VI (PLA2G6)* or *SYNJ1*) were strongly associated with several circulating phospholipids and lysophospholipids. Although lipids are essential to brain function, and phospholipids in particular are crucial for synaptic plasticity, neurotransmission and memory [379], the brain can only synthesize a limited number of lipids. However, plasma fatty acids can cross the BBB as NEFA or esterified in lysophospholipids such as lysophosphatidylcholine (LPC) [380,381]. Some of the genes in the phospholipid metabolism cluster encode *PLA2G6*, which catalyses the hydrolysis of the sn-2 position of glycerophospholipids to yield NEFA and lysophospholipids. These phospholipids may therefore mediate the effects of AT on cognition.

We also identified three highly interconnected clusters of genes related to the inflammatory response, including the complement cascade (*C4A* and *C4B*) and IL-4, IL-10, IL-13 interleukin signalling (*IL-18* and *TIMP metallopeptidase inhibitor 1 (TIMP1)*). Chronic low-grade inflammation is a hallmark of obesity, and the association between obesity and cognitive decline has recently been shown to be mediated by inflammation [209,382]. In addition, complement-dependent synapse elimination has recently been identified as a mechanism for memory loss[383]. Consistent with our findings, NLRP3 from the VAT has recently been shown to impair cognition in mice by activating the microglial IL-1 receptor [250], whereas IL-4 has shown to mediate the protective effects of beige fat on obesity-induced cognitive impairment by restoring synaptic plasticity in the hippocampus [273]. Consistent with the recent finding that inhibition of Na,K-ATPase signalling results in improved cognitive function [223], we also identified a cluster containing the Na$^+$/K$^+$ ATPase transport subunit beta 1 (*ATP1B1*) gene. Notably, the Na,K-ATPase pathway requires activation of PIP 3-kinase, and we identified a cluster of pathways involved in PIP metabolism that are strongly associated with cognition. Finally, the genes involved in the inflammatory cluster (*C4A, C4B, IL-18,*

and *TIMP1*) had a strong positive association with circulating IL-6 levels and a strong negative association with plasma IL-4 levels. Therefore, these adipokines may be released by AT and mediates its effects on cognition. Accumulating evidence suggests that peripheral inflammation contributes to increased neuroinflammation [384] and could be a potential causal mechanism for obesity-related cognitive impairment [385,386].

Other significant clusters included nuclear receptor transcription (*NR4A1, NR4A2,* and *NR2F1*) and vitamin metabolism (*ATP binding cassette subfamily C member 1 (ABCC1), Transcobalamin 2 (TCN2)*), particularly vitamin A (*Retinol binding protein 1 (RBP1)* and Glypican 4 (*GPC4)*). Recent studies have shown that *NR4A2* activation improves LTM in young mice and ameliorates age-related memory impairments in old mice [387]. Several studies have also suggested that water-soluble vitamins (C, E, and Bs) may affect cognitive performance by reducing the generation of ROS and pro-inflammatory mediators such as the NLRP3 inflammasome [388]. Retinoic acid, the active form of vitamin A, is essential for regulating synaptic plasticity in brain regions involved in memory and learning [389]. Notably, we found a strong positive association between the expression levels of genes involved in vitamin metabolism in the AT, in particular *TCN2* and *ABCC1*, and circulating levels of retinoic acid. In particular, *RBP1*, which encodes the cellular retinol binding protein 1 involved in the transport of retinol, had a strong negative association with plasma levels of retinoic acid. Taken together, these results suggest that AT may modulate cognitive performance through vitamin A metabolism.

We want to validate these previous results using an additional cohort, *Validation Cohort 3*, which consists of VAT from 40 subjects with and without obesity who underwent ROCF testing 4 to 10 years later (**Table 5**). We analysed the expression levels of *EZR, UNC5B, NUDT2* and *NR4A2*.

Consistent with previous findings in the *Discovery Cohort*, the expression of *EZR* and *UNC5B* was negatively associated with ROCF scores in subjects with morbid obesity; and positively associated with executive function in subjects with BMI less than 35 kg/m^2. *NUDT2* expression was positively associated with ROCF in morbidly obese subjects, but not in subjects with a BMI less than 35 kg/m^2. We found no significant association with *NR4A2* expression.

While the brain regulates the performance of AT, we show that the reverse is also plausible. We found that the expression of genes associated with axon guidance, nervous system

development, neuronal system, tryptophan, and inflammatory activity in human AT were all associated with cognition in three different cohorts of subjects.

6.1.2 Blood expression levels of key genes linked to cognitive performance

To further validate these findings, we measured the expression of the most promising genes across the different neuropsychological tests in the *Discovery Cohort* (*NUDT2, AMPH, UNC5B* and *OAT*) and *Validation Cohort 1* (*EZR* and *NR4A2*). We used PBMC mRNA from 816 subjects aged ≥ 50 years to provide non-invasive biomarkers of cognitive function as an alternative to AT biopsies (Table 5). PBMC mRNA levels of adipogenic genes decreased after weight loss in obese subjects [390], while HFD-induced cognitive impairment led to changes in the PBMC transcriptome in rats [391].

Circulating levels of *NUDT2* were negatively associated with executive function, while circulating expression of *AMPH* was negatively associated with processing speed and memory. Elevated levels of *OAT* and *UNC5B* tended to be associated with delayed memory and executive function. Finally, there were negative associations between circulating expression of *EZR* and executive function, and quintiles of *NR4A2* with memory.

We showed that the expression of genes in PBMCs that were most strongly associated with cognition in AT (*NUDT2, AMPH, UNC5B, OAT, EZR,* and *NR4A2*) were also associated with cognitive traits in a cohort of 816 subjects.

6.1.3 Downregulation of candidate genes in the fat body of *Drosophila melanogaster* improves cognition

We next investigated the causal effect of AT expression of candidate genes (*AMPH, UNC5B, NUDT2, OAT, NR4A2, NR4A3,* and *EZR*) on cognitive function using *Drosophila melanogaster*. We down-regulated *Amph, unc-5, Datp, Oat, Hr38,* and *Moe* (the well-conserved orthologues of *AMPH, UNC5B, NUDT2, OAT, NR4A2/NR4A3* and *EZR*, respectively) specifically in the *Drosophila* fat body, which corresponds to AT in humans. To assess cognition in *Drosophila*, we used the courtship conditioning paradigm to measure associative learning and memory capabilities [350] (*see section 3.2.1.4.*)

In at least one of the RNAi lines tested, down-regulation of *unc-5, Datp, Hr38,* and *Moe* led to a significant decrease in learning capabilities compared to their respective genetic background controls. Down-regulation of *Amph* resulted in an improvement in learning capabilities in one RNAi line. Down-regulation of *Oat* was lethal in one RNAi line or had no effect on learning capabilities in a second RNAi line.

These results show that specific down-regulation of genes in the fat body modulates learning, suggesting a direct effect on cognition that is uniquely dependent on their expression and/or function in the fat body. Taken together, these results demonstrate that altered expression of genes associated with cognition in humans in the fat body of *Drosophila* modifies cognition in the latter.

6.1.4   Neurotransmitter release cycle-associated genes *SLC18A2* and *RIMS1* modulate cognition in mice AT or *Drosophila* fat body

Among the genes associated with cognition in VAT and SAT from *Discovery Cohort* and *Validation Cohort 1*, the cluster of genes involved in neurotransmitter release (*RIMS1* and *SLC18A2*) had the largest number of significant associations across different cognitive domains. *SLC18A2* encodes for vesicle monoamine transporter member 2 (VMAT2), a protein that transports cytoplasmic monoamine neurotransmitters (dopamine, norepinephrine, histamine, and serotonin) into presynaptic vesicles and has been implicated in the pathophysiology of several neuropsychiatric and neurological disorders [392]. The *Drosophila* and mouse *RIMS1* orthologs have been shown to be a central component in the regulation of synaptic vesicle exocytosis and neurotransmitter regulation of synaptic vesicle exocytosis and neurotransmitter release [393]. Mice lacking *Rim1α* show severely impaired learning and memory [394], and *RIMS1* was recently identified as the top candidate gene for autism spectrum disorder [395]. For this reason and given the associations of both AT *SLC18A2* and *RIMS* mRNA with cognitive function, we selected these genes associated with the neurotransmitter release to test their possible functional relevance.

6.1.4.1   SLC18A2

First, we validated previous associations in cohort 3. Again, we found that *SLC18A2* expression was negatively associated with ROCF performance 4 to 10 years later in subjects with morbid obesity, whereas it was positively associated in subjects with a BMI less than 35 kg/m^2.

To demonstrate a possible causal effect of AT *SLC18A2* on cognition, we studied two preclinical models. In a mouse model, we used a vector expressing GFP and a miRNA to selectively down-regulate *Slc18a2* in AT, followed by tests to assess short- and LTM and locomotor activity (*see section 3.2.2*). The expression levels of GFP contained in the vector were significantly increased in both iWAT and mWAT of mice from the vector-injected groups compared to the saline groups, indicating that the vector was able to reach the AT. We also found a significant decrease in Slc18a2 protein levels in the mWAT of virus-injected mice fed an HFD compared to their respective controls.

As expected, mice fed an HFD gained more weight than those fed a ND. There is good evidence that obesity affects cognition in rodents [386]. Consistently, mice fed an HFD had poorer short- and LTM than mice fed a ND. Down-regulation of *Slc18a2* in mice AT reversed the memory impairment induced by an HFD. Although we found an effect of diet effect on locomotion, down-regulation of *Slc18a2* had no significant effect.

To further investigate the role of AT *SLC18A* on cognition, we specifically down-regulated *Vmat* (the orthologue of *SLC18A2*) in the fat body of *Drosophila* using two RNAi lines, followed by a courtship conditioning paradigm to assess STM.

Males of *Vmat*-RNAi1 were able to suppress courtship significantly better than the corresponding genetic background control. As a result, the LI was significantly increased, suggesting that *Vmat*-RNAi had better STM. Next, we wanted to prove that *Vmat* was specifically downregulated in the fat body, but not in the heads of the flies. qPCR showed that when *Vmat* expression was reduced only in the fat body, the flies were able to learn better.

To elucidate a potential mechanism by which *Vmat* expression in the fat body might affect cognition, we performed qPCR to evaluate the expression of *rutabaga (rut), dunce (dnc), amnesiac (amn), homer, calcium / calmodulin dependent protein kinase II (CAMKII)* and *orb2* in *Drosophila* heads. These genes are part of the cAMP pathway, which has been demonstrated to affect

learning and STM in the courtship conditioning assay [396]. RNAi-mediated down-regulation of *Vmat* in the fat body resulted in a significant increase in memory related genes (*rut, dnc, CAMKII* and *orb2*) in the fly head.

We used a RNAi2 to further validate our findings. When we down-regulate Vmat in the fat body with RNAi2, we observed a significant increase in STM and a significant over-expression of *dnc, CAMKII* and *orb2* in the head of the fly, confirming our previous data.

Down-regulation of *Vmat* in the fat body of two different *Drosophila* lines also improved STM.

6.1.4.2 RIMS1

First, we validated previous associations in cohort 3. *RIMS1* expression was negatively associated with ROCF in morbid subjects, but positively associated with ROCF in subjects with a BMI below 35 kg/m^2.

To test for a possible causal effect, we assessed learning in *Drosophila* after down-regulation or over-expression of *Rim* (the well-conserved orthologue of *RIMS1*) in the fat body. A significant decrease in CI after learning was observed in two different RNAi lines, but we did not observe significant differences in LI. However, when *Rim* was overexpressed (UAS-*Rim*) in the fat body, males were able to suppress courtship significantly better than the corresponding genetic background control flies, resulting in a significant increase in LI. These results suggest that flies with overexpression of *Rim* exclusively in the fat body increase their learning capability, resulting in better learning. Next, we used qPCR to show that *Rim* was uniquely expressed in the fat body, but not in the brain. The improvement in learning was exclusively due to the altered expression *Rim* in the fat body and not due to a "leak" of RNAi into the brain.

To elucidate the potential mechanisms underlying the overexpression of *Rim* in learning, we performed RNA-seq in the fat body and heads of overexpressed *Rim* flies. We identified the differentially expressed genes between the flies overexpressing *Rim* and the corresponding genetic backgrounds in the fat body and fly heads. In the fat body, enrichment analysis identified an over-representation of pathways involved in vitamin metabolism and lipid metabolism, including the hydrolysis of LPC and glutamate neurotransmitter release cycle,

consistent with our findings in humans. It also identified genes involved in other pathways involved in biological oxidations and cytochrome P450 (*Cyp4*)(*cyp4e1, cyp4ac2, cyp4ac3, cyp4p1, and cyp4p2*). Gene ontology (GO) enrichment analysis identified biological processes involved in neurotransmitter regulation, in particular the metabolism of biogenic amines (dopamine, serotonin and norepinephrine), which is highly consistent with our findings in humans. At the molecular level, we identified functions involved in monooxygenase and oxidoreductase activity. We also identified functions involved in PIP transfer and phospholipid transfer and transport. These results were replicated in the fly heads. We found an over-representation of pathways involved in lipid metabolism (phospholipids and hydrolysis of LPC), vitamins and biological oxidations. An analysis based only on up-regulated genes also identified changes in DNA metabolism, while a GO analysis identified molecular functions related to monooxygenase and oxidoreductase activity.

Oxidative damage and antioxidant depletion are associated with cognitive decline due to neurodegeneration [397]. Vitamins can act as potent antioxidant molecules, protecting neurons from oxidative stress and improving overall neuronal function [398]. Reducing oxidative stress in *Drosophila* has been associated with increased lifespan [399] and ameliorates age-related memory impairment [397]. Monooxygenase and oxidoreductase enzymes contribute to cellular levels of ROS, and members of the cytochrome P450 family have been found to be up-regulated in the presence of oxidative stress in *Drosophila*, with a detoxifying and antioxidant function [400]. Low-grade inflammation is associated with cellular oxidative imbalance and is one of the physiopathological mechanisms behind obesity-associated syndromes [401]. Phospholipids are abundant molecules in the *Drosophila* brain, where they play a role in cognition, both by providing energy for brain activity and by participating in membrane trafficking and neurotransmission [402]. Similar to mammals, the main source of phospholipids in *Drosophila* is LD within the fat body cells [403]. In *Drosophila*, phospholipid homeostasis has been shown to be important for the regulation of dendrite morphogenesis [404], and lipid imbalance is used as a target to protect against Aβ42-induced cytotoxicity in the AD fly model [405].

We have shown that overexpression of *Rim* uniquely in the *Drosophila* fat body is sufficient to promote an increase in learning, and that the effect of *Rim* overexpression in the fat body can mediate changes at the transcriptional level in the AT itself and in peripheral tissues such as the brain, modulating pathways associated with neuronal function, cellular oxidative balance and detoxification, and genes involved in phospholipid metabolism.

Taken together, these results suggest that changes in *Vmat* or *Rim* expression in the fat body mediate changes in gene expression in the brain via a putative fat body-to-brain axis. These findings suggest a systemic developmental program that changes in parallel in different tissues and cells, and is reflected in neuronal networks.

6.2 DOWNREGULATED ADIPOSE TISSUE EXPRESSION OF BROWNING GENES WITH INCREAESD ENVIRONMENTAL TEMPERATURES

Gene expression analysis of SAT were performed in a large cohort of 1070 participants (*Adipomit Cohort*) with and without obesity to investigate the possible effect of outdoor temperature on AT physiology and metabolic traits. Subjects were recruited in different regions of Spain, and the outdoor temperature was obtained closest to the place of residence of each individual (Table 5).

The study country, Spain, seems to be particularly suitable to show differences between the North, where BAT would be stimulated in winter (with average minimum temperatures below 10 ℃), and the South, with temperatures between 10 ℃ and 20 ℃. This has not observed in other countries where temperatures are uniformly low or high across territories. As expected, significant differences in environmental temperature across the year were observed, being highest in the Southern nodes (10.95 ℃ and 21.5 ℃; average of minimum and maximum temperature, respectively) compared to the Northern nodes (8.45 ℃ and 18.75 ℃; average of minimum and maximum temperature, respectively).

We found positive and significant associations between environmental temperature, obesity and related metabolic complications, such as BMI, Waist Circumference, Glucose or HbA1c as indicators of T2D, TG and ultrasensitive CRP. Impaired thermogenesis and reduced expression of thermogenesis-related genes are thought to contribute to the development of obesity [406]. In this study, we found inversely significant associations between environmental temperature and genes involved in browning, such as *UCP1*, *PR/SET domain 16 (PRDM16)* and *Cell death inducing DFFA like effector a (CIDEA1)* mRNA. We also found that environmental temperatures were negatively correlated with *ADIPOQ* gene expression, and with genes involved in adipogenesis (*PLIN1*, *Fatty acid synthase (FASN)* and *Solute carrier family 2 member 4 (SLC2A4)*), even when excluding subjects without obesity.

We then performed multivariate linear regression analyses, taking into account the variables associated with environmental temperatures in univariate comparisons. After controlling for age, gender, BMI, sample origin, glucose, TG, HDL-c and ultrasensitive CRP; confounders known to influence obesity, we found that each of the environmental temperatures studied (minimum, maximum and average) independently contributed to *ADIPOQ* mRNA variance.

When subjects without obesity were exclude from the analysis, the contribution of temperatures to *ADIPOQ* mRNA variance were maintained. We also found that minimum temperature contributed independently to adjusted *UCP1* mRNA variance in subjects with obesity; and maximum temperature contributed independently to adjusted *CIDEA1*, *C/EBPA* and *Nicotinamide N-methyltransferase (NNMT)* mRNA variance. All previous analyses were performed with the average, minimum or maximum of the measured temperature of the month in which the AT sample was obtained, but we also examined the temperature of the immediately preceding month of sample collection. Only the minimum temperature independently contributed to the *UCP1* mRNA variance in all subjects and in subjects with obesity.

When participants with T2D were excluded, the previous associations remained significant and additional associations emerged. Minimum temperature independently contributes to adjusted *UCP1* mRNA variance; and maximum temperature independently contributed to adjusted *PLIN1* mRNA, *PPARγ* mRNA and *NNMT* mRNA in the whole cohort and in subjects with obesity.

Given the significant and consistent associations with *ADIPOQ* gene expression and its known associations with healthy metabolic traits, we also analysed circulating adiponectin, which was negatively and significant associated with maximum and average temperature in the immediate previous month prior to tissue collection in all subjects and, with maximum temperature in subjects with obesity. *ADIPOQ* gene expression and circulating adiponectin levels are well known to be inversely associated with obesity [407,408]. ADIPOQ appears to play an important role in thermoregulation, given the findings observed in *Adipoq*[/-] mice under energy-deficient and cold-challenged conditions [409]. Experimental studies have identified adiponectin as a key efferent signal secreted by AT in response to adaptive thermogenesis [410]. The observed results suggest that adiponectin could be involved in thermogenic regulation in humans. *ADIPOQ* expression was inversely associated with all measured temperatures in all participants and in obese subjects.

When the results were stratified according to the season in which the AT samples were obtained, we found that in samples obtained in winter, *UCP1* gene expression was inversely correlated with the minimum environmental temperature in winter, suggesting that exposure to cold increases the expression of this browning marker in WAT, consistent with observations in a previous study with a small number of subjects (n=27) [411]. In subjects with obesity, the association of *UCP1* remained significant. *ADIPOQ* mRNA was negatively

associated with the minimum temperature in the month immediately preceding sample collection in summer. Mean *ADIPOQ* gene expression in samples collected in winter was significantly higher than in samples collected in summer, when the analysis was performed in all subjects and in participants with obesity.

When *UCP1* and *ADIPOQ* transcripts from obese subjects living in the South were compared with those living in the North, the differences were very marked, suggesting that lower temperatures could be a protective factor. This is in line with the results of a previous study in the same regions studied here, which found that increasing time spent in cold environments was associated with a lower prevalence of obesity in the North of Spain compared with the South [315]. In addition, the mean *ADIPOQ* gene expression was higher in subjects living in the North than in those living in the South; and the mean *ADIPOQ* gene expression in the North was also higher in the summer than in the South, in parallel with increased temperatures in the South.

Finally, we analysed the data applying a machine learning variable selection strategy based on multiple random forests as implemented in the Boruta algorithm to identify the most important outcome predictive variables. In line with previous analyses, BMI was independently predicted by environmental temperatures, in addition to several clinical variables, and the expression of genes associated with browning in all subjects as a whole and within subjects with obesity. Importantly, when *ADIPOQ* gene expression was considered the dependent variable, environmental temperatures and several thermogenic genes also contributed as predictive variables to the model, in addition to the adipogenic genes.

In subjects with obesity, given that their AT would play an insulating effect, the decrease in temperature would have a less marked impact and therefore would remain obese. It is possible that decreased environmental temperature in subjects without obesity could lead to increased thermogenesis thus preventing weight gain. In keeping with this hypothesis, previous studies have shown that subjects with obesity exhibited a lower response when exposed to cooling than those without obesity as assessed by heat loss [412]. It could be speculated that the expression of genes associated with browning might provide relevant information about optimal temperature to prevent obesity at individual/populations level.

6.3 GENERAL DISCUSSION

One of the major public health problems around the world is obesity [11]. Obesity is a multifactorial chronic disease [2] that nowadays has reached epidemic proportions [86]. The hallmark for the pathophysiology of obesity is based on energy homeostasis with an imbalance between energy intake and energy expenditure [7], characterised by an excessive peripheral accumulation of fat [9] that lacks of effective treatment and predisposes patients to a large number of adverse co-morbidities. Obesity is associated with an increased risk of cognitive impairment [156,249,251].

It is well known that the brain modulates AT performance, but recent observations in rodents show that AT also regulates brain function [223]. There is a growing awareness that peripheral tissues modulate brain function shaping different cognitive domains. Learning and memory, executive function and attention are the cognitive domains most affected in obese subjects [214], which are evaluated through neuropsychological tests.

In this thesis, we found expression of genes associated with axon guidance, nervous system development, neuronal system, tryptophan and inflammatory activity in human AT with cognition in three different cohorts. In addition, we also found the expression of the same genes in PBMC were also associated with cognitive traits. Demonstrating that although brain regulates performance of AT, reverse is also plausible.

Vitamins act as antioxidant molecules, protecting neurons from oxidative stress, reducing the generation of ROS and improving neuronal function [398]. In particular, retinoic acid, the active form of vitamin A, is essential for the regulation of synaptic plasticity in the brain involved in memory and learning [389] and AT modulates cognitive performance through vitamin A metabolism. Here, we found a negative association between RBP1 (retinol transporter) and plasma levels of retinoic acid.

Lipids are essential for brain function, specifically phospholipids are crucial for synaptic plasticity, neurotransmitters and memory [379]. Here, we also found that the expression of AT genes involved in phospholipid metabolism is associated with circulating phospholipids.

Among all the genes associated with cognition, the neurotransmitters release cluster (RIMS1 and SLC18A2) had the largest number of associations across cognitive domains. Therefore, we aim to demonstrate the causal effect of AT RIMS1 and SLC18A2 on cognition using preclinical models. In a mouse model, down-regulation of Slc18a2 in AT reverses HFD-

induced memory impairment. In a *Drosophila melanogaster* model, down-regulation of *Vmat* in the fat body improves STM and the expression of memory related genes. Whereas, overexpression of *Rim* in Drosophila fat body enhances learning abilities and the effect of this may mediate changes at the transcriptional level in fat body and brain, modulating pathways associated with lipid and vitamin metabolism, neuronal function, cellular oxidative balance and detoxification, consistent with results found in humans.

Given the increasing epidemiology and associated co-morbidities of obesity, there is a growing interest in understanding its aetiology [19]. It is well known that the aetiology of obesity appears to be an interplay between hereditary, environmental, physiological, behavioural, social and economic factors [23]. The environment is an important determinant of health and disease and plays a role in the development of obesity [32]. In recent decades, there has been an increase in the overall temperature of the Earth due to global warming [26,33,139].

Humans are endothermic, we are adapted to live in habitats subject to large temperature variations and keep a constant body temperature through thermoregulatory mechanisms [285]. Cold affects the ability to maintain energy balance by increasing thermogenesis and is also a potent inducer of beige adipocytes. Cold is known to be a protective factor against weight gain. Due to the rising global temperatures, thermogenesis is decreasing and obesity is increasing.

In the present work, we found a positive association between environmental temperatures and obesity, and a negative association between environmental temperatures and genes involved in browning and with *ADIPOQ*, confirming previous studies which found that *ADIPOQ* is associated with healthy metabolic traits and inversely associated with obesity [407,408].

Specifically, in winter samples, *UCP1* gene expression, a browning marker, was inversely correlated with minimum environmental temperature, suggesting that exposure to cold increases the expression of this browning marker in WAT. This is consistent with previous findings [411].

Whether *UCP1* and *ADIPOQ* were compared between warm and cold regions, the differences were very marked, reinforcing the protective factor of cold temperatures found in a previous study in the same regions as our results, when they concluded that increasing

time spent in cold environments was associated with a lower prevalence of obesity in the North of Spain (colder) compared with the South (warmer) [315].

If the outdoor temperature changes by even 1 ºC due to increased global warming, a process of acclimatisation begins that, if prolonged, activates pathways linked to neurodegeneration (oxidative stress, excitotoxicity and neuroinflammation). A 1.5 ºC increase in mean ambient temperature correlates with an increased risk of dementia-related hospital admissions. Exposure to heat stress induces changes in the CNS with long-term neuropathological consequences and effects on neuronal cell degeneration. Chronic heat stress, mainly due to global warming, is critical for the development of neurodegenerative disorders. In humans, environmental hyperthermia (50 ºC) impairs functional connectivity of the brain, alters in cognitive and work performance and short-term visual memory [285].

In summary, the global rise in temperatures in recent decades could be one factor that, together with others, could be linked to the increase of the obesity epidemic worldwide, which in turn obesity can ameliorate the neurological symptoms of pre-existing neurological disorders. It could be speculated, and future research is needed, that temperatures could also ameliorate cognitive disorders.

However, there are some limitations to this work that need to be highlighted.

In the transcriptomics analyses on AT associated with cognitive domains, we focused only on morbidly obese subjects (BMI > 35 kg/m^2); therefore, our results may not be generalisable to other populations. The findings should be confirmed in longitudinal, larger samples of subjects, to generalise these results to the general population.

When we examined the effects of outdoor temperatures on the expression of several genes, we used the mean outdoor temperatures at the meteorological station closest to each study participant's residence. Indoor temperatures where the participants lived or worked were not controlled for. The complexities of measuring indoor temperature exposure have been reviewed in previous articles [308] and are likely to remain a barrier to accessing robust exposure data. It is also important to note that we focused only on outdoor temperature, but other metrics such as humidity and air velocity, and therefore thermal sensation, were not included in this study. However, there is strong evidence linking high environmental temperatures and outdoor meteorological data to general morbidity and mortality [286].

Dietary patterns and physical activity are known to contribute to the development of obesity [2,26] however, these data were not collected in the large *Adipomit* cohort and data analysis was not standardised or adjusted for these parameters.

Finally, there is a huge complexity in obtaining AT samples in the same patient in two different seasons during the same year, which is why the study lacks a case-control element.

7. CONCLUSIONS

1. The expression of genes associated with axon guidance, nervous system development, neuronal system, tryptophan, and inflammatory activity in human AT were all associated with cognition in three different cohorts of subjects.

2. The expression of genes in PBMCs that were most strongly associated with cognition in AT were also associated with cognitive traits in a large cohort of subjects.

3. Specific down-regulation of genes in the fat body modulates learning, suggesting a direct effect on cognition that is uniquely dependent on their expression and/or function in the fat body.

4. Down-regulation of *Slc18a2/Vmat* in AT of mice reversed the memory impairment induced by HFD.

5. Flies with down-regulation of Vmat in fat body had better STM compared to flies without Vmat down-regulation.

6. Expression of *Rim* uniquely in the *Drosophila* fat body is sufficient to promote an increase in learning, and the effect of that can mediate changes at transcriptional level in the AT itself and in peripheral tissues such as brain, modulating pathways associated with neuronal function, cellular oxidative balance and detoxification, and genes involved in phospholipid metabolism.

7. AT expression of genes involved in thermogenic regulation is negatively associated with environmental temperatures and metabolic traits, being more marked in winter and when excluding T2D.

8. REFERENCES

1. Purnell, J. Q. Definitions, Classification, and Epidemiology of Obesity. MDText.com, Inc (2000).

2. Hruby, A. & Hu, F. B. The Epidemiology of Obesity: A Big Picture. *PharmacoEconomics* 33, 673–689 (2015).

3. Sung, H. *et al.* Global patterns in excess body weight and the associated cancer burden. *CA Cancer J Clin* 69, 88–112 (2019).

4. World Health Organization, WHO; Regional office for Europe. Obesity, data and statistics [Internet]. *Geneva, Switzerland: WHO* https://www.euro.who.int/en/health-topics/noncommunicablediseases/ obesity/data-and-statistics (2021).

5. Engin, A. The definition and prevalence of obesity and metabolic syndrome. in *Advances in Experimental Medicine and Biology* 960, 1–17 (Springer New York LLC, 2017).

6. Schwartz, M. W. *et al.* Obesity pathogenesis: An endocrine society scientific statement. *Endocr Rev* 38, 267–296 (2017).

7. Morton, G. J., Cummings, D. E., Baskin, D. G., Barsh, G. S. & Schwartz, M. W. Central nervous system control of food intake and body weight. *Nature* 443, 289–295 (2006).

8. Morton, G. J., Meek, T. H. & Schwartz, M. W. Neurobiology of food intake in health and disease. *Nature Reviews Neuroscience* 15, 367–378 (2014).

9. De Lorenzo, A. *et al.* Obesity: A preventable, treatable, but relapsing disease. *Nutrition* 71:110615 (2020).

10. Malone, J. I. & Hansen, B. C. Does obesity cause type 2 diabetes mellitus (T2DM)? Or is it the opposite? *Pediatric Diabetes* 20, 5–9 (2019).

11. Chooi, Y. C., Ding, C. & Magkos, F. The epidemiology of obesity. *Metabolism* 92, 6–10 (2019).

12. Longo, M. *et al.* Adipose tissue dysfunction as determinant of obesity-associated metabolic complications. *Int J Mol Sci* 20:2358, (2019).

13. Yazıcı, D. & Sezer, H. Insulin resistance, obesity and lipotoxicity. in *Advances in Experimental Medicine and Biology* 960, 277–304 (Springer New York LLC, 2017).

14. Rosen, E. D. & Spiegelman, B. M. What we talk about when we talk about fat. *Cell* 156, 20–44 (2014).

15. Muir, L. A. *et al.* Adipose tissue fibrosis, hypertrophy, and hyperplasia: Correlations with diabetes in human obesity. *Obesity* 24, 597–605 (2016).

16. Jo, J. *et al.* Hypertrophy and/or hyperplasia: Dynamics of adipose tissue growth. *PLoS Comput Biol* 5:e1000324 (2009).

17.   Arner, E. *et al.* Adipocyte turnover: Relevance to human adipose tissue morphology. *Diabetes* 59, 105–109 (2010).

18.   Ghaben, A. L. & Scherer, P. E. Adipogenesis and metabolic health. *Nature Reviews Molecular Cell Biology* 20, 242–258 (2019).

19.   Paradis, A. M., Godin, G., Pérusse, L. & Vohl, M. C. Associations between dietary patterns and obesity phenotypes. *Int J Obes* 33, 1419–1426 (2009).

20.   Apovian, C. M. Obesity: Definition, Comorbidities, Causes, and Burden. *Am J Manag Care* 22:s176–85 (2014).

21.   Bhupathiraju, S. N. & Hu, F. B. Epidemiology of obesity and diabetes and their cardiovascular complications. *Circ Res* 118, 1723–1735 (2016).

22.   Fall, T., Mendelson, M. & Speliotes, E. K. Recent Advances in Human Genetics and Epigenetics of Adiposity: Pathway to Precision Medicine? *Gastroenterology* 152, 1695–1706 (2017).

23.   Blüher, M. Metabolically Healthy Obesity. *Endocr Rev* 4:bnaa004 (2020).

24.   Locke, A. E. *et al.* Genetic studies of body mass index yield new insights for obesity biology. *Nature* 518, 197–206 (2015).

25.   Berthoud, H. R., Münzberg, H. & Morrison, C. D. Blaming the Brain for Obesity: Integration of Hedonic and Homeostatic Mechanisms. *Gastroenterology* 152, 1728–1738 (2017).

26.   Qureshi, S. A., Straiton, M. & Gele, A. A. Associations of socio-demographic factors with adiposity among immigrants in Norway: A secondary data analysis. *BMC Public Health* 20:772 (2020).

27.   Montague, C. T. *et al.* Congenital leptin deficiency is associated with severe early-onset obesity in humans. *Nature* 387, 903–908 (1997).

28.   Clément, K. *et al.* A Mutation in the Human Leptin Receptor Gene Causes Obesity and Pituitary Dysfunction. *Nature* 392, 398–401 (1998).

29.   Yeo, G. S. *et al.* A frameshift mutation in MC4R associated with dominantly inherited human obesity. *Nat Genet* 20, 111–2 (1998).

30.   Vaisse, C., Clement, K., Guy-Grand, B., Froguel, P. A frameshift mutation in human MC4R is associated with a dominant form of obesity. *Nat Genet* 20, 113–114 (1998).

31.   Ling, C. & Rönn, T. Epigenetics in Human Obesity and Type 2 Diabetes. *Cell Metabolism.* 29, 1028–1044 (2019).

32. Lecube, A. *et al.* Prevención, diagnóstico y tratamiento de la obesidad. Posicionamiento de la Sociedad Española para el Estudio de la Obesidad de 2016. *Endocrinol Diabetes Nutr* 64, 15–22 (2017).

33. An, R., Ji, M. & Zhang, S. Global warming and obesity: a systematic review. *Obesity Reviews.* 19, 150–163 (2018).

34. Bäckhed, F. *et al.* The Gut Microbiota as an Environmental Factor That Regulates Fat Storage. *Proc Natl Acad Sci USA* 44, 15718–15723 (2004).

35. Ley, R. E. *et al.* Obesity Alters Gut Microbial Ecology. *Proc Natl Acad Sci USA* 31, 11070–11075 (2005).

36. Heindel, J. J., Newbold, R. & Schug, T. T. Endocrine disruptors and obesity. *Nature Reviews Endocrinology.* 11, 653–661 (2015).

37. Lopez-Minguez, J., Gómez-Abellán, P. & Garaulet, M. Circadian rhythms, food timing and obesity. in *Proceedings of the Nutrition Society.* 75, 501–511 (Cambridge University Press, 2016).

38. Martínez-González, M. A., Martínez, A., Hu, F. B., Gibney, M. J. & Kearney, J. Physical Inactivity, Sedentary Lifestyle and Obesity in the European Union. *Int J Obes Relat Metab disord* 23, 1192–1201 (1999) jo.

39. Razzoli, M., Pearson, C., Crow, S. & Bartolomucci, A. Stress, overeating, and obesity: Insights from human studies and preclinical models. *Neuroscience and Biobehavioral Reviews.* 76 ,154–162 (2017).

40. St-Onge, M. P. Sleep–obesity relation: underlying mechanisms and consequences for treatment. *Obesity Reviews.* 18, 34–39 (2017).

41. Eckel, R. H. *et al.* Prevention conference VII: Obesity, a worldwide epidemic related to heart disease and stroke executive summary. in *Circulation.* 110 2968–2975 (2004).

42. Studies Collaboration, P. Body-mass index and cause-specific mortality in 900 000 adults: collaborative analyses of 57 prospective studies. *Lancet* 373, 1083–1096 (2009).

43. Grundy, S. M. *et al.* Diagnosis and management of the metabolic syndrome: An American Heart Association/National Heart, Lung, and Blood Institute scientific statement. *Circulation.* 112, 2735–2752 (2005).

44. Franssen, R., Monajemi, H., Stroes, E. S. G. & Kastelein, J. J. P. Obesity and Dyslipidemia. *Endocrinology and Metabolism Clinics of North America.* 37, 623–633 (2008).

45. Bray, G. A., Kim, K. K. & Wilding, J. P. H. Obesity: a chronic relapsing progressive disease process. A position statement of the World Obesity Federation. *Obesity Reviews* 18, 715–723 (2017).

46. Rohm, T. V., Meier, D. T., Olefsky, J. M. & Donath, M. Y. Inflammation in obesity, diabetes, and related disorders. *Immunity.* 55, 31–55 (2022).

47. Thomsen, M. & Nordestgaard, B. G. Myocardial infarction and ischemic heart disease in overweight and obesity with and without metabolic Syndrome. *JAMA Intern Med* 174, 15–22 (2014).

48. Kernan, W. N., Inzucchi, S. E., Sawan, C., MacKo, R. F. & Furie, K. L. Obesity: A stubbornly obvious target for stroke prevention. *Stroke.* 44, 278–286 (2013).

49. Rauch, U. *et al.* Thrombus formation on atherosclerotic plaques: pathogenesis and clinical consequences. *Ann Intern Med* 134, 224–38 (2001).

50. Camilleri, M., Malhi, H. & Acosta, A. Gastrointestinal Complications of Obesity. *Gastroenterology* 152, 1656–1670 (2017).

51. Pereira-Santos, M., Costa, P. R. F., Assis, A. M. O., Santos, C. A. S. T. & Santos, D. B. Obesity and vitamin D deficiency: A systematic review and meta-analysis. *Obesity Reviews* 16, 341–349 (2015).

52. Astrup, A. & Bügel, S. Overfed but undernourished: recognizing nutritional inadequacies/deficiencies in patients with overweight or obesity. *International Journal of Obesity.* 43, 219–232 (2019).

53. de Luis, D. A. *et al.* Effect of a hypocaloric diet in transaminases in nonalcoholic fatty liver disease and obese patients, relation with insulin resistance. *Diabetes Res Clin Pract* 79, 74–78 (2008).

54. Sheka, A. C. *et al.* Nonalcoholic Steatohepatitis: A Review. *JAMA* 323, 1175–1183 (2020).

55. O'Brien, P. D., Hinder, L. M., Callaghan, B. C. & Feldman, E. L. Neurological consequences of obesity. *The Lancet Neurology.* 16, 465–477 (2017).

56. Biessels, G. J. & Reagan, L. P. Hippocampal insulin resistance and cognitive dysfunction. *Nat Rev Neurosci* 16, 660–71 (2015).

57. Simó, R., Ciudin, A., Simó-Servat, O. & Hernández, C. Cognitive impairment and dementia: a new emerging complication of type 2 diabetes-The diabetologist's perspective. *Acta Diabetol* 54, 417–424 (2017).

58. Profenno, L. A., Porsteinsson, A. P. & Faraone, S. V. Meta-analysis of Alzheimer's disease risk with obesity, diabetes, and related disorders. *Biol Psychiatry* 67, 505–12 (2010).

59. Ebbeling, C. B., Pawlak, D. B. & Ludwig, D. S. Childhood obesity: public-health crisis, common sense cure. *Lancet* 360, 473–82 (2002).

60. Petry, N. M., Barry, D., Pietrzak, R. H. & Wagner, J. A. Overweight and obesity are associated with psychiatric disorders: Results from the national epidemiologic survey on alcohol and related conditions. *Psychosom Med* 70, 288–297 (2008).

61. Stunkard, A. J. Eating disorders and obesity. *Psychiatric Clinics of North America.* 34, 765–771 (2011).

62. Drager, L. F., Togeiro, S. M., Polotsky, V. Y. & Lorenzi-Filho, G. Obstructive sleep apnea: A cardiometabolic risk in obesity and the metabolic syndrome. *Journal of the American College of Cardiology.* 62, 569–576 (2013).

63. Somers, V. K. *et al.* Sleep Apnea and Cardiovascular Disease. An American Heart Association/American College of Cardiology Foundation Scientific Statement From the American Heart Association Council for High Blood Pressure Research Professional Education Committee, Council on Clinical Cardiology, Stroke Council, and Council on Cardiovascular Nursing In Collaboration With the National Heart, Lung. *Journal of the American College of Cardiology.* 52, 686–717 (2008).

64. Calle, E. E., Rodriguez, C., Walker-Thurmond, K. & Thun, M. J. Overweight, Obesity, and Mortality from Cancer in a Prospectively Studied Cohort of U.S. Adults. N *Engl J Med.* 17, 1625–1638 (2003).

65. Calle, E. E. & Kaaks, R. Overweight, obesity and cancer: Epidemiological evidence and proposed mechanisms. *Nature Reviews Cancer.* 4, 579–591 (2004).

66. Park, J., Morley, T. S., Kim, M., Clegg, D. J. & Scherer, P. E. Obesity and cancer - Mechanisms underlying tumour progression and recurrence. *Nature Reviews Endocrinology.* 10, 455–465 (2014).

67. Guh, D. P. *et al.* The incidence of co-morbidities related to obesity and overweight: A systematic review and meta-analysis. *BMC Public Health* 9:88 (2009).

68. Weaver, J. U. Classical Endocrine Diseases Causing Obesity. *Front Horm Res* 36, 212–228 (2008).

69. Joham, A. E., Palomba, S. & Hart, R. Polycystic Ovary Syndrome, Obesity, and Pregnancy. *Semin Reprod Med* 34, 93–101 (2016).

70. Lainez, N. M. & Coss, D. Obesity, Neuroinflammation, and Reproductive Function. *Endocrinology (United States).* 160, 2719–2736 (2019).

71. Bliddal, H., Leeds, A. R. & Christensen, R. Osteoarthritis, obesity and weight loss: Evidence, hypotheses and horizons - a scoping review. *Obesity Reviews* 15, 578–586 (2014).

72.   Hirt, P. A., Castillo, D. E., Yosipovitch, G. & Keri, J. E. Skin changes in the obese patient. *Journal of the American Academy of Dermatology*. 81 1037–1057 (2019).

73.   Borga, M. *et al.* Advanced body composition assessment: From body mass index to body composition profiling. *Journal of Investigative Medicine*. 66, 887–895 (2018).

74.   Mechanick, J. I., Hurley, D. L. & Garvey, W. T. Adiposity-based chronic disease as a new diagnostic term: The American association of clinical endocrinologists and American college of endocrinology position statement. *Endocrine Practice* 23, 372–378 (2017).

75.   Sahakyan, K. R. *et al.* Normal-weight central obesity: Implications for total and cardiovascular mortality. *Ann Intern Med* 163, 827–835 (2015).

76.   Mayoral, L. P.-C. *et al.* Obesity subtypes, related biomarkers & heterogeneity. *Indian J Med Res* 151, 11–21 (2020).

77.   Frühbeck, G. *et al.* The ABCD of obesity: An EASO position statement on a diagnostic term with clinical and scientific implications. *Obes Facts* 12, 131–136 (2019).

78.   Perona, J. S. *et al.* Waist Circumference and Abdominal Volume Index Can Predict Metabolic Syndrome in Adolescents, but only When the Criteria of the International Diabetes Federation are Employed for the Diagnosis. *Nutrients* 11:1370 (2019).

79.   Grundy, S. M. Obesity, metabolic syndrome, and cardiovascular disease. in *Journal of Clinical Endocrinology and Metabolism*. 89 2595–2600 (2004).

80.   Lin, X. & Li, H. Obesity: Epidemiology, Pathophysiology, and Therapeutics. *Frontiers in Endocrinology*. 12:706978 (2021).

81.   Schwartz, A. & Doucet, E. Relative changes in resting energy expenditure during weight loss: a systematic review. *Obes Rev* 11, 531–47 (2010).

82.   Bray, G. A., Frühbeck, G., Ryan, D. H. & Wilding, J. P. Management of obesity. *Lancet*. 10031, 1947–1956 (2016).

83.   Semlitsch, T., Stigler, F. L., Jeitler, K., Horvath, K. & Siebenhofer, A. Management of overweight and obesity in primary care—A systematic overview of international evidence-based guidelines. *Obesity Reviews*. 20, 1218–1230 (2019).

84.   Ballesteros Pomar, M. D. *et al.* The SEEN Comprehensive Clinical Survey of Adult Obesity: Executive Summary. *Endocrinol Diabetes Nutr (Engl Ed)*. 2, 130–136 (2020).

85.   Sjöström, L. *et al.* Effects of bariatric surgery on mortality in Swedish obese subjects. *N Engl J Med*. 8, 741–752 (2007).

86.   Afshin, A. *et al.* Health Effects of Overweight and Obesity in 195 Countries over 25 Years. GBD 2015 Obesity Collaborators. *N Engl J Med* 377, 13–27 (2017).

87. Hotamisligil, G. S. Inflammation and metabolic disorders. *Nature.* 444, 860–867 (2006).

88. Tremmel, M., Gerdtham, U. G., Nilsson, P. M. & Saha, S. Economic burden of obesity: A systematic literature review. *International Journal of Environmental Research and Public Health.* 14:435 (2017).

89. Bhaskaran, K., dos-Santos-Silva, I., Leon, D. A., Douglas, I. J. & Smeeth, L. Association of BMI with overall and cause-specific mortality: a population-based cohort study of 3·6 million adults in the UK. *Lancet Diabetes Endocrinol* 6, 944–953 (2018).

90. Finkelstein, E. A., Trogdon, J. G., Cohen, J. W. & Dietz, W. Annual medical spending attributable to obesity: Payer-and service-specific estimates. *Health Aff.* 28, 822–831 (2009).

91. Lafontan, M. & Langin, D. Lipolysis and lipid mobilization in human adipose tissue. *Progress in Lipid Research.* 48, 275–297 (2009).

92. Lee, B., Lee, M., Lefevre, M. & Kim, H. R. Anthocyanins Inhibit Lipogenesis During Adipocyte Differentiation of 3T3-L1 Preadipocytes. *Plant Foods for Human Nutrition* 69, 137–141 (2014).

93. Lumish, H. S., O'Reilly, M. & Reilly, M. P. Sex Differences in Genomic Drivers of Adipose Distribution and Related Cardiometabolic Disorders: Opportunities for Precision Medicine. *Arteriosclerosis, Thrombosis, and Vascular Biology.* 40, 45–60 (2020).

94. Carroll, J. F. *et al.* Visceral fat, waist circumference, and BMI: Impact of race/ethnicity. *Obesity* 16, 600–607 (2008).

95. Bora, P. & Majumdar, A. S. Adipose tissue-derived stromal vascular fraction in regenerative medicine: A brief review on biology and translation. *Stem Cell Research and Therapy.* 8:145 (2017).

96. Antonopoulos, A. S. *et al.* Reciprocal effects of systemic inflammation and brain natriuretic peptide on adiponectin biosynthesis in adipose tissue of patients with ischemic heart disease. *Arterioscler Thromb Vasc Biol* 34, 2151–9 (2014).

97. Lee, M. J., Wu, Y. & Fried, S. K. Adipose tissue heterogeneity: Implication of depot differences in adipose tissue for obesity complications. *Molecular Aspects of Medicine.* 34, 1–11 (2013).

98. Trayhurn, P. & Beattie, J. H. Physiological role of adipose tissue: white adipose tissue as an endocrine and secretory organ. *Proceedings of the Nutrition Society* 60, 329–339 (2001).

99. Wu, J. *et al.* Beige adipocytes are a distinct type of thermogenic fat cell in mouse and human. *Cell* 150, 366–376 (2012).

100. Wang, W. & Seale, P. Control of brown and beige fat development. *Nature Reviews Molecular Cell Biology.* 17, 691–702 (2016).

101. Sarjeant, K. & Stephens, J. M. Adipogenesis. *Cold Spring Harb Perspect Biol* 4, (2012).

102. Berry, D. C., Stenesen, D., Zeve, D. & Graff, J. M. The developmental origins of adipose tissue. *Development* 140, 3939–49 (2013).

103. Timmons, J. A. *et al.* Myogenic Gene Expression Signature Establishes That Brown and White Adipocytes Originate from Distinct Cell Lineages. *Proc Ntal Acad Sci USA.* 11, 44501–4406 (2007).

104. Majka, S. M., Barak, Y. & Klemm, D. J. Concise review: Adipocyte origins: Weighing the possibilities. *Stem Cells.* 29, 1034–1040 (2011).

105. Harwood, H. J. The adipocyte as an endocrine organ in the regulation of metabolic homeostasis. *Neuropharmacology.* 63, 57–75 (2012).

106. Macotela, Y., Boucher, J., Tran, T. T. & Kahn, C. R. Sex and depot differences in adipocyte insulin sensitivity and glucose. *Diabetes* 58, 803–812 (2009).

107. Schoettl, T., Fischer, I. P. & Ussar, S. Heterogeneity of adipose tissue in development and metabolic function. *Journal of Experimental Biology.* 121:jeb162958 (2018).

108. Betz, M. J. & Enerbäck, S. Human brown adipose tissue: What we have learned so far. *Diabetes* 64, 2352–2360 (2015).

109. Scheja, L. & Heeren, J. The endocrine function of adipose tissues in health and cardiometabolic disease. *Nature Reviews Endocrinology.* 15, 507–524 (2019).

110. Kahn, C. R., Wang, G. & Lee, K. Y. Altered adipose tissue and adipocyte function in the pathogenesis of metabolic syndrome. *Journal of Clinical Investigation.* 129, 3990–4000 (2019).

111. Zwick, R. K., Guerrero-Juarez, C. F., Horsley, V. & Plikus, M. V. Anatomical, Physiological, and Functional Diversity of Adipose Tissue. *Cell Metabolism.* 27, 68–83 (2018).

112. Tchkonia, T. *et al.* Mechanisms and metabolic implications of regional differences among fat depots. *Cell Metabolism.* 17, 644–656 (2013).

113. Karastergiou, K. & Fried, S. K. Cellular mechanisms driving sex differences in adipose tissue biology and body shape in humans and mouse models. in *Advances in Experimental Medicine and Biology.* 1043, 29–51 (Springer New York LLC, 2017).

114. Wang, Q. A., Tao, C., Gupta, R. K. & Scherer, P. E. Tracking adipogenesis during white adipose tissue development, expansion and regeneration. *Nat Med* 19, 1338–1344 (2013).

115. Zhang, M., Hu, T., Zhang, S. & Zhou, L. Associations of Different Adipose Tissue Depots with Insulin Resistance: A Systematic Review and Meta-analysis of Observational Studies. *Sci Rep* 5, 18495 (2015).

116. Cawthorn, W. P. *et al.* Bone marrow adipose tissue is an endocrine organ that contributes to increased circulating adiponectin during caloric restriction. *Cell Metab* 20, 368–375 (2014).

117. Cypess, A. M. Reassessing Human Adipose Tissue. *N Engl J Med* 386, 768–779 (2022).

118. Morigny, P., Boucher, J., Arner, P. & Langin, D. Lipid and glucose metabolism in white adipocytes: pathways, dysfunction and therapeutics. *Nature Reviews Endocrinology.* 17, 276–295 (2021).

119. Grabner, G. F., Xie, H., Schweiger, M. & Zechner, R. Lipolysis: cellular mechanisms for lipid mobilization from fat stores. *Nat Metab* 3, 1445–1465 (2021).

120. Richard, A. J., White, U., Elks, C. M. & Stephens, J. M. Adipose Tissue: Physiology to Metabolic Dysfunction. MDText.com, Inc (2000).

121. Song, Z., Xiaoli, A. M. & Yang, F. Regulation and metabolic significance of De Novo lipogenesis in adipose tissues. *Nutrients.* 10:1383 (2018).

122. Seo, T. *et al.* Lipoprotein lipase-mediated selective uptake from low density lipoprotein requires cell surface proteoglycans and is independent of scavenger receptor class B type 1. *Journal of Biological Chemistry* 275, 30355–30362 (2000).

123. Harris, C. A. *et al.* DGAT enzymes are required for triacylglycerol synthesis and lipid droplets in adipocytes. *J Lipid Res* 52, 657–667 (2011).

124. Luo, L. & Liu, M. Adipose tissue in control of metabolism. *Journal of Endocrinology.* 231, R77–R99 (2016).

125. Chouchani, E. T. & Kajimura, S. Metabolic adaptation and maladaptation in adipose tissue. *Nature Metabolism.* 1, 189–200 (2019).

126. Kojta, I., Chacińska, M. & Błachnio-Zabielska, A. Obesity, bioactive lipids, and adipose tissue inflammation in insulin resistance. *Nutrients.* 12: 1305 (2020).

127. Braun, K., Oeckl, J., Westermeier, J., Li, Y. & Klingenspor, M. Non-adrenergic control of lipolysis and thermogenesis in adipose tissues. *Journal of Experimental Biology.* 121, jeb165381 (2018).

128. Lafontan, M. *et al.* Adrenergic Regulation of Adipocyte Metabolism. *Hum Reprod.* 12, 6–20 (16997).

129. Jaworski, K., Sarkadi-Nagy, E., Duncan, R. E., Ahmadian, M. & Sul, H. S. Regulation of Triglyceride Metabolism. IV. Hormonal regulation of lipolysis in adipose tissue. *Am J Physiol Gastrointest Liver Physiol* 293, G1–4 (2007).

130. Frühbeck, G., Méndez-Giménez, L., Fernández-Formoso, J. A., Fernández, S. & Rodríguez, A. Regulation of adipocyte lipolysis. *Nutr Res Rev* 27, 63–93 (2014).

131. Lehr, S., Hartwig, S. & Sell, H. Adipokines: a treasure trove for the discovery of biomarkers for metabolic disorders. *Proteomics Clin Appl* 6, 91–101 (2012).

132. Turer, A. T. & Scherer, P. E. Adiponectin: mechanistic insights and clinical implications. *Diabetologia* 55, 2319–26 (2012).

133. Blüher, M. Clinical relevance of adipokines. *Diabetes Metab J* 36, 317–27 (2012).

134. Hajer, G. R., van Haeften, T. W. & Visseren, F. L. J. Adipose tissue dysfunction in obesity, diabetes, and vascular diseases. *Eur Heart J* 29, 2959–71 (2008).

135. Fasshauer, M. & Blüher, M. Adipokines in health and disease. *Trends in Pharmacological Sciences.* 36 461–470 (2015).

136. Hauner, H. Secretory factors from human adipose tissue and their functional role. *Proceedings of the Nutrition Society* 64, 163–169 (2005).

137. Blüher, M. Adipose tissue dysfunction contributes to obesity related metabolic diseases. *Best Practice and Research: Clinical Endocrinology and Metabolism.* 27 163–177 (2013).

138. Berson Award Lecture Mantzoros, S. *et al.* Leptin in human physiology and pathophysiology. *Am J Physiol Endocrinol Metab* 301, 567–584 (2011).

139. Ahima, R. S. Global warming threatens human thermoregulation and survival. *Journal of Clinical Investigation.* 130 559–561 (2020).

140. Denroche, H. C., Huynh, F. K. & Kieffer, T. J. The role of leptin in glucose homeostasis. *J Diabetes Investig* 3, 115–29 (2012).

141. Scherer, P. E. Adipose tissue: From lipid storage compartment to endocrine organ. in *Diabetes.* 55, 1537–1545 (2006).

142. Galic, S., Oakhill, J. S. & Steinberg, G. R. Adipose tissue as an endocrine organ. *Molecular and Cellular Endocrinology.* 316, 129–139 (2010).

143. Kadowaki, T. & Yamauchi, T. Adiponectin and adiponectin receptors. *Endocr Rev* 26, 439–51 (2005).

144. Larsen, C. M. *et al.* Interleukin-1-Receptor Antagonist in Type 2 Diabetes Mellitus. *N Engl J Med.* 356, 1517–1526 (2007).

145. Tack, C. J., Stienstra, R., Joosten, L. A. B. & Netea, M. G. Inflammation Links Excess Fat to Insulin Resistance: The Role of the Interleukin-1 Family. *Immunol Rev.* 1, 239–252 (2012).

146. Hotamisligil, G. S. The role of TNFα and TNF receptors in obesity and insulin resistance. in *Journal of Internal Medicine.* 245, 621–625 (1999).

147. Cypess, A. M. & Kahn, C. R. The role and importance of brown adipose tissue in energy homeostasis. *Current Opinion in Pediatrics.* 22, 478–484 (2010).

148. Nedergaard, J., Bengtsson, T. & Cannon, B. Unexpected evidence for active brown adipose tissue in adult humans. *Am J Physiol Endocrinol Metab* 293, 444–452 (2007).

149. Shabalina, I. G. *et al.* UCP1 in Brite/Beige adipose tissue mitochondria is functionally thermogenic. *Cell Rep* 5, 1196–1203 (2013).

150. Rosenwald, M. & Wolfrum, C. The origin and definition of brite versus white and classical brown adipocytes. *Adipocyte* 3, 4–9 (2014).

151. Sharp, L. Z. *et al.* Human BAT Possesses Molecular Signatures That Resemble Beige/Brite Cells. *PLoS One* 7:e49452(2012).

152. Kaisanlahti, A. & Glumoff, T. Browning of white fat: agents and implications for beige adipose tissue to type 2 diabetes. *Journal of Physiology and Biochemistry.* 75, 1–10 (2019).

153. Scherer, P. E. The many secret lives of adipocytes: implications for diabetes. *Diabetologia.* 62, 223–232 (2019).

154. Omran, F. & Christian, M. Inflammatory Signaling and Brown Fat Activity. *Frontiers in Endocrinology.* 11:156 (2020).

155. Park, J. *et al.* Progenitor-like characteristics in a subgroup of UCP1+ cells within white adipose tissue. *Dev Cell* 56, 985-999.e4 (2021).

156. Tang, Q. Q. & Lane, M. D. Adipogenesis: From stem cell to adipocyte. *Annu Rev Biochem* 81, 715–736 (2012).

157. Bateman, M. E., Strong, A. L., McLachlan, J. A., Burow, M. E. & Bunnell, B. A. The effects of endocrine disruptors on adipogenesis and osteogenesis in mesenchymal stem cells: A review. *Frontiers in Endocrinology.* 7:171 (2017).

158. Hammarstedt, A., Gogg, S., Hedjazifar, S., Nerstedt, A. & Smith, U. Impaired Adipogenesis and Dysfunctional Adipose Tissue in Human Hypertrophic Obesity. *Physiol Rev* 98, 1911–1941 (2018).

159. Blüher, M. Adipose tissue dysfunction in obesity. *Experimental and Clinical Endocrinology and Diabetes*. 117, 241–250 (2009).

160. Van Gaal, L. F., Mertens, I. L. & De Block, C. E. Mechanisms linking obesity with cardiovascular disease. *Nature*. 444, 875–880 (2006).

161. Bays, H. E. Adiposopathy: Is 'sick fat' a cardiovascular disease? *Journal of the American College of Cardiology*. 57, 2461–2473 (2011).

162. Bays, H. E. Adiposopathy, diabetes mellitus, and primary prevention of atherosclerotic coronary artery disease: Treating 'sick fat' through improving fat function with antidiabetes therapies. *American Journal of Cardiology* 110, 4B-12B (2012).

163. Tan, C. Y. & Vidal-Puig, A. Adipose tissue expandability: The metabolic problems of obesity may arise from the inability to become more obese. in *Biochemical Society Transactions*. 36, 935–940 (2008).

164. Gealekman, O. *et al.* Depot-specific differences and insufficient subcutaneous adipose tissue angiogenesis in human obesity. *Circulation* 123, 186–194 (2011).

165. Virtue, S. & Vidal-Puig, A. It's not how fat you are, it's what you do with it that counts. *PLoS Biology*. 6, 1819–1823 (2008).

166. Kabir, M. *et al.* Molecular evidence supporting the portal theory: a causative link between visceral adiposity and hepatic insulin resistance. *Am J Physiol Endocrinol Metab* 288, 454–461 (2005).

167. Alligier, M. *et al.* Visceral fat accumulation during lipid overfeeding is elated to subcutaneous adipose tissue characteristics in healthy men. *Journal of Clinical Endocrinology and Metabolism* 98, 802–810 (2013).

168. Klöting, N. *et al.* Insulin-sensitive obesity. *Am J Physiol Endocrinol Metab* 299, 506–515 (2010).

169. Brakenhielm, E. & Cao, Y. Angiogenesis in adipose tissue. *Methods Mol Biol* 456, 65–81 (2008).

170. Rupnick, M. A. *et al.* Adipose Tissue Mass Can Be Regulated through the Vasculature. *Proc Natl Acad Sci USA*. 16, 10730–10735 (2002).

171. Després, J. P. & Lemieux, I. Abdominal obesity and metabolic syndrome. *Nature*. 444, 881–887 (2006).

172. Ohlson, L.-O. *et al.* The Influence of Body Fat Distribution on the Incidence of Diabetes Mel I It Us 13.5 Years of Follow-up of the Participants in the Study of Men Born in 1913. *Diabetes*. 10, 1055–1058 (1985)

173. Yusuf, S. *et al.* Obesity and the risk of myocardial infarction in 27,000 participants from 52 countries: a case-control study. *Lancet* 366, 1640–9 (2005).

174. Pischon, T. *et al.* General and Abdominal Adiposity and Risk of Death in Europe. *New England Journal of Medicine* 359, 2105–2120 (2008).

175. Spalding, K. L. *et al.* Dynamics of fat cell turnover in humans. *Nature* 453, 783–787 (2008).

176. de Ferranti, S. & Mozaffarian, D. The perfect storm: obesity, adipocyte dysfunction, and metabolic consequences. *Clin Chem* 54, 945–55 (2008).

177. Pellegrinelli, V., Carobbio, S. & Vidal-Puig, A. Adipose tissue plasticity: how fat depots respond differently to pathophysiological cues. *Diabetologia.* 59, 1075–1088 (2016).

178. Trayhurn, P. Hypoxia and adipocyte physiology: Implications for adipose tissue dysfunction in obesity. *Annual Review of Nutrition.* 34, 207–236 (2014).

179. Trayhurn, P. Hypoxia and Adipose Tissue Function and Dysfunction in Obesity. *Physiol Rev* 93, 1–21 (2013).

180. Halberg, N. *et al.* Hypoxia-Inducible Factor 1α Induces Fibrosis and Insulin Resistance in White Adipose Tissue. *Mol Cell Biol* 29, 4467–4483 (2009).

181. Crewe, C., An, Y. A. & Scherer, P. E. The ominous triad of adipose tissue dysfunction: Inflammation, fibrosis, and impaired angiogenesis. *Journal of Clinical Investigation.* 127, 74–82 (2017).

182. Rudich, A., Kanety, H. & Bashan, N. Adipose stress-sensing kinases: linking obesity to malfunction. *Trends in Endocrinology and Metabolism.* 18, 291–299 (2007).

183. Bashan, N. *et al.* Mitogen-activated protein kinases, inhibitory-κB kinase, and insulin signaling in human omental versus subcutaneous adipose tissue in obesity. *Endocrinology* 148, 2955–2962 (2007).

184. Sabio, G. *et al.* A stress signaling pathway in adipose tissue regulates hepatic insulin resistance. *Science* 322, 1539–1543 (2008).

185. Sun, S., Ji, Y., Kersten, S. & Qi, L. Mechanisms of inflammatory responses in obese adipose tissue. *Annual Review of Nutrition.* 32, 261–286 (2012).

186. Singh, R. & Cuervo, A. M. Autophagy in the cellular energetic balance. *Cell Metabolism.* 13, 495–504 (2011).

187. Maixner, N. *et al.* Autophagy in adipose tissue. *Obesity Facts.* 5, 710–721 (2012).

188. Kovsan, J. *et al.* Altered autophagy in human adipose tissues in obesity. *Journal of Clinical Endocrinology and Metabolism* 96, E268–277 (2011).

189. Haim, Y. *et al.* Elevated autophagy gene expression in adipose tissue of obese humans: A potential non-cell-cycle-dependent function of E2F1. *Autophagy* 11, 2074–2088 (2015).

190. Sell, H., Habich, C. & Eckel, J. Adaptive immunity in obesity and insulin resistance. *Nature Reviews Endocrinology.* 8, 709–716 (2012).

191. Cancello, R. *et al.* Reduction of Macrophage Infiltration and Chemoattractant Gene Expression Changes in White Adipose Tissue of Morbidly Obese Subjects After Surgery-Induced Weight Loss. *Diabetes.* 8, 2277–2286 (2005).

192. Harman-Boehm, I. *et al.* Macrophage infiltration into omental versus subcutaneous fat across different populations: Effect of regional adiposity and the comorbidities of obesity. *Journal of Clinical Endocrinology and Metabolism* 92, 2240–2247 (2007).

193. Ye, R. & Scherer, P. E. Adiponectin, driver or passenger on the road to insulin sensitivity? *Molecular Metabolism.* 2, 133–141 (2013).

194. Wu, H. & Ballantyne, C. M. Metabolic Inflammation and Insulin Resistance in Obesity. *Circulation Research.* 126, 1549–1564 (2020).

195. Hwang, I. & Kim, J. B. Two faces of white adipose tissue with heterogeneous adipogenic progenitors. *Diabetes and Metabolism Journal.* 43, 752–762 (2019).

196. Heymsfield, S. B. & Wadden, T. A. Mechanisms, Pathophysiology, and Management of Obesity. *New England Journal of Medicine* 376, 254–266 (2017).

197. Kotas, M. E. & Medzhitov, R. Homeostasis, Inflammation, and Disease Susceptibility. *Cell.* 160, 816–827 (2015).

198. Reilly, S. M. & Saltiel, A. R. Adapting to obesity with adipose tissue inflammation. *Nature Reviews Endocrinology.* 13, 633–643 (2017).

199. Larson, E. B., Yaffe, K. & Langa, K. M. New Insights into the Dementia Epidemic. *New England Journal of Medicine* 369, 2275–2277 (2013).

200. Ward, Z. J. *et al.* Projected U.S. State-Level Prevalence of Adult Obesity and Severe Obesity. *New England Journal of Medicine* 381, 2440–2450 (2019).

201. Sachdev, P. S. *et al.* Classifying neurocognitive disorders: The DSM-5 approach. *Nature Reviews Neurology.* 10, 634–642 (2014).

202. Harvey, P. D. Domains of cognition and their assessment. *Dialogues Clin Neurosci* 21, 227–237 (2019).

203. Feldman, H. *et al.* Behavioral Symptoms in Mild Cognitive Impairment. *Neurology.* 7, 1199–1201 (2004).

204. Tabert, M. H. *et al.* Neuropsychological Prediction of Conversion to Alzheimer Disease in Patients With Mild Cognitive Impairment. *Arch Gen Psychiatry.* 8, 916–924 (2006).

205. Farias, S. T., Mungas, D., Reed, B. R., Harvey, D. & DeCarli, C. Progression of mild cognitive impairment to dementia in clinic- vs community-based cohorts. *Arch Neurol* 66, 1151–1157 (2009).

206. Beydoun, M. A., Beydoun, H. A. & Wang, Y. Obesity and central obesity as risk factors for incident dementia and its subtypes: A systematic review and meta-analysis. *Obesity Reviews.* 9, 204–218 (2008).

207. Livingston, G. *et al.* Dementia prevention, intervention, and care. *The Lancet.* 390, 2673–2734 (2017).

208. Anstey, K. J., Cherbuin, N., Budge, M. & Young, J. Body mass index in midlife and late-life as a risk factor for dementia: A meta-analysis of prospective studies. *Obesity Reviews* 12, e426–437 (2011).

209. Yang, Y. *et al.* The association between obesity and lower working memory is mediated by inflammation: Findings from a nationally representative dataset of U.S. adults. *Brain Behav Immun* 84, 173–179 (2020).

210. Nepal, B., Brown, L. J. & Anstey, K. J. Rising midlife obesity will worsen future prevalence of dementia. *PLoS One* 9, e99305 (2014).

211. Livingston, G. *et al.* Dementia prevention, intervention, and care: 2020 report of the Lancet Commission. *The Lancet.* 396, 413–446 (2020).

212. Whitmer, R. A., Gunderson, E. P., Quesenberry, C. P., Zhou, J. & Yaffe, K. Body Mass Index in Midlife and Risk of Alzheimer Disease and Vascular Dementia. *Current Alzheimer Research.* 4, 103–109 (2007).

213. Albanese, E. *et al.* Body mass index in midlife and dementia: Systematic review and meta-regression analysis of 589,649 men and women followed in longitudinal studies. *Alzheimer's and Dementia: Diagnosis, Assessment and Disease Monitoring.* 8, 165–178 (2017).

214. Restivo, M. R., Mckinnon, M. C., Frey, B. N., Hall, G. B. & Taylor, V. H. Effect of obesity on cognition in adults with and without a mood disorder: study design and methods. *BMJ Open.* 2:e009347 (2016).

215. Brem, A. katharine, Ran, K. & Pascual-leone, A. Learning and memory. in *Handbook of Clinical Neurology.* 116 ,693–737 (Elsevier B.V., 2013).

216. Matthews, B. R. Memory Dysfunction. *Continuum.* 21, 613–626 (2015).

217. Loprinzi, P. D. & Frith, E. Obesity and episodic memory function. *Journal of Physiological Sciences*. 68, 321–331 (2018).

218. Cournot, M. *et al.* Relation between body mass index and cognitive function in healthy middle-aged men and women. *Neurology* 67, 1208–1214 (2006).

219. Gunstad, J. *et al.* Obesity Is Associated with Memory Deficits in Young and Middle-Aged Adults. *Eat Weight Disord.* 11, e15–19 (2006).

220. Alosco, M. L. *et al.* Cognitive function after bariatric surgery: Evidence for improvement 3 years after surgery. *Am J Surg* 207, 870–876 (2014).

221. Conforto, R. M. & Gershman, L. Brief report cognitive processing differences between obese and nonobese subjects. *Addictive Behaviors*. 10, 83–85 (1985).

222. Katz, P. *et al.* Physical activity, obesity, and cognitive impairment among women with systemic lupus erythematosus. *Arthritis Care Res (Hoboken)* 64, 502–510 (2012).

223. Sodhi, K. *et al.* Role of adipocyte Na,K-ATPase oxidant amplification loop in cognitive decline and neurodegeneration. *iScience* 24, 103262 (2021).

224. Rabinovici, G. D., Stephens, M. L. & Possin, K. L. Executive Dysfunction. *Continuum*. 21, 646–659 (2015).

225. Diamond, A. Executive functions. *Annual Review of Psychology*. 64, 135–168 (2013).

226. Vainik, U., Dagher, A., Dubé, L. & Fellows, L. K. Neurobehavioural correlates of body mass index and eating behaviours in adults: A systematic review. *Neuroscience and Biobehavioral Reviews*. 37, 279–299 (2013).

227. Spitznagel, M. B. *et al.* Cognitive function predicts weight loss after bariatric surgery. *Surgery for Obesity and Related Diseases* 9, 453–459 (2013).

228. Friedman, J. M. & Halaas, J. L. Leptin and the Regulation of Body Weight in Mammals. *Nature*. 395, 763–770 (1998).

229. Scarpace, P. J. & Matheny, M. Leptin Induction of UCP1 Gene Expression Is Dependent on Sympathetic Innervation. *Am J Physiol*. 2, E259–264 (1998).

230. Rezai-Zadeh, K. & Münzberg, H. Integration of sensory information via central thermoregulatory leptin targets. *Physiology and Behavior*. 121, 49–55 (2013).

231. Zeng, W. *et al.* Sympathetic neuro-adipose connections mediate leptin-driven lipolysis. *Cell* 163, 84–94 (2015).

232. Arvaniti, K., Deshaies, Y. & Richard, D. Effect of Leptin on Energy Balance Does Not Require the Presence of Intact Adrenals. *Am J Physiol*. 1, R105–111 (1998).

233. Weisberg, S. P. *et al.* Obesity is associated with macrophage accumulation in adipose tissue. *Journal of Clinical Investigation* 112, 1796–1808 (2003).

234. Nguyen, K. D. *et al.* Alternatively activated macrophages produce catecholamines to sustain adaptive thermogenesis. *Nature* 480, 104–108 (2011).

235. Cardoso, F. *et al.* Neuro-mesenchymal units control ILC2 and obesity via a brain–adipose circuit. *Nature* 597, 410–414 (2021).

236. Morrison, S. F. & Nakamura, K. Central Mechanisms for Thermoregulation. *Annu Rev Physiol* 12, 57 (2018).

237. Minhas, P. S. *et al.* Restoring metabolism of myeloid cells reverses cognitive decline in ageing. *Nature* 590, 122–128 (2021).

238. Kanoski, S. E. & Grill, H. J. Hippocampus Contributions to Food Intake Control: Mnemonic, Neuroanatomical, and Endocrine Mechanisms. *Biological Psychiatry.* 81, 748–756 (2017).

239. Min, D. K., Tuor, U. I. & Chelikani, P. K. Gastric distention induced functional magnetic resonance signal changes in the rodent brain. *Neuroscience* 179, 151–158 (2011).

240. Wang, G.-J. *et al.* Gastric stimulation in obese subjects activates the hippocampus and other regions involved in brain reward circuitry. *Proc Natl Acad Sci U S A* 103, 15641–5 (2006).

241. Davidson, T. L. *et al.* Hippocampal Lesions Impair Retention of Discriminative Responding Based on Energy State Cues. *Behavioral Neuroscience* 124, 97–105 (2010).

242. Suarez, A. N. *et al.* Gut vagal sensory signaling regulates hippocampus function through multi-order pathways. *Nat Commun* 9, 2181 (2018).

243. Geisler, C. E., Hepler, C., Higgins, M. R. & Renquist, B. J. Hepatic adaptations to maintain metabolic homeostasis in response to fasting and refeeding in mice. *Nutr Metab (Lond)* 13, 62(2016).

244. Joly-Amado, A. *et al.* Hypothalamic AgRP-neurons control peripheral substrate utilization and nutrient partitioning. *EMBO Journal* 31, 4276–4288 (2012).

245. Miletta, M. C. *et al.* AgRP neurons control compulsive exercise and survival in an activity-based anorexia model. *Nat Metab* 2, 1204–1211 (2020).

246. Dietrich, M. O. *et al.* AgRP neurons regulate development of dopamine neuronal plasticity and nonfood-associated behaviors. *Nat Neurosci* 15, 1108–1110 (2012).

247. Dietrich, M. O., Zimmer, M. R., Bober, J. & Horvath, T. L. Hypothalamic Agrp neurons drive stereotypic behaviors beyond feeding. *Cell* 160, 1222–1232 (2015).

248. Endle, H. *et al.* AgRP neurons control feeding behaviour at cortical synapses via peripherally derived lysophospholipids. *Nat Metab* 4, 683–692 (2022).

249. Qu, Y. *et al.* Association of body mass index with risk of cognitive impairment and dementia: A systematic review and meta-analysis of prospective studies. *Neuroscience and Biobehavioral Reviews.* 115, 189–198 (2020).

250. Gardener, H. *et al.* Obesity Measures in Relation to Cognition in the Northern Manhattan Study. *Journal of Alzheimer's Disease* 78, 1653–1660 (2020).

251. Farruggia, M. C. & Small, D. M. Effects of adiposity and metabolic dysfunction on cognition: A review. *Physiology and Behavior.* 208, 112578 (2019).

252. Moya-Alvarado, G., Gershoni-Emek, N., Perlson, E. & Bronfman, F. C. Neurodegeneration and Alzheimer's disease (AD). What can proteomics tell us about the Alzheimer's brain? *Molecular and Cellular Proteomics* 15, 409–425 (2016).

253. Sonkusare, S. K., Kaul, C. L. & Ramarao, P. Dementia of Alzheimer's disease and other neurodegenerative disorders - Memantine, a new hope. *Pharmacological Research.* 51, 1–17 (2005).

254. Ashrafian, H., Harling, L., Darzi, A. & Athanasiou, T. Neurodegenerative disease and obesity: What is the role of weight loss and bariatric interventions? *Metabolic Brain Disease.* 28, 341–353 (2013).

255. Kothari, V. *et al.* High fat diet induces brain insulin resistance and cognitive impairment in mice. *Biochim Biophys Acta Mol Basis Dis* 1863, 499–508 (2017).

256. Chew, H., Solomon, V. A. & Fonteh, A. N. Involvement of Lipids in Alzheimer's Disease Pathology and Potential Therapies. *Frontiers in Physiology.* 11, 598 (2020).

257. Uranga, R. M. & Keller, J. N. The complex interactions between obesity, metabolism and the brain. *Frontiers in Neuroscience.* 13, 513 (2019).

258. De La Monte, S. M. *et al.* Ceramide-mediated insulin resistance and impairment of cognitive-motor functions. *Journal of Alzheimer's Disease* 21, 967–984 (2010).

259. Dahl, A. K. *et al.* Body mass index across midlife and cognitive change in late life. *Int J Obes (Lond)* 37, 296–302 (2013).

260. Xu, H. *et al.* Chronic inflammation in fat plays a crucial role in the development of obesity-related insulin resistance. *Journal of Clinical Investigation* 112, 1821–1830 (2003).

261. Jiang, L. *et al.* Donepezil Attenuates Obesity-Associated Oxidative Stress and Central Inflammation and Improves Memory Deficit in Mice Fed a High-Fat Diet. *Dement Geriatr Cogn Disord* 48, 154–163 (2020).

262. Mazon, J. N., de Mello, A. H., Ferreira, G. K. & Rezin, G. T. The impact of obesity on neurodegenerative diseases. *Life Sciences.* 182, 22–28 (2017).

263. Saltiel, A. R. & Olefsky, J. M. Inflammatory mechanisms linking obesity and metabolic disease. *Journal of Clinical Investigation.* 127, 1–4 (2017).

264. Iyer, S. S. *et al.* Necrotic Cells Trigger a Sterile Inflammatory Response through the Nlrp3 Inflammasome. *Proc Natl Acad Sci USA.* 48, 20388–20393 (2009).

265. Iyer, S. S. *et al.* Necrotic cells trigger a sterile inflammatory response through the Nlrp3 inflammasome. *Proc Natl Acad Sci U S A* 106, 20388–93 (2009).

266. Vandanmagsar, B. *et al.* The NLRP3 inflammasome instigates obesity-induced inflammation and insulin resistance. *Nat Med* 17, 179–88 (2011).

267. Youm, Y. H. *et al.* Canonical Nlrp3 inflammasome links systemic low-grade inflammation to functional decline in aging. *Cell Metab* 18, 519–532 (2013).

268. Heneka, M. T. *et al.* NLRP3 is activated in Alzheimer's disease and contributes to pathology in APP/PS1 mice. *Nature* 493, 674–678 (2013).

269. Guo, D. H. *et al.* Visceral adipose NLRP3 impairs cognition in obesity via IL-1R1 on CX3CR1+ cells. *Journal of Clinical Investigation* 130, 1961–19766 (2020).

270. Cohena, P. & Spiegelmanb, B. M. Cell biology of fat storage. *Molecular Biology of the Cell.* 27, 2523–2527 (2016).

271. Rao, R. R. *et al.* Meteorin-like is a hormone that regulates immune-adipose interactions to increase beige fat thermogenesis. *Cell* 157, 1279–1291 (2014).

272. Qiu, Y. *et al.* Eosinophils and type 2 cytokine signaling in macrophages orchestrate development of functional beige fat. *Cell* 157, 1292–1308 (2014).

273. Guo, D. H. *et al.* Beige adipocytes mediate the neuroprotective and anti-inflammatory effects of subcutaneous fat in obese mice. *Nat Commun* 12, 4623 (2021).

274. De Felice, F. G. & Ferreira, S. T. Inflammation, defective insulin signaling, and mitochondrial dysfunction as common molecular denominators connecting type 2 diabetes to Alzheimer Disease. *Diabetes.* 63, 2262–2272 (2014).

275. Ramalingayya, G. V. *et al.* Insulin Protects against Brain Oxidative Stress with an Apparent Effect on Episodic Memory in Doxorubicin-Induced Cognitive Dysfunction in Wistar Rats. *Journal of Environmental Pathology.* 36, 121–130 (2017).

276. Craft, S. & Watson, G. S. Insulin and neurodegenerative disease: shared and specific mechanisms. *Lancet Neurol* 3, 169–78 (2004).

277. Dore, S., Kar, S., Rowe, W. & Quirion, R. Distribution and levels of [125I] IFG-I, [125I] IGF-II and [125I] insulin receptor binding sites in the hippocampus of aged memory-unimpaired and-impaired rats. *Neuroscience.* 80, 1033–1040 (1997).

278. Liang, M. *et al.* Identification of a pool of non-pumping Na/K-ATPase. *Journal of Biological Chemistry* 282, 10585–10593 (2007).

279. Liu, J., Kennedy, D. J., Yan, Y. & Shapiro, J. I. Reactive oxygen species modulation of Na/K-ATPase regulates fibrosis and renal proximal tubular sodium handling. *International Journal of Nephrology.* 2012, 381320 (2012).

280. Yan, Y. *et al.* Ouabain-stimulated trafficking regulation of the Na/K-ATPase and NHE3 in renal proximal tubule cells. *Mol Cell Biochem* 367, 175–183 (2012).

281. Tian, J. *et al.* Binding of Src to Na /K-ATPase Forms a Functional Signaling Complex. *Mol Biol Cell* 17, 317–326 (2006).

282. Yan, Y. *et al.* Involvement of reactive oxygen species in a feed-forward mechanism of Na/K-ATPase-mediated signaling transduction. *Journal of Biological Chemistry* 288, 34249–34258 (2013).

283. Yan, Y. *et al.* Protein Carbonylation of an Amino Acid Residue of the Na/K-ATPase α1 Subunit Determines Na/K-ATPase Signaling and Sodium Transport in Renal Proximal Tubular Cells. *J Am Heart Assoc* 5, e003675 (2016).

284. Li, Z. *et al.* NAKtide, a Na/K-ATPase-derived peptide Src inhibitor, antagonizes Quabain-activated signal transduction in cultured cells. *Journal of Biological Chemistry* 284, 21066–21076 (2009).

285. Bongioanni, P. *et al.* Climate change and neurodegenerative diseases. *Environmental Research.* 201, 111511 (2021).

286. Nguyen, J. L., Schwartz, J. & Dockery, D. W. The relationship between indoor and outdoor temperature, apparent temperature, relative humidity, and absolute humidity. *Indoor Air* 24, 103–112 (2014).

287. Springmann, M. *et al.* Global and regional health effects of future food production under climate change: A modelling study. *The Lancet* 387, 1937–1946 (2016).

288. The intergovernmental panel on climate change. https://www.ipcc.ch/report/ar5/wg2/ (2013).

289. Koch, C. A. *et al.* Climate Change and Obesity. *Hormone and Metabolic Research.* 53, 575–587 (2021).

290. Solomon, S., Plattner, G.-K., Knutti, R. & Friedlingstein, P. Irreversible Climate Change Due to Carbon Dioxide Emissions. *Proc Natl Acad sci USA.* 6, 1704–1709 (2009).

291. Mavrogianni, A. *et al.* Historic variations in winter indoor domestic temperatures and potential implications for body weight gain. *Indoor and Built Environment* 22, 360–375 (2013).

292. Hartmann D. L. *et al.* Observations: atmosphere and surface. In: climate change 2013: the physical science basis. Contribution of working group I to the fifth assessment report of the intergovernmental panel on climate change. (2013).

293. Qin, D. *et al.* To the Fifth Assessment Report of the Intergovernmental Panel on Climate Change Summary for Policymakers SPM Drafting Authors: Draft Contributing Authors. Monika Rhein. (2013)

294. Climate Impact Lab. Climate Projections on Impact Map. (2022).

295. Zheutlin, A. R., Adar, S. D. & Park, S. K. Carbon dioxide emissions and change in prevalence of obesity and diabetes in the United States: An ecological study. *Environ Int* 73, 111–116 (2014).

296. Voss, J. D., Masuoka, P., Webber, B. J., Scher, A. I. & Atkinson, R. L. Association of elevation, urbanization and ambient temperature with obesity prevalence in the United States. *Int J Obes* 37, 1407–1412 (2013).

297. Nations, U., of Economic, D., Affairs, S. & Division, P. World Urbanization Prospects The 2018 Revision. (2018).

298. Nieuwenhuijsen, M. J. *et al.* Air pollution, noise, blue space, and green space and premature mortality in Barcelona: A mega cohort. *Int J Environ Res Public Health* 15, 2405 (2018).

299. Bennett, J. E., Blangiardo, M., Fecht, D., Elliott, P. & Ezzati, M. Vulnerability to the mortality effects of warm temperature in the districts of England and Wales. *Nat Clim Chang* 4, 269–273 (2014).

300. Watts, N. *et al.* The Lancet Countdown on health and climate change: from 25 years of inaction to a global transformation for public health. *The Lancet.* 391, 581–630 (2018).

301. Burkart, K. G. *et al.* Estimating the cause-specific relative risks of non-optimal temperature on daily mortality: a two-part modelling approach applied to the Global Burden of Disease Study. *The Lancet* 398, 685–697 (2021).

302. Intergovernamental panel on climate change. Climate change 2014: impacts, adaptation and vulnerability. Part B: regional aspects. Contribution of working group II to the fifth assessment report of the intergovernamental panel on climate change. (2014).

303. Haines, A. & Ebi, K. The Imperative for Climate Action to Protect Health. *New England Journal of Medicine* 380, 263–273 (2019).

304. Cohen, A. J. *et al.* Estimates and 25-year trends of the global burden of disease attributable to ambient air pollution: an analysis of data from the Global Burden of Diseases Study 2015. *The Lancet* 389, 1907–1918 (2017).

305. Furlong, M. A. & Klimentidis, Y. C. Associations of air pollution with obesity and body fat percentage, and modification by polygenic risk score for BMI in the UK Biobank. *Environ Res* 185, 109364 (2020).

306. Kim, K. H., Kabir, E. & Kabir, S. A review on the human health impact of airborne particulate matter. *Environment International.* 74, 136–143 (2015).

307. Kenney, W. L. & Munce, T. A. Invited review: aging and human temperature regulation. *J Appl Physiol (1985)* 95, 2598–603 (2003).

308. Tham, S., Thompson, R., Landeg, O., Murray, K. A. & Waite, T. Indoor temperature and health: a global systematic review. *Public Health.* 179, 9–17 (2020).

309. Willett, W. *et al.* Food in the Anthropocene: the EAT–Lancet Commission on healthy diets from sustainable food systems. *The Lancet.* 393, 447–492 (2019).

310. Swinburn, B. A. *et al.* The Global Syndemic of Obesity, Undernutrition, and Climate Change: The Lancet Commission report. *The Lancet.* 393, 791–846 (2019).

311. Springmann, M., Charles, H., Godfray, J., Rayner, M. & Scarborough, P. Analysis and valuation of the health and climate change cobenefits of dietary change. 113, 4146–4151 (2016).

312. Catalán, V. *et al.* Time to Consider the "Exposome Hypothesis" in the Development of the Obesity Pandemic. *Nutrients.* 14, 1597 (2022).

313. Johnson, F., Mavrogianni, A., Ucci, M., Vidal-Puig, A. & Wardle, J. Could increased time spent in a thermal comfort zone contribute to population increases in obesity? *Obesity Reviews* 12, 543–551 (2011).

314. Boyles, J. G., Seebacher, F., Smit, B. & McKechnie, A. E. Adaptive thermoregulation in endotherms may alter responses to climate change. *Integrative and Comparative Biology.* 51, 676–690 (2011).

315. Valdés, S. *et al.* Ambient temperature and prevalence of obesity in the spanish population: The di@bet.es study. *Obesity* 22, 2328–2332 (2014).

316. Ye, L. *et al.* Fat cells directly sense temperature to activate thermogenesis. *Proc Natl Acad Sci U S A* 110, 12480–12485 (2013).

317. Gao, Y. *et al.* Acute and chronic cold exposure differentially affects the browning of porcine white adipose tissue. *Animal* 12, 1435–1441 (2018).

318. Scheffers, F. R. *et al.* The Association between Indoor Temperature and Body Mass Index in Children: The PIAMA Birth Cohort Study. *BMC Public Health.* 13, 1119 (2013).

319. Valdés, S. *et al.* Ambient temperature and prevalence of diabetes and insulin resistance in the Spanish population: Di@bet.es study. *Eur J Endocrinol* 180, 275–282 (2019).

320. Puig, J. *et al.* The Aging Imageomics Study: rationale, design and baseline characteristics of the study population. *Mech Ageing Dev* 189, 111257 (2020).

321. Corominas Barnadas, J. M. *et al.* Estudio MESGI50: descripción de una cohorte sobre la madurez y el envejecimiento satisfactorio. *Gac Sanit* 31, 511–517 (2017).

322. Martí, R. *et al.* Improving InterMediAte Risk Management. MARK Study. *BMC Cardiovasc Disord.* 11, 61 (2011).

323. Conde-Sala, J. L., Portellano-Ortiz, C., Calvó-Perxas, L. & Garre-Olmo, J. Quality of life in people aged 65+ in Europe: associated factors and models of social welfare—analysis of data from the SHARE project (Wave 5). *Quality of Life Research* 26, 1059–1070 (2017).

324. Deurenberg, P., Weststrate, J. A. & Seidell, J. C. Body mass index as a measure of body fatness: age- and sex-specific prediction formulas. *British Journal of Nutrition* 65, 105–114 (1991).

325. Defronzo, R. A., Tobin, J. D. & Andres, R. Glucose Clamp Technique: A Method for Quantifying Insulin Secretion and Resistance. *Am J Physiol.* 3, E214–223 (1979)

326. Delis D. C., Kramer J. H., Kaplan E. & Ober B. A. California Verbal Learning Test - second edition. Adult Version. Manual. *The psychological corporation* (2000).

327. Wechsler D. Escala de inteligencia de Wechsler para adultos-IV, Manual técnico y de interpretación. *NCS Pearson* (2012).

328. Elwood, R. W. The California Verbal Learning Test: Psychometric Characteristics and Clinical Application. *Neuropsychology Review.* 5, 173–201 (1995).

329. Paolo, A. M., Troster, A. I., Ryan, J. J. & Eisenhower, D. D. Test-Retest Stability of the California Verbal Learning Test in Older Persons. *Neuropsychology.* 11, 613–616 (1997).

330. Donders, J. Subtypes of learning and memory on the California Verbal Learning Test-Second Edition (CVLT-II) in the standardization sample. *J Clin Exp Neuropsychol* 30, 741–748 (2008).

331. Strauss E., Sherman E. M. S & Spreen O. A compendium of neuropsychological tests: administration, norms and commentary. *Arch Clin Neuropsychol.* 8, 819–825 (2006).

332. Golden C. A manual for the clinical and experimental use of the stroop color and word test, in faculty books and book chapters. (1978).

333. Scarpina, F. & Tagini, S. The stroop color and word test. *Frontiers in Psychology.* 8, 557 (2017).

334. Lezak, M. D. Neuropsychological Assessment in Behavibral Toxicology-Developing Techniques and Interpretative Issues. *Scand J Work Environ Health.* 10, 25–29 (1984).

335. Corrigan D, J. & Hinkeldey S, N. Relationships Within the Trail Making Test. *J Clin Psychol* 43, 402–409 (1987).

336. Rey A. L'examen psychologique dans les cas d'encephalopathie traumatique. *Arch Psychol* (1941).

337. Osterrieth P. A. Le test de copie d'une figure complexe. *Arch Psychol* (1944).

338. Shin, M. S., Park, S. Y., Park, S. R., Seol, S. H. & Kwon, J. S. Clinical and empirical applications of the Rey-Osterrieth Complex Figure Test. *Nat Protoc* 1, 892–899 (2006).

339. Muller, H. J. Genetic variability, twin hybrids and constant hybrids, in a case of balanced lethal factors prelimnary crosses and formulation of a working hypothesis. *Genetics.* 5, 422–499 (1918).

340. Muller, H. J. Artificial transmutation of the genes. *Science.* 66, 84–87 (1927).

341. Prokop A. Fruit flies in biological research. *Sciences Review* 28, 10–14 (2016).

342. Pandey, U. B. & Nichols, C. D. Human disease models in drosophila melanogaster and the role of the fly in therapeutic drug discovery. *Pharmacol Rev* 63, 411–436 (2011).

343. Yamaguchi, M. & Yoshida, H. Drosophila as a model organism. in *Advances in Experimental Medicine and Biology.* 1076, 1–10 (Springer New York LLC, 2018).

344. Brand, H. & Perrimon, N. Targeted Gene Expression as a Means of Altering Cell Fates and Generating Dominant Phenotypes. *Development.* 2, 401–415 (1993).

345. Dietzl, G. *et al.* A genome-wide transgenic RNAi library for conditional gene inactivation in Drosophila. *Nature* 448, 151–156 (2007).

346. Rynes, J. *et al.* Activating Transcription Factor 3 Regulates Immune and Metabolic Homeostasis. *Mol Cell Biol* 32, 3949–3962 (2012).

347. Oliveras-Cañellas, N. *et al.* Adipose tissue coregulates cognitive function. *Sci Adv* 9, eadg4017 (2023).

348. Griffith, L. C. & Ejima, A. Courtship learning in Drosophila melanogaster: Diverse plasticity of a reproductive behavior. *Learning and Memory.* 16, 743–750 (2009).

349. Dickinson, A. Associative learning and animal cognition. *Philosophical Transactions of the Royal Society B: Biological Sciences.* 367, 2733–2742 (2012).

350. Koemans, T. S. *et al.* Drosophila courtship conditioning as a measure of learning and memory. *Journal of Visualized Experiments* 124, 55808 (2017).

351. Kamyshev, N. G., Iliadi, K. G. & Bragina, J. V. Drosophila Conditioned Courtship: Two Ways of Testing Memory. *Learn Mem.* 6, 1–20 (1999).

352. Puighermanal, E. *et al.* Cannabinoid modulation of hippocampal long-term memory is mediated by mTOR signaling. *Nat Neurosci* 12, 1152–1158 (2009).

353. Busquets-Garcia, A. *et al.* Differential role of anandamide and 2-arachidonoylglycerol in memory and anxiety-like responses. *Biol Psychiatry* 70, 479–486 (2011).

354. Escudero-Lara, A., Cabañero, D. & Maldonado, R. Kappa opioid receptor modulation of endometriosis pain in mice. *Neuropharmacology* 195, 108677 (2021).

355. Gomis-González, M. *et al.* Protein Kinase C-Gamma Knockout Mice Show Impaired Hippocampal Short-Term Memory While Preserved Long-Term Memory. *Mol Neurobiol* 58, 617–630 (2021).

356. Dobin, A. *et al.* STAR: Ultrafast universal RNA-seq aligner. *Bioinformatics* 29, 15–21 (2013).

357. Li, B. & Dewey, C. N. RSEM: Accurate Transcript Quantification from RNA-Seq Data with or without a Reference Genome. *BMC Bioinformatics.* 12, 323 (2011).

358. Dheda K., *et al.* Validation of hhousekeeping genes for normalizing RNA expression in real-time PCR. *Biotechniques.* 37, 112–114 (2004).

359. Livak, K. J. & Schmittgen, T. D. Analysis of relative gene expression data using real-time quantitative PCR and the 2-ΔΔCT method. *Methods* 25, 402–408 (2001).

360. Wikoff, W. R., Pendyala, G., Siuzdak, G. & Fox, H. S. Metabolomic analysis of the cerebrospinal fluid reveals changes in phospholipase expression in the CNS of SIV-infected macaques. *Journal of Clinical Investigation* 118, 2661–2669 (2008).

361. Ritchie, M. E. *et al.* Limma powers differential expression analyses for RNA-sequencing and microarray studies. *Nucleic Acids Res* 43, e47 (2015).

362. Robinson, M. D., McCarthy, D. J. & Smyth, G. K. edgeR: A Bioconductor package for differential expression analysis of digital gene expression data. *Bioinformatics* 26, 139–140 (2009).

363. Kamburov, A., Stelzl, U., Lehrach, H. & Herwig, R. The ConsensusPathDB interaction database: 2013 Update. *Nucleic Acids Res* 41, D793–800 (2013).

364. Szklarczyk, D. *et al.* STRING v11: Protein-protein association networks with increased coverage, supporting functional discovery in genome-wide experimental datasets. *Nucleic Acids Res* 47, D607–D613 (2019).

365. Ulgen, E., Ozisik, O. & Sezerman, O. U. PathfindR: An R package for comprehensive identification of enriched pathways in omics data through active subnetworks. *Front Genet* 10, 858 (2019).

366. Kursa, M. B. Robustness of Random Forest-Based Gene Selection Methods. *BMC Bioinformatics.* 15, 8 (2014).

367. Kivipelto, M., Mangialasche, F. & Ngandu, T. Lifestyle interventions to prevent cognitive impairment, dementia and Alzheimer disease. *Nature Reviews Neurology.* 14, 653–666 (2018).

368. Anazi, S. *et al.* Clinical genomics expands the morbid genome of intellectual disability and offers a high diagnostic yield. *Mol Psychiatry* 22, 615–624 (2017).

369. Diaz, F. *et al.* Novel NUDT2 variant causes intellectual disability and polyneuropathy. *Ann Clin Transl Neurol* 7, 2320–2325 (2020).

370. Takei, K., Slepnev, V. I., Haucke, V. & De Camilli, P. Functional Partnership between Amphiphysin and Dynamin in Clathrin-Mediated Endocytosis. *Nature Cell Biology.* 1, 33–39 (1999).

371. Bergström, S. *et al.* Multi-cohort profiling reveals elevated CSF levels of brain-enriched proteins in Alzheimer's disease. *Ann Clin Transl Neurol* 8, 1456–1470 (2021).

372. Sheng, C. *et al.* Experience-dependent structural plasticity targets dynamic filopodia in regulating dendrite maturation and synaptogenesis. *Nat Commun* 9, 3362 (2018).

373. Yu, Y. *et al.* PICALM rescues glutamatergic neurotransmission, behavioural function and survival in a Drosophila model of Aβ42 toxicity. *Hum Mol Genet* 29, 2420–2434 (2020).

374. Ginguay, A., Cynober, L., Curis, E. & Nicolis, I. Ornithine aminotransferase, an important Glutamate-Metabolizing enzyme at the crossroads of multiple metabolic pathways. *Biology.* 6, 18 (2017).

375. Arnoriaga-Rodríguez, M. *et al.* Obesity Impairs Short-Term and Working Memory through Gut Microbial Metabolism of Aromatic Amino Acids. *Cell Metab* 32, 548-560.e7 (2020).

376. Arnoriaga-Rodríguez, M. *et al.* Obesity-associated deficits in inhibitory control are phenocopied to mice through gut microbiota changes in one-carbon and aromatic amino acids metabolic pathways. *Gut* 70, 2283–2296 (2021).

377. Carulli, D., de Winter, F. & Verhaagen, J. Semaphorins in Adult Nervous System Plasticity and Disease. *Frontiers in Synaptic Neuroscience.* 13, 672891 (2021).

378. Südhof, T. C. Neuroligins and Neurexins Link Synaptic Function to Cognitive Disease.*Nature.* 455, 903–911 (2008).

379. García-Morales, V. *et al.* Membrane-Derived Phospholipids Control Synaptic Neurotransmission and Plasticity. *PLoS Biol* 13, e1002153 (2015).

380. Mitchell, R. W. & Hatch, G. M. Fatty acid transport into the brain: Of fatty acid fables and lipid tails. *Prostaglandins Leukot Essent Fatty Acids* 85, 293–302 (2011).

381. Nguyen, L. N. *et al.* Mfsd2a is a transporter for the essential omega-3 fatty acid docosahexaenoic acid. *Nature* 509, 503–506 (2014).

382. Bourassa, K. & Sbarra, D. A. Body mass and cognitive decline are indirectly associated via inflammation among aging adults. *Brain Behav Immun* 60, 63–70 (2017).

383. Wang, C. *et al.* Microglia mediate forgetting via complement-dependent synaptic elimination. *Science* 367, 688–694 (2020).

384. Dantzer, R., O'Connor, J. C., Freund, G. G., Johnson, R. W. & Kelley, K. W. From inflammation to sickness and depression: When the immune system subjugates the brain. *Nature Reviews Neuroscience.* 9, 46–56 (2008).

385. Miller, A. A. & Spencer, S. J. Obesity and neuroinflammation: A pathway to cognitive impairment. *Brain Behav Immun* 42, 10–21 (2014).

386. Guillemot-Legris, O. & Muccioli, G. G. Obesity-Induced Neuroinflammation: Beyond the Hypothalamus. *Trends in Neurosciences* vol. 40 237–253 Preprint at https://doi.org/10.1016/j.tins.2017.02.005 (2017).

387. Chatterjee, S. *et al.* Pharmacological activation of Nr4a rescues age-associated memory decline. *Neurobiol Aging* 85, 140–144 (2020).

388. Shah, H. *et al.* Revisiting the Role of Vitamins and Minerals in Alzheimer's Disease. *Antioxidants* 12, 415 (2023).

389. Wołoszynowska-Fraser, M. U., Kouchmeshky, A. & Mccaffery, P. Vitamin A and Retinoic Acid in Cognition and Cognitive Disease. *Annual Review of Nutrition.* 40, 247–272 (2020).

390. De Brún, A. & McAuliffe, E. Exploring the potential for collective leadership in a newly established hospital network. *J Health Organ Manag* 34, 449–467 (2020).

391. Cifre, M., Palou, A. & Oliver, P. Cognitive impairment in metabolically-obese, normal-weight rats: Identification of early biomarkers in peripheral blood mononuclear cells. *Mol Neurodegener* 13, 14 (2018).

392. Ng, J., Papandreou, A., Heales, S. J. & Kurian, M. A. Monoamine neurotransmitter disorders - Clinical advances and future perspectives. *Nature Reviews Neurology.* 11, 567–584 (2015).

393. Kaeser, P. S., Deng, L., Fan, M. & Südhof, T. C. RIM genes differentially contribute to organizing presynaptic release sites. *Proc Natl Acad Sci U S A* 109, 11830–11835 (2012).

394. Powell, C. M. *et al.* The Presynaptic Active Zone Protein RIM1α Is Critical for Normal Learning and Memory. *Neuron.* 42, 143–153 (2004).

395. Krumm, N. *et al.* Excess of rare, inherited truncating mutations in autism HHS Public Access Author manuscript. *Nat Genet* 47, 582–588 (2015).

396. Raun, N., Jones, S. & Kramer, J. M. Conditioned courtship suppression in Drosophila melanogaster. *Journal of Neurogenetics.* 35, 154–167 (2021).

397. Haddadi, M. *et al.* Brain aging, memory impairment and oxidative stress: A study in Drosophila melanogaster. *Behavioural Brain Research* 259, 60–69 (2014).

398. Wang, D. *et al.* Antioxidants Protect PINK1-Dependent Dopaminergic Neurons in Drosophila. *Proc Natl Acad Sci USA.* 103, 13520–13525 (2006).

399. Bahadorani, S., Bahadorani, P., Phillips, J. P. & Hilliker, A. J. The Effects of Vitamin Supplementation on Drosophila Life Span Under Normoxia and Under Oxidative Stress. *J Gerontol A Bio Sci Med Sci.* 63, 35–42 (2008).

400. Roeterdink, W. G., Strecker, K. E., Hayden, C. C., Janssen, M. H. M. & Chandler, D. W. Imaging the rotationally state-selected NO (A,n) product from the predissociation of the A state of the NO-Ar van der Waals cluster. *Journal of Chemical Physics* 130, 134305 (2009).

401. Kawai, T., Autieri, M. V. & Scalia, R. Adipose tissue inflammation and metabolic dysfunction in obesity. *Am J Physiol Cell Physiol* 320, C375–C391 (2021).

402. Liu, Z. & Huang, X. Lipid metabolism in Drosophila: Development and disease. *Acta Biochimica et Biophysica Sinica.* 45, 44–50 (2013).

403. Kühnlein, R. P. The contribution of the Drosophila model to lipid droplet research. *Progress in Lipid Research.* 50, 348–356 (2011).

404. Meltzer, S. *et al.* Phospholipid Homeostasis Regulates Dendrite Morphogenesis in Drosophila Sensory Neurons. *Cell Rep* 21, 859–866 (2017).

405. Muffat, J., Walker, D. W. & Benzer, S. Human ApoD, an apolipoprotein up-regulated in neurodegenerative diseases, extends lifespan and increases stress resistance in Drosophila. *Proc Natl Acad Sci USA.* 105, 7088–7093 (2008).

406. Turner, J. B., Kumar, A. & Koch, C. A. The effects of indoor and outdoor temperature on metabolic rate and adipose tissue – the Mississippi perspective on the obesity epidemic. *Reviews in Endocrine and Metabolic Disorders.* 17, 61–71 (2016).

407. Hu, E., Liang, P. & Spiegelman, B. M. AdipoQ Is a Novel Adipose-Specific Gene Dysregulated in Obesity*. *J Biol Chem.* 271, 10697–10703 (1996).

408. Arita Y., *et al.* Paradoxical decrease of an adipose-specific protein, adiponectin, in obesity. *Biochem Biophys Res Commun.* 257, 79–83 (1999).

409. Wei, Q. *et al.* Adiponectin is required for maintaining normal body temperature in a cold environment. *BMC Physiol* 17, 8 (2017).

410. Hui, X. *et al.* Adiponectin Enhances Cold-Induced Browning of Subcutaneous Adipose Tissue via Promoting M2 Macrophage Proliferation. *Cell Metab* 22, 279–290 (2015).

411. Kern, P. A. *et al.* The effects of temperature and seasons on subcutaneous white adipose tissue in humans: Evidence for thermogenic gene induction. *Journal of Clinical Endocrinology and Metabolism* 99, E2772–E2779 (2014).

412. Bittel, J. H. M. Heat Debt as an Index for Cold Adaptation in Men. *J Appl Physiol.* 62, 1627–1634 (1987).

9. ANNEX I

Table 20 | Primer sequences used in this thesis

Gene ID	Forward Sequence (5' -> 3')	Reverse Sequence (5' -> 3')
HUMAN		
ADIPOQ	GGTCTTATTGGTCCTAAGGG	GTAGAAGATCTTGGTAAAGCG
AMPH	CCTGACATAAAGAATCGCATC	CAAACACTTTCTGTGCTTTC
CEBPA	AGCCTTGTTTGTACTGTATG	AAAATGGTGGTTTAGCAGAG
CIDEA1	TTATGGGATCACAGACTAAGC	ATCCAGAGTCTTGCTGATG
CPA3	CTCCATTCCTAACACCAATG	CCATAGGGAAACAATAGCATC
DIO2	TCTATGACTCGGTCATTCTG	AATTTCACCTGTTTGTAGGC
EZR	TGACTTTGTGTTTTATGCCC	CTCCTTTTCTTCTCTGTTTCC
FASN	CAATACAGATGGCTTCAAGG	GATGTATTCAAATGACTCAGGG
IL6	GCAGAAAAAGGCAAAGAATC	CTACATTTGCCGAAGAGC
IL8	GTTTTTGAAGAGGGCTGAG	TTTGCTTGAAGTTTCACTGG
NNMT	CTGACTACTCAGACCAGAAC	TCTGTTCCCTTCAAGATCAC
NR4A2	GACTATCAAATGAGTGGAGATG	GACCTGTATGCTAATCGAAG
NRG4	AGTCATGAACAACACTGAAG	ATGATACGAGTTACACAAGC
NUDT2	TTCTGCTTCGGTCCTTAG	AACTCAATTGCATTGTTCGTC
OAT	CAGACCTGATATAGTCCTCC	CTTCTTCTAAAACCTCAAGGG
PLIN1	CCCTGAAAAGATTGCTTCTG	AGGACCTTGTCTGAAGTG
PPARG	AAAGAAGCCAAC ACTAAACC	TGGTCATTTCGTTAAAGGC
PPARGC1A	GCAGACCTAGATTCAAACTC	CATCCCTCTGTCATCCTC
PPARGC1B	ACATTCAAAATCTCTCCAGC	CTCTCCTATTTCTTGTCAGC
PRDM16	TCTACAGCAGGGTAGAAAAG	TCTCTGTCATGGTCTCTATG
SLC2A4	CCATTGTTATCGGCATTCTG	ATTCTGGATGATGTAGAGGTAG
TFAM	GAAAGATTCCAAGAAGCTAAGG	CGTCCAACTTCAATCATTTG
TMEM26	CTTCTTCTTATGTTTGTGGGG	CCTCACATTTTGTTCTTCTAGG
TNF	AGGCAGTCAGATCATCTTC	TTATCTCTCAGCTCCACG
TRPM8	GAAGCTGCTTTGGTACTATG	ACTGTCTCACTTCATCACAG
UCP1	ACAGCACCTAGTTTAGGAAG	CTGTACGCATTATAAGTCCC

UCP2	AGTTTTTCTCCATCTCCTGG	CTTTCTCCTTGGATCTGTAAC
UNC5B	AGGACAGTTACCACAACC	GGGGATCTCCTGGTATTTG
GAPDH	ACAGTTGCCATGTAGACC	TTGAGCACAGGGTACTTTA
PPIA	CTCCACAATATTCATGCCTTC	ATGGTTCCCAGTTTTTCATC
MOUSE		
GFP	CAACAGCCACAACGTCTATATCATG	TGTGCACTTTTATTGGTCT
Actb	GATGTATGAAGGCTTTGGTC	TGTGCACTTTTATTGGTCT
DROSOPHILA		
Amn	CAAATGTTCCGAGCGTCCAC	GCAGCGGTTCCGTTTGATAC
CaMKII	GGGAGCCATACTTACGACAATG	TCGGTTGATTCTTTGACCTGTG
Dnc	CAAACGCATGCTCAACAAGG	GATGGCAAGTCGAACTCCTG
Orb2	AACTGTGACTCCCTCTCCAG	TTGCGCAGACTAACTTCGTC
Rim	CAGCAACAGCCCAGATCAG	CTCATCAGGCCATCGAGTTC
Rut	GAAACGTTCAGGTGTCGGAG	CGATTCGTTGGCTGATGGTG
1tub23cf	TAATGGGCTCGGTCTACTCC	CCGCGATACTTCTCTCCAC
RNApol2	CCGCGATACTTCTCTCCAC	GACCAGCTAGGCGACATTC

Table 21 | TaqMan Probe Set used in this thesis

Gene ID	Probe TaqMan Assay
RIMS1	Hs01112189_m1
SLC18A2	Hs00996835_m1
PPIA	Hs99999904_m1

10. ANNEX II

Additional publications related to the thesis topic generated during the PhD program.

Latorre J, Ortega FJ, Liñares-Pose L, Moreno-Navarrete JM, Lluch A, Comas F, <u>Oliveras-Cañellas N</u>, Ricart W, Höring M, Zhou Y, Liebisch G, Nidhina Haridas PA, Olkkonen VM, López M, Fernández-Real JM. **Compounds that modulate AMPK activity and hepatic steatosis impact the biosynthesis of microRNAs required to maintain lipid homeostasis in hepatocytes**. EBioMedicine. 2020. 53:102697. doi: 10.1016/j.ebiom.2020

Impact factor (JCR 2022): 11.1 (D1, 10/136 Medicine, Research & Experimental)

Comas F, Latorre J, Ortega F, <u>Oliveras-Cañellas N</u>, Lluch A, Ricart W, Fernández-Real JM, Moreno-Navarrete JM. **Permanente cystathionine-β-Synthase gene knockdown promotes inflammation and oxidative stress in immortalized human adipose-derived mesenchymal stem cells, enhancing their adipogenic capacity**. Redox Biol. 2021. 42:101668. doi: 10.1016/j.redox.2020

Impact factor (JCR 2022): 11.4 (D1, 20/285 Biochemistry & Molecular Biology)

Comas F, Díaz-Trelles R, Gavaldà-Navarro A, Milbank E, Dragano N, Morón-Ros S, Mukthavaram R, Latorre J, Ortega F, Arnoriaga-Rodriguez M, <u>Oliveras-Cañellas N</u>, Ricart W, Karmali PP, Tachikawa K, Chivukula P, Villarroya F, Giralt M, López M, Fernández-Real JM, Moreno-Navarrete JM. **Downregulation of peripheral lipopolysaccharide binding protein impacts on perigonadal adipose tissue only in female mice**. Biomed Pharmacother. 2022. 151:113156. doi: 10.1016/j.biopha.2022.

Impact factor (JCR 2022): 7.5 (D1, 27/136 Medicine, Research & Experimental)

Latorre J, Ortega F, <u>Oliveras-Cañellas N</u>, Comas F, Lluch A, Gavaldà-Navarro A, Morón-Ros S, Ricart W, Villarroya F, Giralt M, Fernández-Real JM, Moreno-Navarrete JM. **Specific adipose tissue *Lbp* gene knockdown prevents diet-induced body weight gain, impacting fat accretion-related gene and protein expression.** Mol Ther Nucleic Acids. 2022. 27:870-879. doi: 10.1016/j.omtn.2022.

Impact factor (JCR 2022): 8.8 (Q1, 18/136 Medicine, Research & Experimental)

Martínez C, Latorre J, Ortega F, Arnoriaga-Rodríguez M, Lluch A, <u>Oliveras-Cañellas N</u>, Díaz-Sáez F, Aragonés J, Camps M, Gumà A, Ricart W, Fernández-Real JM, Moreno-Navarrete JM. **Serum neuregulin 4 is negatively correlated with insulin sensitivity in humans and impairs mitochondrial respiration in HepG2 cells**. Front Physiol. 2022. 13:950791. doi: 10.3389/fphys.2022.

Impact factor (JCR 2022): 4.0 (Q2, 21/79 Physiology)

Latorre J, Díaz-Trelles R, Comas F, Gavaldà-Navarro A, Milbank E, Dragano N, Morón-Ros S, Mukthavaram R, Ortega F, Castells-Nobau A, <u>Oliveras-Cañellas N</u>, Ricart W, Karmali PP, Tachikawa K, Chivukula P, Villarroya F, López M, Giralt M, Fernández-Real JM, Moreno-Navarrete JM. **Downregulation of hepatic lipopolysaccharide binding protein improves lipogenesis-induced liver accumulation**. Mol Ther Nucleic Acids. 2022; 5(29):599-613. doi: 10.1016/j.omtn.2022.08.003

Impact factor (JCR 2022): 8.8 (Q1, 18/136 Medicine, Research & Experimental)

Latorre J, Mayneris-Perxachs J, <u>Oliveras-Cañellas N</u>, Ortega F, Comas F, Fernández-Real JM, Moreno-Navarrete JM. **Adipose tissue cysteine dioxygenase type 1 is associated with an anti-inflammatory profile, impacting on systemic metabolic traits**. EBioMedicine. 2022. 85:104302. doi: 10.1016/j.ebiom.2022.

Impact factor (JCR 2022): 11.1 (D1, 10/136 Medicine, Research & Experimental)

Latorre J, Martínez C, Ortega F, <u>Oliveras-Cañellas N</u>, Díaz-Sáez F, Aragonés J, Camps M, Gumà A, Ricart W, Fernández-Real JM, Moreno-Navarrete JM. **The relevance of EGFR, ErbB receptors and neuregulins in human adipocytes and adipose tissue in obesity**. Biomed Pharmacother. 2022. 156:113972. doi: 10.1016/j.biopha.2022

Impact factor (JCR 2022): 7.5 (Q1, 27/136 Medicine, Research & Experimental)

Lluch A, Latorre J, Serena-Maione A, Espadas I, Caballano-Infantes E, Moreno-Navarrete JM, <u>Oliveras-Cañellas N</u>, Ricart W, Malagón MM, Martin-Montalvo A, Birchmeier W, Szymanski W, Graumann J, Gómez-Serrano M, Sommariva E, Fernández-Real JM, Ortega FJ. **Impaired plakophilin-2 in obesity breaks cell cycle dynamics to breed adipocyte senescence.** Nat Commun. 2023; 14(1): 5106. doi: 10.1038/s41467-023-40596-0

Impact factor (JCR 2022): 16.6 (D1, 6/73 Multidisciplinary Sciences)

Quesada-Vázquez S, Castells-Nobau A, Latorre J, <u>Oliveras-Cañellas N</u>, Puig-Parnau I, Tejera N, Tobajas Y, Baudin J, Hildebrand F, Beraza N, Burcelin R, Martinez-Gili L, Chilloux J, Dumas ME, Federici M, Hoyles L, Caimari A, Del Bas JM, Escoté X, Fernández-Real JM, Mayneris-Perxachs J. **Potential therapeutic implications of histidine catabolism by the gut microbiota in NAFLD patients with morbid obesity**. Cell Rep Med. 2023. 4(12):101341. doi: 10.1016/j.xcrm.2023

Impact factor (JCR 2022): 14.3 (D1, 17/191 Cell Biology)

<u>Oliveras-Cañellas N</u>, Latorre J, Santos-González E, Lluch A, Ortega F, Mayneris-Perxachs J, Fernández-Real JM, Moreno-Navarrete JM. **Inflammatory response to bacterial lipopolysaccharide drives iron accumulation in human adipocytes**. Biomed Pharmacother. 2023. 166:115428. doi: 10.1016/j.biopha.2023

Impact factor (JCR 2022): 7.5 (Q1, 27/136 Medicine, Research & Experimental)